CENTRE D'HYDROGEOLOGIE
CENTRE OF HYDROGEOLOGY

UNIVERSITE DE NEUCHATEL
FACULTE DES SCIENCES
INSTITUT DE GÉOLOGIE

A conceptual model of flow and transport in a karst aquifer based on spatial and temporal variations of natural tracers

PhD thesis presented to the Faculty of Sciences of
the University of Neuchâtel to satisfy the requirements
of the Degree of Doctor of Philosophy in Science

By

Jérôme Perrin

Geologist graduated from the University of Lausanne

Thesis Jury Defense Date: 14.02.2003
Public Presentation Date: 28.03.2003

Prof. F. Zwahlen	University of Neuchâtel	Thesis Director
Dr. P-Y. Jeannin	University of Neuchâtel	Thesis Co-Director
Dr. M. Bakalowicz	University of Montpellier	Jury member
Prof. K. Föllmi	University of Neuchâtel	Jury member
Prof. H. Hötlz	University of Karlsruhe	Jury member
Prof. K-P. Seiler	GSF, Institute für Hydrologie, Munich	Jury member

IMPRIMATUR POUR LA THESE

A conceptual model of flow and transport in a karst aquifer based on spatial and temporal variations of natural tracers

de M. Jérôme PERRIN

UNIVERSITE DE NEUCHATEL

FACULTE DES SCIENCES

La Faculté des sciences de l'Université de Neuchâtel, sur le rapport des membres du jury

MM. F. Zwahlen (directeur de thèse), P.-A. Jeannin (co-directeur de thèse), K. Föllmi, H. Hoetzl (Karlsruhe D), K.-P. Seiler (Neuherberg D) et M. Bakalowicz (Montpellier F)

autorise l'impression de la présente thèse.

Neuchâtel, le 23 juin 2003

Le doyen:

François Zwahlen

Remerciements

Ce travail de thèse n'aurait pu aboutir sans le concours et le soutien de nombreuses personnes que je tiens à remercier chaleureusement.

F. Zwahlen, directeur du Centre d'hydrogéologie (CHYN), et P-Y. Jeannin, responsable du groupe karst au Centre, m'ont accordé leur confiance dès le début de l'étude ; leurs encouragements et leur enthousiasme ont largement contribué à la réussite de ce travail. M. Bakalowicz, de l'Université de Montpellier, H. Hötzl, de l'Université de Karlsruhe, K-P. Seiler, de l'Institut d'Hydrologie du GSF à Münich, et K. Föllmi, de l'Université de Neuchâtel ont accepté de juger la qualité scientifique de cette thèse. Leurs remarques constructives ont sensiblement amélioré sa qualité.

Au CHYN, de nombreuses personnes ont été impliquées dans ce projet. Je pense tout d'abord à Tong Ettlin, notre efficace laborantine, qui ne s'est jamais découragée devant l'abondance des échantillons souvent sales que je ramenais des entrailles de Milandre… François Bourret a réussi la prouesse de gérer jusqu'à 15 appareils de mesure en continu localisés en milieu souterrain. Certains n'ont pas toujours fonctionné mais les abondantes mesures présentées dans cette thèse lui doivent beaucoup. Stéphane Cattin n'a pas ménagé ses efforts sous terre et sur son Mac pour rendre des données indispensables accessibles et utilisables.

Plusieurs collègues m'ont fait partagé leur compétences scientifiques, techniques, ou linguistiques. Je pense en particulier à V. Puech, A. Kovacs, F. Bosch, F. Cornaton, E.Milnes, H. Surbeck, I.Mueller, P.Renard, D. Hunkeler, P-A. Schnegg.

Quelques étudiants ont eu le mérite de ne pas se laisser effrayer par la complexité du karst et ont réalisé des travaux de diplôme tout à fait intéressants et utiles. Merci à L. Savoy, I. Favre, P. Monnot et G. Madec.

B. Wenger et L. Kopp, valeureux civilistes, ont renforcé le groupe karst de manière efficace. Les stagiaires bretons G. Carré et R. Le Fanic ont apporté des contributions très intéressantes par leurs expériences de terrain. P. Tacchini, d'une disponibilité rare, a rendu de fiers services lors des échantillonnages sur le site de Milandre.

Grâce aux nombreux travaux du Spéléo Club Jura, la grotte de Milandre et sa rivière souterraine est devenue un laboratoire souterrain idéal. Les agriculteurs du Maira se sont montrés très intéressés par l'étude et n'ont pas rechigné à ouvrir leur carnet des champs pour me communiquer les charges d'engrais administrées aux parcelles. Le village de Boncourt, par l'intermédiaire de son employé de commune M. Schuler, a participé aux campagnes d'échantillonnage de la source du Saivu. Les bureaux d'ingénieurs MFR et RWB, ainsi que le service de l'environnement du canton du Jura (OEPN) ont fourni gracieusement de nombreuses données utiles à l'étude.

Pour terminer, je me dois de remercier ma famille qui m'a toujours encouragé et aidé à suivre le chemin qui me plaisait. Cette thèse doit beaucoup à leur soutien.

Abstract

Karst aquifers represent an important groundwater resource world-wide. They are highly vulnerable to contamination due to fast transport through the system and limited attenuation of contaminants. The two main hydrogeological approaches developed for studying flow and transport are: inference of the system structure from karst spring hydrographs and chemographs; numerical modelling of flow and transport using a theoretical distribution of flow and transport field parameters. These two approaches lack of validation by detailed field measurements and observations. The main objective of this thesis is to “fill the gap” existing between field and model data. Observations of flow and transport parameters at several locations within the system were used to develop a conceptual model. This model was then compared to the existing models.

The main field test site is the Milandre karst aquifer, located in the Swiss tabular Jura. Natural tracers (major ions, oxygen-18, specific conductance) and discharge were measured on the underground river, its main tributaries, percolation waters, and the main spring. These data were collected on a long-term basis in order to assess the spatial variability of the parameters, and on a short time scale (i.e. flood events) in order to investigate the dynamic processes. Complementary sites (Brandt and Grand Bochat) were used for more observations at the base of the epikarst.

The proposed conceptual model considers four sub-systems: the soil zone, the epikarst, the unsaturated zone, and the phreatic zone. Each has its own specificity with respect to flow and transport.

The soil zone controls the actual infiltration into the system. It contributes efficiently to groundwater storage. It mixes quickly stored water with fresh infiltrated water. Its thickness determines land-use: thick soils are generally cultivated whereas thin soils are under forested areas. The solutes concentration of soil waters depends on land-use for pollution-related parameters (nitrate, chloride, sulfate, potassium, sodium). Moreover the soil zone is the main source of CO_2 which controls the limestone dissolution-related parameters.

The epikarst zone contributes largely to groundwater storage. It distributes groundwater into vadose flow through conduits, and base flow through low permeability volumes (LPV) in the unsaturated zone. It is the sub-system where dissolution-related parameters are mostly acquired.

The unsaturated zone is seen as a transmissive zone connecting the epikarst to the horizontal conduit network of the phreatic zone. In case of flood events, some dissolution still occurs in this sub-system.

The phreatic zone is the partly flooded conduit network draining groundwater to the spring. It collects waters issued from the unsaturated zone, mixes the tributaries, and drain the water towards the discharge area. The role of phreatic storage appears to be limited for both hydraulics and transport. Tributary mixing is a prominent process that shapes spring chemographs during flood events.

In steady-state conditions, base flow is mainly sustained by the epikarst reservoir. Tracer concentrations are stable as the chemical equilibrium is already reached in the epikarst. Waters issued from the different tributaries mix in the conduit network, and the spring chemistry is the result of this mixing.

During flood events, transient flow induces non-linear mixing of the tributaries. The respective contributions of the tributaries change throughout the flood, and the spring chemographs vary accordingly. In case of important recharge, waters issued from other sources than the epikarst participate to the flood. First, soil water reaches the phreatic zone. Its characteristics are a dampened isotopic signal, and ionic concentrations differing from those of the epikarst. Second, fresh water directly issued from rainfall, may reach the phreatic zone. Its characteristics are a varying isotopic signal, and diluted ionic concentrations. The mixing components participating to the flood are controlled by the actual infiltration volume (or height). The limestone dissolution process is effective for the fresh and soil components of flow. However mixing processes play a more important role than dissolution for shaping the spring chemographs.

From a practical point of view, the project confirmed the prominent role of the soil zone and the epikarst on the solute transport in karst systems. This was already integrated in karst vulnerability mapping methods recently developed (EPIK, PI, VULK).

Key-words: karst aquifer, carbonate aquifer, Milandre test site, epikarst, infiltration, transport, isotope, nitrate, dissolution, natural tracers, mixing, chemographs, spatio-temporal variability, structure, storage, transit times, vulnerability, local scale, catchment scale.

Résumé

Les aquifères karstiques représentent une importante ressource en eaux souterraines à l'échelle planétaire. Cette ressource est très vulnérable aux contaminants car les eaux transitent rapidement dans l'aquifère et les phénomènes d'atténuation sont limités. Les hydrogéologues ont développé deux approches différentes pour étudier l'écoulement et le transport des aquifères karstiques : la première infère la structure du système karstique à partir des réponses hydrauliques et chimiques à la source ; la seconde est une modélisation numérique de la réponse en utilisant une distribution théorique des paramètres d'écoulement et du transport. Ces deux approches sont insuffisamment validées par des observations de terrain détaillées. Le principal objectif de cette thèse est de combler le vide existant entre les mesures de terrain et les modèles numériques. Pour ce faire, nous avons observé les paramètres d'écoulement et de transport en différents endroits du système pour en extraire un modèle conceptuel de fonctionnement cohérent. Ce modèle a ensuite été comparé aux modèles existant dans la littérature.

Le site test principal est l'aquifère karstique de Milandre situé dans le Jura tabulaire. Les traceurs naturels (ions majeurs, oxygène-18, conductivité) et le débit ont été mesurés sur la rivière souterraine, ses affluents principaux, des eaux de percolation et la source principale du système. Les paramètres furent mesurés sur le long terme afin de caractériser leur variabilité spatiale, ainsi qu'à l'échelle d'une crue afin de décrire les processus dynamiques. Des sites complémentaires (Grand Bochat et Brandt) ont été utilisés afin de compléter les mesures effectuées à la base de l'épikarst.

Le modèle conceptuel proposé se structure en quatre sous-systèmes : le sol, l'épikarst, la zone non saturée et le zone phréatique. Chacun de ces sous-systèmes a ses propres particularités en terme d'écoulement et de transport.

Le sol contrôle la recharge effective du système. Il contribue de manière efficace au stockage de l'eau. C'est dans cette zone que l'eau fraîchement infiltrée se mélange rapidement avec l'eau stockée. Son épaisseur contrôle l'occupation du sol : les sols épais sont généralement cultivés alors que les sols minces sont des secteurs boisés. La concentration des ions dépend de l'occupation du sol pour les paramètres liés aux contaminations (nitrate, chlorures, sulfate, potassium, sodium). De plus le sol est la source principale de CO_2 qui contrôle les paramètres liés à la dissolution des calcaires.

L'épikarst contribue efficacement au stockage de l'eau souterraine. A l'image d'un entonnoir, il canalise les écoulements vers les fractures perméables de la zone non saturée C'est dans ce sous-système que les paramètres associés à la dissolution sont principalement acquis.

La zone non saturée se résume essentiellement à une zone transmissive qui connecte l'épikarst aux conduits sub-horizontaux de la zone phréatique. Lors des crues, les phénomènes de dissolution peuvent encore être significatifs dans cette zone.

La zone phréatique est constituée d'un réseau de conduits partiellement noyés qui drainent les écoulements en direction de la source. Cette zone collecte les écoulements issus de la zone non saturée, mélange les affluents, et achemine l'eau souterraine en direction des exutoires. Le stockage dans les volumes peu perméables (VPP) de la zone phréatique semble jouer un rôle limité sur l'écoulement et le transport. Le mélange des différents affluents est un phénomène prépondérant qui influence les chimiogrammes à la source lors des événements de crue.

En conditions d'étiage, l'écoulement de base est essentiellement issu des réserves de l'épikarst. Les concentrations en traceurs sont stables puisque les équilibres chimiques sont déjà atteints dans l'épikarst. Les eaux provenant des différents affluents se mélangent dans le réseau de conduits et la chimie à la source est le résultat de ce mélange.

Lors des événements de crue, la non stationnarité des écoulements induit un mélange non linéaire des affluents. Les contributions respectives des affluents évoluent au cours de la crue, conditionnant les chimiogrammes à la source. En cas d'une importante infiltration, des eaux issues d'autres sources que l'épikarst participent à la crue. Dans un premier temps, l'eau du sol court-circuite l'épikarst et gagne la zone phréatique. Ses caractéristiques sont un signal isotopique tamponné et des concentrations en ions différentes de celles de l'épikarst. Si la recharge continue, l'eau fraîchement infiltrée, directement issue de l'eau de pluie, peut rejoindre également la zone phréatique. Ses caractéristiques sont un signal isotopique contrasté et des concentrations ioniques basses. La provenance des eaux participant à la crue est contrôlée par la hauteur de l'infiltration efficace correspondant à l'événement pluvieux. La dissolution du calcaire est significative pour les eaux provenant du sol et de la pluie. Les chimiogrammes sont plus influencés par les mélanges que par les processus de dissolution.

D'un point de vue pratique, cette étude confirme le rôle prépondérant du sol et de l'épikarst sur le transport de solutés dans les aquifères karstiques. Cet aspect avait déjà été intégré dans les méthodes de cartographie de la vulnérabilité développées récemment (EPIK, PI, VULK).

Table of contents

1. Introduction

Carbonate aquifers differ from other reservoirs as they develop an important secondary porosity by limestone dissolution processes: groundwater infiltrates through pre-existent fissures and enlarges them, generating a conduit network. This process is a major specificity of carbonate aquifers, which are an important groundwater resource in many areas of the world. It is estimated that carbonate rocks cover 20 % of the world's continents, 35 % of the European continent, and 20 % of the Swiss territory. Carbonate aquifers are a future resource of primary importance for the following reasons:

- Groundwater volumes are important due to large catchment areas.
- Catchments are often located in sparsely populated areas making the application of land-use restrictions easier than in other regions.
- Carbonate aquifers are particularly abundant in the areas surrounding the Mediterranean basin, where the water demand is high.

The organised heterogeneity of carbonate aquifers due to solution processes leads to a specific structure and behaviour which need adequate methods of investigation.

Over the last 30 years, conceptual and numerical models have been developed in order to reproduce the karst aquifer behaviour (see § 1.1.3.). Generally these models consider the karst system at a global scale and infer the structure of the aquifer from a global response (i.e. the spring of the karst aquifer). Even if they succeed in reproducing the observations, verifications of the proposed inferences by detailed field observations are still lacking.

The present study aims at describing the spatial variability of the physico-chemical parameters of waters at different locations in the aquifer first, and then their time-concentration evolution. The data were collected in different parts of the aquifer (the unsaturated zone, the conduit network and its tributaries, the spring). These observations should then allow to improve or validate existing global models and propose new insights on the aquifer structure and flow parameters.

The main study area is the Milandre test site located in the Swiss tabular Jura. The hydrodynamics of the system has been extensively studied (Jeannin 1998). The existence of two springs, an underground river, several tributaries, and numerous boreholes offer a unique observation network.

Detailed field investigations are first made, and then conceptual models are developed from these field data and verified by numerical modelling. In the thesis report, the results are presented following this logical order:

- The first step is a complementary study of the hydraulic behaviour of several tributaries. These observations complete those of Jeannin (1998). (chapter 2.2)
- The second step is a characterisation of the spatial variability of the groundwater chemistry. (chapter 2.3)
- The third step is a study of the temporal variability of stable isotopes in groundwater and in rainfall. The major issue is the determination of the storage characteristics in the unsaturated zone. (chapter 2.4)
- The fourth step is an analysis of karst spring chemographs. The role of mixing processes is evaluated and modelled. (chapter 2.5)
- The fifth step is an evaluation of the dissolution and mixing processes in the unsaturated zone (chapter 2.6)
- The sixth step is a discussion on the adequacy of the proposed transport conceptual model with existing concepts of vulnerability assessment. (chapter 2.7)

1.1. Karst aquifers

1.1.1. Definition

Karst aquifers include any karstified geological unit which contains groundwater. Most common rocks are limestone, dolomite, gypsum, and halite.

The term karst aquifer is generally used instead of **carbonate aquifer**, which is limited to limestone and dolomite rocks.

Mangin (1975) showed that the term **karst system** is more adapted than karst aquifer. Unlike classical aquifers, unsaturated and saturated zones are not necessarily superimposed in karst, and the recharge can include part of a non-karstic catchment. Hence karst system is defined as “the entity where the flow constitutes a drainage unit”.

In the present study, karst aquifer or karst system is the used terminology. However, it refers always to systems in carbonate rocks. Karst hydrology of gypsum or halite is another topic which is not considered here.

1.1.2. The specificity of karst aquifers

Karst aquifers need to be studied on their own as they have a very peculiar structure and behaviour. The main feature of a karst aquifer is its **organised heterogeneity**.

“Unlike porous or fissured aquifers, in karst aquifers it is impossible to determine a representative elementary volume (REV) for the whole aquifer because karstification creates cavities and organises flow between them in a **hierarchical** manner“ (Bakalowicz et al. 1994)

“The organised heterogeneity of many karst aquifers may be schematised by a high permeability, generally unknown channel network with kilometres wide meshes, which is immersed in a low permeability fractured limestone volume, and is well connected to a local discharge area, the karst spring. The **duality** of karst aquifers is a direct consequence of this structure:

- Duality of the infiltration processes (diffuse or slow infiltration into the low permeability volumes, concentrated or rapid infiltration into the channel network).
- Duality of groundwater flow field (low flow velocities in the fractured volumes, high flow velocities in the channel network).
- Duality of the discharge conditions (diffuse seepage from the low permeability volumes, concentrated discharge from the channel network at the karst springs).” (Kiraly 1998).

1.1.3. The conceptual models of karst aquifers

Several conceptual models of karst aquifers can be found in the literature (Blavoux and Mudry 1983, Drogue 1992, Lee and Krothe 2001, Mangin 1975, Doerfliger et al. 1999) (figure 1). They generally take into account the main features of the system, which can be separated in sub-systems:

- **Infiltration** sub-system where recharge is autogenic, allogenic, diffuse or concentrated.
- **Soil and epikarst** sub-systems which store part of the infiltrated water.
- **Unsaturated zone** (or infiltration zone, vadose zone) sub-system connecting the former sub-system to the phreatic zone by drainage through a vertical network of fissures and conduits.
- **Phreatic** zone (or saturated zone) sub-system split into a network of high permeability conduit and low permeability volumes (LPV) with a high storage capacity.

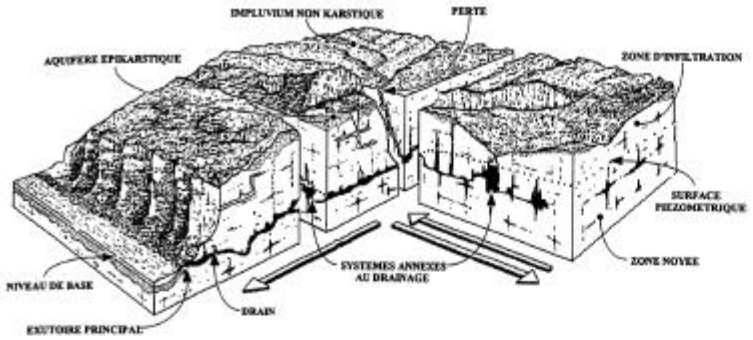

1.

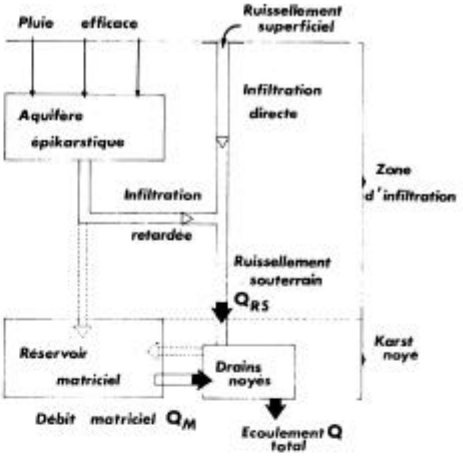

2.

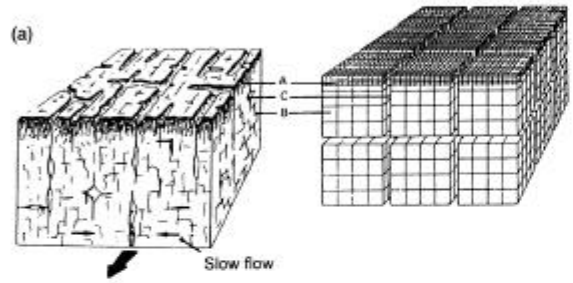

Drainage of rapid flow to the spring

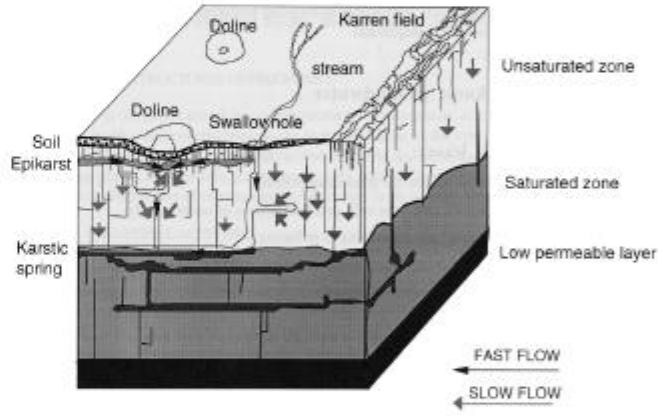

4.

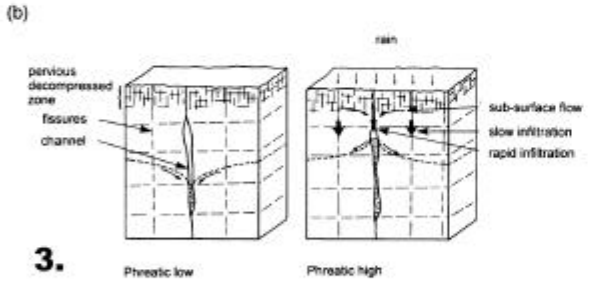

3.

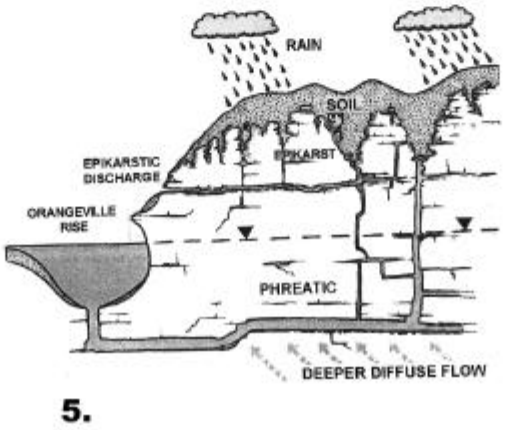

5.

Figure 1: Conceptual models of karst aquifers existing in the literature (1. Mangin 1975, 2. Blavoux and Mudry 1983, 3. Drogue 1992, 4. Doerfliger et al. 1999, 5. Lee and Krothe 2001).

The major differences are the following:

- The low permeability volumes in the phreatic zone are represented either as volumes of fissured limestone (Drogue 1992, Lee and Krothe 2001) or as large cavities connected to the drain (Mangin 1975).
- Base flow originates either from the low permeability volume of the phreatic zone (Drogue 1971, Mangin 1975, Kiraly and Mueller 1979) or from the epikarst storage (at least a fraction) (Williams 1983, Sauter 1992, Klimchouk 2000).
- Waters participating to flood events have different origin: concentrated infiltration, diffuse infiltration and phreatic water stored in the low permeability volumes (LPV) (Vervier 1990), phreatic water and fresh infiltrated water (Kiraly and Mueller 1979, Blavoux and Mudry 1983), epikarst storage, conduit storage, and fresh infiltrated water (Williams 1983, Sauter 1992), mixing of fresh infiltrated water, soil water, epikarst water, and phreatic water (Lee and Krothe 2001), mixing of several tributaries (Hess and White 1988).

Practical approaches of this theoretical conceptual model can be very different:

- Hobbs and Smart (1986) reproduced the shape of karst spring hydrographs on the basis of three cascading systems (figure 2): first recharge can be diffuse or concentrated, second storage can be low or high, and third the flow can be diffuse or concentrated. The combination of these three systems can lead to very different hydrograph shapes.

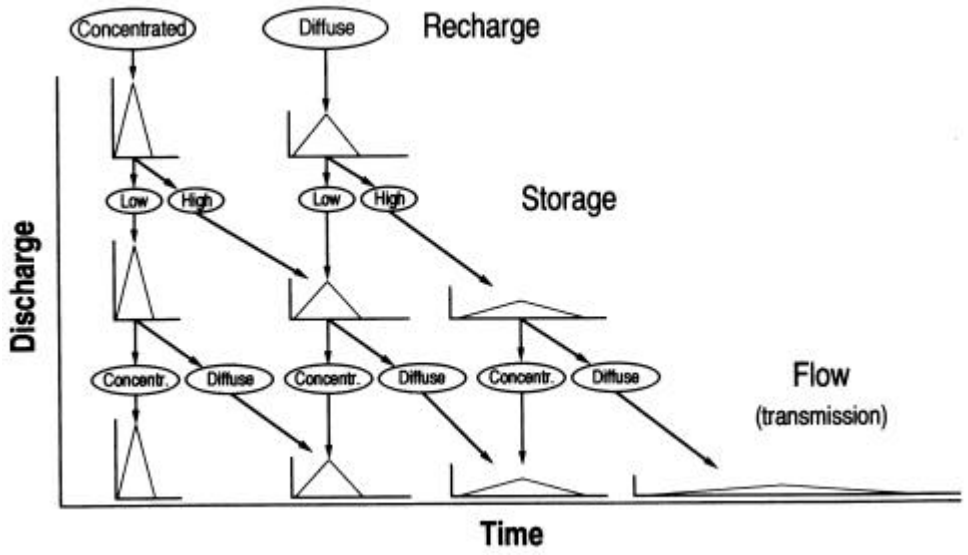

Figure 2: A three cascading sub-systems model can reproduce observed hydrographs at karst springs (from Hobbs and Smart 1986).

- Mangin (1975) developed a **functional approach**. He analysed karst spring hydrographs (temporal behaviour) by time series analyses such as cross-correlation, spectral analysis, wavelets. The karst system is considered as a black-box where only the input and output functions are used. From this approach, he proposed interpretations allowing to infer structural information on the system (storage, memory effect, degree of karstification, type of infiltration). The main drawback of this approach is that no validation is possible. Eisenlohr et al. (1997a and 1997b) tested this approach on a synthetic numerical model. They showed that the results depend not only on the structure but also on the recharge events frequency. Grasso (1999) reached the same conclusions from a detailed analysis of the Milandre test site data.
- Drogue (1971) and Kiraly (1975) proposed a **structural approach**. The karst aquifer is represented by a network of high permeability conduits embedded in a fissured media of low permeability. Such a representation is adapted for simulating karst spring hydrographs by the mean of physically based models. Kiraly (1988) developed a three dimensional numerical model

where groundwater flow is simulated by the resolution of laminar flow equations in finite elements. The major drawback of this approach is that a thorough knowledge of the aquifer geometry (dimensions and conduit location) is necessary to reproduce a real temporal evolution of discharge at the spring. Another limitation is the use of Darcian flow only, when it is established that flow in the conduits is mainly turbulent.

None of these approaches is ideal and it is necessary to combine or choose one of them regarding the problem to be solved and the data available.

1.1.4. Used terminology

Some terms used in the following chapters may have different meanings in the existing literature. Here they are used according to the definitions given below.

Terms of flow:

Flow divides in **diffuse flow** and **concentrated flow** (Hobbs and Smart 1986). Diffuse flow is also described as **seepage flow** or **percolation water** through the LPV. Concentrated flow is also called **conduit flow** or **quick flow** through the **conduit network** (or karstic network, channel network, drainage axis). More specifically, **vadose flow** is conduit flow in the infiltration zone (vertical), and flow through the (sub)**horizontal conduit network** is conduit flow in a phreatic zone of reduced thickness (e.g. partially filled conduits).

Base flow is the part of stream discharge that is not attributable to rapid infiltration, and generally sustained by groundwater storage.

Flood event is a high-discharge event due to important precipitations. It does not necessarily generate a flooding downstream of the spring.

Terms of storage:

Storage can exist in the low permeability volumes (LPV) of the phreatic zone, and in the soil and epikarst sub-systems. **Dynamic storage** is groundwater issued from the phreatic zone (Mangin 1975). For groundwater issued from the epikarst, **epikarst dynamic storage** should be used.

A **reservoir** corresponds to a groundwater store, e.g. the epikarst nappe, or the phreatic zone.

1.2. The epikarst

1.2.1. The role of the epikarst in karst aquifers behaviour

Kiraly (1998) showed by several numerical simulations the need of an epikarst layer concentrating infiltration water near the ground surface (figure 3). If this concentration of diffuse infiltration does not occur, the spring hydrograph stays too flat compared to real systems.

An important consequence of the existence of an epikarst layer, as modelled by Kiraly (1998), is the “Faraday cage” effect. In concentrating infiltration, epikarst limits greatly the recharge of the low permeability volumes by diffuse infiltration through the unsaturated zone. In a deep phreatic zone karst configuration, the low permeability volumes can still be recharged by inversion of gradients during flood events, but in the case of shallow karst configuration (e.g. Milandre test site), the recharge of low permeability volume can be non-existent.

This numerical simulation showed clearly that the epikarst sub-system plays an important role in the behaviour of karst aquifers.

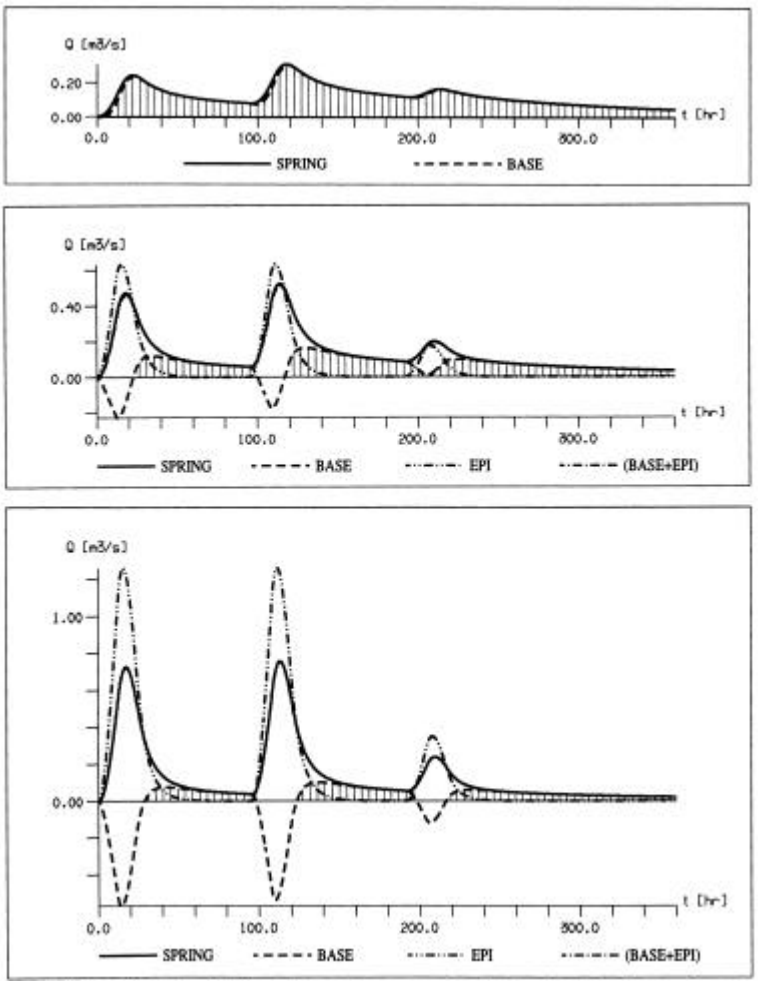

Figure 3: Simulations of karst spring hydrographs: no epikarst is present in the upper graph, epikarst concentrates 50 % of infiltration in the middle graph, and 100 % in the lower graph (from Kiraly 1998). Hydrographs are separated in springflow, baseflow, and epiflow (rapid concentrated infiltration).

1.2.2. Definition

The **epikarstic zone** (also referred to as the **subcutaneous zone**) is the uppermost zone of exposed karstified rocks, in which permeability due to fissuring and diffuse karstification is substantially greater, as compared to the underlying main vadose zone (Klimchouk 1997).

The observed exponential increase in fissure density towards the ground surface is the result of rock decompression and biochemical processes (dissolution is the most effective in this zone and vegetation can break away fissured limestone).

1.2.3. Representation of the epikarst

Several authors attempted to schematise this epikarstic zone (Mangin 1975, Gouisset 1981, Gunn 1981, Williams 1985, Smart and Friederich 1986, Klimchouk 2000) (figure 4). These representations have in common the following hydraulic characteristics which are summarised by Klimchouk (2000):

- Vertical hydraulic conductivity is high and quasi-uniform at the surface and within the top of the epikarst zone, so that diffuse infiltration dominates.
- As jointing density and diffused karstification rapidly diminishes with depth, hydraulic conductivity also rapidly diminishes in that direction.

- Infiltration in the top of the epikarst zone is much easier than drainage out of it. Further downwards percolation occurs mainly via major tectonic fissures which are distant and non-uniformly distributed.
- Consequently, retention of percolation and storage of groundwater occurs in the epikarst zone.
- Contrast in permeability between the epikarst zone and underlying low permeability volumes causes a temporary aquifer to form within the epikarst zone. Perched above the vadose zone, it leaks into it along major tectonic fissures.
- Flow has an important lateral component in the epikarst zone. Water stored in this zone flows laterally towards the nearest vertical fissure.

Thus, by its **storage capacity**, epikarst contributes to support base flow to shafts and an overall base flow to the karst aquifer through quite prolonged period of drought.

By its "**funnelling" effect**, epikarst concentrates water fluxes in the upper part of the unsaturated zone and is the key factor that explains nervous hydraulic responses at karst springs.

This epikarst hydraulic functioning has been detailed at the Centre of Hydrogeology of Neuchâtel during the last years (Puech 1996, Puech and Jeannin 1997). Sprinkling experiments above cave systems located near the ground surface showed generally a common hydraulic response:

1. sprinkled water is stored in the epikarst nappe till a threshold capacity is reached
2. then water is rapidly transmitted to the cave vadose flow. A permanent flow regime can be reached
3. after the sprinkling stopped, stored water in the epikarst discharges slowly to the observed vadose flow

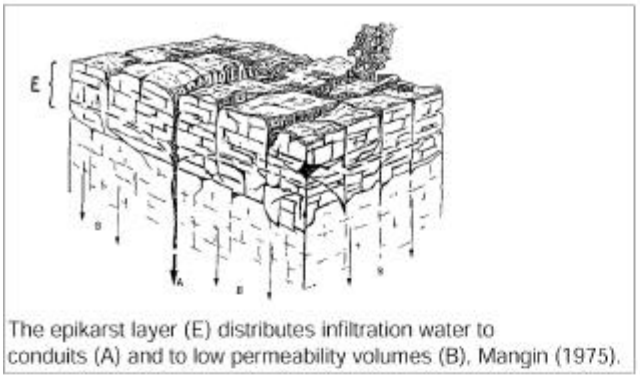

The epikarst layer (E) distributes infiltration water to conduits (A) and to low permeability volumes (B), Mangin (1975).

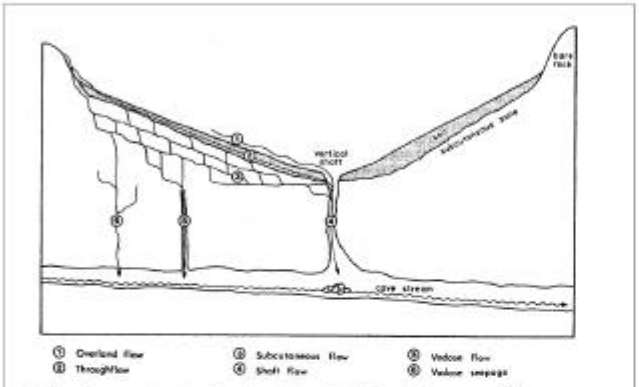

Infiltration water is diverted in six different types of flow. Subcutaneous flow corresponds to epikarst, Gunn (1981).

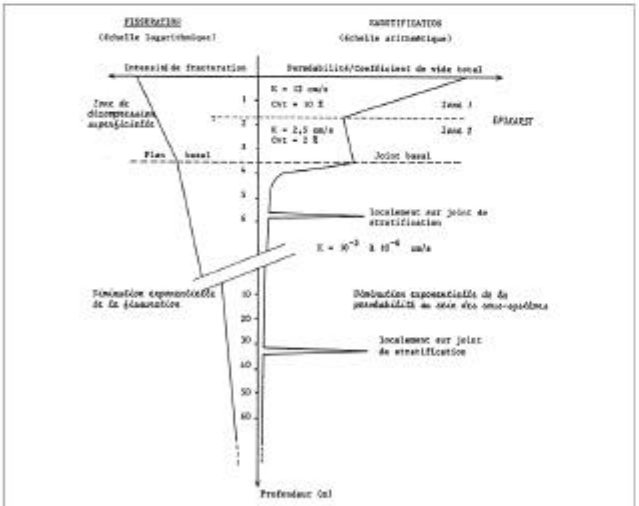

Synthetic representation of hydraulic parameters in the epikarst sub-system, Gouisset (1981).

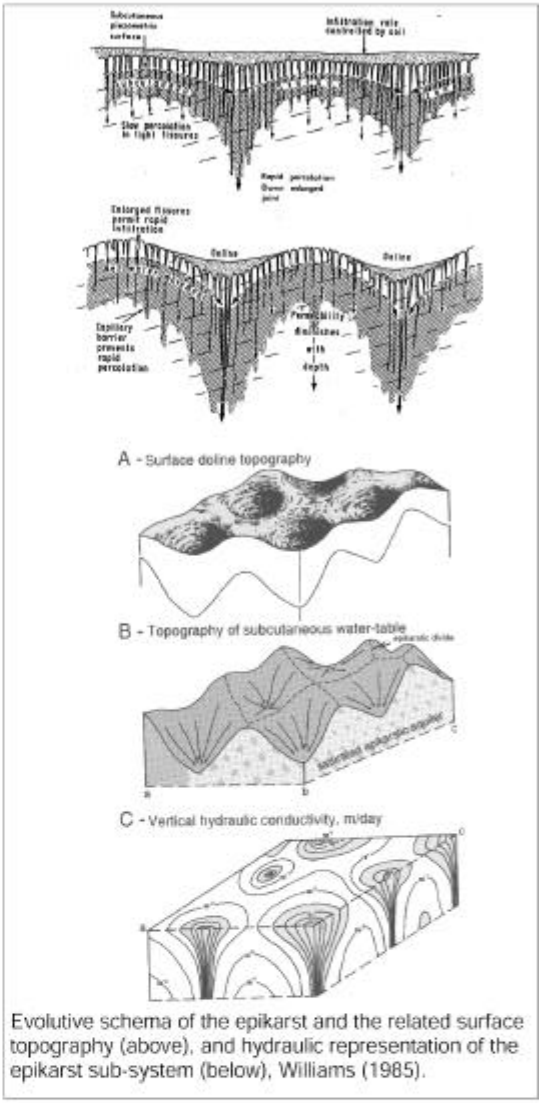

Evolutive schema of the epikarst and the related surface topography (above), and hydraulic representation of the epikarst sub-system (below), Williams (1985).

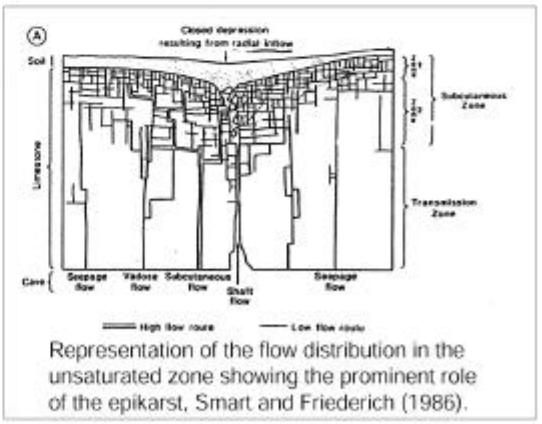

Representation of the flow distribution in the unsaturated zone showing the prominent role of the epikarst, Smart and Friederich (1986).

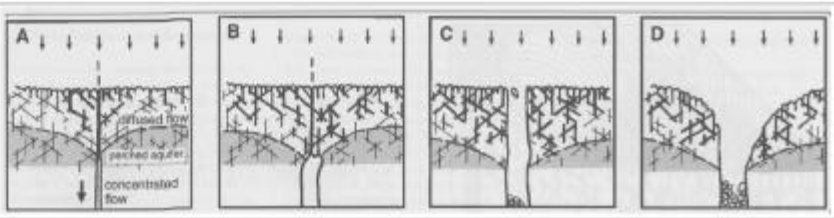

Epikarst evolution and its role in the formation of shafts, Klimchouk (2000).

Figure 4: Existing representations of the epikarst sub-system.

1.3. Hydrogeochemistry in karst aquifers

1.3.1. Definitions

Hydrogeochemistry is the “geochemistry of water as related to the occurrence of subsurface water” (Field 1999). The term **hydrochemistry** is often used instead, which in its original sense includes surface waters.

Tracer is a particle or solute carried by groundwater having specific properties which allow identification of hydrogeological processes.

A **natural tracer** is present in groundwater without being related to a scientific experiment. It can be natural or from anthropogenic sources (e.g. agriculture).

An **artificial tracer** is added to groundwater for scientific studies. Use of artificial tracers is referred to as **tracer** (or tracing) **tests** (or experiments).

A **chemograph** is the record of the time-concentration variations of a chemical parameter (e.g. specific conductance) in groundwater at one point of the aquifer (generally the spring).

Transit time (or travel time, flow through time) is the time needed for groundwater to flow from one point to another.

Transfer time (or pulse through time, piston through time) is the time needed for the groundwater pressure wave to displace from one point to another.

1.3.2. Use of hydrochemistry in hydrogeology

Chemical composition of groundwater is ruled by three main processes:

- Dissolution (or hydration) of elements (rocks, particles, liquids, gases) located along flow paths
- Modification along flow paths linked to physical and chemical processes (evaporation, cationic exchange, sorption, diffusion, dispersion, mixing)
- Modifications of the groundwater physico-chemistry along the flow path leading to chemical reactions such as dissolution, incongruent dissolution, precipitation, redox processes

Several useful hydrogeological informations can be inferred from these processes:

- Groundwater quality assessment
- Determination of the groundwater origin (i.e. catchment area) by the mean of natural tracers (e.g. sulfate indicator of gypsum, nitrate indicator of agricultural pollution)
- Determination of the physico-chemical state of the aquifer (e.g. reducing conditions inducing the degradation of nitrates)
- Tool allowing to infer flow characteristics (transit times, flow paths, storage)
- Tool allowing to infer the aquifer structure (sub-catchments, mixing)

The present study concentrates mainly on the two last points: by the study of the hydrochemical parameters evolution of a karst aquifer, we aim at better describing its flow and structure characteristics.

1.3.3. Hydrochemical methods in karst hydrology

The peculiar hydrochemical behaviour of karst systems requires specific investigation methods (Plagnes 2000). The main characteristic is the prominent role of hydrometeorological events (e.g. flood events) on chemical changes in the aquifer. This peculiarity has two important consequences:

The sampling frequency has to be adapted to the objective of the study (e.g. a flood event needs generally hourly sampling (or even more detailed) in order to get a realistic representation of the chemical variations).

Any hydrochemical information needs to be coupled with a hydraulic information (e.g. discharge, water level).

Several tools have been developed for the study of karst aquifers hydrochemistry. They can be classified as follows:

A.- Descriptive tools

A.1. Chemograph shapes (figure 5)

The chemograph is generally interpreted as the result of the relative contribution of different waters. Most characteristic chemographs occur at the first flood event after the low stage period (Bakalowicz and Aminot 1974). Three models of chemographs are described in the literature (Plagnes 2001):

Model 1: Water having a similar chemistry than pre-event water occurs during the rising limb of the hydrograph. Then diluted water arrives and, at the end of the flood, water recovers progressively to its pre-event chemistry.

Model 2: More mineralised water appears during the rising limb of the hydrograph. Then mineralisation decreases below the values of pre-event water, and during recession water returns to its pre-event concentrations.

Model 3: It shows invariant or very regular chemical variations.

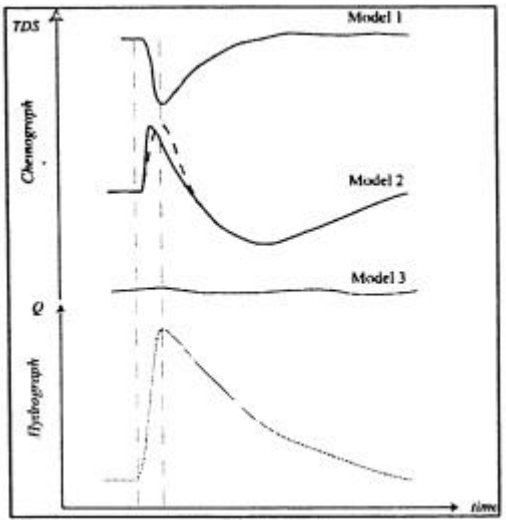

Figure 5: The three main types of karst spring chemographs according to Plagnes (2001).

A.2. Binary, ternary diagrams

Such diagrams are used for illustrating the correlation between two parameters (e.g. bicarbonate and specific conductance, or calcium and total dissolved solids) and the presence of different types of water (Mazor 1991, Mayer 1999).

Figure 6 gives an example of ternary diagrams used for chemical analyses at Milandre test site.

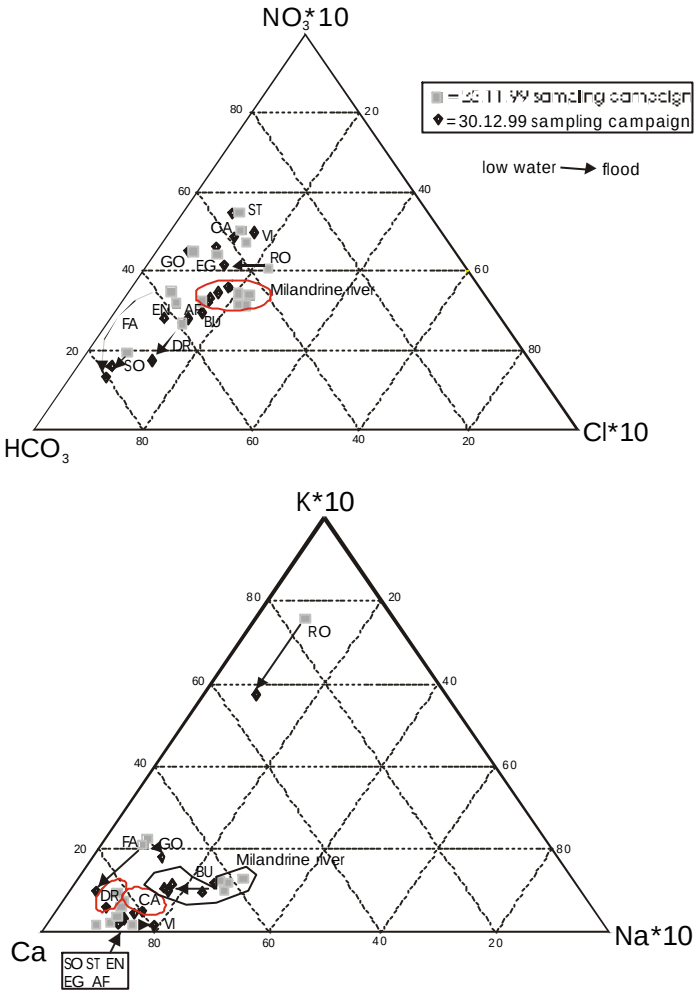

Figure 6: Ternary diagrams for anions and cations showing analyses from two sampling campaigns at Milandre test site: one at low water in November 1999, the other during a flood event in December 1999. Arrows indicate the evolution from the low water to the flood (Perrin et al. 2000).

A.3. Concentration – discharge relations

Concentration is plotted against discharge and the result is generally a cyclic relationship (hysteresis). The shape and sense of the hysteresis has been exploited in surface hydrology by Evans and Davies (1998), but not yet in karst hydrology. Grasso and Jeannin (1998) represented discharge and TDS on a log-log plot in order to obtain a straight line indicating the chemically based recession flow (CBRF phase).

A second representation is the plot mass flux (concentration multiplied by discharge) against discharge (Mudry 1990). Such an approach leads to the identification of the mixing poles chemistry, the degree of heterogeneity of the system, and the characteristic discharge where the switch between the flood decreasing limb and the recession occurs (figure 7).

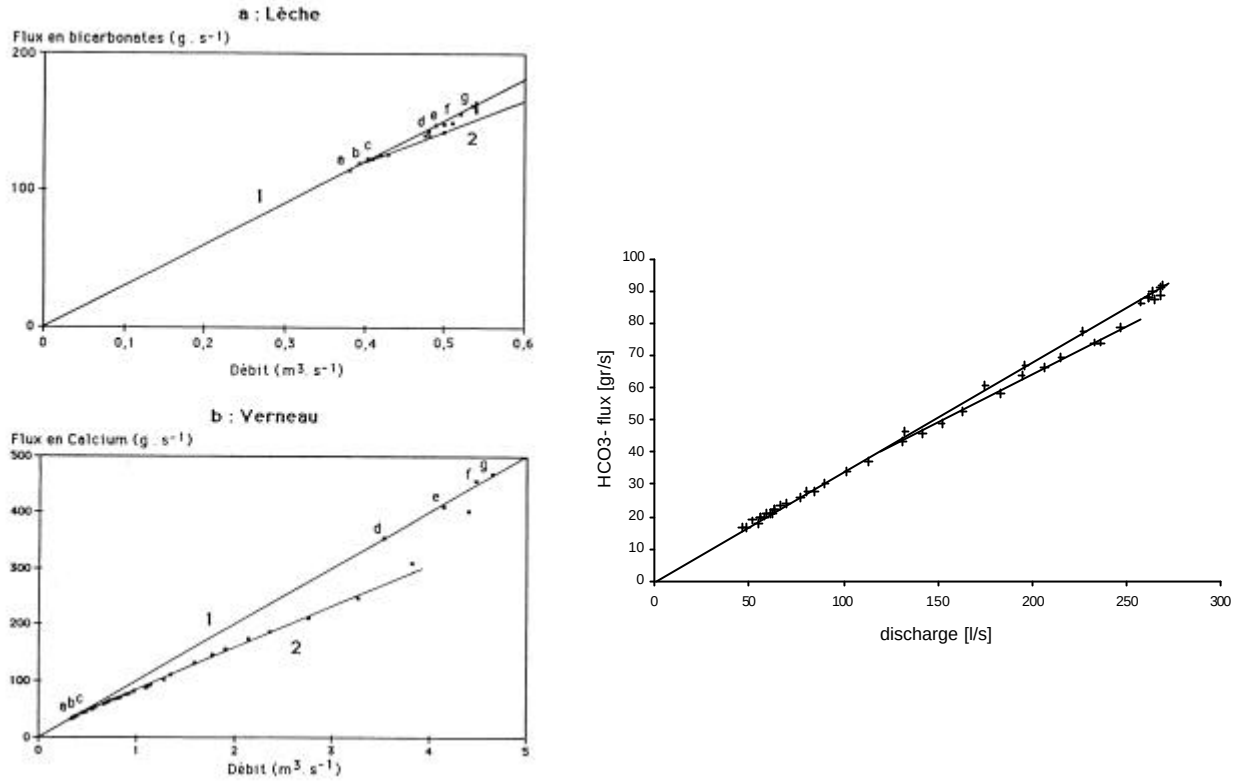

Figure 7: Relationship flux-discharge according to Mudry (1990), two diagrams to the left. The points d, e, f, g represent the piston-effect inherent to karst springs. The points a, b, c represent the base flow conditions. The straight line 1 is given by the base flow chemistry (note that the line passes through the point 0, 0). The straight line 2 results from the mixing of base flow with fresh infiltrated water. The right diagram is an application to the data at Milandrine upstream (June 2001 flood event).

A.4. Conductivity recovery fitting (Hess and White 1988)

The specific conductance (Sc) recovery after a flood event can be fitted to an exponential model (figure 8):

$$Sc\ (low\ stage) - Sc\ (t) = A\ e^{-bt}$$

1/b is called the characteristic response time for recovery and seems to be correlated with the importance of the recharge event.

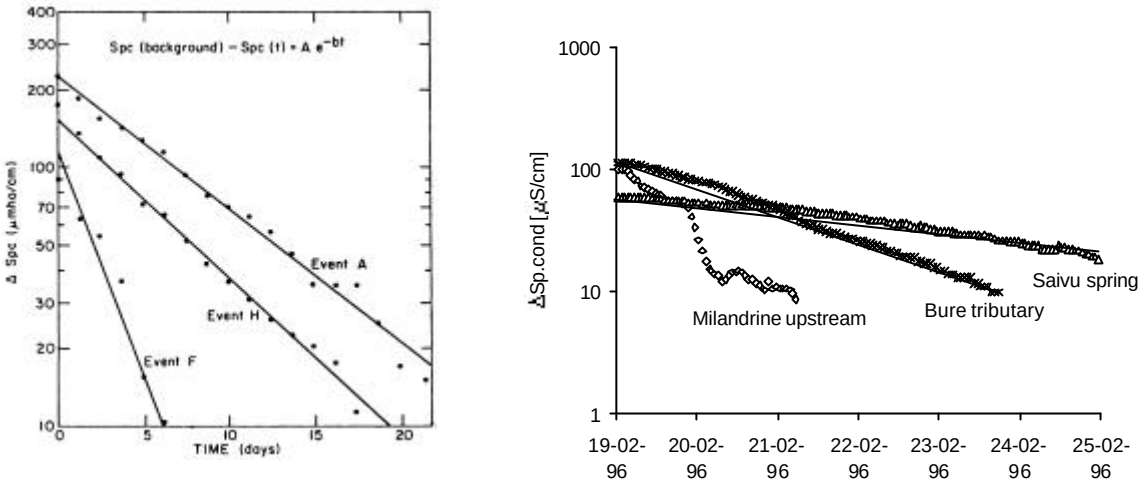

Figure 8: Specific conductance recovery curve fitted by an exponential model for several flood events on the same karst system, left diagram (Hess and White 1988). Application to the Milandre aquifer is shown on the right diagram: a same flood event is considered at three measurement sites: Bure tributary and Saivu spring fit to the exponential model whereas Milandrine upstream follows a completely different pattern.

A.5. Relation of water hardness to CO_2 availability (White 1988)

Dissolution processes giving groundwater its hardness are highly dependant on the CO_2 partial pressure available in the system (figure 9). The main source of CO2 is the soil, and hence differences in groundwater hardness at karst springs can indicate differences in soil development in the respective catchments (White 1988).

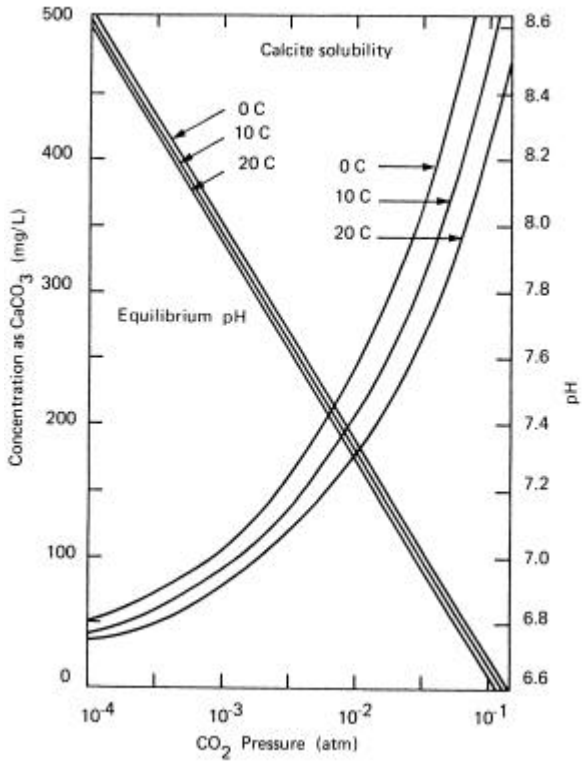

Figure 9: Pathways to equilibrium for undersaturated waters from various initial CO_2 pressures (White 1988).

This graph allows to predict equilibrium concentrations for open systems as a function of the CO_2 partial pressures. Concentrations of Ca^{2+} and HCO_3^- presented in the table below are calculated from the equilibrium equation:

$$CaCO_3 + CO_2 + H_2O = Ca^{2+} + 2\ HCO_3^-$$

pCO_2 [%]	HCO_3^- [mg/l]	Ca^{2+} [mg/l]	pH
0.1	100	40	8.0
0.3	150	60	7.7
1	220	100	7.4
3	330	120	7.1

Water chemistry in Milandre aquifer corresponds closely to an equilibrium pCO_2 of 3 %. Measurements carried out in the soil and the cave (Appendix 7) are in agreement.

B.- Statistical tools

B.1. Mineralisation frequency distribution

Bakalowicz (1979) represents measured specific conductance over an annual cycle on a frequency distribution plot for several karst systems (figure 10). The distribution can be very variable and illustrates the degree of development of the karst system: fissured carbonate aquifer gives an unimodal distribution whereas systems drained by a developed conduit network give plurimodal and spread distributions. Figure 11 shows that waters of Milandre aquifer follow a plurimodal distribution, in agreement with its well karstified structure.

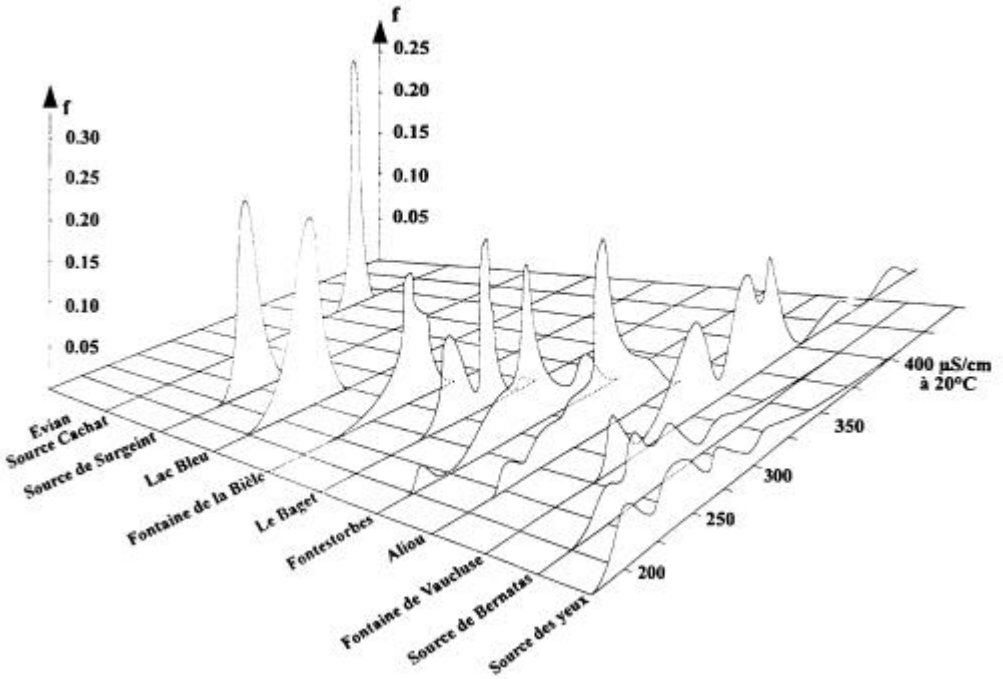

Figure 10: Frequency distribution of specific conductance for several karst systems (Bakalowicz 1979).

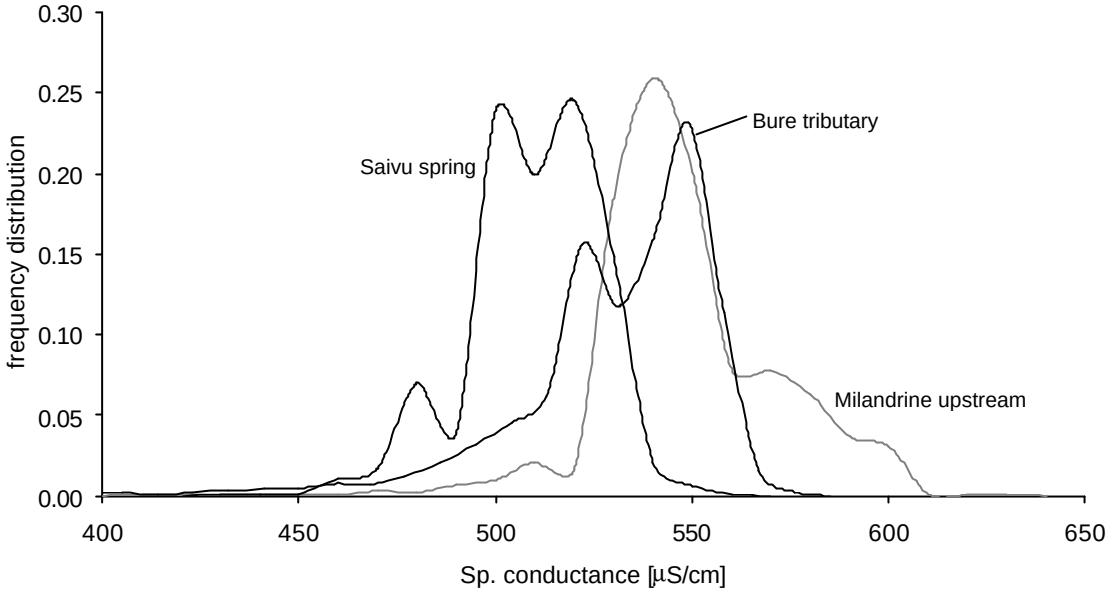

Figure 11: Frequency distribution of specific conductance for Saivu spring, Milandrine upstream (hourly data from year 1996), and Bure tributary (half hourly data from year 1999).

B.2. Coefficient of variation

Ternan (1972) showed that karst springs from the Pennine Hills (UK) can have very different hardness variations. The chosen statistical expression is the coefficient of variation (CV), that is the average concentration divided by the standard deviation. From the knowledge of the hydrogeological specificity of each system, Ternan proposed the following relation:

$CV = 35\ t^{-0.524}$

Where t is the flow through time in days. This relation seems only valid for small and well defined basins in temperate climate (White 1988). It has been applied at Milandre aquifer in chapter 2.3.

B.3. Principal component analysis (PCA)

PCA is a powerful tool for analysing the cross-correlation between a large data set of variables (the chemical parameters for instance). Technical aspects of the method can be found in Davies (1986). PCA done on karst springs data showed that most of the variance is explained by the “mineralisation” factor and by the “spatial variability of the recharge water” factor (Kiraly and Mueller 1979, Mudry and Blavoux 1986). These two factors account for at least 75 % of the total variance. A flood event can then be plotted on a graph factor 1- factor 2, and the chemical temporal evolution illustrated (figure 12) (Lastennet and Mudry 1997).

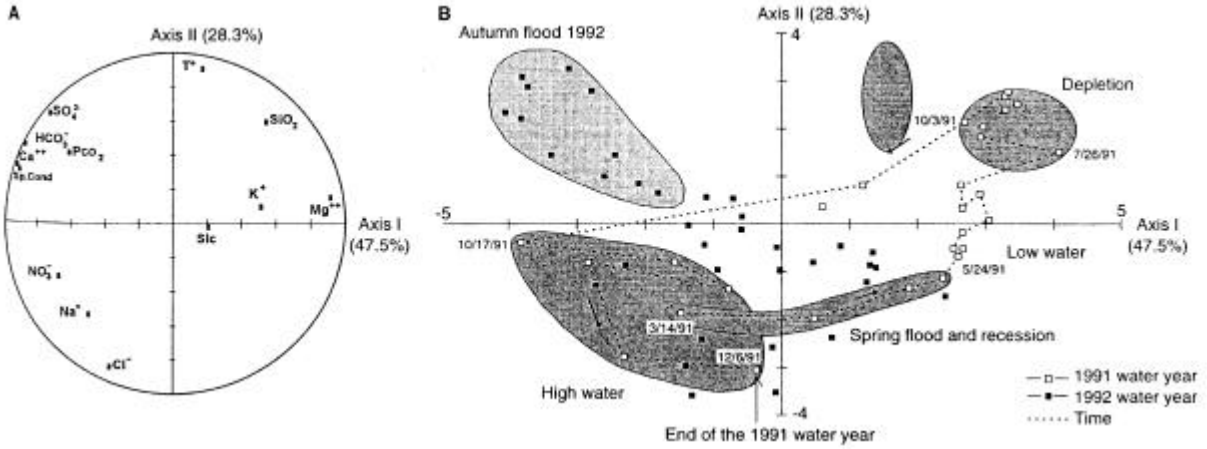

Figure 12: Temporal evolution of a flood event on the two first factors of a PCA analysis, N. D.-des-Anges karst system. A is the projection of the variables, and B of the water samples (Lastennet and Mudry 1997).

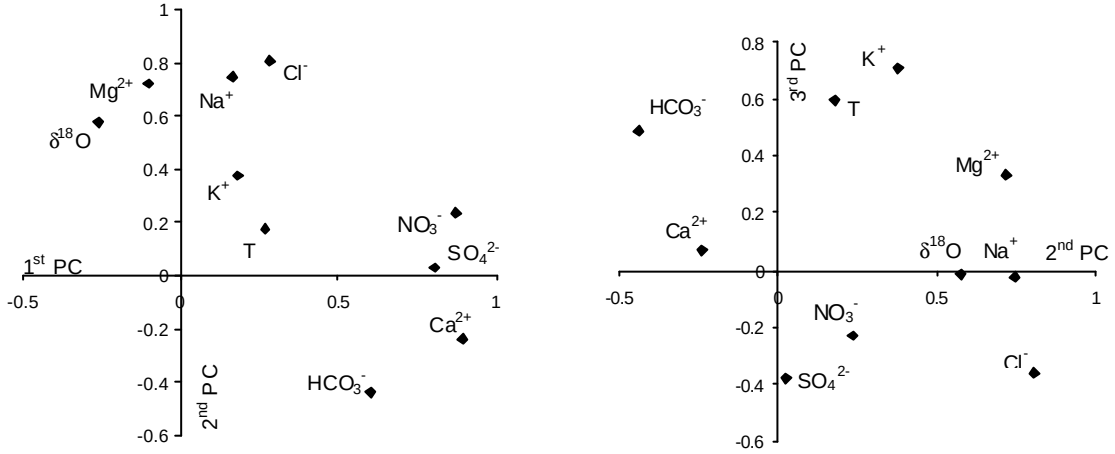

Figure 13: Results of the PCA analysis from the monthly sampling at Milandre test site (15 sampling points corresponding to tributaries of various size feeding the underground river). The number of analyses considered is 148 and only RO site has been discarded.

Figure 13 shows the PCA analysis of Milandre site sampling points plotted on the first three axes (the first accounts for 29% of the variance, the second for 25% and the third for 15%). The percentage of variance explained by the two first axes is lower than in other studies considering only one sampling point (generally the spring). The distribution of the parameters on the axes 1-2 projection do not follow a classical interpretation: in the present case, axis 1 accounts for NO_3^- – SO_4^{2-}, Ca^{2+} – HCO_3^- mainly; axis 2 for Na^+, Mg^{2+}, Cl^-, $\delta^{18}O$ and axis 3 for T, K^+. Such differences with previous studies could be caused by the prominent role of the spatial variability of the anthropogenic activities on the Milandre water chemistry.

B.4. Cross-correlation

Bakalowicz and Jusserand (1987) tried to cross-correlate the oxygen 18 stable isotope signals between the input (rain) and the output (percolation water in a cave) located 300 m below in the unsaturated zone (figure 14). Negative r-values between 0-10 weeks signify that water flow through time is more than 10 weeks. The gravity centre of the curve at 18 weeks gives a rough estimate of the mean transit time of percolation water. However part of the water takes more than 25 weeks to pass through the system as the cross-correlogram is still significantly different of 0 at that time.

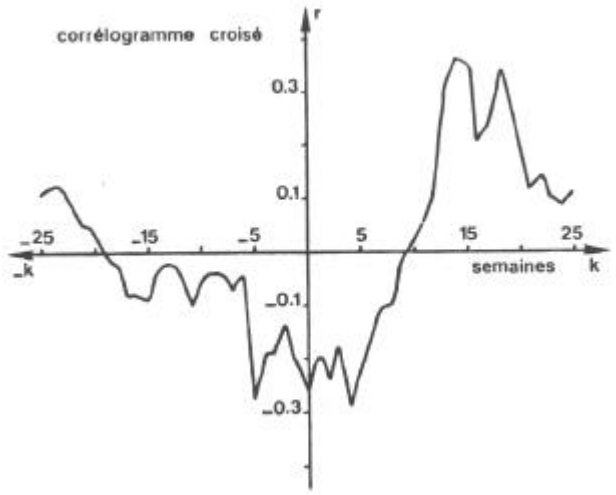

Figure 14: Cross-correlogram of oxygen-18 signal in the rain and in percolation water in a cave (Bakalowicz et Jusserand 1987).

B.5. Convolution models

When the input and output functions of a conservative tracer (e.g. stable isotopes) are known, it is possible to model the output by a convolution integral (Maloszewski et al. 1992).

$$C_{out}(t) = \int_0^{\infty} C_{in}(t-t)\,g(t)\exp(-l\,t)\,dt$$

where l is the decay constant (l= 0 for stable isotopes), and $g(t)$ is the weighting function defined for the dispersion model as:

$$g(t) = \left[Pe/(4p\,t\,/T)\right]^{0.5} \exp\left[-Pe(1-t\,/T)^2/(4t\,/T)\right]/t$$

where T is the mean transit time, and Pe (the Peclet number) is equal to 1/(D/vx).

Best fit results give the mean transit time of the system and an "artificial" dispersion parameter. The main drawback is that the model is valid under steady-state conditions only (i.e. constant volumetric flow rate through the system and constant volume of water in the system). Later, Dzikowski et al. (1995) developed a convolution model taking into account transient flow conditions.

B.6. Analysis of residuals

Grasso and Jeannin (1998) simulate the temporal evolution of the mineralisation at a spring by the following empirical relation discharge (Q) – temporary hardness (TAC):

$$TAC(t) = 225e^{-0.087Ln(Q(t))}$$

Because of the short time variability of the observed and simulated data, a moving average over 30 days is calculated for both time series. The difference between the observed and the simulated temporary hardness curves is then calculated. The resulting residual curve is analysed by a spectral analysis which allows to find some periodicity in the signal. This periodicity seems to be related to seasonal effects.

C.- Numerical and analytical modelling

C.1. Deterministic relation concentration – discharge

Grasso (1999) expresses the calcite dissolution rate as a function of discharge. This relation allows to simulate the evolution of the calcium concentration during a flood event. Results show the prominent role of the aquifer geometry (volume/surface ratio and mean flow path length) and of the saturation concentration (dependant on the temperature and the CO_2 partial pressure) on the concentration – discharge relationship (figure 15).

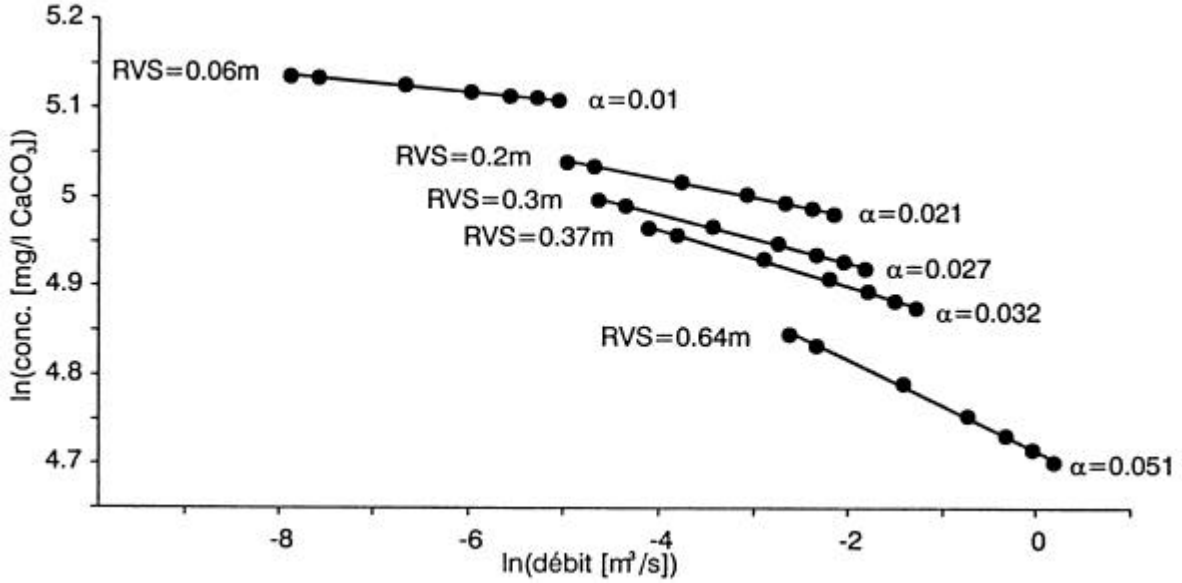

Figure 15: Relationship concentration-discharge for different modelling scenario (Grasso 1999). RVS is the ratio volume-surface of the conduit network. For a single conduit, it is the internal volume of the tube divided by the internal surface area of the tube. The slope α is directly related to the ratio RVS (volume-surface ratio) – PME (mean flow path length).

C.2. Double-continuum model with particle tracking (Sauter 1992)

A one-dimensional double-continuum model is used for simulating the hydraulics of the karst aquifer. The slope of the aquifer bottom is taken into account. Then the transport is modelled by particle tracking which is well adapted to transport simulation in advection dominated problems. Tracer input can either be a point source or spatially distributed.

C.3. Mixing models

These models aim at reproducing chemographs by the mixing of waters of different compositions. The most frequently applied model considers two end-members (Blavoux and Mudry 1983, Lakey and Krothe 1996). It is based on the conservation of the water flux and the mass flux:

$$Q = Q_b + Q_q$$

$$C\,Q = C_b\,Q_b + C_q\,Q_q$$

The validity of the model needs several assumptions: only two water types mix (Q_b as baseflow and Q_q as quickflow), their respective concentrations (C_b and C_q) stay constant throughout the flood, and pure mixing occurs (no chemical reactions). Some authors propose three end members models (Lee 1999) or even four end members models (Lee and Krothe 2001).

A mixing model has been applied to Brandt cave site in chapter 2.6.

C.4. Inverse modelling

Pinault et al. (2001a, 2001b) consider magnesium as the tracer of base flow conditions (low rate of dissolution). A representative tracer of the rapid flow component should have a concentration significantly different from its concentration in base flow conditions (i.e. its concentration in the aquifer reservoir). Depending on the considered karst systems, calcium, chloride, or sulfate have been used.

From these assumptions, the authors can calculate the transfer function of the calcium (or chloride, sulfate) and magnesium fluxes. Then the hydrogram is separated in base flow and rapid flow components by inverse modelling.

C.5. Network chemical reactors (figure 16)

Lanini et al. (2001) developed a grey box model aiming at reproducing chemographs. The hydrogeology of the system is simplified by cascading reservoirs (the epikarst, the saturated zone and a bypass source reaching directly the saturated zone). Each reservoir is a chemical reactor where each significant chemical reaction is calculated over time. Calculated chemographs are then compared to the reality, and differences should lead to a refinement of the model.

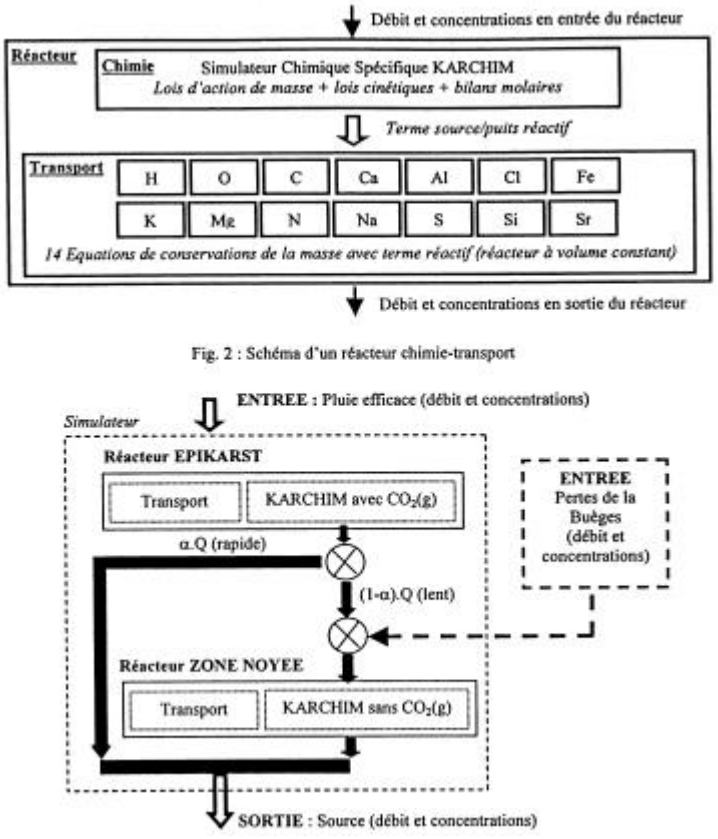

Figure 16: Schematic diagram of the network chemical reactors model developed for reproducing karst spring chemographs (Lanini et al. 2001).

C.6. Speleogenetic models

Results of lab experiments on calcite dissolution are applied for modelling cave formation. The interest of such models is to infer a mean time for a karst system development from an initial fracture network. It gives also an insight on the conduit network pattern.

Palmer (1991) and then Svensson and Dreybrodt (1992) showed the importance of the switch to a higher kinetic order in calcite dissolution for solutions close to saturation: if the dissolution rate was thoroughly linear, speleogenesis would never take place. The concept of penetration length is developed: it is the length along a fissure where dissolution is efficient. The penetration length is highly

correlated with flow velocity (controlled by fissure aperture and hydraulic head distribution) and the rate law of dissolution. As soon as turbulent flow is reached the penetration length jumps from around 100 metres to several kilometres. In the earlier stage of karstification fissures of less than 0,05 cm are calcite-saturated after a travel distance of around 20 m. The time when penetration length reaches the outflow of the system is called breakthrough time. Typical breakthrough times obtained are on the order of several 10'000 years (figure 17). From this time onwards, the principle of the positive feedback for the karst network development is enhanced: the flow is concentrated in the larger fissures (flow path determined during the penetration length phase), dissolution becomes more efficient, fissures enlarge, and more flow is again drained to this preferential flow path. Hence flow in the smaller fissures decreases through time (Jeannin 1998). This karstification process has important consequences on the structure of karst aquifers.

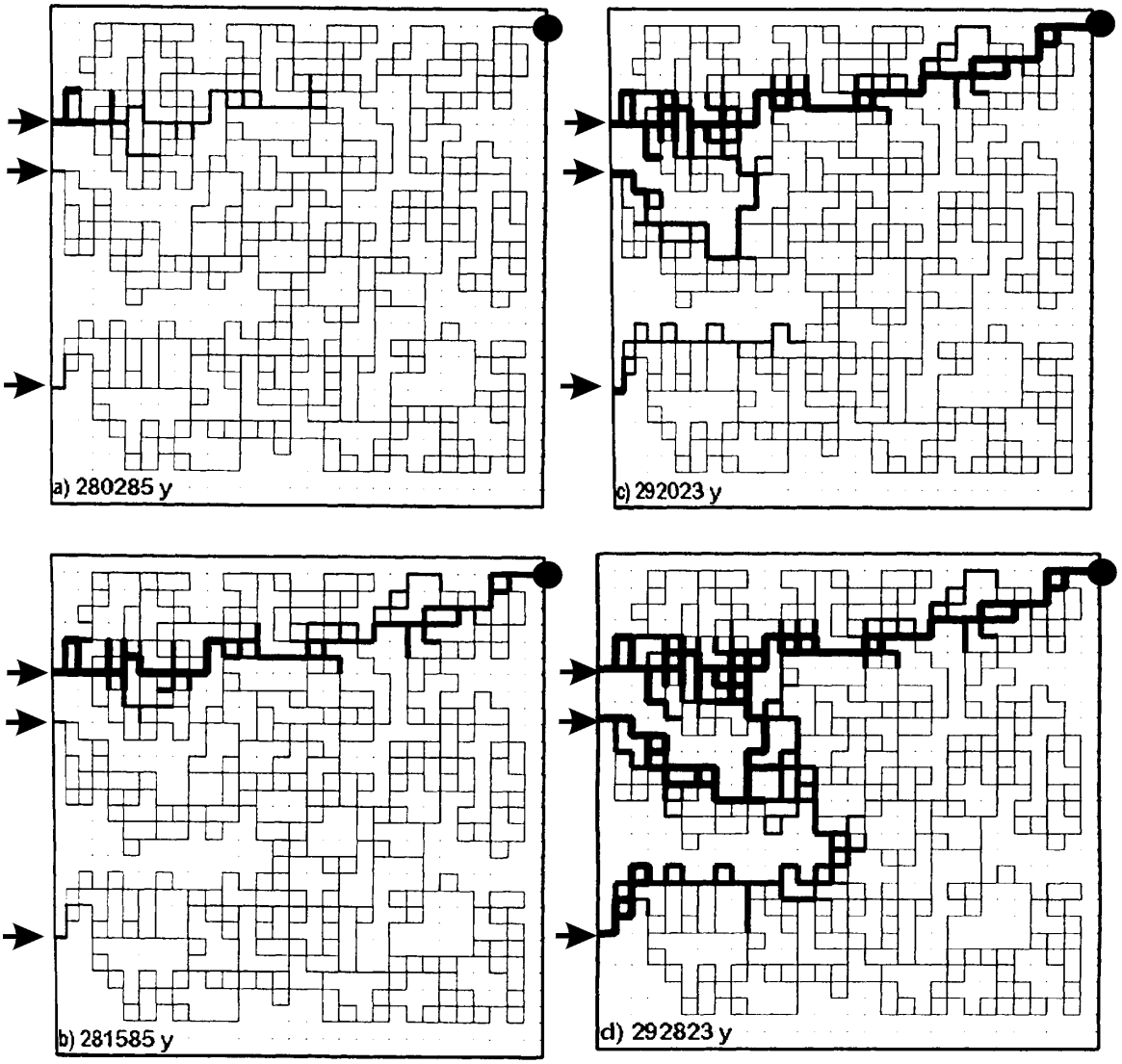

Figure 17: Simulation of the creation of a karstic network based on speleogenetic models (Dreybrodt 1997). Arrows indicate inputs, and the black circle the output.

1.4. Objectives of the study

Transport processes in karst aquifers have been studied extensively with two main objectives: 1) the use of both natural and artificial tracers to delimit the catchment areas, and 2) the inference of the aquifer structure and characteristics based on time-concentration variations (i.e. chemographs) at the outlet of the system. Our project is mainly concentrated on the latter topic and the ultimate objective is to obtain a consistent model of transport and hydraulics of our field test site. Previous studies on transport in karst aquifers have been done at two different scales: lab scale experiments which confirm theoretical models and allow more adequate models to be developed, and catchment scale studies which provide global information on the structure and the behaviour of the karst system. The link between these two approaches requires observations at an intermediate scale, within the karst system. This type of observations can be achieved in our field test sites (Milandre site mainly).

The study is limited to the observation of natural tracers. However former artificial tracing experiments are available for comparison and for completing the results (Maréchal 1994, Grétillat 1996, Doerfliger 1996, Hauns 1998, Favre 2001).

Three types of natural tracers are considered, each having their own specificities:

- **Stable isotopes** (mainly oxygen 18) are used as non reactive tracers homogeneously distributed on the whole catchment.
- **Pollution-related solutes** (nitrates, chloride, potassium) are considered as mainly non reactive tracers which are heterogeneously distributed on the catchment.
- **Dissolution-related parameters** (calcium, bicarbonate, specific conductance, hardness, total dissolved solids) represent reactive tracers relatively homogeneously distributed on the whole catchment.

In the following paragraphs, we present the main issues of the thesis, as well as previous studies and their interpretations.

1.4.1. Stable isotopes

Main issues

- What is the spatial variability of the stable water isotopes within Milandre karst aquifer under steady state flow conditions? For that, monthly sampling was done on 16 observation points (underground river, spring, tributaries, percolation water).
- How can global models, which simulate isotopic response at the spring from rainfall data, be applied to Milandre system? What is the significance of the computed mean residence time? For that, weekly samples were collected at the spring and in the rain during two years.
- To what extent is rainfall isotopic signal dampened in the unsaturated zone of the aquifer? What can we tell about the hydraulic functioning of the soil and epikarst sub-systems? For that, three flood events were sampled in details (rainfall, tributaries, underground river).

Previous studies and interpretations

The **mean elevation of the catchment area** of a spring can be calculated on the basis of the isotope composition of spring water (Dubois et al. 1993, Bakalowicz 1974, Mudry 1981). This method has to be used on karst systems only during steady state conditions in order to get a representative isotopic composition of the aquifer. Two relations are proposed in the literature for computing the elevation of a spring catchment located in the Swiss Jura:

$Z\ (m) = -367\ \delta^{18}O - 3112$ (Vuataz 1981)

$Z\ (m) = (\delta^{18}O + 8.62) / -0.0018$ (Blavoux et al. 1979)

At Saivu spring, main outflow of Milandre karst aquifer, the mean annual oxygen-18 ratio is –9.05 ‰. The catchment elevation is 210 m with the first relation, and 240 m with the second relation. In reality the mean elevation of the catchment is 500 m, hence the proposed equations are not adapted to the climate of the area (northern Jura).

Models have been developed for calculating **mean groundwater residence time** on the basis of the isotopic fluctuations at the spring and in the precipitation (Maloszewski et al. 1992; Behrens 1992, Reichert et al. 1997, Kattan 1997, Frederickson and Criss 1999). These models are black-boxes and generally consider the karst system as linear (constant volumetric flow rate). These simplifications limit the validity of the results. The most adapted approach has been proposed by Maloszewski et al. (1992) who consider two different residence times: the conduit network transit time, and the matrix porosity transit time. The first is estimated by the lag between marked stable isotopes anomalies in rainfall and at the spring, the second by a convolution integral of an advective-dispersive model. At Milandre, oxygen-18 at the spring are highly dampened compared to rainfall (chapter 2.4.)

Seepage velocity in the vadose zone can be estimated by sampling both precipitation and cave percolation waters, followed by isotopic analyses. This approach has been tested in the USA by Harmon (1979), Yonge (1985), Chapman et al. (1992), Lee et al. (1998). In Europe similar studies were carried out by Atkinson et al. (1985) and more recently by Caballero et al. (1996). At Milandre site, isotopic signals are strongly dampened at the base of the unsaturated zone, even in case of important flood event. This confirms the storage function of the epikarst.

1.4.2. Pollution-related solutes

Main issues

- What is the spatial variability of the pollution-related parameters within the Milandre aquifer? For that, monthly sampling was done on 16 observation points (underground river, spring, tributaries, percolation water).
- To what extent are spring chemographs influenced by the mixing of tributaries, respectively under steady-state and transient flow conditions? For that, three flood events were sampled at Milandrine upstream and Saivu spring, and continuous measurements of specific conductance and nitrate concentrations on the main tributaries were used.
- What is the temporal evolution of the pollution-related parameters concentrations, on a long term basis (a few years) and at the flood event scale? For that, three flood events were sampled at Milandrine upstream and Saivu spring, and a few observation points were sampled monthly during three years.
- Where do occur chemical reactions capable of modifying pollution-related parameters concentrations?

Previous studies and interpretations

Chemical reactivity of nitrogen within the aquifer shows two opposite trends: denitrification has been proven by Edmunds et al. (1983, 1984) in the Lincolnshire limestone aquifer (England) caused by strong reducing conditions. Nitrification has been illustrated in karst aquifers of the Swiss Jura (Montandon et al. 1995, Lièvre 1989): sewage waters are oxygenated in the aquifer and nitrogen is transformed into nitrates. At Milandre, the oxidation of nitrogen compounds occurs entirely in the vadose zone, although it is only around 50 m thick.

Temporal variations and mass balances of nitrates have been carried out by Dubreucq (1987) in the French Jura. Several factors influence the changes in concentration: hydraulics, seasonal cycles, agriculture.

The influence of land use is of great concern for agronomy engineers. Benoit et al. (1997a, 1997b) and Limaux et al. (1998) have studied the relations between nitrate concentrations in soils, karst spring waters and agriculture practice. At Milandre, the link between land use and groundwater quality is clearly established.

The influence of soils on the nitrate concentrations observed in karst aquifers has been investigated by Wells and Krothe (1989) and Iqbal and Krothe (1995). They showed the importance of preferential pathways through cracks and root channels leading to nitrate pulses. Feast et al. (1998) were able to prove the effective denitrification processes taking place in the glacial deposits overlying the chalk aquifer of SE England. In an opposite manner, Mühlherr et al. (1998) show the existence of nitrification processes within the unsaturated zone of limestone aquifers in the UK and the production of large amount of nitrous oxides. At Milandre, pulses of nitrates occur after fertilizers spreading and denitrification seems to be very limited. However detailed investigations on the processes occurring in the soil zone have not been carried out yet.

In order to better distinguish the participating reservoirs, attempts have been made to determine **natural tracers** from the different parts of the karst system: magnesium and sulfate are tracers of the LPV in the phreatic zone (slow dissolution kinetics), chloride and sodium tracers of the epikarst (reconcentration by evaporation) (Bakalowicz 1979, Bakalowicz et al. 1994). At Milandre test site, the influence of agriculture invalidates the used assumptions.

1.4.3. Limestone dissolution-related parameters

In the thesis, "limestone dissolution-related parameters" are often referred to as "dissolution-related parameters"

Main issues

- What is the spatial variability of the dissolution-related parameters concentrations within the Milandre karst system? What is the role of soil air pCO_2 on this variability? For that, monthly sampling was carried out on 16 observation points (underground river, spring, tributaries, percolation water). Soil air pCO_2 was measured at several locations and at different depths.
- Where occur most of the dissolution processes (epikarst, unsaturated zone, whole system), under steady state flow conditions? And under transient flow conditions? For that, three flood events were sampled in details (rainfall, tributaries, underground river). Additional data were acquired on complementary sites.
- What is the role of dissolution compared to mixing in shaping the spring chemographs during flood events? For that, three flood events were sampled in details (rainfall, tributaries, underground river) and continuous measurements of specific conductance on the main tributaries were used.

Previous studies and interpretations

Plagnes (2001) showed the existence of three main types of dissolution parameters responses (i.e. chemographs) at the spring (see paragraph 1.3.3). In the literature, two distinct models are applied to explain these variations: The first is based on the **mixing** of different types of water (Blavoux and Mudry 1983, Dreiss 1983, Williams 1983, Vervier 1990, Sauter 1992, Hess and White 1988, Plagnes 2001). The second is based on the disequilibrium between **dissolution kinetics** and flow velocity: during flood events, water flows too quickly for reaching thermodynamic equilibrium (Shuster and White 1971, Ternan 1972, Grasso 1999).

At Milandre site, the last model is not valid: generally groundwater reaches the base of the unsaturated zone in equilibrium with respect to calcium carbonate (Milandrine upstream and Saivu spring were always at 100 % ± 5 % of saturation). This model should only be used in systems with clear evidence of undersaturated water reaching the spring (e.g. recharge occurring by point infiltration).

1.5. Study areas

The main experiments were conducted on the Milandre test site located in the Swiss Jura near Porrentruy town (figure 18).

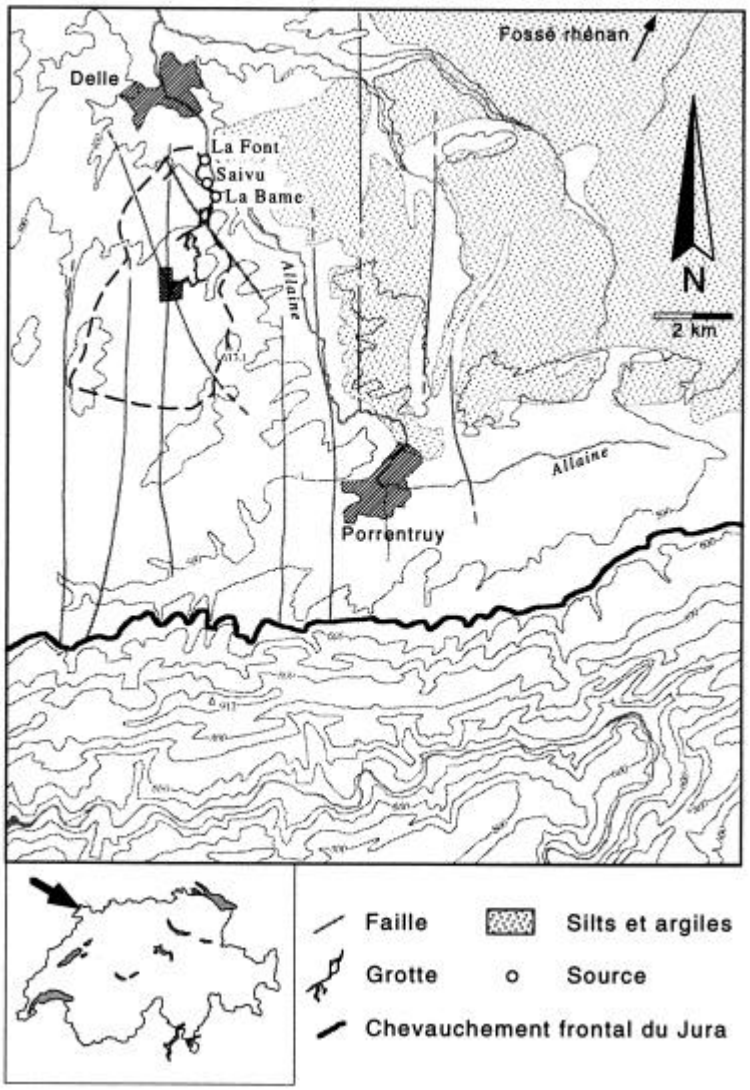

Figure 18: Geographical and geological location of the Milandre test site (from Jeannin 1998).

1.5.1. Main geological features

The area belongs structurally to the tabular Jura, which extends behind the folded Jura (Jeannin 1998). Bedding planes are subhorizontal and show the following stratigraphy (figure 19):

Quaternary deposits: 0 to 20 metres of silty loams from loess deposits during the latest glacial period. Colluvium in karstic depressions.

Upper Oxfordian (Sequanian): 30 metres of marly limestones with Astartes and Natices. This formation has been eroded on a large part of the catchment area. Below, Astartes limestones that are chalky in some places.

Middle Oxfordian (Rauracian): compact limestones with abundant corals. The thickness is between 60 and 76 metres.

Lower Oxfordian (Oxfordian s.s.): 80 to 90 metres of marls.

The horizontal bedding planes are cut by several fracture systems: the first is oriented N-S and is associated to the Rhine graben located to the north-west; the second oriented N040° to N070° and the third oriented N130° to N150° are associated to the folded Jura existing to the south.

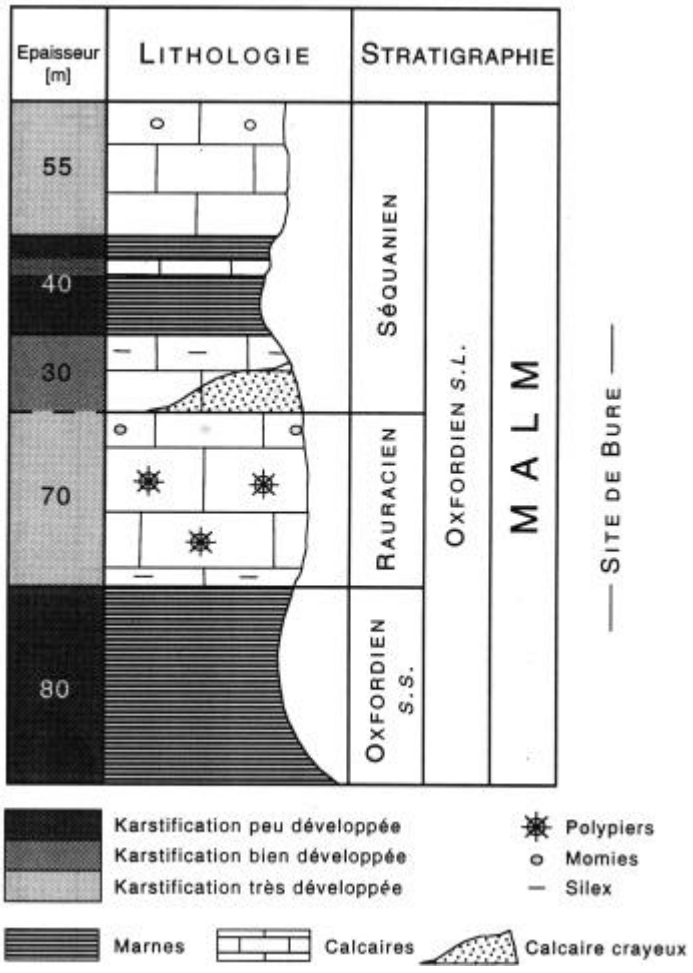

Figure 19: Synthetic stratigraphy of the study area. The Milandrine river flows around 15 m above the Oxfordian marls (from Jeannin 1998).

1.5.2. Regional hydrogeology

Numerous tracing experiments allow to delineate accurately the catchment area of the Milandre karst aquifer (figure 20). The area of 13 km^2 is constituted of Rauracian limestones covered by quaternary deposits and soils. This unit forms the main aquifer and is limited downwards by the aquiclude of the oxfordian marls. The recharge is mainly diffuse through the soil zone, as no swallow hole is present on the whole catchment.

The conduit network draining the karst aquifer is partly known by the Milandre cave system (Gigon and Wenger 1986). Water levels measured in boreholes are systematically higher than the levels in the conduits. Through time, levels can fluctuate strongly in some boreholes, whereas they can be fairly stable in others (Jeannin 1998). Infiltration is mainly diffuse through the soil zone. Flow velocities determined by tracing experiments are between 100 and 400 m/h (Favre 2001). In the conduits, velocities depend on the discharge and are between 70 and 700 m/h (Maréchal 1994). The catchment area is partly cultivated and the groundwater is contaminated by agriculture (nitrates, bacteria).

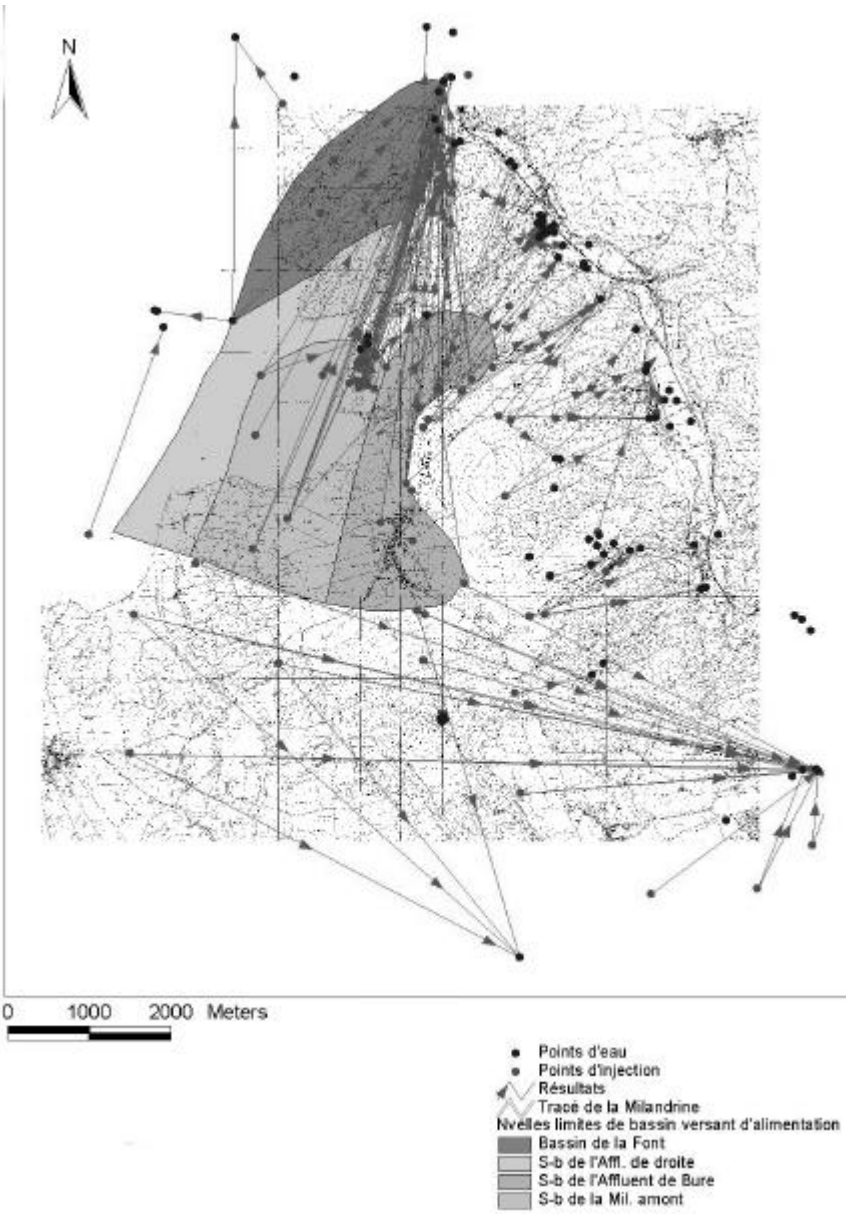

Figure 20: Map synthesising the tracing experiments carried out on the Milandre karst system. The catchment areas corresponding to the three main tributaries of the system are indicated in grey (Affluent de Droite is Droite tributary (AF), Affluent de Bure is Bure tributary (BU), Mil. amont is Milandrine upstream (AM)), (Favre, 2001).

1.5.3. The experimental site

Sampling has been carried out at several locations throughout the project: the first phase, focused on the spatial variability, necessitated sampling points all along the Milandre cave and in some boreholes. The second phase, focused on the temporal variability, was limited to the upstream part of the cave and the spring.

The following table summarises the sampling points. For each, a short description of the location is given.

Table 1: List of the sampling sites and of the measurement points used throughout the study.

	Site ID	Site name	X	Y	Z	measured parametrers
Milandrine cave	EC	base échelle	567087	257059	475	Q-K-T, ions, 18O
	SO	le robinet	567092	257104	468	Q-K-T, ions, 18O
	AM	Milandrine upstream	567093	257098	469	Q-K-T, ions, 18O
	VI	la niche	567088	257141	466	Q, ions, 18O
	EN	l'entonnoir	567100	257145	465	Q-K-T, ions, 18O
	ST	la colonne	567224	257334	458	Q, ions, 18O
	EG	l'égout	567320	257436	453	ions, 18O
	GO	drops 5m downstream EG	567323	257432	453	ions, 18O
	CA	grande cascade	567400	257443	445	ions, 18O
	BU	Bure tributary	567819	257439	425	Q-K-T, ions, 18O
	RO	source rouge	567742	257753	415	Q, ions, 18O
	RI	milandrine au niveau de FA	567716	257965	411	ions, 18O
	FA	fausse source	567716	257965	412	Q, ions, 18O
	AF	Droite tributary	567588	258622	389	ions, 18O
	DR	right bank tributary	567867	258749	385	ions, 18O
	AV	Milandrine downstream	567854	258788	385	ions, 18O
Springs	SAI	Saivu spring	567970	259700	373	Q-K-T, ions, 18O
	BAM	Bame spring	568175	259530	374	Q-K-T, ions, 18O
Meteo	Maira		567475	257600	520	rainfall
	Fahy		563300	252050	567	rainfall
Epikarst	EPI 1	Epikarst borehole	567093	256887		pCO2
	EPI 3	Epikarst borehole	567097	256890		pCO2
	EPI 4	Epikarst borehole	567089	256890		pCO2
	EPI 5	Epikarst borehole	567096	257059		pCO2
	EPI 7	Epikarst borehole	567080	257063		pCO2
Soil	CO2-1	CO2 borehole	567144	257220	517	pCO2
	CO2-2	CO2 borehole	567145	257224	517	pCO2
	CO2-4	CO2 borehole	567472	257763	530	pCO2
	CO2-5	CO2 borehole	567474	257762	530	pCO2
	CO2-6	CO2 borehole	567482	257719	528	pCO2
	CO2-7	CO2 borehole	567474	257720	528	pCO2
	CO2-8	CO2 borehole	567053	257900	515	pCO2
	CO2-9	CO2 borehole	566955	257852	523	pCO2

EC

Drops at the base of the third ladder (access to the upstream part of the cave by the Maira shaft). Collection was made by a plastic sheet fixed on the cave wall. Discharge was measured with a pluviometer (figure 21). Specific conductance and temperature were measured with a datalogger.

Figure 21: the pluviometer installed at EC is used for discharge measurement. At the outflow a conductivity-temperature probe is connected to a datalogger.

SO

Tributary located 1m above the Milandrine river, on its right bank about 10 m after the gallery has reached the river. Water was impounded and directed in a pipe of 30 m in order to measure discharge with a super-pluviometer (figure 22) (see paragraph 1.6. below).

Figure 22: SO tributary is collected into a pipe. At its end, discharge is continuously measured by a super pluviometer (grey PVC tube on the picture).

AM
Milandrine upstream. Samples were taken at the weir (figure 23) and continuous measurements of discharge, specific conductance and temperature in the upstream basin of the weir.

Figure 23: the Milandrine upstream weir at low water stage. The dark pipe behind is the SO impoundment.

VI
Drops falling in a nook located on the left bank of the underground river, approximately 50 m downstream of the AM weir. Discharge was measured with a pluviometer.

EN
Small tributary arriving at the roof of the gallery 10 m downstream of VI (and 60 m downstream of AM weir). Discharge was measured with a super-pluviometer. Specific conductance and temperature were recorded with a datalogger.

ST
Drops feeding a large speleothem (about 60 cm diameter and 3 m high) located on the right bank of the river and 165 m upstream of the confluence with EG (Gratte roche gallery). Discharge continuous measurements were made with a pluviometer.

EG
Gratte roche tributary arriving on the left bank of the Milandrine river.

GO
Drops falling from the roof (along speleothems) 5 m downstream of Gratte roche tributary (EG).

CA
Tributary flowing on the large speleothem located at the base of the “Grande Cascade”.

BU
Bure tributary. Continuous measurement of discharge, specific conductance and temperature were made in the lake created by the weir.

RO
"Source rouge", polluted tributary located on the left bank of the Milandrine river. A weir was constructed in order to measure discharge (figure 24).

Figure 24: Plastic weir constructed at RO tributary in order to measure continuously discharge with a water level probe.

FA
Small tributary arriving on the left bank of the river about 2 m higher than the river bed. Located 260 m downstream of RO. A weir was constructed in order to measure discharge.

RI
Milandrine river at FA tributary.

AF
Droite tributary.

DR
Small tributary arriving on the right bank of the river, 320 m downstream of the AF confluence.

AV
Milandrine river in the downstream part. Sampling location is the point where the river is first reached when accessing from the natural entrance of the Milandre cave system.

Other measurement points (figure 25) are the Saivu and Bâme springs (Boncourt village), pluviometric station at Maira and Fahy village (Jeannin 1998), epikarst boreholes (Thierrin 1996), and soil boreholes (Carré 2001).

Figure 25: The Saivu spring (upper left), the pluviometer near Maira village (upper right), pCO_2 measurements in an epikarst borehole (lower left), and in a soil under forest (lower right).

1.6. Measurement methods, precision and validation

1.6.1. Discharge measurements

Direct measurement of discharge was carried out by filling a container of known volume for low discharge rates, by dilution gauging or current meters for higher discharge rates.

Continuous measurements of discharge were done following three principles:

- Very low discharge rates: a pluviometer is connected to a recording station which sums the number of tilting at each time step. Each tilting corresponds to a certain volume of water.
- Low discharge rates: “super-pluviometers” were built based on former developments carried out by V. Puech (pers. comm.) It consists of a PVC tube perforated on a part of its height by small holes following a helicoidal trajectory. A pressure probe is set at the bottom of the tube for measuring the water height. The height is then converted to discharge by a rating curve.
- High discharge rates: construction of weirs allowed to install pressure probe in the upstream lake. Conversion height- discharge is done with a rating curve (appendix 1). Weirs discharge formulas are not adapted as it was impossible to obtain an upstream basin with a sufficient extension.

Accuracy of discharge measurements is on the order of 10 %.

1.6.2. In situ physico-chemical parameters measurements

Specific conductance and temperature were measured for each sample collected for a chemical analysis. WTW field conductimeters, regularly calibrated in the lab, were used. In some cases, dissolved oxygen (WTW field oxymeter) was also measured. However, groundwater was always saturated in dissolved oxygen, and measurements were not continued further.

pH was first measured in the field but, due to technical difficulties (stability of the measure and transport problems), we decided to determine pH in the lab within 12 hours after sampling. Several tests showed that this delay allows to keep a representative pH value if the water sample is kept in a tight bottle without air bubbles, and stays at sampling temperature (appendix 2).

1.6.3. Analyses of major ions

Bicarbonate was determined within 24 hours by titration with HCl 0.1 M to a pH of 4.3. Preliminary tests showed that within 24 hours, bicarbonate is well preserved if the sample is kept at constant temperature and in a tight bottle without air bubbles.

The other parameters (K^+, Na^+, Mg^{2+}, Ca^{2+}, SO_4^{2-}, Cl^-, NO_3^-) were analysed by ion chromatography (IC) after a 0.45µm filtration. For cation preservation, filtered samples were acidified to pH < 2 with HNO_3 suprapur. Nitrate concentrations in samples with or without formol were equivalent (table 2), therefore most samples were taken without it. Analyses were carried out within the month following sampling. The used IC is a Dionex model DX-120, with a column n° AS14A for anions, and n° CS12A for cations.

In some samples, traces of other solutes were detected (nitrite, organic compounds, fluorite), however no quantitative determination were made.

Table 2: nitrates analyses of samples with formol and without formol.

site	no formol	formol
BU	7.3	7.4
EG	11.7	11.8
AM	10.4	10.7
SAI	8.1	8.0
BAM	8.0	8.0
DR	5.7	5.8
CA	47.1	47.0
RO	29.4	30.8

The quality of the analyses was checked with the charge-balance error (E) calculated by:

$$E = \frac{\sum z_c m_c - \sum z_a m_a}{\sum z_c m_c + \sum z_a m_a} \cdot 100$$

where $z_{c,a}$ is the ionic valence, m_c the molality of cation species, m_a the molality of anion species. The analysis is considered as acceptable if $E \leq 5\%$. The charge-balance error is given for each analysis (appendix 3). The measured specific conductance was also compared to the calculated specific conductance according to Rodier (1978).

Accuracy and reproducibility of the measured parameters are given in the table 3.

Table 3: Major ions analyses, precision of the measure.

Parameter	**Reproducibility** [mg/l]	**Accuracy** [mg/l]
Calcium	± 0.2	± 2
Magnesium	± 0.1	± 0.5
Sodium	± 0.1	± 0.5
Potassium	± 0.1	± 0.5
Sulfate	± 0.1	± 0.5
Chloride	± 0.1	± 0.5
Nitrate	± 0.1	± 0.5
Bicarbonate*	± 5	± 10

* = analysis by titration

For most of the ions measurement uncertainties are included in the used graphical representation, i.e. points used on graphs have a size comparable to the uncertainty. This is not true for bicarbonate, but only significant variations are interpreted.

1.6.4. Analyses of stable isotopes

Water for isotope analysis was collected in 50 ml plastic bottles carefully filled and sealed in order to avoid any degassing or contamination by air. Stable isotope analyses were carried out at Hydroisotop Gmbh, Germany within six months after sampling. Isotope compositions are reported in the usual δ-scale in parts per thousand (‰):

$$d_{sample} = \left(\frac{R_{sample} - R_{SMOW}}{R_{SMOW}} \right) \cdot 10^3$$

where *R* is the ratio $^{18}O/^{16}O$ or $^{2}H/^{1}H$. Accuracy is +/- 0.15 ‰ for $^{18}O/^{16}O$ and +/- 1.5 ‰ for $^{2}H/^{1}H$.

Oxygen-18 results are synthesised in appendix 4. Regular duplicates confirmed the quality of the analyses. They are presented in appendix 5 together with analyses of deuterium. Error bars are not represented in graphs used for the interpretation (chapter 2). However, only significant variations are interpreted.

1.6.5. Continuous measurement of specific conductance and temperature

Continuous measurements of specific conductance and temperature were generally made with modified WTW probes coupled to a datalogger. In some cases, ready to use datalogger systems were installed. Regular manual measurements were taken in order to calibrate the data. Accuracy of the measurements is at around 5 %. Calibration curves for continuous measurements are given in appendix 6.

1.6.6. Air gas pCO_2 measurements

Air gas pCO_2 was measured in the soil and in Milandre cave. Details of the measurement method can be found in Carré (2001). Measurements were carried out with a CO2 analyser from Environmental Instruments (UK), model Anagas CD 98HR. Its measurement range is 0 to 40 % per volume.

Measurements were done by pumping until stable concentrations were reached. Soil gas measurements were done at different depths in boreholes equipped as follows: the 10 cm diameter hole was filled with 15 cm of gravel, and then with 30 cm of bentonite. This was repeated until the hole was filled. Into each gravel level, an aluminium tube of 6 mm internal diameter was set, and was cut to the length necessary for being 20-40 cm above ground surface at the other end. The outside end was used for a measurement at the depth corresponding to the gravel pack, and was sealed between each measurement in order to prevent possible contamination and wetting. Results are presented in appendix 7.

1.6.7. Continuous measurement of nitrates

The methodology developed during the project has been presented in the following paper published in the proceedings of the 7th Conference on Limestone Hydrology and Fissured Media.

All the recorded data are presented in appendix 8.

Continuous measurement of nitrates concentrations, lab tests and field results in a karstic aquifer.

J. Perrin, B. Wenger[1]

[1]Centre d'Hydrogéologie, Université de Neuchâtel, 11 rue E-Argand, 2007 Neuchâtel, Suisse.

Abstract

The Milandre test site is a karstic aquifer located in the tabular Jura. The observation network is particularly complete: an underground river with many tributaries, boreholes, springs, pluviometric stations. Part of the catchment area is used for an intensive agriculture with plants of tobacco, maize and cereals. Scattered water sampling within the karstic system gave a first insight on the spatial variability in nitrates concentrations. These results encouraged to develop a system for continuous recording of nitrates concentrations with the objective to test the response of this parameter to hydrodynamic pulses.

An electrochemical-measuring device was assumed to be the most appropriate: the system is made of a nitrate selective electrode, a reference electrode and an ionometer combined with a datalogger. The different available electrodes have been tested in the lab first in order to optimise continuous measurements in the field. Nevertheless some unexpected technical problems had to be solved for getting the first convincing results.

Résumé

Le site de Milandre situé dans le Jura tabulaire est un aquifère karstique comportant de nombreux points d'observation :rivière souterraine et affluents, forages, sources, stations pluviométriques. De plus, une partie du bassin d'alimentation est utilisée pour une pratique intensive de l'agriculture : tabac, céréales et maïs. Des prélèvements ponctuels d'échantillons d'eau dans le système karstique ont mis en évidence la variabilité spatiale des concentrations en nitrates. Ce constat a encouragé le développement d'un appareillage de mesure in situ et en continu des concentrations en nitrates afin de caractériser la réponse de ce paramètre à des événements hydrodynamiques.

Un système de mesure par électrochimie s'est avéré le plus approprié : Le dispositif comprend une électrode spécifique nitrates, une électrode de référence et un ionomètre couplé à un datalogger. Différentes électrodes disponibles sur le marché ont été testées en laboratoire dans le but d'optimiser la mesure en continu sur le terrain. Pourtant quelques problèmes techniques inattendus ont nécessité quelques aménagements afin d'obtenir les premiers résultats fiables.

Introduction

Karstic aquifers show rapid change in water chemistry during flood events because of their highly transmissive structure (FORD & WILLIAMS 1996). This behaviour encourages continuous measurement of chemical parameters in order to get a realistic image of the temporal variability of the chemistry. Such observations were already encouraged by MUELLER (1976). However only a few studies were carried out afterwards: MUELLER *et al.* (1982) recorded sodium on the Areuse karstic spring. WACKER & WITTWER (1982) published also sodium continuous measurement on the Orbe resurgence. DUCLUZAUX (1999) used a iodide specific electrode for several tracing experiments and for studying the natural variations of this parameter.

The karstic aquifer studied at CHYN for the last decade is located in a cultivated area; nitrates concentrations at the spring are on the order of 25 mg/l and are known to change during the year (PERRIN *et al.* 2000). Thus it has been decided to follow the nitrate parameter during flood events in different parts of the aquifer. The most appropriate device appeared to be a nitrate selective electrode combined with a datalogger. This paper focuses on theoretical and practical aspects of this measurement and gives an example of obtained data. This project is still ongoing and more results will be published in the near future.

Methodology

Theoretical background

A typical device for ion-selective measurements is made of a working electrode containing an ion-selective membrane and a reference electrode (Fig. 1) (RUNDLE, 2000). Although one can find combined electrode on the market, half-cells are preferred to improve flexibility. Nitrate ion-selective electrodes (ISE's) sensitive part is a PVC membrane containing ion carriers that form a potential difference by complexation of nitrate ions. On the other side of the cell, the reference electrode provides a stable potential. Since the KCl solution used in most reference electrode is slowly introduced in the sample, we use a double junction filled with NaH_2PO_4 0.1M to avoid the interference of chloride ions with the ion-selective membrane. Different approaches may be used to measure the concentration with an ISE. The simplest way is to measure the potential directly and deduce the concentration from a calibration graph. This method is straightforward but does not consider the difference in ionic strength, a drift in electrode potential or contamination of the selective membrane between the measurement and the calibration. In this regard, it is preferable to use

the known-addition method and an ionic strength adjustment buffer (ISAB) in laboratory measurements. Nevertheless these methods are not convenient for continuous field analysis.

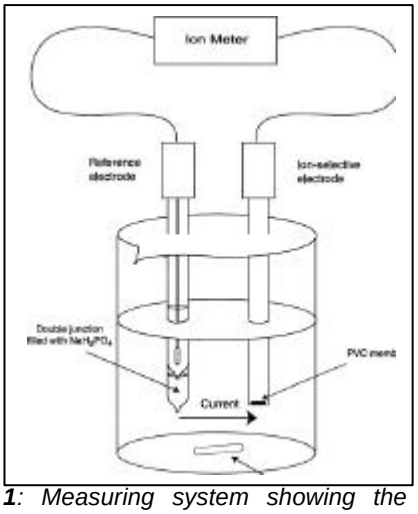

Fig. 1*: Measuring system showing the reference electrode with a double junction for avoiding chloride contamination in the water, the selective electrode with its PVC membrane sensitive to nitrates and the measuring device.*

Laboratory tests

A main difficulty in direct potentiometry measurements is to obtain a representative calibration graph. Theoretically, the slope of a pX vs. potential curve is given by the term 2.303RT/nF in the Nernst equation. At 25 °C the slope should be therefore 59 mV per decade. However values between 50 and 60 mV/decade are encountered depending on the temperature, the conduction across the ion-selective membrane and the deviation from the ideal behaviour. A calibration achieved with deionised water may therefore lead to an error of several mg/l if the sample contains a high concentration of ionic species (Fig. 2). One way to optimise the calibration is to use water with similar chemical composition as standards. In karst waters, the ionic strength is mainly determined by the dissolution of calcium carbonate, and the best calibrations were obtained with water having similar chemical characteristics. Use of electrodes from different brands leads to different calibration graphs and none is interchangeable. It is therefore recommended to use the same set ISE/reference electrode in the field as in the lab for calibration. In the laboratory the standards were weakly swirled during the measurement. No ISAB was used and potentials were measured directly. Between each measurement, the electrodes were rinsed with a jet of deionised water, then soaked for 30 seconds in the same media. The value stabilised after less than 30 seconds. Standard solutions containing 0.5, 5, 50 and 100 mg/l of nitrates were used with deionised water and 6.5, 11, 56 and 106 mg/l with karstic water.

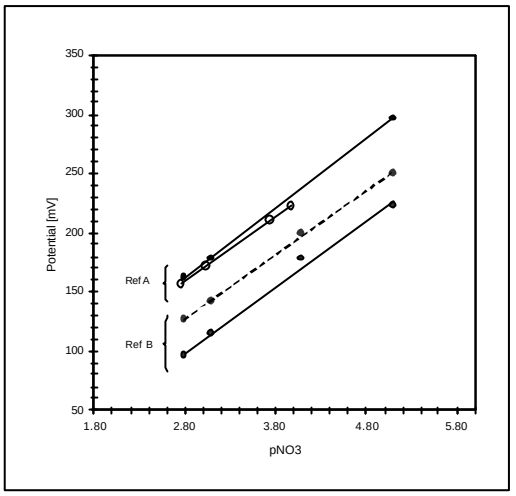

Fig. 2: Calibration graphs. Full line: ISE Metrohm NO_3, dashed line: ISE Orion 93-07. Ref A: Radiometer REF251, Ref B: Radiometer REF451. ● deionised water . ○: karstic water.

Application in the field

The first site chosen for continuous measurement has been the upstream part of the underground river. The reasons were: a stable air and water temperature throughout the year, a good protection against vandalism, known important variations on nitrates concentrations (from 20 to more than 100 mg/l) and parallel measurement of discharge and water conductivity. The site is illustrated in Fig. 3 where a conceptual model of the infiltration zone is also proposed. The measured water is a mixing of direct infiltration from the surface through drains and stored waters issued from the soil, the epikarst and the low permeability volume of the aquifer. The proportion of each component of the flow changes during storm pulses.

Measurement device

The setup of the measurement device is given in Fig. 3. The electrodes are fixed on a wood floater in order to avoid drowning during floods: the changes in water levels in the conduit are represented by Δh, which is about 80 cm. The floater is protected by a PVC tube with small circular perforations allowing water renewal. The role of this tube is also to break partly the turbulence of the flow during floods. A rod in the middle of the tube guides the floater and avoids clamping. On both end a stop limits the movement of the floater. The PVC tube is firmly fixed to the wall. On the top a waterproof box contains the ionometer and the datalogger.

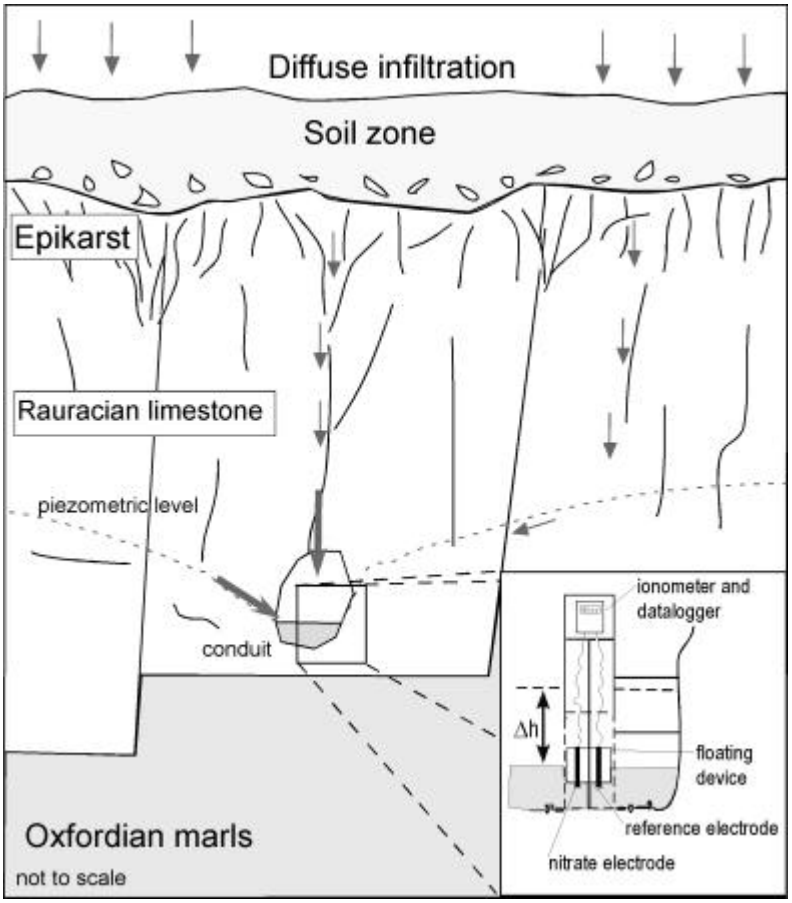

***Fig. 3**: Field location of the nitrates continuous measuring system. The river of the Milandrine upstream is about 40 metres underground and is fed by diffuse infiltration from the upper zone of the catchment area. The measurement system is installed in the conduit surrounding the river, which is never completely flooded. The variation in water levels is about 80 cm.*

First results

Differences in calibration slopes between lab and field measurements were observed due to water temperature decrease and presence of suspended load. Moreover preliminary field data showed an important potential drift. Therefore calibration curves obtained in the lab could not be used for determining the nitrates concentrations. It was decided to install an automatic sampler (ISCO 6700) in order to adjust potentiometric measures with samples analysed in the lab. These samples were taken every 12 hours and analysed on a Dionex DX 500 Ion chromatography system (IC).

As an example, the recording of nitrates between the 1st and the 13th of March 2001 is represented in Fig. 4. The interval between two measurements is 15 minutes for nitrates and 30 minutes for discharge. The validity of the continuous measurement of nitrates is confirmed by samples analysed by IC. It is interesting to see the progressive drift of the continuous measurement, which starts just after the first flood event. Two main causes can explain this deviation:

a) Accumulation of particles such as sediments, biofilms, bacteria in the vicinity of the membrane leads to changes in the equilibrium between the free and the adsorbed species.
b) Refilling holes of the reference electrode must stay open in order to ensure a continuous flow through the junctions. During flood events, river water infiltrates into the inner compartments and causes dilution of the reference solution.

The observed drift is more likely due to the dilution effect since it started after the first flood event and the decrease in chloride concentration leads to a lower potential difference (and an overstatement of the nitrates amount).

The discharge data indicates the strong correlation between storm pulses and concentration decreases by dilution effect. This dilution is generally retarded compared to discharge. The recovery of the pre-event concentration is never complete.

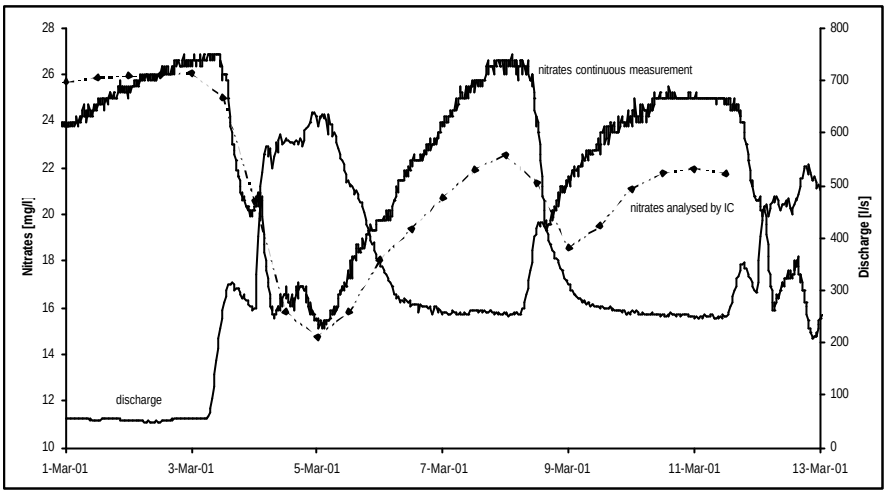

***Fig. 4**: Continuous measurement of nitrates obtained on Milandrine upstream. The raw data of the continuous measurement in mV has been converted in mg/l with the calibration curve determined in the lab. The curve with dots is interpolated from nitrates analyses done by IC. Comparison between this curve and the continuous recording gives an insight on the drift. The third curve gives the discharge measured beside. It is clear that nitrates are diluted during each storm pulses.*

Maintenance of the measurement setup

A regular maintenance of the electrodes is necessary: refilling of the reference electrode and cleaning of the sensing parts. In this regard an epoxy body reference electrode would be more appropriate than a breakable glass body. To avoid dilution of the inner solutions, the use of a gas permeable plug is highly recommended.

The saturated humidity in the cave atmosphere is a threatening parameter for the electronics. A solution is to install the ionometer and the datalogger in a protective box together with silicagel, which has to be renewed on a regular basis.

Conclusions and further work

The setup of the nitrates continuous measurement station took more time than foreseen, since various problems appeared due to the cave environment (humidity, water levels during flood) and to the material (fragile electrodes, datalogger and autosampler failures). However, these preliminary difficulties have been solved and the first results are promising. Continuous recording of chemical parameters offers several advantages:

- Work as a remote operating system.
- Flexibility: different chemical parameters can be measured at the same time.
- Low cost of the installation: prices are on the order of 650 € for an ionometer, between 200 and 500 € for a datalogger, 130-200 € for the reference electrode and between 200 and 500 € for the specific electrode. The total averages around 1600 € including material for the field installation.

In the near future, it is planned to install complementary stations on other sites within the aquifer. The results should give an interesting insight on the dynamic behaviour of nitrates.

More generally, continuous measurement of chemical parameters appears to be a very useful tool for karstic aquifer investigations and this method has to be recommended.

Acknowledgements

This project is supported by the Swiss National Science Foundation, Grant n° 20-61717.00. We are indebted to the Jura caving club, who gave us the permission to install the measurement device and let us full access to this part of the cave. At CHYN, F. Bourret, S. Cattin and T. Ettlin gave us a priceless support for the field and the lab work.

References

DUCLUZAUX, B. 1999: Mesure en continu et in situ des traceurs pour les traçages artificiels et naturels. *Published on the web: www.traceauto.com/article-1.htm.*

FORD, D. & WILLIAMS, P. 1996. Karst geomorphology and hydrology. Chapman & Hall Ed.

MUELLER, I. 1976. L'importance d'un dispositif, in situ et en continu, pour l'observation des paramètres physiques et chimiques dans les sources karstiques. *2ème Colloque d'Hydrologie en Pays calcaire, Besançon: 317-320*.

MUELLER, I., SCHOTTERER, U. & SIEGENTHALER, U. 1982. Etude des caractéristiques structurales et hydrodynamiques des aquifères karstiques par leurs réponses naturelles et provoquées. *Eclogae geol. Helv. 75/1: 65-75.*

PERRIN, J., JEANNIN, P-Y. & ZWAHLEN, F. 2000. Spatial variability of groundwater chemistry within a karst aquifer (Milandre test site, Swiss Jura). *Proceedings of New trends in karst studies, Marmaris, Sept. 2000.*

WACKER, C. & WITTWER, C. 1982. Approche hydrogéologique de la résurgence de l'Orbe. *Actes 7ème Congrès nat. Spéléologie, Schwytz: 239-248.*

RUNDLE, C. C. 2000. A Beginners Guide to Ion-Selective Electrode Measurements. *Published on the web: www.nico2000.net.*

1.7. References

Atkinson, T.C., Hess, J.W. and Harmon, R.S., 1985. Stable isotope variations in recharge to a karstic aquifer, Yorkshire dales, England. Annales de la Société Géologique de Belgique, 108: 225.

Bakalowicz, M., 1979. Contribution de la géochimie des eaux à la connaissance de l'aquifère karstique, Pierre et Marie Curie, Paris, 257 pp.

Bakalowicz, M. and Aminot, A., 1974. Géochimie des eaux d'aquifères karstiques: premiers résultats obtenus sur le système karstique du Baget durant le cycle hydrologique 1983. Annales de Spéléologie, 29(4): 484-493.

Bakalowicz, M., Blavoux, B. and Mangin, A., 1974. Apports du traçage isotopique naturel à la connaissance du fonctionnement d'un système karstique - teneurs en oxygène 18 de trois systèmes des Pyrénées, France. Journal of Hydrology, 23: 141-158.

Bakalowicz, M., Crochet, P., D'Hulst, D., Mangin, A., Marsaud, B., Ricard, J. and Rouch, R. 1994. High discharge pumping in a vertical cave: fundamental and applied results. In: N. Crampon and M. Bakalowicz (Editor), Basic and applied hydrogeological research in French karstic areas. COST 65 action., Montpellier-Millau., pp. 93-110.

Bakalowicz, M. and Jusserand, C., 1987. Etude de l'infiltration en milieu karstique par les méthodes géochimiques et isotopiques. Cas de la grotte de Niaux (Ariège, France). Bulletin d'Hydrogéologie, Neuchâtel, 7: 265-283.

Behrens, H. et al., 1992. Investigations with natural and artificial tracers in the karst aquifer of the Lurbach system (Peggau-Tanneben-Semriach, Austria). Steir. Beitr. z. Hydrogeologie, Graz, 43: 9-158.

Benoît, M., Deffontaines J.-P., Gras, F., Bienaimé, E., Riela- Cosserat R., 1997. Agriculture et qualité de l'eau, une approche interdisciplinaire de la pollution par les nitrates d'un bassin d'alimentation. Cahiers Agricultures(6): 97-105.

Benoît, M., Bonneau, M., Dambrine, E., 1997. Influence du sol et de sa mise en valeur sur la qualité des eaux infiltrées et superficielles. L'Eurobiologiste, 31(230): 53-58.

Blavoux, B., Burger, A., Chauve, P., Mudry, J. 1979. Utilisation des isotopes du milieu à la prospection hydrogéologique de la chaîne karstique du Jura. Rev. géol. dynamique et géogr. physique, 21 : 295-306.

Blavoux, B. and Mudry, J., 1983. Décomposition chimique des hydrogrammes du karst. Hydrogéologie-Géologie de l'Ingénieur, 4: 270-278.

Caballero, E., Jimenez de Cisneros, C. and Reyes, E., 1996. A stable isotope study of cave seepage waters. Applied Geochemistry, 11(4): 583-587.

Carré, G., 2001. Mesures du CO_2 dans l'air de la zone non-saturée, site de Milandre. Rapport de stage, Centre d'Hydrogéologie, unpublished.

Chapman, J.B., Ingraham, N.L., Hess, J.W., 1992. Isotopic investigation of infiltration and unsaturated zone flow processes at Carlsbad Cavern, New Mexico. Journal of Hydrology, 133: 343-363.

Davies, J.C., 1986. Statistics and data analysis in Geology, New-York, 646 pp.

Doerfliger, N., 1996. Advances in karst groundwater protection strategy using artificial tracer tests analysis and multiattribute vulnerability mapping (EPIK method). PhD thesis, Neuchâtel Unversity: 308 p.

Doerfliger, N., Jeannin, P.-Y. and Zwahlen, F., 1999. Water vulnerability assessment in karst environments: a new method of defining protection areas using a multi-attribute approach and GIS tools (EPIK method). Environmental Geology, 39(2): 165-176.

Dreiss, S.J., 1989. Regional scale transport in a karst aquifer: 1. Component separation of spring flow hydrographs. Water Resources Research, 25(1): 117-125.

Dreybrodt, W., 1988. Processes in karst Systems. Physical Environment. Springer Verlag, 288 pp.

Dreybrodt, W., 1996. Principles of early development of karst conduits under natural and man-made conditions revealed by mathematical analysis of numerical models. Water Resources Research, 32(9): 2923-2935.

Drogue, C., 1971. Coefficient d'infiltration ou infiltration efficace, sur les roches calcaires, Actes colloque d'hydrologie en pays calcaire, Besançon, pp. 121-131.

Dubois, J.-D., Mazor, E., Jaffé, F. and Bianchetti, G., 1993. Hydrochimie et géothermie de la région de Saillon. Bulletin d'Hydrogéologie, 12: 71-85.

Dubreucq, F., 1987. Le chimisme des eaux de la Cuisance en amont d'Arbois (Jura) : influence du karst, des sols et de l'activité humaine. Mémoires n°3, 156 pp.

Dzikowski, M., Delay, F., Sauty, J.-P., Crampon, N. and De Marsily, G., 1995. Convolution à débit variable à partir des réponses de traçages artificiels; application à un système karstique (Causse de Gramat, France). Journal of Hydrology, 61: 305-324.

Edmunds, W.M. and Walton, N.R.G., 1983. The Lincolnshire Limestone - Hydrochemical evolution over a ten years period. Journal of Hydrology(61): 201-211.

Edmunds, W., Miles, D.M., Cook, J.M., 1984. A comparative study of sequential redox processes in three British aquifers. In: E. Erikson (Editor), Hydrochemical balances of fresh water systems, pp. 55-77.

Eisenlohr, L., Bouzelboudjen, M., Kiraly, L. and Rossier, Y., 1997a. Numerical simulation as a tool for checking the interpretation of karst springs hydrographs. Journal of Hydrology, 202: 306-315.

Eisenlohr, L., Bouzelboudjen, M., Kiraly, L. and Rossier, Y., 1997b. Numerical versus statistical modelling of natural response of karst hydrogeological system. Journal of Hydrology, 202: 244-262.

Evans, C. and Davies, T.D., 1998. Causes of concentration/discharge hysteresis and its potential as a tool for analysis of episode hydrochemistry. Water Resources Research, 34(1): 129-137.

Favre, I., 2001. Base de données des essais de traçage du plateau karstique de Bure, SIG, interprétations statistiques. MSc diploma thesis CHYN, unpublished, 62 p.

Feast, N.A., Hiscock, K.M., Dennis, P.F., Andrews, J.N., 1998. Nitrogen isotope hydrochemistry and denitrification within the Chalk aquifer system of north Norfolk, UK. Journal of Hydrology, 211: 233-252.

Field, M., 1999. A lexicon of cave and karst terminology with special reference to environmental karst hydrology. United States Environmental Protection Agency, 201 pp.

Frederickson, G.C. and Criss, R.E., 1999. Isotope hydrology and residence times of the unimpounded Meramec River basin, Missouri. Chemical Geology, 157(3-4): 303-317.

Gigon, R. and Wenger, R. 1986. Inventaire spéléologique de la Suisse, 2: canton du Jura. Comm. Spéléo. Soc. Helv. Sc. Nat., Porrentruy: 291 pp.

Gouisset, Y., 1981. Le karst superficiel: genèse, hydrodynamique et caractéristiques hydrauliques., Univ. des Sciences et techniques du Languedoc, France, Montpellier, 218 pp.

Grasso, D.A., 1999. Interprétation des réponses hydrauliques et chimiques des sources karstiques., PhD thesis, Neuchâtel, 135 pp.

Grasso, D.A. and Jeannin, P-Y., 1998. Statistical approach to the impact of climatic variations on karst spring chemical response. Bulletin d'Hydrogéologie.-Special issue Modelling in Karst systems., 16: 59-76.

Grétillat, P.-A., 1996. Les aquifères karstiques et poreux de l'Ajoie (Jura, Suisse), PhD thesis, Neuchâtel, 209 pp.

Gunn, J., 1981. Hydrological processes in karst depressions. Zeit. Geomorph. NF, 25: 313-331.

Harmon, R.S., 1979. An isotopic study of groundwater seepage in the Central Kentucky karst. Water Resources Research, 15(2): 476-480.

Hauns, M., Jeannin, P.-Y. and Hermann, F., 1998. Tracer transport in karst underground rivers: tailing effect and channel geometry. Bulletin d'Hydrogéologie : special issue on modelling in karst systems,, 16: 123-144.

Hess, J.W. and White, W.B., 1988. Storm response of the karstic carbonate aquifer of southcentral Kentucky. Journal of Hydrology, 99: 235-252.

Hobbs, S.L. and Smart, P.L., 1986. Charaterisation of carbonate aquifers: a conceptual base, 9th International Congress of Speleology, Barcelona.

Iqbal, M.Z. and Krothe, N.C., 1995. Infiltration mechanisms related to agricultural waste transport through the soil mantle to karst aquifers of southern Indiana, USA. Journal of Hydrology(164): 171-192.

Jeannin, P.-Y., 1998. Structure et comportement hydraulique des aquifères karstiques, PhD thesis, Neuchâtel, 237 pp.

Kattan, Z., 1997. Environmental isotope study of the major karst springs in Damascus limestone aquifer systems; case of the Figeh and Barada springs. Journal of Hydrology, 193: 161-182.

Kiraly, L., 1975. Rapport sur l'état actuel des connaissances dans le domaine des caractères physiques des roches karstiques. In: A. Burger and L. Dubertet (Editors), Hydrogeology of karstic terrains. International Union of Geological Sciences, pp. 53-67.

Kiraly, L., 1988. Large scale 3-D groundwater flow modelling in highly heterogeneous geologic medium. In: E. Custodio (Editor), Groundwater flow and quality modelling. NATO ASI series 224, pp. 761-775.

Kiraly, L., 1998. Modelling karst aquifers by the combined discrete channel and continuum approach. Bulletin d'Hydrogéologie, 16: 77-98.

Kiraly, L., Mueller, I., 1979. Hétérogénéité de la perméabilité et de l'alimentation dans le karst : effet sur la variation du chimisme des sources karstiques. Bulletin du Centre d'Hydrogéologie, 3: 237-285.

Klimchouk, A., 1997. The nature and principal characteristics of epikarst. In: P.-Y. Jeannin (Editor), 12th International Congress of Speleology, La Chaux-de-Fonds, pp. 306.

Klimchouk, A.B., 2000. The formation of Epikarst and Its role in Vadose Speleogenesis. In: A.B. Klimchouk, D.C. Ford, A.N. Palmer and W. Dreybrodt (Editors), Speleogenesis. Evolution of Karst Aquifers. National Speleological Society, pp. 91-99.

Lakey, B. and Krothe, N.C., 1996. Stable isotopic variation of storm discharge from a perennial karst spring, Indiana. Water Resources Research, 32(3): 721-731.

Lanini, S., Ladouche, B., Doerfliger, N. and Bakalowicz, M., 2001. Développement d'une modélisation hydrogéochimique d'un système karstique de l'Hérault (France) selon l'approche des réacteurs

chimiques en réseau. In: J. Mudry and F. Zwahlen (Editors), 7th Conference on Limestone Hydrology and Fissured Media. Franche-Comté University, Besançon, pp. 225-228.

Lastennet, R. and Mudry, J., 1997. Role of karstification and rainfall in the behavior of a heterogeneous karst system. Environmental Geology, 32(2): 114-123.

Lee, E.S., Krothe, N.C. and Anonymous, 1998. Chemical and isotopic characterization of epikarstic water; a major water storage component of a karst aquifer in south-central Indiana, Geological Society of America, 1998 annual meeting, 30(7): 321-322.

Lee, E.S., 1999. Hydrological investigation in south central Indiana, USA: delineating flow systems and mixing problems using major ions, water isotopes, and solute isotopes as tracers, PhD thesis, Indiana University.

Lee, E.S. and Krother, N.C., 2001. A four-component mixing model for water in a karst terrain in south-central Indiana; USA. Using solute concentration and stable isotopes as tracers. Chemical Geology, 179: 129-143.

Lièvre, A., 1989. Evolution de la qualité chimique de la source karstique du Betteraz à Porrentruy. Gaz-Eaux-Eaux usées(69): 5-14.

Limaux, F., 1998. Le devenir des fertilisants azotés: utilisation par la plante, immobilisation, lixiviation et pertes par voies gazeuses. Comptes rendus de l'académie d'agriculture de France, 84(5): 95-114.

Maloszewski, P., Rauert, W., Trimborn, P., Herrmann, A., Rau, R, 1992. Isotope hydrological study of mean transit times in an alpine basin (Wimbachtal, Germany). Journal of Hydrology, 140: 343-360.

Mangin, A., 1975. Contribution à l'étude hydrodynamique des aquifères karstiques. Thèse Univ. Dijon. Annales de spéléologie, 29/3: 283-332, 29/4: 495-601, 30/1: 21-124.

Mayer, J., 1999. Spatial and temporal variation of groundwater chemistry in Petitjohns cave, Northwest Georgia, USA. Journal of Cave and Karst studies, 61(3): 131-138.

Mazor, E., 1991. Applied chemical and isotopic groundwater hydrology. Open University Press, UK: 274 pp.

Montandon, P.-E., Mages, J-F., Miserez, J-J., 1995. Etude de l'écoulement et de l'autoépuration du système karstique : exemple de la vallée de la Ronde. Bulletin d'Hydrogéologie, 14: 177-198.

Maréchal, J.-C., 1994. Etude et modélisation de l'hydraulique et du transport dans les drains karstiques, MSc thesis, Neuchatel, 128 pp.

Mudry, J., 1981. Sur l'origine des gradients de teneurs isotopiques et géochimiques dans les eaux karstiques du Jura (France). Journal of Hydrology, 50: 167-178.

Mudry, J., 1990. Les courbes flux chimique-débit et le fonctionnement des aquifères karstiques. Journal of Hydrology, 120: 283-294.

Mudry, J. and Blavoux, B., 1986. Utilisation de l'analyse en composantes principales pour l'étude du fonctionnement hydrocinématique de trois aquifères karstiques du Sud-Est de la France. Hydrogéologie.(1): 53-59.

Mühlherr, I.H. and Hiscock, K.M., 1998. Nitrous oxide production and consumption in British limestone aquifers. Journal of Hydrology, 211: 126-139.

Palmer, A. 1991. The origin and morphology of limestone caves. Geol. Soc. of America Bull., 103: 1-21.

Perrin J., Jeannin P.-Y., Zwahlen F., 2000. Spatial variability of groundwater chemistry within a karst aquifer (Milandre test site, Swiss Jura).In Karst 2000: New trends in karst studies, Marmaris Turkey.

Pinault, J.-L., Ladouche, B., Doerfliger, N., Bakalowicz, M., 2001a. Modélisation inverse des relations pluie-débits et des chimiogrammes. In: J. Mudry and F. Zwahlen (Editors), 7th Conference on Limestone Hydrology and Fissured Media. Franche-Comté University, Besançon, pp. 289-292.

Pinault, J.-L., Plagnes, V., Aquilina, L., Bakalowicz, M., 2001b. Inverse modeling of the hydrochemical behavior of hydrosystems : Characterization of karst system functioning. Water resources research, vol. 37, n°8, pp. 2191-2204.

Plagnes, V., 2000. Structure et fonctionnement des aquifères karstiques. Caractérisation par la géochimie des eaux. Documents du BRGM, 294. BRGM, 352 pp.

Plagnes, V. and Bakalowicz, M., 2001. May it propose a unique interpretation for karstic spring chemographs? In: J. Mudry and F. Zwahlen (Editors), 7th Conference on Limestone Hydrology and Fissured Media. Franche-Comté University, Besançon, pp. 293-298.

Puech, V. 1996. Etude préliminaire à une classification des zones épikarstiques en fonction de leurs propriétés hydrauliques. MSc. Hydrogeology, Univ. Neuchâtel, unpublished : 101 p.

Puech, V. and Jeannin, P-Y. 1997. Contribution à la compréhension du fonctionnement hydraulique de l'épikarst ; expériences d'arrosage sur le site de Bure. Proceedings of the 12th Int. Congress of Speleology, La Chaux-de-Fonds. Vol 1 : 293-296.

Reichert, B., Hötzl, H., Stichler, W., Trimborn, P., 1997. Hydrodynamic behaviour of a karst aquifer (Trnovski gozd Plateau, Slovenia). Proceedings of the 12th International Congress of Speleology, 2: 303-306.

Rodier, J., 1978. L'analyse de l'eau.- Dunod, Paris, 1135 pp.

Sauter, M., 1992. Quantification and forecasting of regional groundwater flow and transport in a karst aquifer (Gallusquelle, SW Germany), Tübingen, Tübingen, 151 pp.

Shuster, E.T. and White, W.B., 1971. Seasonal fluctuations in the chemistry of limestone springs: A possible means for characterizing carbonate aquifers. Journal of Hydrology, 14: 93-128.

Smart, P.L. and Friederich, H., 1986. Water movement and storage in the unsaturated zone of a maturely karstified carbonate aquifer, Mendip Hills, England. In: D. National Water Well Association, Ohio. (Editor), Proc. Conf. env. problems of karst terrains and their solutions, pp. 59-87.

Svensson, and Dreybrodt, W. 1992. Dissolution kinetics of natural calcite minerals in CO_2-water systems approaching calcite equilibrium. Chem. Geol., 100: 129-145.

Ternan, J.L., 1972. Comments on the use of a calcium hardness variability index in the study of carbonate aquifers; with references to the central Pennines, England. Journal of Hydrology., 16: 317-321.

Drogue, C., 1992. Hydrodynamics of karstic aquifers: experimental sites in the mediterranean karst, Southern France. In: W. Back, J.S. Herman and H. Paloc (Editors), Hydrogeology of selected karst regions, International contributions to Hydrogeology, Vol. 13. Heinz Heise, Hannover: 133-149.

Vervier, P., 1990. Hydrochemical characterization of the water dynamics of a karstic system. Journal of Hydrology, 121: 103-117.

Vuataz, F.D. 1981. Hydrogéologie, géochimie et géothermie des eaux thermales de Suisse et des régions alpines limitrophes. PhD thesis, Geneva University.

Wells, E.R. and Krothe, N.C., 1989. Seasonal fluctuation in d15N of groundwater nitrate in a mantled karst aquifer due to macropore transport fertilizer-derived nitrate. Journal of Hydrology(112): 191-201.

White, W.B., 1988. Geomorphology and hydrology of karst terrains. Oxford University Press, Oxford, 464 pp.

Williams, P.W., 1983. The role of the subcutaneous zone in karst hydrology. Journal of Hydrology, 61: 45-67.

Williams, P.W., 1985. Subcutaneous hydrology and the development of doline and cockpit karst. Zeit. Geomorph. NF., 29: 463-482.

2. Results and Interpretation

2.1. Introduction

This chapter is made of five papers. As most of the data are taken from Milandre test site, the introduction and study area presentation is somewhat similar in all the papers. They are presented in a logical order which has been followed for reaching the main goal of the project: the building of a consistent flow and transport conceptual model of the Milandre aquifer, and the practical consequences of this model. We start with a conceptual model of flow based on a detailed investigation of the hydrodynamics of the aquifer. Then, we look at the spatial variability of the physico-chemical parameters in the aquifer. The role of this variability on global responses at the spring is assessed. The next step is to consider the temporal variability of non-reactive tracers (i.e. stable isotopes) in the unsaturated zone. This should help at refining the model of flow and transport in the soil, epikarst, and unsaturated zone sub-systems. Then, temporal variations of the chemical parameters are investigated in the saturated zone (the conduit network). A model is proposed which take into account the knowledge acquired in the previous steps. Finally, ideas from the conceptual models are confronted to vulnerability assessments scheme used in karst aquifers.

The first paper, accepted by the “Bulletin d’Hydrogéologie” is based on hydrodynamic data only. It aims at describing the hydraulic behaviour of the sub-systems of the aquifer (soil, epikarst, unsaturated zone, and phreatic zone). Measurements on several tributaries showed that the hydrographs can be very different for the same recharge events. These differences are used to classify the tributaries in categories corresponding to their location in the karst aquifer. Observed hydrographs show that the spring hydraulic characteristics are already established in the unsaturated zone. The epikarst confirms its prominent role of storage and distribution of infiltrated water towards the drains and the low permeability volumes.

The second paper, accepted by Hydrogeology journal, is limited to the spatial variability of the physico-chemical parameters in the Milandre karst aquifer. Regular sampling on the tributaries, the spring, and some boreholes indicated a clear heterogeneity. Main causes of the spatial variability are: nature and location of agricultural inputs, chemical reactions, and mixing of different waters.

The third paper, accepted by the Journal of Hydrology, is based on isotopic data collected on a weekly basis in rainfall and at the spring, and at several locations every half an hour during flood events. Important storage is evidenced and the following model is proposed: the soil zone has a mixing function due to the presence of capillary water storage. Thus epikarst is fed by water having dampened concentrations. The epikarst zone acts as the storage element and distributes water as either a base flow component or a quick flow component. Phreatic storage is thought to be limited.

The fourth paper, submitted to the Journal of Hydrology, is focused on the role of the phreatic zone on the chemical responses (i.e. chemographs) at the karst spring. Water issued from the epikarst has contrasted chemistry due to land use differences mainly (spatial variability illustrated in the second paper) and the phreatic zone mixes these waters. A mixing numerical model is able to reproduce the spring chemograph from time-concentration data at the three main tributaries of the system.

The chapter 2.6. presents the observations made within the unsaturated zone. The evolution of natural tracers during flood events are presented for three sites: Brandt, Grand Bochat, and Milandre (EC percolation water). Each of these sampling points is seepage flow fed by the epikarst and soil sub-systems. Mixing of waters issued from the soil, the epikarst, and rainfall is clearly evidenced. Their respective contribution is controlled by the recharge intensity. Dissolution caused by fresh infiltrated is estimated, and a simple dissolution model allows to work out a mean transit time.

The last paper, published in the proceedings of the 32nd Congress of the IAH, is a reflection on the existing vulnerability assessment methodologies. New concepts are proposed based on the ideas developed during the project: the role of the soil and epikarst sub-systems, the mixing in the phreatic zone. Complementary informations are taken from other field test sites (Brandt and Lionne).

2.2. Hétérogénéité des écoulements dans la zone non saturée d'un aquifère karstique (site de Milandre, Jura suisse)

Par Jérôme Perrin* et Lionel Kopp*

Paper accepted by Bulletin d'Hydrogéologie

Résumé
Entre 1999 et 2001, des débits ont été mesurés sur neuf affluents karstiques qui alimentent la rivière souterraine de la Milandrine. Les hydrogrammes montrent trois types de réponses différentes : le premier présente une cyclicité annuelle des débits (réponse tamponnée), le deuxième se distingue par des crues abruptes et fréquentes (réponse nerveuse) et le troisième a un comportement intermédiaire (réponse intermédiaire). Ces comportements contrastés illustrent l'hétérogénéité des écoulements dans la zone vadose du karst.

La taille des bassins d'alimentation respectifs a pu être calculée à partir des infiltrations efficaces et du débit moyen : les valeurs s'échelonnent entre 42 m^2 et 4.5 km^2, illustrant la large gamme des débits mesurés. La combinaison de l'infiltration efficace et de l'hydrogramme des affluents à réponses nerveuses a permis de calculer pour chaque crue les volumes d'eau alimentant le flot de crue, le flot de base et le stockage dans les volumes peu perméables. Les valeurs moyennes montrent qu'environ 50 % de l'infiltration contribue au flot de crue, 25-30 % au flot de base, et 20-25 % au stockage. La hauteur maximale du stock est comprise entre 13 et 32 mm.

Un modèle conceptuel simple permet d'expliquer le fonctionnement de l'infiltration : la pluie brute est modulée en infiltration efficace dans le sous-système sol. Cette infiltration est ensuite dirigée vers deux types de réservoir dans le sous-système épikarst : le premier conduit à des réponses hydrauliques nerveuses par l'existence d'un trop plein (*vadose flow*), le second donne des réponses tamponnées par l'existence d'un seul exutoire (*seepage flow*). La combinaison de ces deux réservoirs en proportions variables génère des réponses nerveuses dans le réseau karstique (*conduit flow*) d'une part, et à des réponses intermédaires (*intermediate flow*) d'autre part. Ce modèle montre que les caractéristiques hydrauliques de l'aquifère karstique peuvent s'acquérir dans la zone non saturée : à cet égard, il semble que l'épikarst confirme son rôle prépondérant dans le stockage et la distribution de l'eau infiltrée vers les drains et les volumes peu perméables.

Mots-clés

Karst, épikarst, hydrogramme, infiltration efficace, bilan hydrologique, bassin d'alimentation

Abstract
Between 1999 and 2001, discharges have been measured on nine karstic tributaries of the Milandrine underground river. Hydrographs showed three types of behaviour: the first with variations on a one year cycle (buffered response), the second with rapid and frequent flood events (nervous response), and the third with a intermediate behaviour (intermediate response). These different responses illustrate the flow heterogeneity in the karst vadose zone.

The size of the catchment areas has been estimated by a water budget calculation: values are comprised between 42 m^2 and 4.5 km^2. Hence measured discharges cover a large range of values. For each flood event at nervous inlets, it was possible to estimate the volume of water feeding quick flow, base flow, and low permeability volumes by combining computed actual infiltration and measured discharges. Results showed that on average 50 % of the actual infiltration contributes to quick flow, 25-30 % to base flow, and 20-25 % is stored in low permeability volumes. The storage maximum height is comprised between 13 mm and 32 mm.

A simple conceptual model is developed in order to explain the functioning of infiltration in the Milandre karst system. Rainfall is transformed in actual infiltration in the soil sub-system. Then, infiltration is directed to two types of reservoir in the epikarst sub-system: the first has a temporary outlet giving nervous hydraulic responses (*vadose flow*), whereas the second has only one outlet leading to buffered hydraulic responses (*seepage flow*). Different combinations of these two reservoirs can generate nervous responses in the conduit network (*conduit flow*), or responses intermediate between nervous and buffered (*intermediate flow*). This model shows that the hydraulic behaviour of a karst system can be established in the unsaturated zone already. It appears that the epikarst confirms its prominent role of storage and distribution of infiltrated water to the drains and the low permeability volumes.

Keywords

Karst, epikarst, hydrograph, actual infiltration, water budget, catchment area

2.2.1. Introduction et buts

La recharge d'un aquifère karstique peut soit être concentrée par des pertes reliées directement au réseau de conduits souterrains, soit se produire de manière diffuse. Dans ce deuxième cas, l'eau infiltrée est dirigée pour partie vers le réseau de conduits, et pour partie vers les volumes peu perméables du calcaire (SMART & FRIEDERICH 1986, WILLIAMS 1983, JEANNIN & GRASSO 1995b). Les grottes peuvent être considérées comme de véritables lysimètres naturels et permettent d'observer directement la répartition de l'infiltration dans la zone non saturée. Des études récentes (SANZ & LOPEZ 2000, PERRETTE *et al.* 2001) montrent la grande variabilité des réponses hydrauliques des eaux de percolation : certaines réponses présentent des crues fréquentes alors que d'autres sont complètement tamponnées.

La présente étude est également basée sur des mesures de débit en grotte. Son originalité réside dans le nombre de points d'observation (neuf), parmi lesquels certains sont des eaux de percolation alors que les autres sont des affluents à fort débits. L'interprétation de ces mesures doit permettre d'aboutir à un modèle conceptuel cohérent de l'infiltration. La démarche suivie passe par l'établissement d'un bilan hydrologique pour chaque point de mesure, puis par la décomposition des hydrogrammes. Cette décomposition informe sur la répartition des infiltrations vers les volumes peu perméables d'une part, et vers le réseau de conduits d'autre part. L'analyse est effectuée sur une chronique annuelle ou crue par crue (JEANNIN & GRASSO 1995b).

2.2.2. Site d'étude

Le système karstique de Milandre est situé dans le Jura tabulaire à proximité de Porrentruy (canton du Jura, Suisse). La recharge de l'aquifère est purement diffuse, aucune perte n'est visible en surface. La zone saturée est drainée par un conduit qui peut être visité sur plus de 4000 m (la grotte de Milandre). Le long du parcours, de nombreuses arrivées d'eau viennent grossir le débit de la rivière souterraine de la Milandrine. Les débits ont été mesurés en continu pour neuf d'entre elles (figure 1).

L'aquifère est situé dans les calcaires du Rauracien qui reposent sur les marnes de l'Oxfordien. L'épaisseur de la zone non saturée varient grandement entre les volumes peu perméable et le drain (JEANNIN 1998) : elle est comprise entre 40 et 80 m. La zone saturée est moins épaisse : quelques mètres au niveau du drain et jusqu'à 30-40 m dans les volumes peu perméables (figure 1). Les points mesurés dans la partie amont (SO, AM, EC, EN, VI, ST) sont situés 40 à 60 m sous la surface, Les points plus en aval (BU, RO, FA) sont couverts d'environ 100 m de calcaires. La zone non saturée a une structure très hétérogène avec des sols aux épaisseurs variables (0 à plus de 5 m), un épikarst souvent bien développé et des failles importantes qui forment des drains verticaux en direction de la zone saturée.

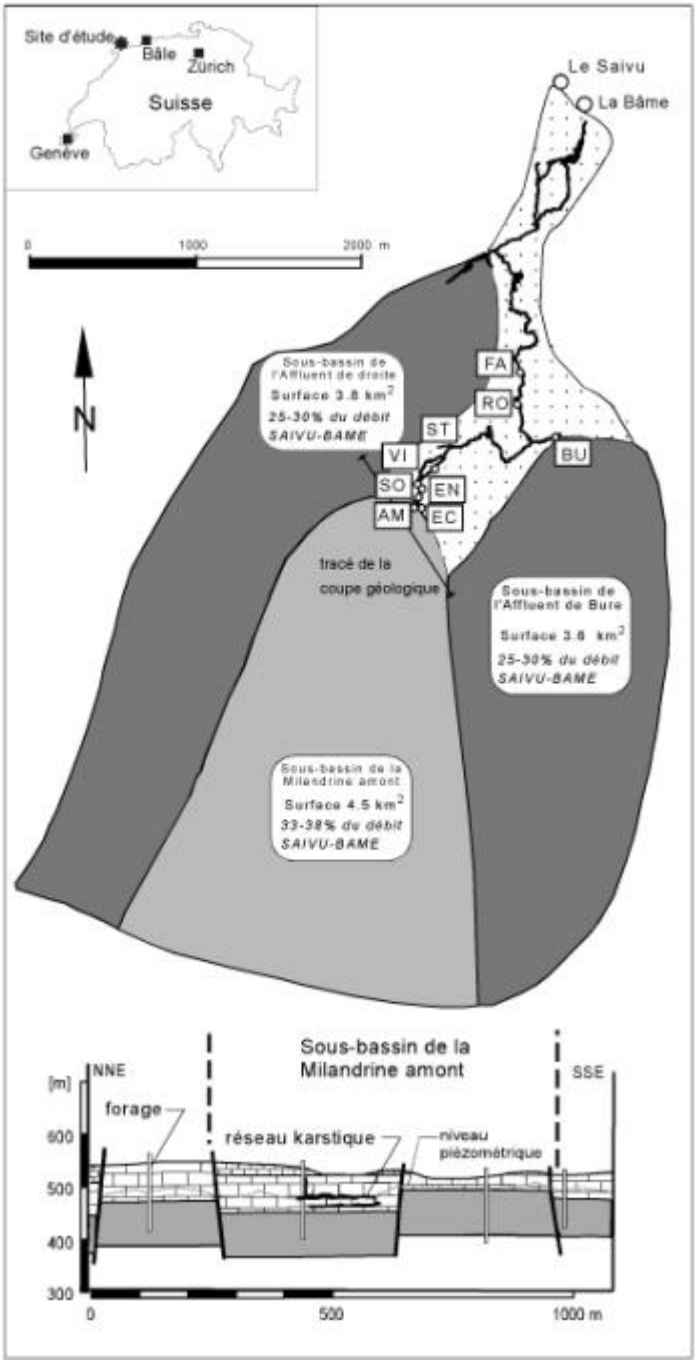

Figure 1 : Le bassin d'alimentation de l'aquifère karstique de Milandre. La rivière souterraine est représentée par le trait noir. La surface pointillée correspond aux bassins d'alimentation des affluents de moindre importance. Les sites de mesure sont localisés par des points et leur abréviation. La coupe géologique montre la situation du réseau karstique et une représentation schématique du niveau piézométrique (modifié de GRASSO & JEANNIN 1994).

2.2.3 Acquisition des données et méthodes de traitement

Mesures des débits
Les neuf arrivées d'eau ont été aménagées pour la mesure du débit : concentration du flux par un entonnoir ou un tuyau, déversoir. Les débits sont mesurés à pas de temps très rapproché (généralement 30 minutes) selon différentes méthodes indirectes choisies en fonction de l'importance du débit à mesurer :

- Très faibles débits : un pluviomètre est utilisé et l'enregistreur comptabilise le nombre de basculements par pas de temps. Chaque basculement correspond à un certain volume d'eau.
- Faibles débits : des « super-pluviomètres » ont été construits. Il s'agit d'un tube PVC percé, sur une partie de sa hauteur, de petits trous selon une trajectoire hélicoïdale. Une sonde de pression est placée au bas du tube et permet de mesurer la charge dans le tube. La charge est ensuite convertie en débit par une courbe de tarage.
- Débits importants : la construction de déversoirs a permis d'installer une sonde de pression dans le bassin créé à l'amont. Les hauteurs d'eau enregistrées sont converties en débit par une courbe de tarage. Les formules hydrauliques utilisées généralement pour la conversion hauteur – débit ne conviennent pas car les déversoirs construits ne permettent pas d'obtenir des bassins suffisamment étendus vers l'amont.

Les mesures ponctuelles de débits ont été réalisées par empotement et par traçage chimique au NaCl.

Calcul du bilan hydrologique
Sur un cycle hydrologique annuel, le bilan hydrologique peut s'exprimer de la façon suivante (DRACOS 1980) :

$$I_{eff} = L_{lame\ écoulée} \quad (1)$$

avec :
$$I_{eff} = P_{brute} - ETR - \delta V_{Stock} \quad (2)$$

et :
$$L_{lame\ écoulée} = (Q + R + \delta V_{réserves}) / A \quad (3)$$

où : I_{eff} = Infiltration efficace [m]

$L_{lame\ écoulée}$ = Lame d'eau écoulée [m]

P_{brute} = Pluie brute [m]

ETR = Evapotranspiration réelle [m]

V = Ecoulement souterrain mesuré [m^3]

R = Ruissellement de surface [m^3]

A = Superficie du bassin d'alimentation [m^2]

δV_{Stock} = Variation du stock d'humidité du sol [m]

$\delta V_{réserves}$ = Variation du volume d'eau souterraine [m^3]

R est négligeable sur le bassin de la Milandrine. Les paramètres hydrauliques sont extraits des hydrogrammes. Pour obtenir Q et $\delta V_{réserves}$ en [mm], le volume d'eau souterraine doit être divisé par la superficie du bassin d'alimentation (voir 2.2.2.) Les paramètres météorologiques sont donnés par la station de Fahy appartenant à L'Institut Suisse de Météorologie (ISM) et située à quelques kilomètres du bassin d'alimentation de l'aquifère.

Calcul de l'ETR
L'équation pour retrouver l'ETR à partir de l'ETP (évapotranspiration potentielle) est la suivante :

$$ETR = Humidité\ (sol) - ETP + P_{brute} \quad (4)$$

Le stock d'humidité du sol a été fixé à 140 mm après plusieurs essais de calibration (JEANNIN & GRASSO 1995a). L'ETP est calculée par la formule de PRIMAULT (1963) :

$$ETP = E * C * i \quad (5)$$

où: E = Evaporation calculée ou mesurée directement dans un bac à la station ISM de Fahy d'avril à septembre [mm]

C = Coefficient dépendant de l'altitude (0.7-1.1). Pour Fahy, alt. =596m : C=0.92

i = Coefficient dépendant de la végétation (0.1-1.1), varie en fonction des saisons

L'évaporation pendant les mois d'hiver (octobre à mai) est donnée par :

$$E = [(103 - H) / 100] * (S + 2 * n) \quad (6)$$

où: H = Humidité relative de l'air [%]

S = Durée d'insolation [h]

n = Nombre de jours considérés (n=1 pour un pas de temps journalier)

Calcul de la superficie du bassin d'alimentation
La superficie des bassins d'alimentation A est calculée par l'équation (3). Le calcul de $\delta V_{réserves}$ (variation du volume d'eau souterraine) se fait par l'analyse des courbes de tarissement en fin d'année hydrologique (août – septembre) : en reportant une courbe de récession (subdivisée en une courbe de décrue et une courbe de tarissement) dans un repère semi-logarithmique, la partie terminale de la courbe s'ajuste généralement bien sur une droite. En soustrayant les ordonnées de la droite aux ordonnées de la courbe de récession, on obtient une deuxième courbe dont la partie terminale s'ajuste sur une droite. En procédant ainsi, la courbe de récession peut généralement être représentée par la superposition de trois droites de pentes α_n (FORKASIEWICZ & PALOC 1967, GRASSO 1998) (figure 2) :

$$Q(t) = Q_{01} * e^{-\alpha 1*t} + Q_{02} * e^{-\alpha 2*t} + Q_{03} * e^{-\alpha 3*t} \quad (7)$$

Pour déterminer le temps t_i à partir duquel s'écoule les réserves de tarissement de l'aquifère (i.e. les volumes d'eau issus des parties peu perméables de l'aquifère), GRASSO (1998) propose de considérer le temps où le débit correspondant à la deuxième exponentielle devient inférieur à 1 % du débit dû à la troisième exponentielle :

$$t_i = [1 / (\alpha_2 - \alpha_3)] * \ln [Q_{02} / (0.01 * Q_{03})] \quad (8)$$

$V_{réserves}$ se calcule comme suit :

$$V_{réserves} = (Q_{ti} / \alpha_3) * C \quad (9)$$

Où : Q_{ti} = Débit au temps t_i [l/s]

C = Constante: C=86.4 [$jour^{-1}$], lorsque Q_{ti} est en l/s et α_3 en $jour^{-1}$

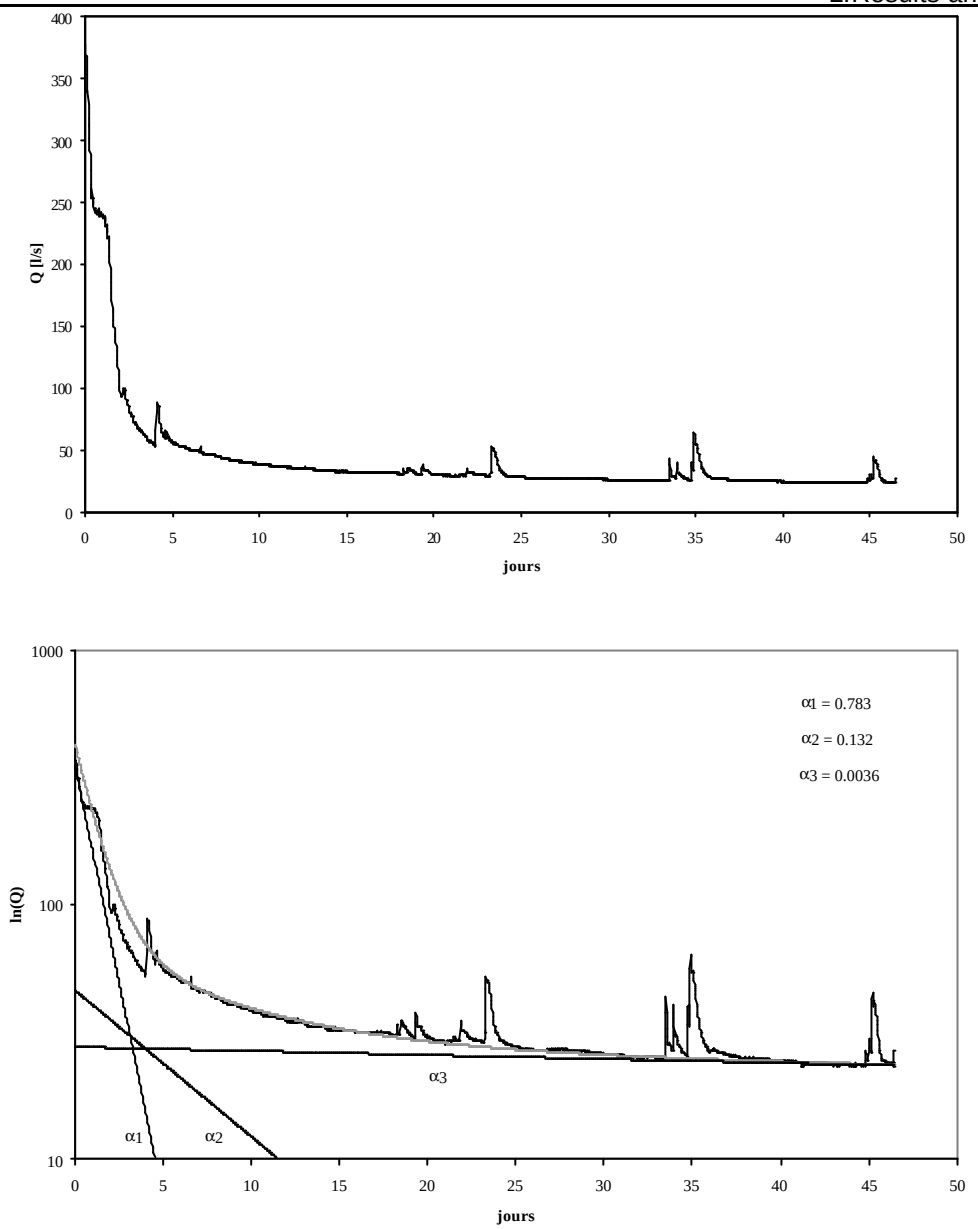

Figure 2 : Courbe de récession de la Milandrine amont (décrue et tarissement du 16/07/01 au 31/08/01). Le graphique du haut présente l'hydrogramme ; le graphique du bas reprend l'hydrogramme dans un repère semi-logarithmique (courbe noire). La décomposition de l'hydrogramme en trois courbes de récession (de pente α1, 2 et 3) permet de modéliser le débit Q(t) par la somme des trois courbes de récession (courbe grise).

Evolution du flot de base par rapport au flot total pour chaque site de mesure et analyse détaillée des crues

Le débit total à l'exutoire est décomposé en un débit de base, lié à la vidange des volumes de roche peu perméable, et un débit de crue. Ces débits sont ensuite transformés en volumes écoulés :

$$V_{crue}\ (V_c) = V_{Total}\ (V_t) - V_{base}\ (V_b) \qquad (10)$$

La séparation entre flot de base et flot de crue se fait d'après la méthode graphique présentée par SHAW (1994) : le début de la crue correspond à l'inflexion de la courbe de débit qui est en général bien délimitée dans le temps. La fin de la crue est déterminée dans un repère semi-logarithmique (figure 3). Elle correspond au point où la courbe se transforme en une droite. Cette méthode a été choisie pour sa facilité de mise en œuvre, comparativement à la méthode de décomposition de l'hydrogramme.

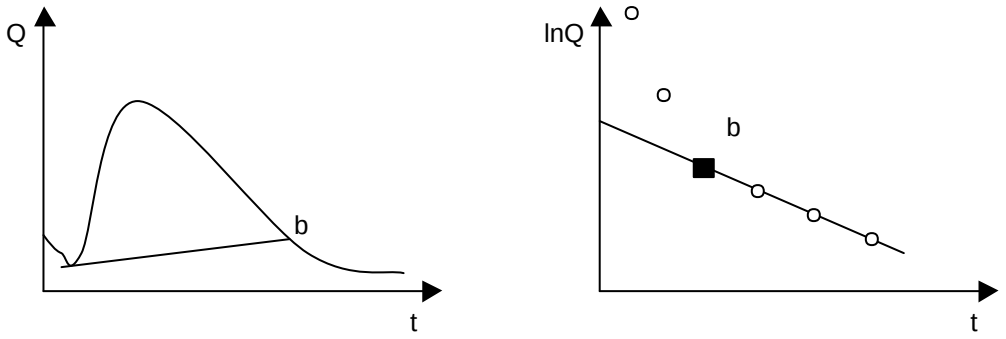

Figure 3 : Méthode graphique utilisée pour séparer le flot de crue du flot de base (d'après SHAW 1994).

2.2.4. Résultats

La réponse hydraulique des affluents

Trois types de réponse ressortent de l'observation directe des hydrogrammes des neuf points de mesure (figure 4). Un premier comportement, de type cycle annuel, est caractéristique des sites VI et ST avec des écoulements plus importants en hiver. Le débit commence à augmenter environ deux mois plus tard à ST et l'augmentation est nettement plus marquée que sur VI (Le rapport Qmax/Qmin est de 43.6 pour ST et 1.4 pour VI). Un deuxième comportement de type crues fréquentes apparaît pour de nombreux affluents (EC, la Milandrine amont (AM), l'affluent de Bure (BU), la source rouge (RO), FA). Il se caractérise par de fortes augmentations du débit lors d'évènements pluvieux. L'hydrogramme présente une asymétrie typique avec une forte montée initiale du débit, sur une période de temps très courte, puis, une récession beaucoup plus lente. Plusieurs sites montrent des chroniques très semblables : ils réagissent en moyenne deux heures après le début des pluies et atteignent un pic de crue en même temps (figure 5). Quelques différences existent toutefois entre les affluents: certaines petites crues (à fin décembre 2000 par exemple) n'apparaissent pas sur FA; l'importante crue de début janvier 2001 se marque par un double pic pour BU et RO; et la décrue sur AM est moins brutale et peut même marquer un plateau (interprété comme un stockage temporaire par GRASSO & JEANNIN 1994).

Enfin, deux affluents (SO, EN) se caractérisent par un comportement intermédiaire : des crues surviennent en période hivernale ; par contre le débit reste relativement stable et bas en période estivale, malgré l'existence d'averses importantes. Il semble toutefois que SO soit plus sensible aux crues d'été qu'EN (juillet 2001).

SMART & FRIEDERICH (1986) utilisent le débit maximum et le coefficient de variation du débit pour classer les différentes arrivées d'eau dans leur système. En s'inspirant de leur classification, il est possible de distinguer quatre types d'écoulement pour lesquels nous proposons la nomenclature suivante (figure 6) :

1. écoulement de suintement pour le comportement cycle annuel (*seepage flow*)
2. écoulement vadose pour EC se distinguant par son faible débit et sa claire provenance de la zone non saturée (*vadose flow*)
3. écoulement de conduit pour AM, BU, RO et FA (*conduit flow*),
4. écoulement à régime « intermédiaire » pour SO et EN (*intermediate flow*).

Type cycle annuel

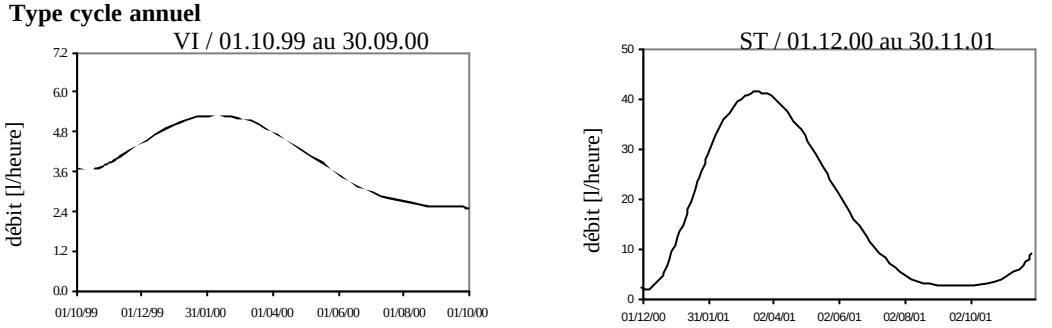

Type crues fréquentes

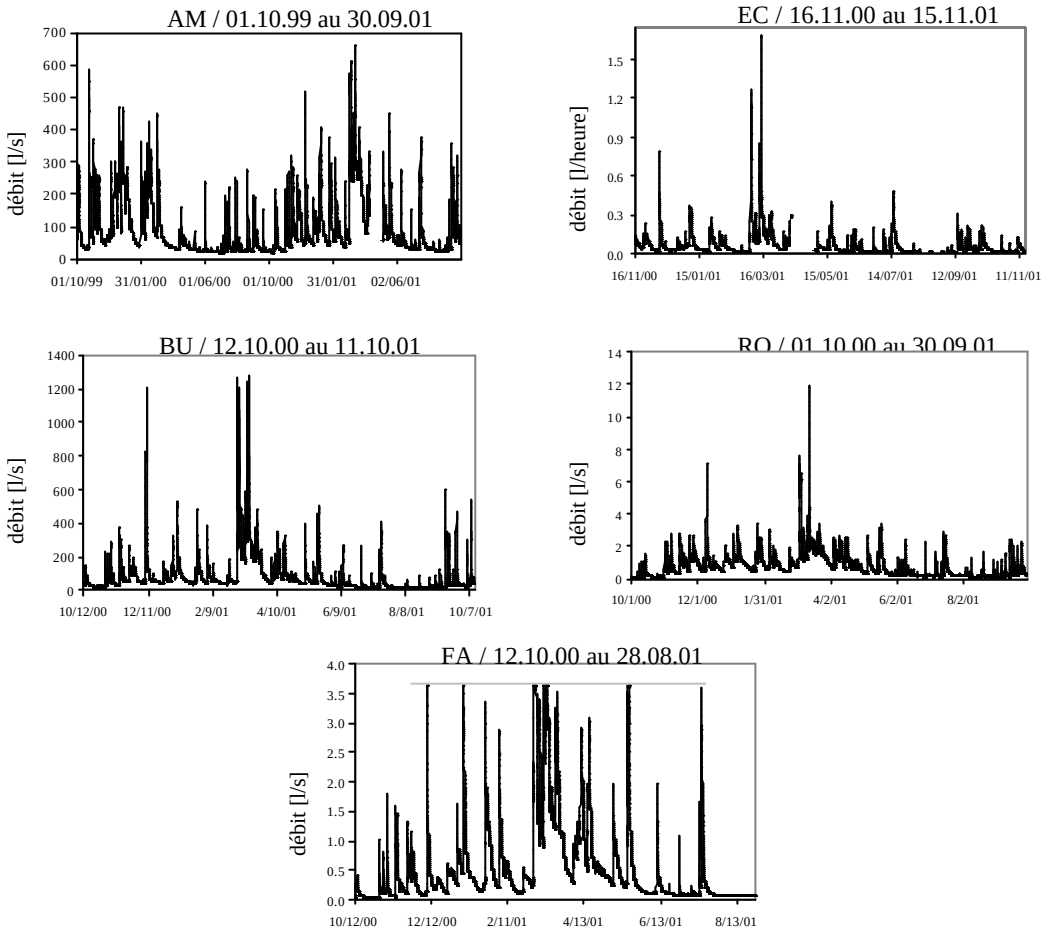

Type intermédiaire

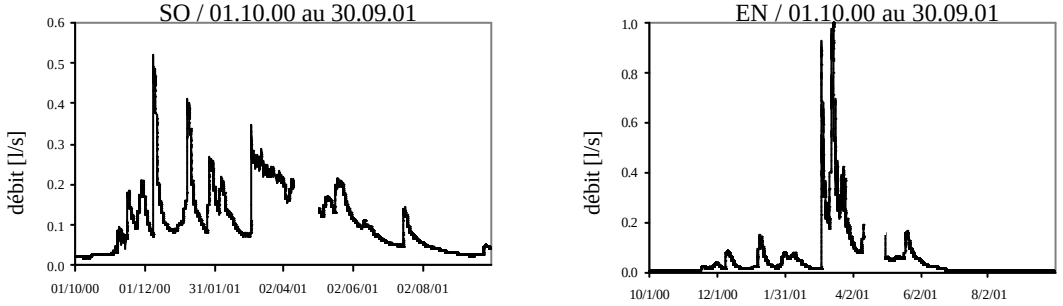

Figure 4 : Classification des hydrogrammes en trois types de réponses différentes : le premier à cycle annuel, le deuxième à crues fréquentes et le troisième à comportement intermédiaire.

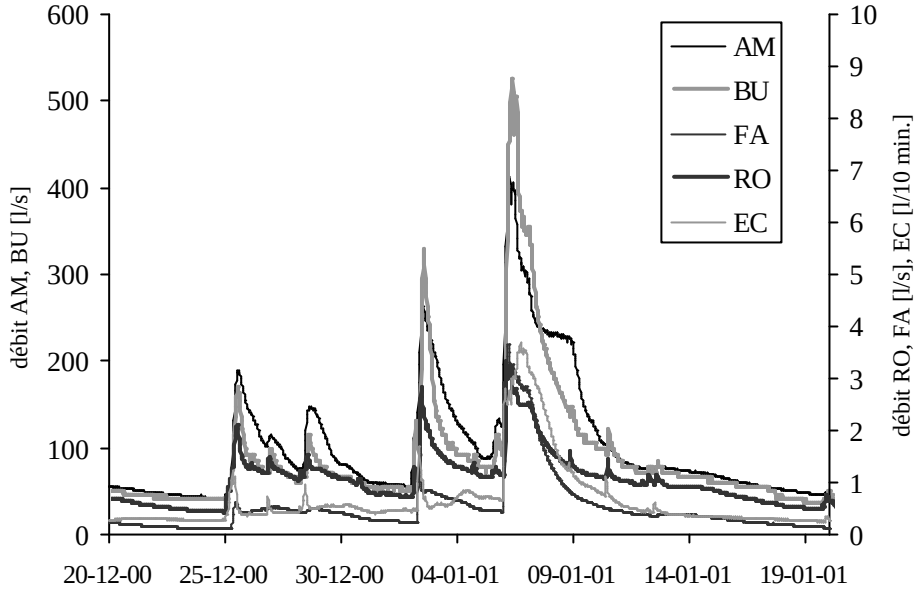

Figure 5 : Comparaison de la forme des hydrogrammes des cinq affluents à réponse hydraulique nerveuse.

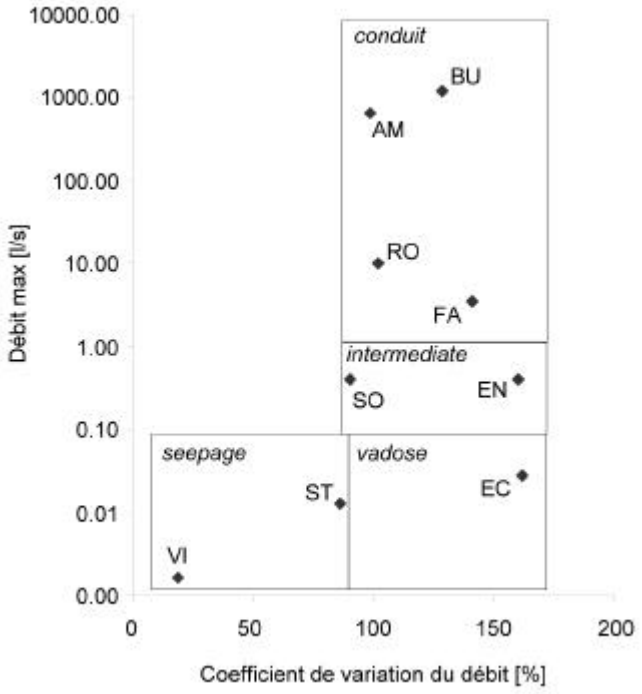

Figure 6 : Classification des affluents en fonction du coefficient de variation du débit et du débit maximum. Le coefficient de variation est obtenu en divisant l'écart type sur les débits par le débit moyen.

Estimation de l'infiltration efficace

La pluie brute est mesurée par la station ISM de Fahy. De plus, une station pluviométrique a été installée dans le village du Maira par le bureau RWB et une dernière station a été mise en place plus tardivement à proximité de l'entrée amont de la grotte.

Ce réseau d'observation détaillé permet de comparer la variabilité spatiale de la pluie brute. Les données mensuelles montrent des écarts entre les stations de quelques pour cents en général (tableau 1). Des écarts dépassant 10 % ont été déterminés en décembre 1999, juin et décembre 2000, février et mars 2001. Ces écarts n'ont qu'une conséquence très limitée sur le bilan annuel puisque pour l'année hydrologique 1999/2000, la pluie totale au Maira est de 1167 mm et de 1140 mm à Fahy. Par contre, des écarts non négligeables peuvent exister à l'échelle du bassin d'alimentation sur une période d'averse.

En vue du calcul du bilan hydrologique, la recharge a été calculée à partir des données météorologiques de la station ISM de Fahy. Il en ressort que plus de 50 % des pluies brutes rechargent l'aquifère comme infiltration efficace, le reste est repris par l'évapotranspiration (tableau 2).

Le modèle utilisé pour le calcul de l'évapotranspiration est global. Il semble convenir pour les bilans de bassins de plusieurs km^2. Par contre, il peut générer une importante imprécision dans les bilans effectués sur des arrivées d'eau de petite taille où les conditions locales d'infiltration sont de prime importance.

Tableau 1 : comparaison des pluies mensuelles sur trois stations pluviométriques situées dans le bassin d'alimentation de Milandre (Maira) ou à proximité (Fahy).

	Maira CHYN	Maira RWB	Fahy
Oct-99	non existant	119.5	134.6
Nov-99	non existant	77.4	87.0
Dec-99	non existant	193.1	150.7
Jan-00	non existant	41.4	41.4
Fév-00	non existant	143.0	117.2
Mar-00	non existant	60.6	62.3
Avr-00	non existant	60.8	66.2
Mai-00	non existant	92.8	85.6
Juin-00	non existant	31.6	49.4
Juil-00	non existant	169.6	172.7
Août-00	non existant	103.4	110.7
Sep-00	non existant	74.3	61.7
Oct-00	non existant	83.9	83.0
Nov-00	non existant	116.1	105.4
Dec-00	69.3	88.9	68.7
Jan-01	59.8 (gel)	103.2	96.0
Fév-01	58.1	60.3	45.3
Mar-01	273.2	300.3	243.0
Avr-01	en panne	134.6	122.2
Mai-01	105.7	98.2	105.9
Juin-01	117.3	?	121.1
Juil-01	136.4	?	119.5
Août-01	89.0	?	81.4

Tableau 2 : Tableau récapitulatif des précipitations brutes (d'après ISM (Institut Suisse de Météorologie), station de Fahy), de l'évapotranspiration, des infiltrations efficaces et de la variation du stock d'humidité du sol, déterminés sur le bassin entier pour deux années.

	Oct 99 / Oct 00	Oct 00 / Oct 01
$\mathbf{P_{brute}}$ [mm]	1140	1330
ETR [mm]	573	504
$\mathbf{I_{eff}}$ [mm]	634	751
$\delta\mathbf{V_{Stock}}$ [mm]	-67	75

Les bilans hydrologiques et le calcul des bassins d'alimentation
Les réserves de tarissement sont calculées selon la relation (9) (tableau 3) et permettent d'établir la variation des réserves. La pluie efficace est déterminée selon l'équation (2), puis la superficie des différents bassins d'alimentation est établie selon la relation (3). Les résultats (tableau 4) montrent l'extrême variabilité des surfaces des divers bassins considérés. La variation de réserve n'a pas pu être calculée pour EC car seule une année hydrologique a été enregistrée. Cette absence d'information peut tout au plus induire une erreur de quelques pour cents sur la superficie calculée. Le volume minimum de base est simplement le débit annuel minimum intégré sur l'année.

Pour la Milandrine amont (AM), deux cycles annuels (99-00) et (00-01) sont disponibles. Un bassin d'alimentation moyen de 4.5 km^2 (correspondant à l'analyse de JEANNIN & GRASSO 1995a) a été utilisé dans le calcul des bilans. Les écarts sur le bilan sont de 2.5 % pour 1999-2000 et -13 % pour 2000-2001. L'année 2001 a été anormalement humide, ce qui peut expliquer l'important écart sur le bilan : il est possible que le modèle du calcul de la recharge surestime les infiltrations dans des conditions climatiques particulières, ou que les forts débits soient sous-estimés par les mesures *in situ*.

Tableau 3 : Réserves écoulables calculées pour AM, RO, FA, BU, EN, SO selon la méthode de FORKASIEWICZ & PALOC (1967).

	$V_{rés}$ 1999 [m^3]	$V_{rés}$ 2000 [m^3]	$V_{rés}$ 2001 [m^3]
AM	561'917	756'584	590'400
RO		1377	1905
FA		250	1364
BU		154'585	96'748
EN		100	59
SO		377	414

Répartition des infiltrations entre flots de base et de crue
La décomposition de l'hydrogramme en débit de base et débit de crue a été réalisé sur tous les affluents présentant un régime d'écoulement en conduits, vadose ou intermédiaire selon la méthode présentée au paragraphe 3.3. Dans le cas de ST et VI (*seepage flow*), il semble clair que la totalité du volume écoulé correspond au flot de base.

Pour la majorité des affluents, environ 50% du volume annuel écoulé représente des volumes de crues, les 50% restants, représentent les volumes du flot de base (tableau 4). Dans le cas de RO le flot de base est proportionnellement plus important tandis que pour FA, il est sensiblement moins important. Dans tous les cas, il est intéressant de constater que les pourcentages respectifs des flots de base et de crue peuvent être similaire pour des écoulements de type vadose, intermédiaire ou de conduit.

Tableau 4 : La partie 1 donne les valeurs caractéristiques des débits de chaque affluent pour l'année hydrologique considérée, ainsi que les volumes écoulés (total, base, crue et minimum de base). La partie 2 présente les résultats du calcul du bassin d'alimentation de chaque affluent, selon l'équation (7).

Partie 1	**EC 00-01** 16/11/00-15/11/01	**AM 99-00** 01/10/99-31/09/00	**AM 00-01** 01/10/00-31/09/01	**SO 00-01** 01/10/00-31/09/01	**VI 99-00** 01/10/99-31/09/00
Débit moyen [l/s]	0.001	82	97	0.11	0.001
Débit minimum [l/s]	0.00008	19	20	0.02	0.0007
Débit maximum [l/s]	0.028	592	665	0.4	0.002
Débit max. / Débit min.	350	31	33	20	2.9
Volume tot. écoulé (Vt) [m^3]	32.4	2590307	3151530	3194	35.2
Volume de base (Vb) [m^3]	16.8	1146323	1402140	1795	-
Volume de crue (Vc) [m^3]	15.6	1443984	1749390	1399	-
Volume min. de base (Vm) [m^3]	2.6	610278	624377	599	24.8
Vb / Vt [%]	52	44	44	56	-
Vc / Vt [%]	48	56	56	44	-
Vm / Vt [%]	8	24	20	19	70
Partie 2					
I eff. calculée [mm]	769	634	751	751	634
δV réserves [m^3]	Pas calculé	194667	-166184	37	Pas calculé
Bassin d'alimentation estimé	**42** m^2	**4.39** km^2	**3.98** km^2	**4300** m^2	**55** m^2

Partie 2	**EN 00-01** 01/10/00-31/09/01	**ST 00-01** 01/12/00-30/10/01	**BU 00-01** 11/10/00-10/10/01	**RO 00-01** 01/10/00-31/09/01	**FA 00-01** 10/10/00-09/10/01
Débit moyen [l/s]	0.055	0.005	76.0	0.75	0.51
Débit minimum [l/s]	0.004	0.0002	10	0.08	0.024
Débit maximum [l/s]	1.0	0.013	1280	12.9	3.6
Débit max. / Débit min.	250	65	128	162	150
Volume tot. écoulé (Vt) [m^3]	1832.7	125.4	2397010	23723	14247
Volume de base (Vb) [m^3]	842.8	-	1232052	14523	4499
Volume de crue (Vc) [m^3]	989.9	-	1164958	9200	9748
Volume min. de base (Vm) [m^3]	126.1	5.4	302728	2617	666
Vb / Vt [%]	46	-	51	61	32
Vc / Vt [%]	54	-	49	39	68
Vm / Vt [%]	7	4	13	11	5
Partie 2					
I eff. calculée [mm]	751	789	769	751	706
δV réserves [m^3]	-41	Pas calculé	-57837	529	1114
Bassin d'alimentation estimé	**2390** m^2	**160** m^2	**3.04** km^2	**0.032** km^2	**0.022** km^2

2.2.5. Discussion

Variabilité spatiale de la réponse hydraulique

La réponse hydraulique à un événement pluvieux diffère d'un point de mesure à l'autre. Cette variabilité spatiale a déjà été illustrée dans plusieurs études récentes se limitant à la zone non saturée de l'aquifère (DELANNOY *et al.* 1999, SANZ & LOPEZ 2000, DESTOMBES *et al.* 1997, SMART & FRIEDERICH 1986). Dans notre cas, les mesures comprennent des arrivées d'eau en zone non saturée mais également des chroniques sur des drains pouvant être alimentés par la zone saturée. Les réponses hydrauliques peuvent être nerveuses (*conduit* ou *vadose flow*), tamponnées (*seepage flow*) ou intermédiaires (*intermediate flow*). Une classification hiérarchique des arrivées d'eau selon leur importance (débit moyen et taille du bassin d'alimentation) montre que les affluents modestes (VI, ST, EC) présentent les deux types de réponses hydrauliques. Les affluents légèrement plus importants (EN, SO) sont un mélange des deux réponses. Les réponses des petits drains (RO, FA) sont nerveuses. Toutefois leur coefficient de tarissement (α = 0.005 j^{-1}), est environ 10 fois plus faible qu'EC (α = 0.03 j^{-1}), montrant la participation d'écoulement de type tamponné à l'alimentation de ces drains. Cette remarque est valable pour les drains majeurs (AM, BU) qui sont alimentés essentiellement par des écoulements nerveux type EC, mais également par des affluents tamponnés (type VI) et probablement par des affluents intermédiaires (type EN, SO).

Ces réponses hydrauliques contrastées confirment l'existence de deux types de recharge dans la zone d'infiltration. Les affluents à réponse tamponnée (*seepage flow*) sont issus d'un réservoir suffisamment capacitif permettant de niveler les impulsions de recharge. Ce réservoir peut être localisé dans la zone vadose (sol – épikarst) ou dans les volumes peu perméables de la zone saturée. Les affluents à réponse nerveuse (*vadose flow*) sont alimentés par un réservoir peu capacitif pouvant transmettre rapidement un événement de recharge. Finalement les drains sont un mélange de ces types de réservoir. Cependant les réservoirs permettant une réponse hydraulique nerveuse dominent largement.

La répartition de l'infiltration

(i) à l'échelle inter-annuelle

Sur un cycle hydrologique, l'infiltration efficace représente plus de 50 % de la pluie brute, le reste étant repris par l'évapotranspiration (tableau 2). Ces données et celles de JEANNIN & GRASSO (1995a) pour 1990/91, 1991/92, 1992/93 montrent une relation linéaire entre les précipitations et l'infiltration efficace (figure 7). La pente de 0.77 indique que les années pluvieuses participent proportionnellement moins à l'infiltration efficace. Ce résultat a priori surprenant s'explique par la distribution des pluies au cours de l'année : les années pluvieuses sont nettement plus humides en été et participent de fait plus efficacement à l'évaporation potentielle ; l'infiltration efficace est proportionnellement moins importante.

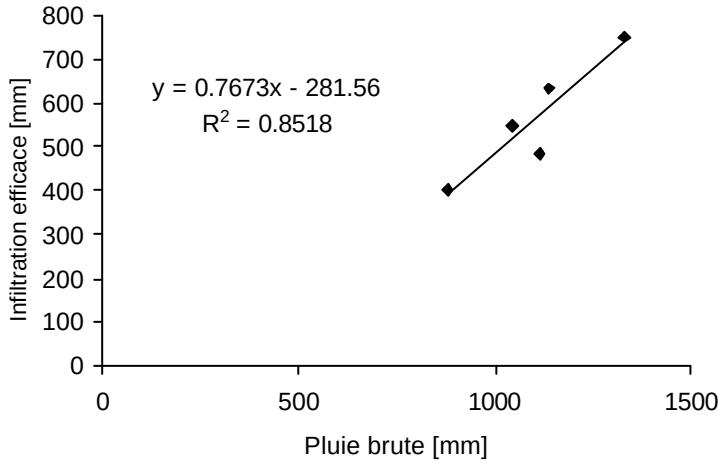

Figure 7 : relation entre pluie brute annuelle et infiltration efficace calculée par le modèle. Les années hydrologiques considérées sont 1990/91, 1991/92, 1993/94, 1999/2000, 2000/01.

L'eau infiltrée se répartit dans l'aquifère en flot de base et flot de crue. Les pourcentages respectifs sont d'environ 50 % chacun. Pour la Milandrine amont (AM) par exemple, 44 % correspond au flot de base

et 56 % au flot de crue pour les deux années mesurées (tableau 4). Des valeurs similaires ont été obtenues par JEANNIN & GRASSO (1995b), soit respectivement 47 % et 53 % pour la période 1990 - 1993. Les valeurs plus élevées du flot de base (61 %) pour RO pourraient indiquer une participation plus importante d'affluents de type *seepage flow* à son alimentation. Au contraire, le faible pourcentage de flot de base à FA (32 %) pourrait indiquer une importante contribution de *vadose flow* dans l'alimentation (écoulements temporaires par exemple). Des mesures sur plusieurs cycles sont toutefois nécessaires pour confirmer de telles tendances.

Dans le cas des *intermediate flow* (SO, EN), la séparation en flot de base et de crue peut être discutée. En effet, les crues de ces deux affluents regroupent plusieurs évènements de crue enregistrés sur les affluents nerveux, indiquant un fonctionnement hydraulique très différent. De fait, la séparation des flots de crue et de base devient arbitraire et il est possible que les pourcentages des volumes de base écoulés (56 et 46 %) soient sensiblement plus élevés.

(ii) à l'échelle annuelle

La décomposition des hydrogrammes selon la relation (10), crue par crue, permet de tester la validité du modèle de calcul des infiltrations efficaces. La correspondance entre les infiltrations efficaces calculées et les volumes écoulés mesurés est satisfaisante (figure 8). Pour les crues peu importantes, les infiltrations efficaces sont surestimées. Cette déviation a déjà été notée au paragraphe précédent. Le calcul de la recharge devrait donc être affiner pour ce type d'évènement. Il est possible que le stock d'humidité du sol soit sous-estimé, en tout cas pour AM et RO : leurs bassins d'alimentation respectifs sont essentiellement situés en zone agricole avec des sols épais permettant un stock d'humidité plus important.

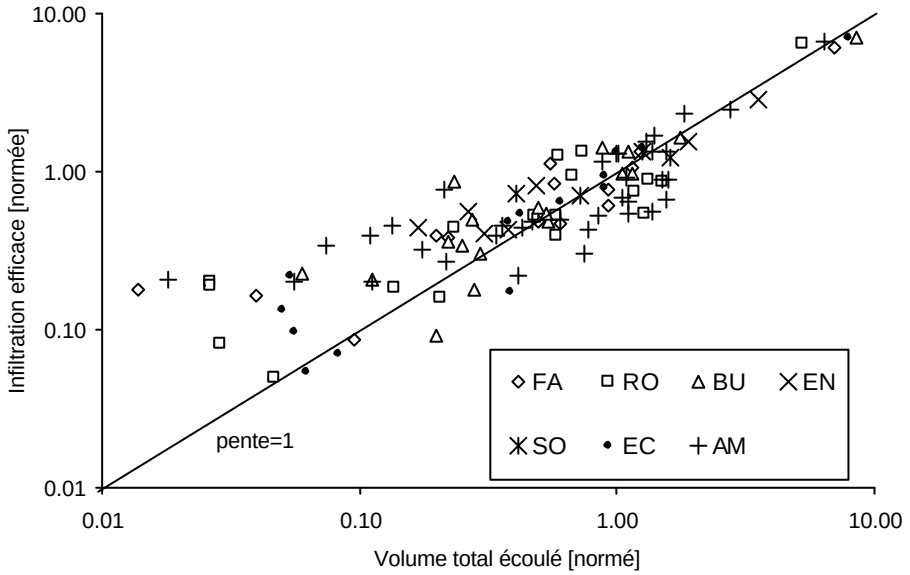

Figure 8 : corrélation entre les infiltrations efficaces calculées et le volume écoulé mesuré pour chaque crue. Les valeurs sont normées par la moyenne annuelle.

Les effets de l'évapotranspiration peuvent être mis en évidence en calculant pour chaque crue le taux de restitution des averses de pluie brute dans les crues (soit le rapport entre le volume d'eau précipitée et le débit à l'exutoire) : le taux peut dépasser 60 % en hiver et se réduit à moins de 20 % l'été, bien que les pluies soient réparties sur toute l'année. Cette saisonnalité traduit le rôle de l'évapotranspiration qui soustrait proportionnellement plus d'eau aux précipitations en été qu'en hiver. Ces tendances saisonnières se retrouvent dans tous les affluents de type *conduit* ou *vadose flow*, l'exemple de la Milandrine amont est donné à la figure 9.

L'estimation satisfaisante de l'infiltration efficace permet de calculer pour chaque site à réponse hydraulique nerveuse la répartition du volume d'eau infiltré (*Vi*) en volume de flot de base (*Vb*), volume de flot de crue (*Vc*) et volume stocké (*Vs*) :

$$V_i = I_{eff} A = V_b + V_c + V_s = V_t + V_s \quad (11)$$

La relation (11) suppose que l'aire d'alimentation (A) ne varie pas notablement en fonction des conditions hydrologiques. La figure 8 montre que cette hypothèse est valable pour le site de Milandre.

Pour les sites à réponses hydrauliques intermédiaires (SO, EN), les résultats du calcul ont montré des *Vs* moyens négatifs, prouvant l'inadéquation de la décomposition des hydrogrammes sur ces points de mesure.

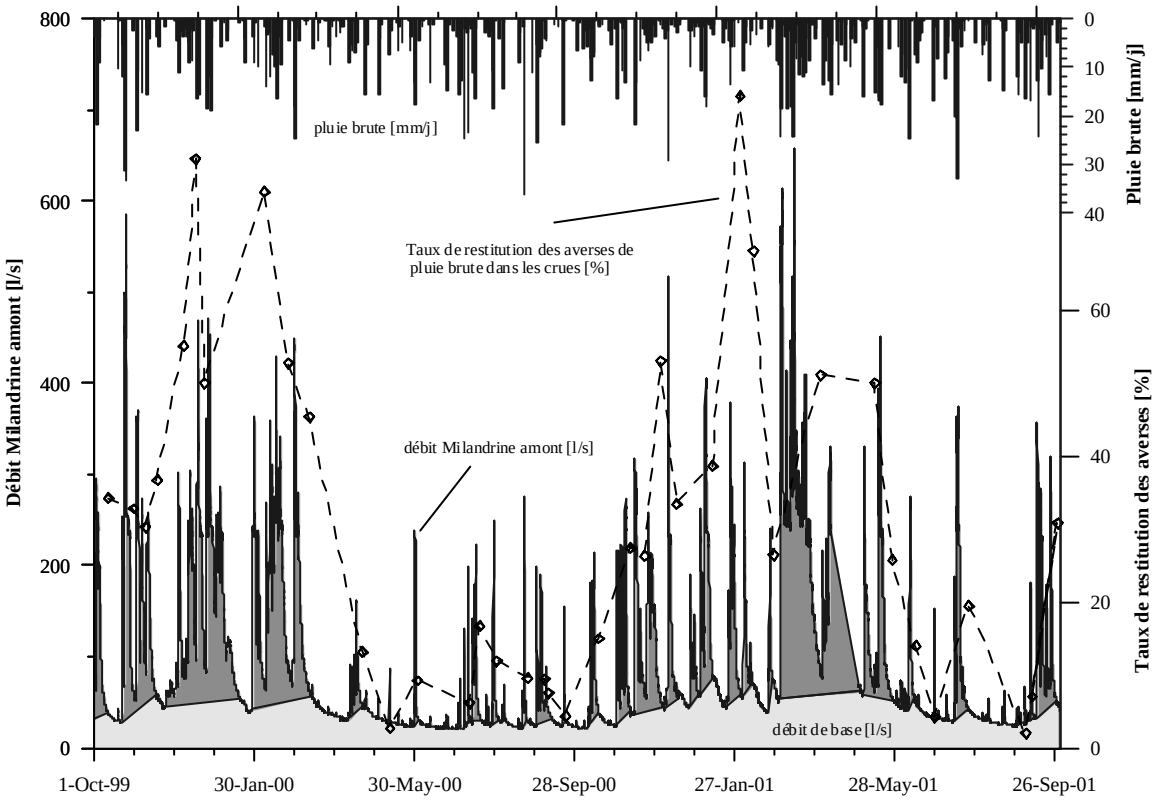

Figure 9 : Hydrogramme de la Milandrine amont d'octobre 1999 à octobre 2001. Décomposition du débit total en un débit de crue et en un débit de base, et comparaison avec les précipitations brutes. La courbe trait tillée représente le taux de restitution des averses calculé pour la plupart des crues.

Pour les autres affluents, l'équation a été appliquée à chaque crue (n= 14 à 20) et les résultats synthétiques sont présentés dans le tableau 5. Pour les volumes de crue et de base, les pourcentages sont variables d'une crue à l'autre (CV entre 50 et 70 %), mais les valeurs moyennes montrent qu'environ 50 % de l'infiltration correspond au volume de crue et 25-30 % au volume de base. Le volume stocké est nettement plus variable (CV entre 110 et 275 %) car il dépend du stock préalable, c'est à dire des conditions climatiques précédant la crue analysée. Les valeurs moyennes du volume stocké sont de l'ordre de 20 à 25 %. Il est intéressant de constater que le volume stocké pour AM passe de 30 % en 2000 à 17 % en 2001, année clairement plus humide (tableau 2). Ce volume stocké calculé crue par crue est comparable aux réserves écoulables calculées pour le bilan hydrologique (tableau 6).

Il semble que les estimations des différents volumes dépendent en partie des conditions météorologiques et probablement des répartitions des précipitations au cours de l'année. Les pourcentages moyens des volumes de base, de crue et stocké sont proches pour les cinq affluents considérés. Le modèle d'infiltration retenu pour ces écoulements à réponses hydrauliques nerveuses semble donc cohérent.

La répartition des différents volumes d'eau peut être schématisée par un réservoir à deux exutoires (figure 9). Le stock maximum, soit *Vs* (max) */A*, doit permettre d'approcher la valeur du seuil h (tableau 5). Les valeurs sont comprises entre 13 mm pour EC et 32 mm pour AM et illustrent la variabilité

spatiale de la hauteur h du réservoir. L'évolution des isotopes stables de l'oxygène pendant des crues sur AM et EC ont montré que, jusqu'à 20 mm d'infiltration efficace, seule de l'eau stockée participait à la crue (PERRIN *et al.* [soumis]). Le seuil h basé sur l'analyse des hydrogrammes est donc compatible avec les données isotopiques.

Tableau 5 : estimation des volumes moyens de base, de crue et stocké. CV est le coefficient de variation, n le nombre de crues considérées. Le dernier tableau présente la hauteur moyenne et maximale du stockage.

Volume de base (*Vb*)

	moyenne [%]	CV [%]	n
EC	27.4	70.3	14
FA	20.8	68.9	14
RO	35.5	72.0	18
AM 00	25.1	59.7	20
AM 01	34.8	54.2	16
BU	24.6	68.7	18

Volume stocké (*Vs*)

	moyenne [%]	CV [%]	n
EC	16.8	246	14
FA	30.5	113	14
RO	19.4	259	18
AM 00	29.8	155	20
AM 01	16.9	275	16
BU	26.6	137	18

Volume de crue (*Vc*)

	moyenne [%]	CV [%]	n
EC	55.8	45.6	14
FA	48.8	49.7	14
RO	45.1	61.1	18
AM 00	45.1	72.4	20
AM 01	52.2	59.9	16
BU	48.8	48.1	18

Hauteur du stock

site	stock moy. [mm]	stock max. [mm]
EC	3.2	13.2
FA	6.8	26.0
RO	6.4	26.6
AM 00	7.6	32.4
AM 01	6.2	19.5
BU	6.2	22.0

Tableau 6 : Comparaison du volume d'eau stocké calculé crue par crue (V_s, équation 11) et par l'analyse de la courbe de tarissement en fin d'année hydrologique ($V_{rés}$, équation 9) pour la Milandrine amont.

	2000	**2001**
$V_{rés}$ [m^3]	756'584	590'400
Σ **V_s [m^3]**	681'415	447'229

(iii) limites de l'interprétation

Les interprétations ci-dessus pourraient être affinées par une meilleure connaissance de plusieurs paramètres : l'infiltration efficace devrait être distribuée dans l'espace de manière à tenir compte de la couverture végétale et de l'épaisseur des sols ; la taille des bassins d'alimentation pourrait être précisée par l'établissement d'un bilan hydrologique sur plusieurs années ; une détermination plus précise des débits serait en outre souhaitable.

Modèle conceptuel de fonctionnement hydraulique

Le modèle de réservoir (figure 10) a le mérite d'être simple. Toutefois il ne permet pas de reproduire le comportement des affluents de type intermédiaire ou tamponné. De plus, la taille des bassins d'alimentation des affluents est fort différent (42 m^2 pour EC et 4.5 km^2 pour AM), nécessitant une hiérarchisation du système d'écoulement. Le modèle conceptuel (figure 11) tente de tenir compte de ces spécificités hydrauliques et géométriques. La zone d'infiltration est représentée par la succession dans le plan vertical de quatre sous-systèmes : le sol, l'épikarst, la zone non saturée et la zone saturée. Le sol est le siège de l'évapotranspiration et transforme le signal de pluie brute en infiltration efficace (I_{eff}). L'épikarst est schématisé par deux types de réservoir : le premier est identique à la figure 10 et distribue un flot de base (Q_b) et un flot de crue (Q_c) ; le second n'a pas d'écoulement de trop-plein et distribue uniquement un flot de base. A cheval entre la zone non saturée et la zone saturée, un autre réservoir représente un mélange d'eaux issus des deux réservoirs de l'épikarst. Finalement, la zone saturée est parcourue par un drain karstique qui collecte les écoulements de ces différents réservoirs et les mélange.

Les observations de terrain ont toutes été réalisées dans le drain karstique : les affluents ayant de petits bassins d'alimentation (moins de 160 m^2) sont alimentés uniquement par un réservoir de l'épikarst (réservoir sans trop plein pour les écoulements tamponnés ST et VI, réservoir à trop plein pour l'écoulement nerveux EC). Les affluents avec des tailles de bassin plus importantes (de l'ordre de 3000 m^2 pour SO et EN) sont un mélange d'eaux issues des deux réservoirs de l'épikarst. Leur réponse hydraulique relativement tamponnée semble indiquer une contribution importante du réservoir sans trop plein. Finalement les affluents alimentés par des bassins de grande taille (plus de 20'000 m^2) sont alimentés par un mélange de ces trois types d'écoulements (seepage, intermediate et vadose). Le comportement hydraulique nerveux de tous ces affluents (*conduit flow*) indiquent que la contribution du *vadose flow* est prépondérante.

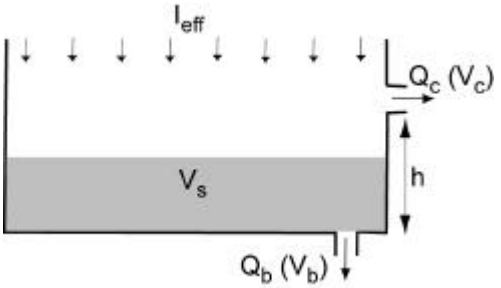

Figure 10 : modèle de réservoir permettant la répartition des infiltrations (Ieff) en volume de flot de base (Vb), volume de flot de crue (Vc) et volume stocké (Vs).

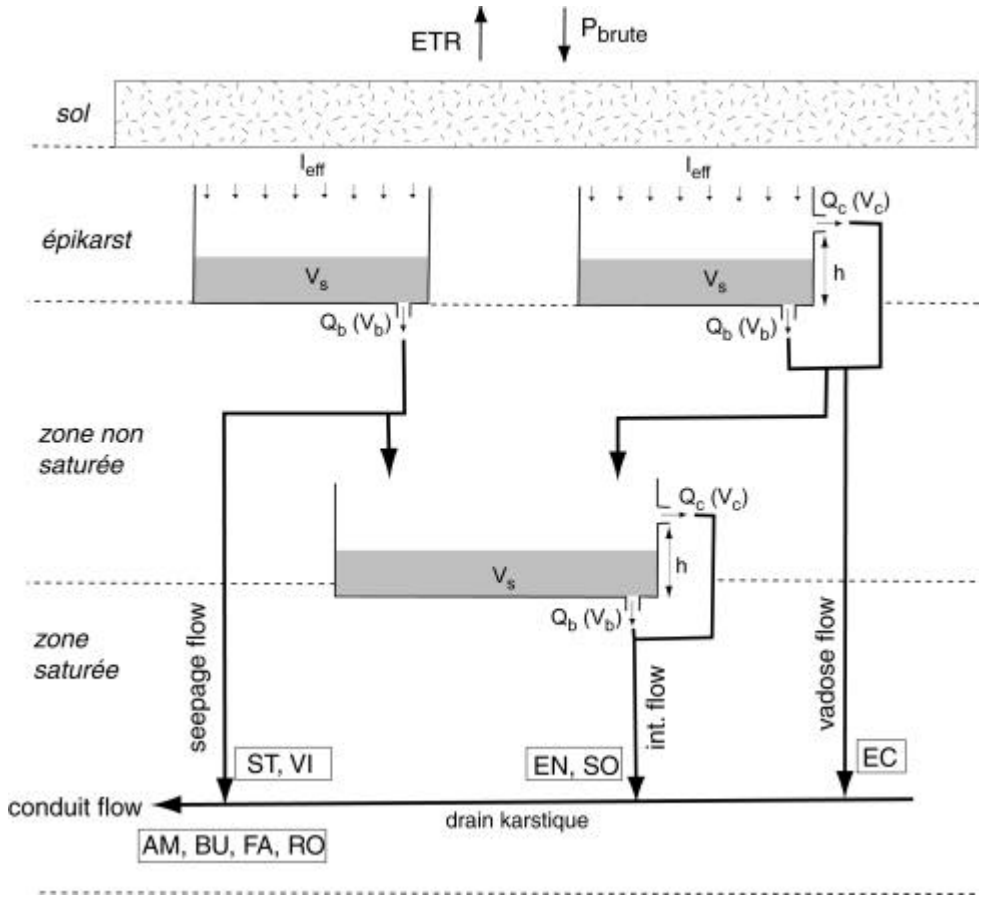

Figure 11 : modèle conceptuel représentant la hiérarchisation des infiltrations à partir de deux réservoirs situés dans l'épikarst. Les points mesurés lors de l'étude sont encadrés et regroupés en quatre familles correspondant au vadose flow, seepage flow, intermediate flow et conduit flow.

2.2.6. Conclusions

Les mesures en grotte de débits d'eau d'infiltration se sont multipliées ces dernières années : certaines études se sont limitées à l'observation d'une arrivée d'eau dans la zone non saturée (BAKALOWICZ & JUSSERAND 1987, MANGIN 1988, GENTY & DEFLANDRE 1998). Les résultats montrent l'existence d'un réservoir capacitif en sub-surface. D'autres études ont été réalisées également dans la zone non saturée mais sur plusieurs arrivées d'eau (SMART & FRIEDERICH 1986, SANZ & LOPEZ 2000, PERRETTE *et al*. 2001) : un comportement hydraulique très variable d'un point de mesure à l'autre a généralement pu être mis en évidence. Certains hydrogrammes ont une allure nerveuse comparable à la source du système karstique, montrant que le régime hydraulique du système peut s'acquérir dans la zone non saturée déjà. Toutes ces mesures ont été réalisées sur des arrivées de faibles débits (égouttement de stalactites par exemple), de l'ordre de 0.0005 l/min à 0.001 l/min.

Dans la présente étude, les débits sont beaucoup plus importants et couvrent une large gamme (0.06 l/min à 6000 l/min). Bien que la quantification des volumes des précipitations superficielles et ceux écoulés à la source de chaque affluent soit relativement précise, la répartition des infiltrations dans le milieu souterrain l'est quant à elle beaucoup moins. Cette étude a permis d'illustrer quelques spécificités du fonctionnement de l'infiltration :

- Plusieurs types d'écoulement existent également pour cette gamme de débits (nerveux, tamponnés et intermédiaires). Ces différences illustrent l'hétérogénéité spatiale du mode d'infiltration et des écoulements dans la zone vadose du karst.
- L'eau infiltrée lors d'une crue se répartit en moyenne en flot de crue pour 50 %, en flot de base pour 25-30 % et en volume stocké pour 20-25 %. Ces pourcentages sont valables pour toutes arrivées d'eau de type nerveuse.
- Le volume maximum stocké permet d'estimer le seuil des réservoirs alimentant les arrivées d'eau entre 13 mm et 32 mm. Cette hétérogénéité spatiale de la hauteur du stock est probablement liée à la grande variabilité des épaisseurs de sol et de l'épikarst observée sur le site.
- La gamme des débits mesurés oblige à hiérarchiser les écoulements. Le modèle conceptuel résultant (figure 10) indique que deux types de réservoir permettent d'expliquer tous les hydrogrammes mesurés. Ces deux réservoirs produisent des écoulements de *seepage flow* (ST, VI) et de vadose flow (EC). La combinaison de *seepage flow* et de *vadose flow* permet de générer les écoulements de *conduit flow* (AM, BU, FA, RO) et *intermediate flow* (SO, EN). Le *conduit flow* est essentiellement alimenté par du *vadose flow*.

Ces résultats indiquent que les caractéristiques hydrauliques du système karstique de Milandre s'acquièrent dans la zone non saturée, et qu'à priori, la zone saturée de l'aquifère n'a qu'un rôle limité. Le sous-système de l'épikarst devient le lieu privilégié pour la localisation des deux réservoirs définis dans le modèle conceptuel. Cette zone de décompression et d'intense dissolution a une porosité largement plus élevée que les calcaires sous-jacents. Les valeurs de porosité données dans la littérature sont comprises entre 1 et 10 % (GOUISSET 1981, WILLIAMS 1985, SMART & FRIEDERICH 1986). Ces auteurs soulignent également l'importante fonction de réservoir de l'épikarst. SMART & FRIEDERICH (1986) proposent un modèle de réservoirs permettant de reproduire les mesures de débit. Outre le *seepage flow* et le *vadose flow*, ils introduisent deux autres réservoirs alimentant le *shaft flow* et le *subcutaneous flow*. Ce dernier correspond simplement à des arrivées d'eau temporaire. Sur notre modèle, il pourrait s'agir de mesures sur le trop plein (Q_c) uniquement. Le *shaft flow* par contre pourrait être considéré comme la combinaison de plusieurs *vadose flow*.

Une exploitation plus approfondie de ces données pourrait apporter davantage d'informations sur les réservoirs : une modélisation journalière de l'évolution du stock au sein des réservoirs permettrait de connaître l'évolution de la charge et de mieux contraindre la géométrie. Il serait souhaitable de raffiner la connaissance de l'infiltration efficace : le paramètre devrait être distribué en fonction de l'assolement et devrait pouvoir être calculé à un pas de temps inférieur au jour. Des études complémentaires sur d'autres sites sont souhaitables afin de confirmer et de généraliser les idées présentées dans cet article. Il est toutefois primordial de maîtriser avec une précision suffisante les différents termes du bilan hydrologique.

Remerciements

Nous tenons à remercier le Professeur J-J. Delannoy de l'Université de Savoie et le Dr A. Grasso de l'Office Fédéral des Eaux et de la Géologie pour leurs remarques constructives lors de la relecture de cet article. Nous remercions le Spéléo Club Jura de nous avoir facilité l'accès à la grotte. Les données enregistrées par l'Institut Suisse de Météorologie ont été très utiles pour mener à bien ce travail. Au Centre d'Hydrogéologie, nous avons apprécié les compétences de P-Y. Jeannin, F. Bourret, S. Cattin et V. Puech. Cette étude a bénéficié du soutien du Fonds national de la recherche scientifique, subside n° 20-61717.00.

Références

BAKALOWICZ M. & JUSSERAND C. 1987. Etude de l'infiltration en milieu karstique par les méthodes géochimiques et isotopiques. Cas de la grotte de Niaux (Ariège, France). Bulletin du Centre d'Hydrogéologie de Neuchâtel 7 : 265-283.

DELANNOY J.-J., PEIRY J.-L., PERRETTE Y. & DESTOMBES J.-L. 1999. Articulation des aspects expérimentaux, théoriques et méthodologiques de l'étude d'un système karstique à des fins environnementales: le laboratoire de Choranche (Vercors-France). Karst 99 – European Conference, Etudes de géographie physique, supplément n° 18 : 77-82.

DESTOMBES J-L., CORDONNIER M., GADAT, J-Y., DELANNOY, J-J. 1997. Periodic and aperiodic forcing of water flow through sodastraw stalactites (Choranche,Vercors, France). Proceedings of the International Congress of Speleology, Switzerland, Volume 2 : 69-73.

DRACOS Th. 1980. Hydrologie, eine Einführung für Ingenieure. Springer Verlag Ed., 194 pp.

FORKASIEWICZ J. & PALOC H. 1967. Le régime de tarissement de la Foux de la Vis, Etude préliminaire. Chronique d'hydrogéologie n° 10 : 59-73.

GENTY D. & DEFLANDRE G. 1998. Drip flow variations under a stalactite of the Père Noël cave (Belgium). Evidence of seasonal variations and air pressure constraints. Journal of Hydrology 211 : 208-232.

GOUISSET Y. 1981. Le karst superficiel: genèse, hydrodynamique et caractéristiques hydrauliques. Univ. des Sciences et techniques du Languedoc, France, Montpellier, 218 pp.

GRASSO A. D. 1998. Interprétation des réponses hydrauliques et chimiques des sources karstiques. (Essai d'inférence de la structure des systèmes karstiques). Thèse de Doctorat, Univ. de Neuchâtel. 135 pp.

GRASSO A. D. & JEANNIN P.-Y. 1994. Estimation des pertes dans la partie aval du réseau karstique de Milandre : bilan hydrique au sein de l'aquifère karstique. Bulletin d'Hydrogéologie 13 : 115-128.

JEANNIN P.-Y. 1998. Structure et comportement hydraulique des aquifères karstiques. Thèse de Doctorat, Univ. de Neuchâtel. 237 pp.

JEANNIN P.-Y. & GRASSO A. D. 1995a. Estimation des infiltrations efficaces journalières sur le bassin karstique de la Milandrine (Ajoie, JU, Suisse). Bulletin d'Hydrogéologie 14 : 83-93.

JEANNIN P.-Y. & GRASSO A. D. 1995b. Recharge respective des volumes de roche peu perméable et des conduits karstiques, rôle de l'épikarst. Bulletin d'Hydrogéologie 14 : 95-111.

MANGIN A. 1988. Réflexions sur l'infiltration dans les karsts à partir de l'exemple de Niaux. Bulletin du Centre d'Hydrogéologie de Neuchâtel 8 : 3-25.

PERRETTE Y., DELANNOY J.-J., DESTOMBES J.-L. & PEIRY J.-L. 2001. Différents modes d'écoulement de la zone vadose du système de Choranche (massif du Vercors, France). Proceedings 7th Conference on Limestone Hydrology, Besançon : 269-272.

PERRIN J., JEANNIN P.-Y. & ZWAHLEN F . Epikarst storage in a karst aquifer : a conceptual model based on isotopic data. Milandre test site, Switzerland. soumis à Journal of Hydrology.

PRIMAULT B. 1963. Du calcul de l'évapotranspiration. Arch. Met. Geoph. Biokl. B., Bd. 12, H. 1, Zürich :124-150.

SANZ E. & LOPEZ J.J. 2000. Infiltration measured by the drip of stalactites. Ground water, Vol. 38, n° 2 : 247-253.

SMART, P.L. & FRIEDERICH, H. 1986. Water movement and storage in the unsaturated zone of a maturely karstified carbonate aquifer, Mendip Hills, England. In: D. National Water Well Association, Ohio. (Editor), Proc. Conf. env. problems of karst terrains and their solutions: 59-87.

SHAW E. M. 1994. Hydrology in Practice, Third Edition. Published by Chapman & Hall : 569 pp.

WILLIAMS P.W. 1983. The role of the subcutaneous zone in karst hydrology. Journal of Hydrology, 61: 45-67.

WILLIAMS P.W. 1985. Subcutaneous hydrology and the development of doline and cockpit karst. Zeit. Geomorph. NF. 29: 463-482.

2.3. Implications of the spatial variability of the infiltration water chemistry for the investigation of a karst aquifer. A field study at Milandre test site, Swiss Jura.

J. Perrin • P-Y. Jeannin • F. Zwahlen

Paper accepted by Hydrogeology journal

Abstract

The Milandre test site is an ideal karstic aquifer for studying the spatial heterogeneity of groundwater chemistry. Numerous observation points can be sampled: the spring, the underground river and its tributaries, and boreholes at different depths. Main causes of the spatial variability of the chemical parameters are: nature and localisation of the input, the structure of the infiltration zone, chemical reactions (transit time vs. reaction kinetics) and mixing of different waters. Observed chemograms at the spring of the karstic system represent the sum of this spatial heterogeneity. Therefore, it is difficult to interpret the global chemical response with a simple mixing model of the aquifer sub-systems (runoff, matrix reservoir, epikarst). Parameters issued from agricultural inputs show important seasonal variations (Coefficient of variation around 15 %) and parameters linked to rainfall ($\delta^{18}O$) and to the aquifer (Ca, HCO_3^-) present variations of a less than 5 %. This result indicates important water storage (a couple of months) in the epikarstic aquifer.

Résumé

Le site test de Milandre est un aquifère karstique idéal pour étudier l'hétérogénéité spatiale des éléments chimiques majeurs car de nombreux points d'observation sont accessibles : source, rivière souterraine et affluents, forages à différentes profondeurs. Les principales causes de la variabilité spatiale des paramètres chimiques sont : nature et localisation des intrants, la structure de la zone d'infiltration, la réactivité des paramètres (temps de transit vs. cinétique de réaction) et le mélange des eaux. Les chimiogrammes observés à la source du système karstique représentent la somme de cette hétérogénéité spatiale. Il est de fait difficile, pour un tel aquifère, d'interpréter la réponse chimique globale en termes de mélanges d'eau des différents sous-systèmes de l'aquifère (ruissellement, réservoir matriciel, épikarst). Les éléments chimiques correspondant aux intrants agricoles montrent des variations saisonnières relativement importantes (Coefficient de variation d'environ 15%) alors que les paramètres liés à la pluie ($\delta^{18}O$) et à l'aquifère (Ca, HCO_3^-) présentent des variations de quelques pour cents. Un tel résultat indique un stockage d'eau d'au minimum quelques mois dans l'épikarst.

Keywords: karst, solute transport, heterogeneity, contamination, hydrochemistry.

2.3.1. Introduction

Groundwater physico-chemical parameters are increasingly used for obtaining information on the structure and behaviour of karstic aquifers. Combined with hydraulic observations, they are used to estimate water transit times, percentage of waters issued from different parts of the aquifer, reactivity within the aquifer, vulnerability, and transport processes. Parameters recorded during flood events have been interpreted in terms of proportions of diffuse and point recharge (Scanlon and Thraikill 1987, Wicks 1997, Mayer 1999, Lakey and Krothe 1996, Hess and White 1988, Vervier 1990, Worthington et al. 1992), existence and importance of subsurface storage (Williams 1983, Lastennet and Mudry 1997, Bakalowicz et al. 1974), percentage of quick and matrix flow (Blavoux and Mudry 1983, Kiraly and Müller 1979). Hydrochemistry can also be used for testing conceptual models of the hydraulic behaviour of karst aquifers (Kiraly and Müller 1979, Grasso and Jeannin 1998).

Often these studies try to extrapolate observations done at the spring to the basin scale. Such an upscaling can cause some limitations in the validation of the interpretation. In order to avoid such a drawback, several authors started to record chemical parameters inside the karstic aquifer. These

studies consider several topics, such as the chemical evolution and kinetic processes along drains (Wicks and Engeln 1997, Groves 1992), residence times of waters issued from different tributaries (Wicks 1997), description of the spatial and temporal variability in the water chemistry (Perrin 1997, Mayer 1999, Liñan et al. 1999).

Our project enters in this second category of hydrochemical studies in which observations are made at different points in the aquifer. The first step, presented in this paper, considers the spatial variability of groundwater chemistry. The second step, which will be published later, aims at describing the temporal variability of some points selected from the observations made in the first phase. The main objectives are as follows:

- characterisation of the spatial variability of the parameters by sampling different tributaries within the aquifer;
- determination of the causes that control the spatial variability;
- evaluation of the information that can be inferred from the different types of natural tracers at the spring of a karstic system.

Such an empirical approach should improve the interpretation of karstic spring chemical responses and bring new ideas on solute transport and vulnerability of karst groundwater. The Milandre test site has been chosen for its accessibility and its well documented hydrodynamic behaviour (Jeannin 1996), which plays a prominent role in the chemistry of karstic aquifers (Kiraly and Müller 1979, Grasso 1999).

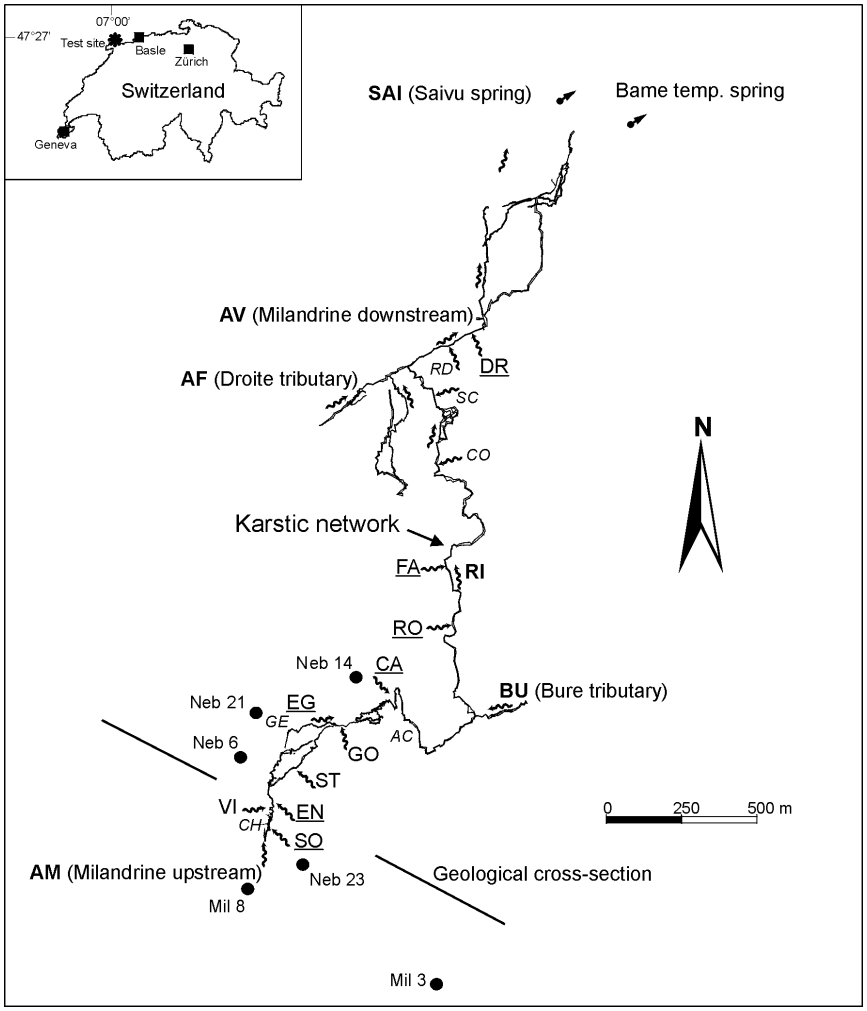

Fig. 1 *Map of the karstic network with location of the sampling points. Sites in bold correspond to main tributaries and the underground river, sites underlined to secondary tributaries, and other sites to percolation water. Sites in italic were sampled once. Dots indicate the location of the sampled boreholes.*

2.3.2. Study area

The Milandre test site is a karstic aquifer located in the Swiss tabular Jura in the vicinity of Basle, (Fig. 1). Fig. 2 presents a geological cross-section of the area illustrating the structure of the aquifer; diffuse infiltration recharges the Rauracian limestone overlying the Oxfordian marls, which limit the flow downwards. Piezometric levels are highly variable (Jeannin 1996), but the unsaturated zone is about 40 to 80 metres thick and the saturated zone is limited to a few tens of metres. A well developed karstic network drains the aquifer towards Saivu spring (Fig. 1). Sampling points are located along the drain and include the spring, the underground river and several tributaries.

The area receives around 1000 mm annual precipitation, which recharges the karst aquifer mainly by diffuse infiltration. The springs of the system are the Saivu, with a discharge varying between 20 and 150 l/s, and the Bame temporary spring with a discharge reaching up to 1500 l/s (overflow of the system). The regional flow system is mainly controlled by the karst conduit network and the dip direction of the Oxfordian marls aquiclude. The faulting has a limited effect on flow paths. The catchment area of Milandre karst system has a common limit to the W with the catchments of Val and Doux karst springs located further W (Fig. 3). To the E, Oxfordian marls plunges eastwards, and direct groundwater towards several small karst springs located along the Allaine alluvial plain. This plain limits the basin to the N, and controls the position of the discharge area. To the S, a change in the dip direction directs flow to the important Beuchire karst spring situated 5 km to the SE. The groundwater divides have been specified by numerous tracing experiments and piezometric measurements (Gretillat 1996, Jeannin 1995, 1996). The surface area of the whole catchment area is 13 km^2, which corresponds to estimation made from water budget calculations. It can be further divided into four sub-basins (Fig. 3):

1. Milandrine upstream sub-basin: its surface of 4.6 km^2 is occupied by cultivated land for 30 %, forests for 30 %, and meadows for 40 %. The small farming village of “Villars le Sec” (France) is entirely located in the basin. Several tracing experiments allowed to determine precisely the limits of the catchment (Favre 2001).
2. Bure tributary sub-basin: its surface of 3.6 km^2 is occupied by cultivated land for 10 %, forests for 20 %, and meadows for 50 %. The Bure village and a military camp are partly located within the catchment. Its limits have been confirmed by tracing experiments (Favre 2001).
3. Droite tributary sub-basin: its surface of 3.8 km^2 is occupied by cultivated land for 10 %, forests for 80 %, and meadows for 10 %. No tracer test was carried out in the catchment, and the limits are based on the geology and a water budget calculation.
4. Small tributaries and percolation waters: This basin includes all the water inlets encountered along the Milandre cave system. Surfaces of the different sub-basins have been estimated by water budget calculations, and the basins have been located directly above the respective inlets, as no tracing tests were available. The catchment is mainly cultivated in the upstream part, and occupied by forests and pasture in the downstream part.

The underground river, as well as several tributaries, have been equipped with continuous recording stations measuring parameters such as water levels that are converted in discharge with a rating curve, water specific conductance and temperature.

Tributaries discharge rates react differently to flood pulses: the drainage axis is very sensitive and shows repeated flooding, whereas some tributaries have delayed responses and others show completely dampened hydraulic signals.

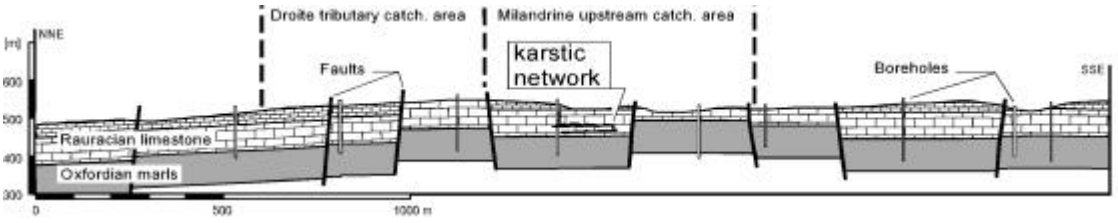

Fig. 2 *Geological cross-section showing the aquifer in the Rauracian limestone, the location of the karstic network and some boreholes.*

2.3.3. Methods and analyses

A preliminary study on the spatial variability of the chemical parameters has shown the adequacy of the site for illustrating the prominent role of land use, mixing processes and structure of the infiltration zone on the groundwater chemistry (Perrin et al. [in press]).

Sampling was carried out every month from June 1999 to July 2000. The day of sampling was chosen for its stable hydraulic conditions in the aquifer. This choice was made in order to get a sample set representative of the spatial variability, and the least influenced by concentration changes occurring during flood events (e.g. dilution by fresh infiltrated water). Each time, fifteen samples were collected, i.e. three along the main drain (SAI, AV, AM), two on the main tributaries (AF, BU), seven on secondary tributaries (DR, FA, RO, CA, EG, EN, SO) and three of percolation water (VI, GO ST) (Fig. 1). Water specific conductance and temperature were measured directly on site, pH was determined within 12 hours at sampling temperature, bicarbonate within 24 hours by titration and the other parameters were analysed by ionic chromatography after a 0.45µ filtration. For cation preservation, filtered samples were acidified to pH < 2 with HNO_3 suprapur. Nitrate concentrations in samples with or without formol were equivalent, therefore most samples were taken without it.

The quality of the analyses has been checked by ionic balances, which have to be comprised between 0 and 5 %, and by comparing calculated conductivity vs. measured conductivity. Oxygen-18 analyses have been carried out by the lab Hydroisotop Gmbh with the standard method of CO_2 equilibration and purification. The analytical precision is ± 0.15 ‰.

Raw data are available on the web at the following address: www.unine.ch/chyn (under karst hydrogeology research topic).

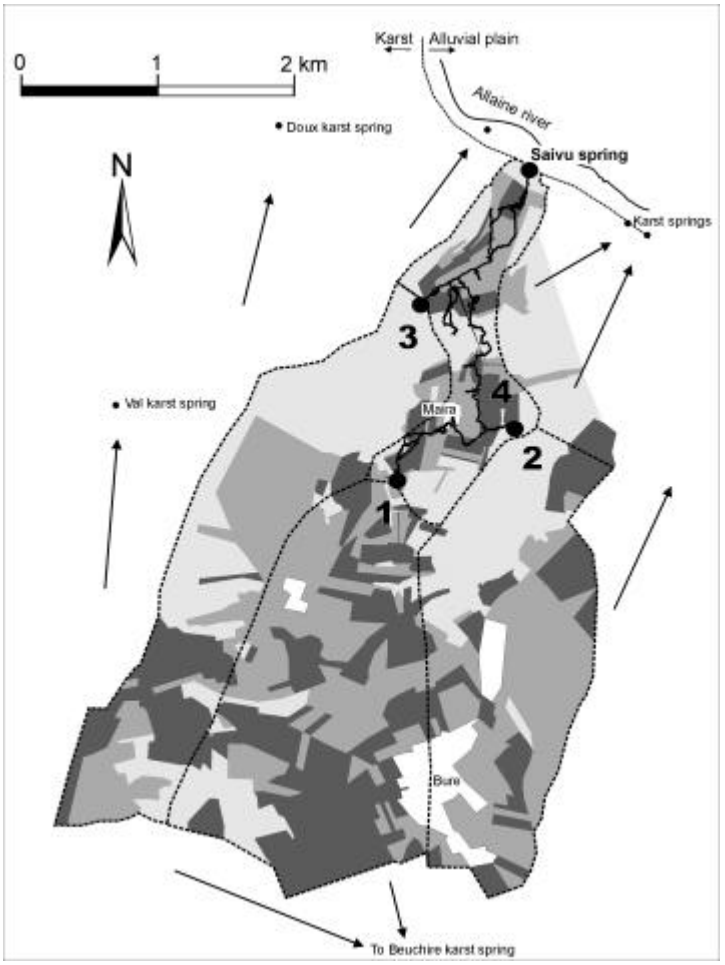

Fig. 3 *Simplified land use map of the Saivu catchment area. Pale gray represents forests, gray meadows and dark gray cultivated areas. Villages are represented in white and the Milandre cave system is indicated by the thick line. The four main sub-catchments are delineated by dashed lines: 1 is Milandrine upstream (AM), 2 is Bure tributary (BU), 3 is Droite tributary (AF), and 4 corresponds to the catchment of all the secondary tributaries encountered along the cave (i.e. SO, EN, EG, RO, FA, etc…)*

2.3.4. Data processing

Spatial variability of the water chemistry can be assessed only if the temporal variability of the available data is known and can be removed.

Physico-chemical and hydraulic parameters are illustrated in Fig. 4 for AM and SO tributaries. The first (AM) is the underground river in the upstream part: the discharge varies sharply in a short period of time but other parameters appear to be stable throughout the year. The main reason is the fact that sampling campaigns were carried out in base flow conditions. The second (SO) is a secondary tributary with a stable discharge during the dry season and marked floods in winter. It is less contaminated by nitrates and chloride than AM. The physico-chemical parameters also appear to be stable, similar to other sampling sites. Therefore, it can be hypothesized that average concentrations should give a good approximation of the representative chemistry of each outlet under base flow conditions. This hypothesis has been tested by estimating the importance of the temporal variability.

In order to work on the spatial variability, it is necessary to quantify the temporal variability of the data, and to reduce it if necessary. A simple way to characterize the temporal variability of a parameter is the coefficient of variation (CV, the standard deviation divided by the mean and expressed as a percent). The CV are given in Table 1. It appears that the most sensitive sites are RO, FA and to a lesser extent the underground river (AM, AV, SAI). The first is an outlet fed partly by sewage water from the Maira village, the second is an outlet very sensitive to rain events. Other sites have a low temporal variability.

An objective approach for testing the importance of the temporal variability is to compare the standard deviation intra-sites (temporal variability) and the standard deviation inter-sites (spatial variability). The principle is illustrated in Fig. 5 with a theoretical example of frequency distribution curves. Three categories can be distinguished:

1. the standard deviation (SD) intra-site is lower than the SD inter-site;
2. the SD intra-site is higher than the SD inter-site;
3. both are comparable.

The first case means that the temporal variability of the considered site is less important than the spatial variability, the second illustrates the opposite and the third indicates that the temporal variability of a site is comparable to the spatial variability.

Results are compiled in Table 2, and it appears that the inter-site SD is generally higher than the intra-site SD: the temporal variability of the samples is limited and the spatial variability is important for the data of Milandre test site (case 1). The parameters that best illustrate the spatial variability are nitrate, potassium, sulfate, chloride and magnesium. In contrast, temperature and $\delta^{18}O$, bicarbonate and even calcium show close intra-site and inter-site SD (case 3).

In karst systems, flood water can present a very different chemistry than base flow water. As an example, at AM specific conductance can decrease to 520 µS/cm, Ca^{2+} to 94 mg/l, or HCO_3^- to 300 mg/l (data not used in the present study). These values are far from the average values presented in Table 1. Hence the temporal variability of the data set has to be tested in order to keep only the data which represent the base flow chemistry of the sampling site.

The following procedure has been applied: analyses, which are out of the interval delimited by the standard deviation around the mean are discarded and thus the intra-site SD is strongly reduced. Corrected mean values have been compared to raw values in Table 1. The difference is systematically lower than 5 %. It demonstrates that the raw data are little affected by temporal variations and can be used for the study of spatial variability.

Mean values are given in Table 1. They can be considered as representative for base flow conditions at each station. The waters are all calcium-bicarbonate types with the exception of RO, which has anomalous high concentrations in sodium, potassium and chloride. This outlet is partly fed by sewage effluent from the small village of Maira. Major ion concentrations of sewage water are the following according to Dubreucq (1987): K^+: 44 mg/l, Na^+: 91 mg/l, Mg^{2+}: 8.5 mg/l, Ca^{2+}: 107 mg/l, SO_4^{2-}: 51 mg/l, Cl^-: 57 mg/l, NO_3^-: 11 mg/l. These values confirm the influence of sewage on RO tributary chemistry.

Owing to its peculiar chemistry, RO has been discarded in the statistical analysis presented in the following section.

Measured parameters can be split into two groups: the first, comprising nitrates, sodium, potassium, magnesium, chloride and even sulfates, is characterized by an important spatial variability and high CV. The second includes parameters with a more homogeneous distribution and low CV: pH, oxygen isotopic ratio, temperature, calcium and bicarbonates.

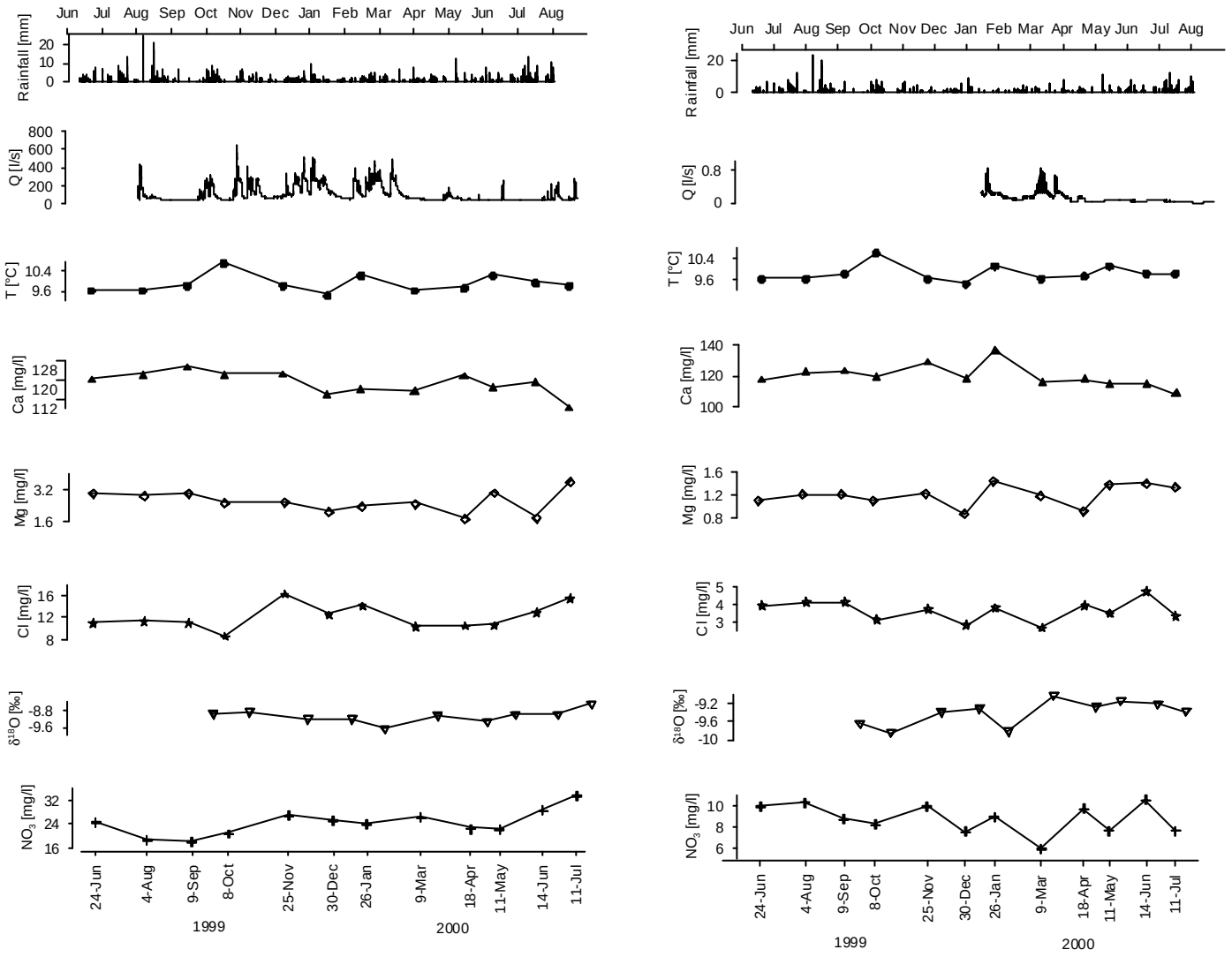

Fig. 4 *Temporal variation of the physico-chemical parameters for two differing tributaries: AM (river upstream) on the left and SO (secondary tributary) on the right.*

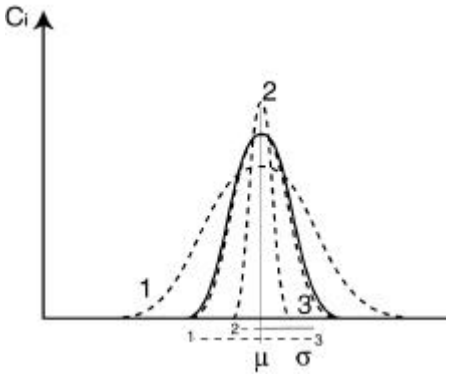

Fig. 5 *Theoretical frequency distribution curves for a parameter. The black curve represents the distribution of the intra-site concentrations. Dashed curves represent the three cases of inter-site distribution.* m *represents the mean and* s *the corresponding standard deviations.*

Table 1 *Data from the 15 sites located on Fig. 1. Means and coefficient of variation were calculated based on 12 measurements for the physico-chemical parameters and 10 measurements for* $d^{18}O$*. Sampling point are classified in three categories of decreasing flow rate: M.r.= Milandrine river, Tr.= Tributary, P.w.= Percolation water.*

average		Flow [l/s]	pH	Temp [°C]	Cond [mS/cm]	Na^+ [mg/l]	K^+ [mg/l]	Mg^{2+} [mg/l]	Ca^{2+} [mg/l]	Cl^- [mg/l]	SO_4^{2-} [mg/l]	NO_3^- [mg/l]	HCO_3^- [mg/l]	$d^{18}O$ [‰]
AM	M.r.	69.55	7.17	9.78	610.4	3.71	2.38	2.58	122.4	12.00	8.84	24.22	351.9	-9.14
BU	Tr.	44.16	7.27	9.84	586.9	3.67	2.30	*2.61*	114.6	8.71	9.69	17.08	344.1	-9.01
AF	Tr.	39.10	7.24	9.51	571.2	1.87	0.44	1.27	116.8	7.42	8.75	16.14	340.8	-9.19
AV	M.r.	140.25	7.25	9.86	598.6	3.17	1.87	2.25	117.3	10.20	9.31	21.01	347.8	-9.07
SAI	M.r.	140.25	7.26	9.90	598.7	3.42	1.94	2.34	119.5	10.50	9.62	21.55	349.0	-9.10
SO	Tr.	0.16	7.23	9.77	554.7	1.95	0.32	1.19	119.4	3.63	8.37	8.73	352.7	-9.36
VI	P.w.	0.001	7.27	9.98	610.9	3.21	0.27	2.62	125.9	13.33	11.27	43.50	324.6	-9.02
EN	P.w.	0.04	7.30	9.71	576.7	2.34	0.31	1.51	123.2	5.85	11.35	18.21	360.5	-9.37
ST	P.w.	0.02	7.26	9.98	663.0	2.46	0.40	1.37	137.3	9.79	16.55	55.93	357.6	-9.32
GO	P.w.	0.01	7.34	10.13	711.3	2.41	4.32	2.08	147.4	5.62	12.32	41.92	414.1	-9.51
EG	Tr.	0.98	7.29	9.65	636.6	2.21	0.84	1.75	133.5	8.37	13.06	30.06	373.0	-9.24
CA	Tr.	0.74	7.14	9.81	671.2	2.51	1.12	2.05	139.1	11.96	12.47	46.47	367.9	-9.10
RO	Tr.	0.43	7.28	10.35	683.1	4.72	25.24	3.80	118.5	14.66	10.92	27.60	371.8	-8.64
FA	Tr.	0.38	7.26	10.07	564.7	1.51	1.37	1.70	115.8	5.80	6.07	13.52	349.9	-9.27
DR	Tr.	1.02	7.24	9.97	585.7	1.77	0.99	2.92	119.3	7.72	8.15	13.00	353.5	-8.97
coefficient of variation [%]														
AM	M.r.	79.08	1.68	3.60	5.77	28.59	46.48	21.90	3.87	19.47	11.44	17.45	5.09	3.39
BU	Tr.	75.00	2.24	3.01	5.72	18.13	24.07	34.15	7.91	14.79	6.99	17.36	7.52	1.65
AF	Tr.	86.45	1.40	1.58	2.46	9.83	14.38	17.32	3.82	15.38	12.69	22.98	2.97	0.58
AV	M.r.	65.07	2.08	2.05	3.85	21.90	47.38	23.11	6.14	20.60	9.51	17.43	6.31	1.50
SAI	M.r.	65.07	2.12	1.86	3.94	35.00	51.90	14.86	6.14	22.87	13.42	19.19	6.73	3.51
SO	Tr.	156.32	1.29	3.30	5.08	14.25	20.08	14.73	6.21	16.27	17.41	16.07	3.32	2.95
VI	P.w.	18.75	2.38	3.81	4.52	18.61	33.80	16.46	5.64	5.87	7.56	9.75	1.72	1.29
EN	P.w.	158.97	2.57	3.57	6.18	13.06	28.55	16.90	4.20	9.48	14.18	14.30	1.90	1.38
ST	P.w.	158.47	1.40	3.61	5.26	13.30	23.09	16.28	4.73	8.07	7.55	6.64	2.31	1.24
GO	P.w.	117.89	2.60	3.12	5.59	12.82	6.74	13.39	2.58	10.08	9.17	10.61	1.74	1.09
EG	Tr.	65.21	1.40	3.83	5.49	12.18	13.10	15.52	3.48	12.35	7.87	17.44	2.21	1.39
CA	Tr.	60.97	1.06	1.76	7.63	12.33	8.59	17.09	2.43	8.41	7.74	6.91	1.74	1.66
RO	Tr.	110.47	2.04	1.32	7.41	39.03	52.64	23.84	5.85	38.43	24.82	32.14	5.96	3.28
FA	Tr.	220.29	2.26	1.60	4.19	27.37	68.79	20.80	4.41	36.15	36.91	43.61	5.56	3.30
DR	Tr.	101.61	1.61	1.44	3.64	18.31	22.15	29.18	4.68	16.26	24.47	27.59	5.33	2.26

Table 2 *Comparison of the standard deviation inter-site and intra-site in order to evaluate the importance of the temporal variability of the parameters. The corrected data column gives the standard deviation computed after suppression of the values, which are the most distant from the mean in both directions. Number in brackets indicates the quantity of values removed. RO site is not considered due to its specific chemistry.*

		Temp.		Na^+		K^+	Mg^{2+}		Ca^{2+}	Cl^-	SO_4^{2-}	NO_3^-	HCO_3^-		$d^{18}O$	
		raw data	corr. data	raw data	corr. data	raw data	raw data	corr. data	raw data	raw data	raw data	raw data	raw data	corr. data	raw data	corr. data
st. deviation																
inter-site		0.21	0.21	0.91	0.87	6.26	0.71	0.72	9.97	3.14	2.54	14.13	20.06	20.01	0.21	0.21
	AM	0.36	019 (3)	1.13	0.73 (1)	1.11	0.56		4.73	2.34	1.01	4.23	17.90		0.31	0.16 (2)
	BU	0.30	0.18 (1)	0.67		0.55	0.97	0.55 (1)	9.06	1.29	0.68	2.97	25.86	15.90 (1)	0.15	
	AF	0.15		0.18		0.06	0.22		4.45	1.14	1.11	3.71	10.14		0.05	
	AV	0.20		0.70		0.88	0.52		7.20	2.10	0.89	3.66	21.84	18.56 (1)	0.14	
st. deviation	SAI	0.18		1.20	0.50 (2)	1.01	0.35		7.34	2.40	1.29	4.14	23.47	16.98 (2)	0.32	0.17 (2)
intra-site	SO	0.32	0.19 (2)	0.28		0.06	0.18		7.42	0.59	1.46	1.40	11.70		0.28	0.16 (3)
	VI	0.39	0.20 (4)	0.60		0.09	0.43		7.10	0.78	0.85	4.24	5.57		0.12	
	EN	0.35	0.18 (3)	0.31		0.09	0.26		5.18	0.55	1.61	2.60	6.86		0.13	
	ST	0.36	0.21 (4)	0.33		0.09	0.22		6.49	0.79	1.25	3.72	8.25		0.12	
	GO	0.32	0.21 (4)	0.31		0.29	0.28		3.80	0.57	1.13	4.45	7.19		0.10	
	EG	0.38	0.19 (2)	0.27		0.11	0.27		4.65	1.03	1.03	5.24	8.24		0.13	
	CA	0.17		0.31		0.10	0.35		3.38	1.01	0.97	3.21	6.41		0.15	
	FA	0.16		0.41		0.94	0.35		5.11	2.10	2.24	5.90	19.47		0.30	0.18 (3)
	DR	0.14		0.32		0.22	0.87	0.68 (2)	5.59	1.25	1.99	3.59	18.86		0.20	

2.3.5. Illustration of the spatial variability

The Piper diagram (Fig. 6) represents average values obtained for the fifteen sites and additional single measurements taken from six boreholes and six tributaries (Table 3). The boreholes are located in forested areas (Neb 6, Neb 23), in meadows (Neb 21, Mil 8) and in cultivated land (Neb 14, Mil 3). Additional tributaries are distributed along the underground river. The spatial variability of the water chemistry is clearly illustrated by the elongated cloud of sampling points. It is possible to distinguish several groups: boreholes Mil 3 and Mil 8 are contaminated by NaCl inherited from former salt tracing experiments. These tracer tests were carried out in order to test the relation between the boreholes and the Milandrine upstream (Maréchal 1995).

Sewage water RO deviates in the direction of the NaCl pole. The points near the Ca^{2+}-HCO_3^- pole represent waters not influenced by human activities (CO, Neb 23, SC, Neb 6, SO). The points approaching the Mg^{2+}-NO_3^- pole are the most influenced (Neb 21, Neb 14, ST, CA, VI, GE) and the points in between seem to be a mixing of these tendencies (Milandre underground river and its main tributaries BU and AF).

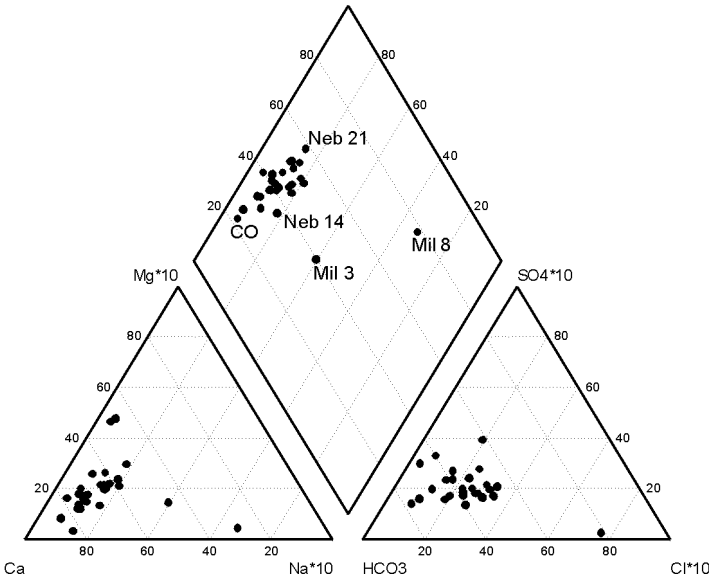

Fig 6 *Piper diagram showing the spatial variability of the data set. Concentrations in Mg^{2+}, Na^{+}, SO_4^{2-}, Cl^{-} are multiplied by a factor 10 in order to improve the readability of the graph.*

Table 3 *Data for samples collected once on one tributary (Tr.), five percolation waters (P.w.), and six boreholes (Bor.)*

Site		Flow	pH	Temp	Cond	Na^+	K^+	Mg^{2+}	Ca^{2+}	Cl^-	SO_4^{2-}	NO_3^-	HCO_3^-
		[l/s]		[°C]	[µS/cm]	[mg/l]	[mg/l]	[mg/l]	[mg/l]	[mg/l]	[mg/l]	[mg/l]	[mg/l]
RD	Tr.	0.2	7.19	9.9	570	1.57	0.78	2.08	122.6	5.58	13.2	8.3	356
CH	P.w.	0.003	7.16	9.8	496	2.20	0.20	2.40	91.0	6.60	8.2	12.0	298
AC	P.w.	0.1	7.18	9.8	633	1.97	0.81	1.87	115.8	7.51	9.0	27.3	364
SC	P.w.	0.01	7.29	10.1	566	1.47	0.94	6.79	110.0	2.81	6.0	2.7	351
CO	P.w.	0.05	7.11	9.6	587	0.96	0.54	1.54	120.0	2.39	5.3	0.1	372
GE	P.w.	0.08	7.16	10.0	770	3.49	5.24	2.88	144.0	14.50	12.4	55.6	394
Mil 3	Bor.		7.12	9.3	543	10.61	1.89	2.10	109.1	8.64	6.0	17.2	337
Mil 8	Bor.		7.22	9.3	824	36.67	0.62	1.30	137.9	75.33	3.5	15.4	367
Neb 6	Bor.		7.11	8.5	122	1.24	0.00	0.75	125.8	1.07	12.7	13.2	359
Neb 14	Bor.		7.12	8.8	779	4.56	0.03	1.86	158.4	6.71	8.1	112.9	377
Neb 21	Bor.		7.26	9.5	130	2.39	0.00	0.31	125.4	7.70	21.7	67.8	289
Neb 23	Bor.		7.20	8.4	563	1.20	0.09	6.58	113.6	2.42	15.4	3.0	356

2.3.6. Main causes of the spatial variability

Land use

Man induced inputs are highly variable at the basin scale, with large amounts of fertilizers used in cultivated areas to nothing in forested land. On the Milandre test site, about 20 % of the catchment is cultivated, 40 % is grazing pasture and 40 % forest (Fig. 3). The most contaminated sampling points drain cultivated catchment only (ST, EN, VI, Neb 14, Neb 23), whereas slightly contaminated tributaries are fed by a mixing of pristine and contaminated waters (Perrin et al. [in press]).

Solute inputs issued from agriculture can be estimated with the help of Table 4, which summarizes data found in the literature and our data. The values from Milandre are based on quantities of fertilizers used by the farmers and on two analyses of rainwater. Missing information has been completed with data presented by Pedersen et al. (1991). Their data are a compilation from several agricultural statistical tables.

The theoretical leachate chemistry is computed with the following equations:

$$M_{pi}(leachate) = M_{pi}(rain) + M_{pi}(fertilizer) + M_{pi}(manure) - M_{pi}(plant) \quad (1)$$

$$V_w = I_a S \quad (2)$$

$$C_{pi}(leachate) = \frac{M_{pi}(leachate)}{V_w} 10^3 \quad (3)$$

with

M_{pi} = mass of parameter p_i [kg/ha/year]

C_{pi} = concentration of parameter p_i [mg/l]

V_w = yearly water volume infiltrated on 1 hectare [m^3/ha/year]

I_a = actual infiltration [m/year]

S = surface [m^2]

Equation (1) gives the mass of fertilizer available for leaching per hectare and per year. This mass is converted in a concentration by equations (2) and (3) using a yearly actual infiltration of 500 mm.

Results (Table 4) are in agreement with concentrations measured in Milandre (Table 1) except for calcium. Such a result indicates that the source of the ions K^+, Na^+, Mg^{2+}, SO_4^{2-}, Cl^-, NO_3^- is mainly due to fertilizers. Farmers use mainly combined chemical fertilizers containing nitrogen, phosphorus, potassium, and magnesium. Manure and liquid manure are used as complementary sources, which contain all the pollution related parameters. Thus, land use in the sub-catchment plays a key role in the spatial variability of groundwater chemistry at least for these parameters.

Inputs are also dependent on the actual infiltration, knowing that evapotranspiration processes act in a completely different manner depending on if the area is cultivated or forested. This process can increase concentrations of the ions, influence the temperature of the infiltrated water or even change isotopic ratios. Evapotranspiration can cause a $\delta^{18}O$ enrichment of around 1.2 ‰ in rain compared to the water collected in lysimeters (Blavoux 1978). This process should be determinant for the differences of isotopic ratios of the sampling sites (from -8.64 ‰ for RO to -9.51 ‰ for EG), as the altitude effect on precipitation isotopic composition is negligible at the Milandre site.

Table 4 *Origin and quantification of the chemical parameters issued from agriculture based on the literature and original data. The last column gives an approximation of leachate concentration based on a mean actual infiltration of 500 mm (Jeannin and Grasso 1995). Values taken from Pedersen et al. (1991) and accepted for this study are shown in italic.*

		rain	fertilizer	manure	plant remov.	available for leaching	
		[kg/ha/year]	[kg/ha/year]	[kg/ha/year]	[kg/ha/year]	[kg/ha/year]	[mg/l]
K^+	this study	5	50	37	*80*	12	2.4
	Dubreucq (1987)	1.9	5		50		
	Pedersen et al. (1991)	3	45	85	80	53	
Na^+	this study	3	*1*	*15*	*6*	13	2.6
	Dubreucq (1987)	2.6					
	Pedersen et al. (1991)	2	1	15	6	30	
Mg^{2+}	this study	0	4	6	*6*	4	0.8
	Dubreucq (1987)	0.7	2.5		10		
	Pedersen et al. (1991)	3	4	10	6	11	
Ca^{2+}	this study	10	*29*	20	*25*	34	6.8
	Dubreucq (1987)	18	25		25		
	Pedersen et al. (1991)	3	29	30	25	40	
SO_4^{2-}	this study	16	*33*	*45*	*21*	73	14.6
	Dubreucq (1987)	35	8.5		12		
	Pedersen et al. (1991)	39	33	45	21	96	
Cl^-	this study	6	*38*	*30*	*35*	39	7.8
	Dubreucq (1987)	19	3				
	Pedersen et al. (1991)	37	38	30	35	70	
NO_3^-	this study	10	340	320	*330*	330	66
	Dubreucq (1987)	20	62		530		
	Pedersen et al. (1991)	75	550	528	330	823	

Chemical reactions

In case of limestone dissolution along the drainage axis, dissolution related parameters (calcium, bicarbonate and specific conductance) concentrations should increase from AM to AV and SAI. The contrary occurs due to dilution by less mineralised waters issued from the major tributaries BU and AF.

Even if pH has not been measured in the field, qualitative values of calcite saturation indices could be calculated by the Phreeqe software with an accuracy of ±0.15. Saturation indices are comprised between 0.12 and 0.25 (unpublished data). Highest values are obtained for seepage waters issued from speleothems located at the base of the unsaturated zone (EN, ST, GO). Other samples are close to equilibrium with respect to calcite. However, dissolution related parameters show a clear spatial variability. As dissolution processes occur mainly in the unsaturated zone, the observed spatial variability is acquired in this sub-system. It is well known that water gets its acidity by dissolution of soil CO_2 (White 1988). Unpublished measurements on the Milandre site show that soil pCO_2 is spatially heterogeneous with generally more CO_2 in thicker soils; at 90 cm depth on the same day, pCO_2 changes from 1.2 % under a forested area to 3.6 % under tillage. This variability is likely to directly influence the differences observed in Ca^{2+} and HCO_3^- concentrations.

Nitrates and sulfates are subject to redox reactions under certain conditions. At the Milandre test site, oxidation processes are limited to the soil zone and the epikarst. Below the parameters are stable during their transit to the spring. During flood events, the underground river can show traces of nitrites, but in concentrations lower than 1 mg/l.

Mixing processes

The role of mixing is illustrated in Fig. 7. The drainage axis (Milandre River) is located in the middle of the plot, as the water is a mixing of tributaries with contrasting solute concentrations. Nitrates can be less than 10 mg/l in some outlets and over 50 mg/l in others. The underground river stabilizes at around 21 mg/l.

Mixing processes are often described in the literature but generally only two or three end-members are considered: matrix reservoir and direct infiltration (Blavoux and Mudry 1983), rain water and pre-storm water (Lakey and Krothe 1996), concentrated infiltration, diffuse infiltration and water issued from low permeability volumes (Vervier 1990), conduit storage, subcutaneous storage and fresh water (Williams 1983, Sauter 1992) and rain, soil, epikarst, and phreatic water (Lee and Krothe 2001).

From the Milandre test site, we get a more complex image of mixing processes, as chemistry is heterogeneous even at the low stage where only one end-member (storage) should be present. However, it has to be kept in mind that the site probably has a higher heterogeneity than other “better preserved“ aquifers due to the impact of agricultural inputs on groundwater chemistry.

The prominent role of mixing on the water chemistry of the main drain has been tested by a simple mixing model given by the following equation:

$$C = \frac{\sum_i C_i Q_i}{\sum_i Q_i} \qquad (3)$$

with

C = modeled concentration

C_i = measured concentration at site i

Q_i = discharge at site i

Sampling sites with low discharge were not considered, as their impact on the modeled concentration is not significant. Thus, the concentration at site RI (middle part of the main drain) has been computed with data from AM, SO, EG, CA, BU and RO. The concentration at site AV (downstream part of the drain) has been calculated with the same sites as mentioned above, completed with the AF and DR sites.

Measurements taken on July 11, 2000, are given in Table 5 for chloride (conservative ion), nitrate (sensitive to redox processes) and ion indicators of calcite dissolution or precipitation (calcite, magnesium, bicarbonate). Five sets of measurements are summarized in Fig. 8. Normalized differences between modeled and measured values are comparable to the conservative ion chloride, except for magnesium sampled on January 26, 2000. This exception is probably due to inaccurate analyses for RI and AV samples. The normalized difference between modeled magnesium concentration at AV and measured concentration at SAI spring is 4% only.

The consistency of the mixing model pinpoints the absence of significant chemical reactions (dissolution, redox) in the aquifer during stable hydraulic conditions. Changes by mixing in the water chemical composition are mainly caused by the high discharge tributaries BU and AF. The other outlets account for less than 1 mg/l variation even if their chemistry is clearly distinct compared to the underground river.

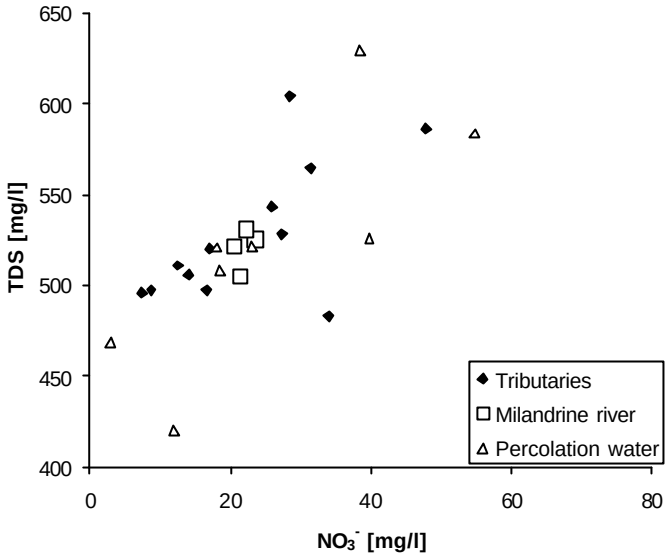

Fig. 7 *Correlation between mineralisation and nitrates, and illustration of the mixed origin of the spring water. The correlation is attributed to changes in the soil thickness in the respective catchment. Forested catchments have thin unfertilized soils, with a low production of CO_2 and thus produce less mineralized waters. On the contrary, cultivated catchments have thick fertilized soils, with an elevated production of CO_2 giving more mineralized waters.*

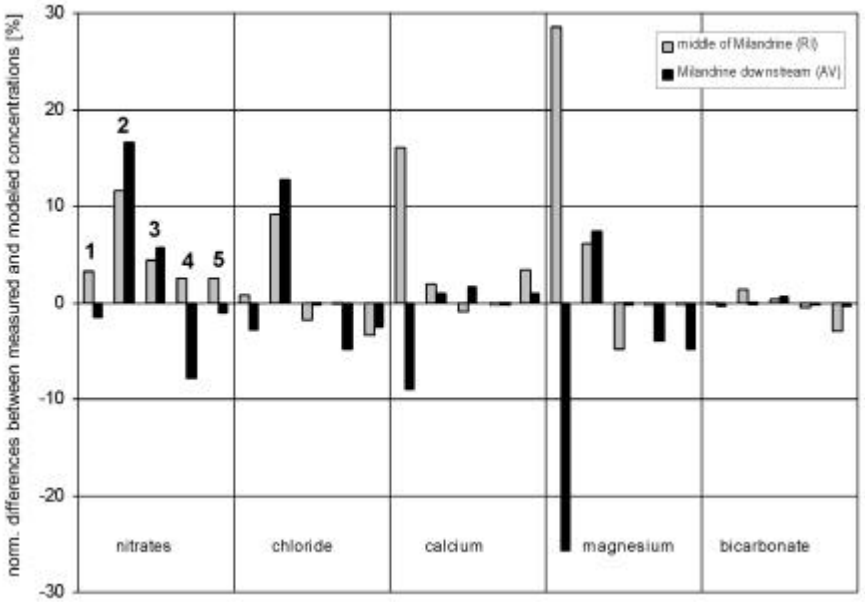

Fig. 8 *Comparison of the concentrations calculated by a simple mixing model and the measured concentrations in the middle part of Milandrine (RI) and on Milandrine downstream (AV). The calculation is based on the results of five sampling campaigns: 26-Jan-00 (1), 11-Jul-00 (2), 30-Dec-99 (3), 11-May-00 (4), 09-Mar-00 (5).*

Table 5 *Results of the mixing model calculation for the 11th of July 2000 sampling campaign.*

	AM	SO	CA	EG	BU	RO	AF	DR
Q [l/s]	32	0.02	0.41	0.78	29	0.14	30	0.26
NO_3^-	33.3	7.6	43.2	21.7	12.8	30.7	12.1	21.6
flux [mg/s]	1065.6	0.2	17.7	16.9	371.2	4.3	363.0	5.6
c_{calc} [mg/l]		33.3	33.4	33.1	23.7	23.7	19.9	19.9
c_{meas} [mg/l]						**26.6**		**23.5**
Cl^-	15.5	3.3	11.6	7.1	6.9	20.9	6.4	5.5
flux [mg/s]	496.0	0.1	4.8	5.5	200.1	2.9	192.0	1.4
c_{calc} [mg/l]		15.5	15.4	15.2	11.4	11.4	9.8	9.7
c_{meas} [mg/l]						**12.5**		**10.9**
Ca^{2+}	112.0	108.0	134.0	127.0	95.0	107.0	112.0	109.0
flux [mg/s]	3584.0	2.2	54.9	99.1	2755.0	15.0	3360.0	28.3
c_{calc} [mg/l]		112.0	112.3	112.6	104.4	104.4	106.9	106.9
c_{meas} [mg/l]						**106.0**		**108.0**
Mg^{2+}	3.6	1.3	2.5	1.8	2.7	4.4	1.3	3.4
flux [mg/s]	115.20	0.03	1.03	1.40	78.30	0.62	39.00	0.88
c_{calc} [mg/l]		3.6	3.6	3.5	3.1	3.2	2.6	2.6
c_{meas} [mg/l]						**3.4**		**2.8**
HCO_3^-	326	346	362	368	281	349	323	314
flux [mg/s]	10432	7	148	287	8149	49	9690	82
c_{calc} [mg/l]		326	326	327	306	306	311	311
c_{meas} [mg/l]						**310**		**311**

2.3.7. Discussion

Specific characteristics of the parameters

The measured physico-chemical parameters can be classified in order to establish what kind of information they supply. This classification is based on the discussion made in the paragraphs preceding and is summarized in Table 6. Three groups can easily be distinguished: land use related parameters, dissolution parameters, and parameters dependent on physical processes. The same type of classification can be extended to karstic aquifers with the following characteristics: agriculture on the catchment, oxygen saturated groundwater, rapid flow, and shallow saturated zone (50 m or less).

The next step is to see what kind of information can be obtained from these groups using spatial and temporal (on a seasonal and on a flood scale) observations.

Table 6 *Classification of the physico-chemical parameters by their statistical and chemical characteristics. S.V.= spatial variability, C.V.= coefficient of variation.*

	High S.V. and C.V.	Low S.V. and C.V.
Non reactive	K^+, Na^+, Mg^{2+}, SO_4^{2-}, Cl^-, NO_3^-	T, $\delta^{18}O$
Reactive		pH, HCO_3^-, Ca^{2+}

Land use related parameters

Spatial variability will denote a contrasted land use in the catchment with cultivated land, pasture, forests and/or urbanized areas. Temporal variability on a seasonal scale will indicate changes in the input rate and/or low storage. For a flood event, it will indicate changes in the respective contribution of the sub-catchments.

Dissolution parameters

Spatial variability will be an indicator of contrasting soil CO_2 availability (dependent on soil thickness, altitude, vegetation type).

Temporal variability on a seasonal scale should denote climatic related changes in CO_2 production. For a flood event, it will be an indication of transit times, as dissolution kinetics will compete with flow velocity. This assertion has been developed by Ternan (1972) and Wicks (1997) for computing groundwater residence using water calcium hardness CV. In both cases, the waters partly issued from a point recharge with high temporal variability and low residence time. In Milandre (Table 7), residence times vary widely, and it appears that shorter times are obtained for tributaries draining forested or urbanized areas whereas, longer times correspond to drainage of cultivated land. Reservoirs in the unsaturated zone seem larger under cultivated areas with thicker soils. However, the calculated residence times have to be considered in a qualitative way as the data set is too fragmented to have strong statistical validity.

Table 7 *Calculated residence time following the equation of Ternan (1972). Values range between 15 and 163 days. The 30 days obtained for Saivu spring illustrates the mixing of waters with different ages. The highest residence times are obtained for tributaries draining catchment located in cultivated areas with thick soils.*

Site	Hard.CV [%]	Res. time [d]
AM	3.63	75
BU	8.35	15
AF	3.15	99
AV	6.02	29
SAI	5.88	30
SO	6.02	29
VI	5.55	33
EN	3.88	66
ST	4.52	49
GO	2.62	140
EG	3.18	97
CA	2.42	163
RO	5.08	40
FA	4.15	58
DR	4.22	56

Parameters dependent on physical processes

Spatial variability will be mainly related to altitude differences of the sub-catchments (not the case in Milandre) but could also denote contrasted evapotranspiration due to land use and vegetation. Temporal variability on a seasonal scale will give an idea of residence times in the aquifer. For a flood event, it will indicate the presence of rapid flow from the surface.

These distinctions will be helpful for the interpretation of the data collected during flood events and should allow a better interpretation of chemograms.

2.3.8. Conceptual model of solute transport

To summarize the observed spatial variability, a conceptual model of solute transport is presented in Fig. 9. It shows the physical and chemical processes, which play a role in the groundwater chemistry of the Milandre test site. Rainwater is a major source of ions in natural areas, especially for sulfate, chloride, nitrate and potassium (Table 2). In cultivated or inhabited areas, fertilizers, sewage and salt for road works release large amounts of ions into the system. Evapotranspiration, plant consumption, ion exchange, oxidation, and CO_2 hydration mainly take place in the soil zone. These processes lead to important solute concentration changes. Soil is therefore the sub-system of major importance, as its thickness governs land use (thick soils are cultivated whereas thin soils are forested) and its physical properties control many biochemical processes.

Below the soil, a significant part of the water is stored in the epikarst sub-system or circulates slowly in the non-saturated zone, as indicated by the low temporal variability of $\delta^{18}O$, which is the sole non-reactive parameter with an evenly distributed input (Table 1). Transit times in the epikarst seem in most cases sufficient for reaching equilibrium with respect to calcite. Water then discharges to the drains and the saturated zone. No chemical reactions (reduction, precipitation) could be observed in normal hydraulic conditions along the drainage axis. Water chemistry changes are essentially caused by mixing of waters issued from different infiltration zones.

Chemographs at the spring represent the sum of the contrasted chemistry of the tributaries. For this type of aquifer, application of a mixing model with two end-members (e.g. runoff and matrix reservoir) would be a dangerous approximation. Such models do not take into account the existing spatial variability of the parameters. However, the chemistry of the tributaries will give information for each catchment on land use, CO_2 production and storage: outlets fed by a large reservoir (e.g. in the epikarst) should have a relatively constant chemistry throughout the year. In contrast, outlets draining rapid infiltration will show contrasted chemograms.

Use of mixing models is correct below the so called “equilibrium line” (Fig. 8). This line represents the trace of the surface below which groundwater becomes chemically equilibrated with respect to a given parameter. Each chemical reaction will have its own surface, depending on the reaction kinetics. This surface is dependent on the transit time and therefore on the hydraulic conditions in the aquifer. During flood events, the line will move downstream and could reach the spring for some dissolved species (e.g. HCO_3^-).

2.3.9. Comparison with models from the literature

Conventional studies (Bakalowicz 1979, Blavoux and Mudry 1983, Lastennet and Mudry 1997) define natural tracers for the aquifer sub-systems. They separate waters issued from the soil – epikarst with high chloride and sodium concentrations, from waters located in low permeability volume of the saturated zone with high magnesium and sulfates concentrations. For the Milandre aquifer, this separation is not possible due to the importance of man induced inputs on these parameters. Natural tracers of the aquifer sub-systems have to be defined after a preliminary study, which determine the spatial variability and the true origin of the parameters.

End-member mixing models (Lee and Krothe 2001) cannot be applied to aquifers such as Milandre. Within each sub-system, the water chemistry is too heterogeneous. The main drawbacks of these models are that they need a unique chemical composition for each system and that they do not take into account possible chemical changes due to reactions during flood events.

These mixing models seem the most appropriate for karst aquifers with a dual recharge mode (point and diffuse). Generally, the point recharge has a chemistry inherited from another geological context, which clearly contrast with diffuse groundwater chemistry (Vervier 1990, Scanlon and Thraikill 1987, Worthington et al. 1992).

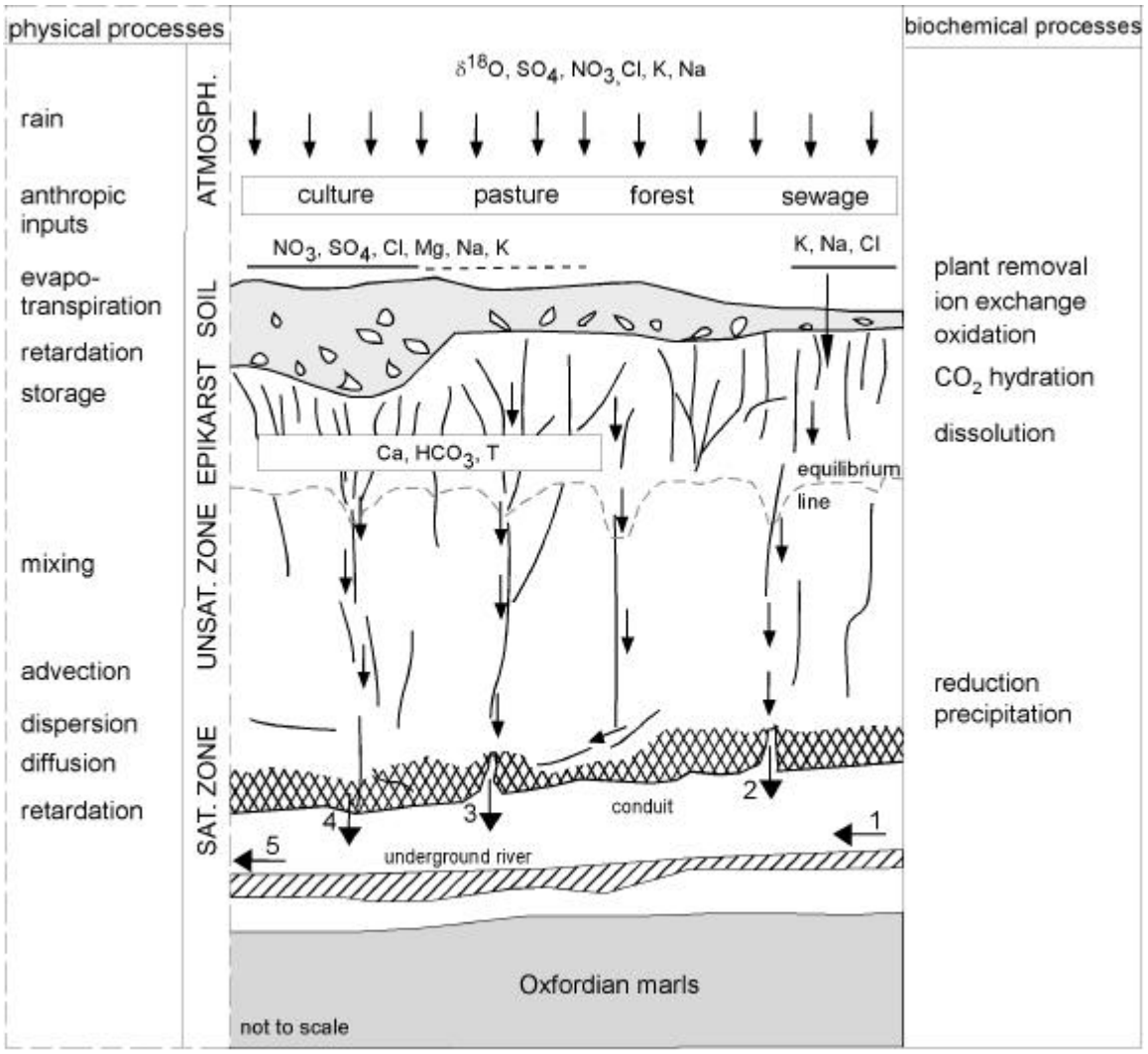

Fig. 9 *Conceptual model of solute transport at Milandre test site. Observation points (i.e. groundwater samples) are located in the conduit. Some waters come directly from the epikarst (2), others from the saturated zone symbolized by the wired surface (4); most of them are a mixing of different origins (3). The chemistry of drain water (1) is changed by the arrival of tributaries 2, 3, 4 and mixing gives drain water 5 a different chemistry.*

2.3.10. Conclusions

The major conclusions of this study are the following:

1. The spatial variability of the groundwater chemistry of the Milandre test site has been clearly established. Land use controls to a large extent concentrations of pollution related parameters in the tributaries of the karst system. The less contaminated are fed by basins which are mainly forested, whereas the more contaminated drain basins which are cultivated. Mixing of waters of contrasted chemistry can modify notably the final water composition. Chemical reactions have a limited effect on the observed spatial variability, at least in normal flow conditions.
2. The soil zone plays a prominent role in the spatial variability of the groundwater chemistry. Its properties control land use and CO_2 production.
3. All the observation points show generally saturated waters with respect to calcite and oxygen. In normal flow conditions, chemical reactions (dissolution, oxido-reduction) are limited to the soil and the epikarst zone. Downstream, change in groundwater chemical composition is mainly due to mixing processes.

4. Different types of tracers can be distinguished: non-reactive spatially heterogeneous tracers such as nitrate, which are directly related to land use, reactive tracers such as bicarbonate which are mainly dependent on dissolution processes, and conservative tracers represented by oxygen isotopes, which have a spatially homogeneous input. These tracers do not have the same time-dependency. Therefore, temporal measurements should allow the inference of transit times and structure of the aquifer.

In the future, detailed investigations in the epikarst and the soil should be carried out in order to better understand the reactivity of these sub-systems. Sampling on flood events will allow estimations on storage and transit times in the unsaturated zone. The importance of mixing compared to chemical reactions will be assessed. The objective is to develop a conceptual model consistent with the observed hydraulics and transport in the infiltration zone. Such a model should help to improve existing aquifer protection methods applied to karst aquifers.

Acknowledgments

This project is supported by the Swiss National Science Foundation, Grant n° 20-61717.00. We are indebted to the Jura Caving Club for access to the cave and to Boncourt local authorities for sending numerous samples from the spring. At the Centre of Hydrogeology, T. Ettlin, F. Bourret, B. Wenger and S. Cattin gave us priceless support for the field and the lab work. John Van Brahana and one anonymous reviewer are thanked for their fruitful comments.

References

Bakalowicz M (1979) Water geochemistry contribution to the study of karst aquifers. PhD dissert, University Pierre et Marie Curie, Paris [in French]

Bakalowicz M, Blavoux B, Mangin A (1974) Apport du traçage isotopique naturel à la connaissance du fonctionnement d'un système karstique [Contribution of natural isotopic tracing to the study of the behaviour of a karstic system]. Journal of Hydrology 23: 141-158

Blavoux B (1978) Study of the water cycle by the mean of Oxygen 18 and Tritium. PhD dissert, University Paris 6 [in French]

Blavoux B, Mudry J (1983) Décomposition chimique des hydrogrammes du karst [Chemical separation of karst springs hydrographs]. Hydrogéologie 4: 270-278

Dubreucq F (1987) Hydrochemistry of Cuisance springs, French Jura: karst, soils and anthropic influences. PhD dissert, University of Besançon, France [in French]

Favre I (2001) A database of tracing experiments at Milandre test site: GIS and statistical analysis. Unpubl. MSc thesis, University of Neuchâtel, Switzerland [in French]

Grasso D A (1999) Interpretation of hydraulic and chemical responses of karstic springs. PhD dissert, University of Neuchâtel, Switzerland [in French]

Grasso D A, Jeannin P-Y (1998) Statistical approach to the impact of climatic variations on karst spring chemical response. Bulletin d'Hydrogéologie 16, special issue Modelling in Karst systems: 59-76

Gretillat P-A (1996) Porous and karstic aquifers of Ajoie (swiss Jura). Data for the 1/25’000 hydrogeological map. PhD dissert, University of Neuchâtel, Switzerland [in French]

Groves C G (1992) Geochemical and kinetic evolution of a karst flow system: Laurel creek, West Virginia. Groundwater, 30(2): 186-191

Hess J W, White W B (1988) Storm response of the karstic carbonate aquifer of south-central Kentucky. Journal of Hydrology 99: 235-252

Jeannin P-Y (1995) Action Cost 65- Projets Bure et Hölloch (Suisse): cadre théorique, position des problèmes, présentation des sites étudiés et des données disponibles [Cost 65 action- Bure and

Hölloch projects (Switzerland): theoretical context, problems and presentation of the studied sites and of the available data]. Bulletin d'Hydrogéologie 14: 53-82

Jeannin P-Y (1996) Structure and behaviour of karstic aquifers. PhD. Dissert, University of Neuchâtel, Switzerland [in French]

Kiraly L, Müller I. (1979) Hétérogénéité de la perméabilité et de l'alimentation dans le karst : effet sur la variation du chimisme des sources karstiques [Heterogeneity of the permeability and the infiltration in the karst: effect on the karstic springs water chemistry variations]. Bulletin du Centre d'Hydrogéologie 3: 237-285

Lakey B, Krothe N C (1996) Stable isotopic variation of storm discharge from a perennial karst spring, Indiana. Water Resources Research 32(3): 721-731

Lastennet R, Mudry J (1997) Role of karstification and rainfall in the behavior of a heterogeneous karst system. Environmental Geology 32(2): 114-123

Lee E S, Krothe N C (2001) A four component mixing model for water in karst terrain in south-central Indiana, USA. Using solute concentration and stable isotopes as tracers. Chemical Geology 179, 129-143.

Liñan C, Andreo B, Carrasco F, Vadillo I (1999) Hidrodinamica e Hidroquimica de las aguas de goteo de la cueva de Nerja. In: C D Andreo (ed) Contribucion del estudio cientifico de las cavidades karsticas al conocimiento geologico Malaga, 393-402

Mayer J (1999) Spatial and temporal variation of groundwater chemistry in Petitjohns cave, Northwest Georgia, USA. Journal of Cave and Karst studies 61(3): 131-138

Maréchal J-C.(1994) Study and modelling of transport processes in karst conduits. MSc. Thesis Hydrogeology Centre, Neuchâtel University [in French]

Pedersen J K, Bjerg P L, Christensen T H (1991) Correlation of nitrate profiles with groundwater and sediment charactersitics in a shallow sandy aquifer. Journal of Hydrology 124: 263-277

Perrin J (1997) Géologie et géochimie des eaux dans le réseau du Grand Cor [Geology and water chemistry in the Grand Cor cave system]. In: P-Y Jeannin (ed), 6th Conference on limestone hydrology and fissured media, La Chaux-de-Fonds, 99-102

Perrin J, Jeannin P-Y, Zwahlen F (in press) Spatial variability of groundwater chemistry within a karst aquifer (Milandre test site, Swiss Jura).In Karst 2000: New trends in karst studies, Marmaris Turkey.

Sauter M (1992) Quantification and forecasting of regional groundwater flow and transport in a karst aquifer (Gallusquelle, SW Germany). PhD dissert, University of Tübingen.

Scanlon B R, Thrailkill J. (1987). Chemical similarities among physically distinct spring types in karst terrain. Journal of Hydrology 89: 259-279

Ternan J L (1972) Comments on the use of a calcium hardness variability index in the study of carbonate aquifers; with references to the central Pennines, England. Journal of Hydrology 16: 317-321

Vervier P (1990) Hydrochemical characterization of the water dynamics of a karstic system. Journal of Hydrology 121: 103-117

Wicks C M (1997) Origins of Groundwater in a Fluviokarst Basin: Bonne Femme Basin in Central Missouri, USA. Hydrogeology Journal 5(3): 89-96

Wicks C M, Engeln J F (1997) Geochemical evolution of a karst stream in Devils Icebox Cave, Missouri, USA. Journal of Hydrology 198: 30-41

Williams P W (1983) The role of the subcutaneous zone in karst hydrology. Journal of Hydrology 61: 45-67

Worthington S R, Davies G J, Quinlan J F (1992) Geochemistry of springs in temperate carbonate aquifers : recharge type explains most of the variation. In: Chauve P, Zwahlen F (ed) 5ème colloque en pays calcaire, Neuchâtel, 341-346

White W.B. (1988) Geomorphology and hydrology of karst terrains. Oxford University Press, Oxford

2.4. Epikarst storage in a karst aquifer: A conceptual model based on isotopic data, Milandre test site, Switzerland.

Jérôme Perrin*, Pierre-Yves Jeannin, François Zwahlen

Centre of Hydrogeology, Neuchâtel University, 11 rue E-Argand, 2007 Neuchâtel, Switzerland

Paper accepted by the Journal of Hydrology

Abstract

The Milandre test site is a karst aquifer characterized by diffuse infiltration, a well developed conduit network, and several tributaries feeding an underground river. Field data include discharge rate measurements, stable isotopes, weekly rainfall and spring-water isotope sampling, and detailed isotope sampling during three flood events. Flood sampling was carried out at several tributaries corresponding to conduit flow, vadose flow and seepage flow.

Weekly sampling showed a strong buffering of the rainfall isotopic signal at the spring. This attenuation suggests an important mixing reservoir in the system. Flood events showed highly peaking hydraulic responses but buffered rain isotope responses. These results indicate that the soil and epikarst sub-systems have an important storage capacity. A conceptual model of flow and transport in the soil and epikarst zone is proposed: Soil plays an important role in mixing due to the presence of capillary water storage. Consequently dampened concentrations reach the epikarst despite a rapid hydraulic response. The epikarst acts as the storage element and distributes water as either a base flow component or a quick flow component. When recharge exceeds a given threshold, excess infiltrated water bypasses the soil and epikarst and reaches the saturated zone as fresh flow. Based on this model, the significance of phreatic storage is thought to be limited, at least in Milandre test site. Hence the saturated zone is seen mainly as a transmissive zone through its well developed conduit network.

Keywords: karst hydrology, solute transport, water storage, stable isotopes, unsaturated zone.

2.4.1. Introduction

Flow behaviour of karst systems is characterized by recharge (diffuse/concentrated), storage (vadose/phreatic), and flow (diffuse/concentrated) (Smart and Friederich, 1986; Ford and Williams, 1989; White, 1988). In the present study we focus on cases with diffuse recharge (no swallow holes or sinking streams) and conduit flow (presence of large cave systems). The aim is to characterize soil and epikarst storage using a coupled approach by means of isotopes and flow. The determination of storage characteristics is done by comparing the input isotopic signals (rain infiltration) with the isotopic content of the underground inlets in the cave roof between 35 and 55 m below ground surface.

These environmental tracers are injected in a diffuse way over the whole catchment during rainfall events. They can be considered as perfect tracers since they belong to the water itself and do not react with the subsurface environment. Stable isotopes (^{2}H and ^{18}O) vary in the rain signal both on a seasonal scale and during a recharge event (Dansgaard, 1964; Blavoux, 1978) and keep a stable ratio in the karst aquifer. Tritium is a radioactive isotope that follows a well-known law of disintegration. However its concentration in rainfall is becoming too low for groundwater dating in karst aquifers with short residence time. Therefore stable isotopes alone were used during the present study.

A few studies using stable isotopes have been completed at the catchment scale in karst systems: Firstly, authors attempted to estimate mean transit time by comparing isotope signal maximum and minimum ratios both in the rain and at a spring on a long term basis. The time shift was used as an indicator of this transit time (Bakalowicz et al., 1974; Mueller et al., 1982; Stichler et al., 1997). This method is correct for linear and stationary systems only, and thus poorly adapted to karst systems (Margrita et al. 1984).

Secondly, some studies observed short term isotopic variations at springs due to important recharge events. These variations are caused by the mixing of fresh infiltrated water having a different isotopic

composition than the aquifer. The time shift between signal input and output was used for estimating conduit flow transit times (Maloszewski et al., 2002). A two end-members model was applied for computing the percentage of fresh infiltrated water contributing to spring flow (Mueller et al., 1982; Lakey and Krothe, 1996).

Other studies have been carried out in the unsaturated zone. A comparison between ^{18}O temporal evolution in the rain and in cave percolation water showed a complete dampening of the signal (Yonge et al., 1985; Chapman et al., 1992; Caballero et al., 1996; Bakalowicz and Jusserand, 1987), or more contrasted responses: some percolation waters showed no variations and others were influenced by strong recharge events (Harmon, 1979; Atkinson et al., 1985).

The present study aims to use isotopes in a more complete manner that links data issued from the unsaturated and the saturated zones. Measurements of ^{18}O have been carried out at different scale both temporally and spatially. Spatially, it was demonstrated (Perrin et al., 2003) that the isotopic values of the tributaries feeding the spring are very similar at steady-state. Temporally, short-term variations are expected. They should allow:

- to test the effectiveness of the buffering in the different part of the aquifer (unsaturated and phreatic zones), and hence to get information on storage and transit times.
- to estimate the effective contribution of newly infiltrated water to quick flow
- to produce a conceptual model of flow and storage in the unsaturated zone allowing the interpretation of flow and transit times in the saturated zone to be derived.

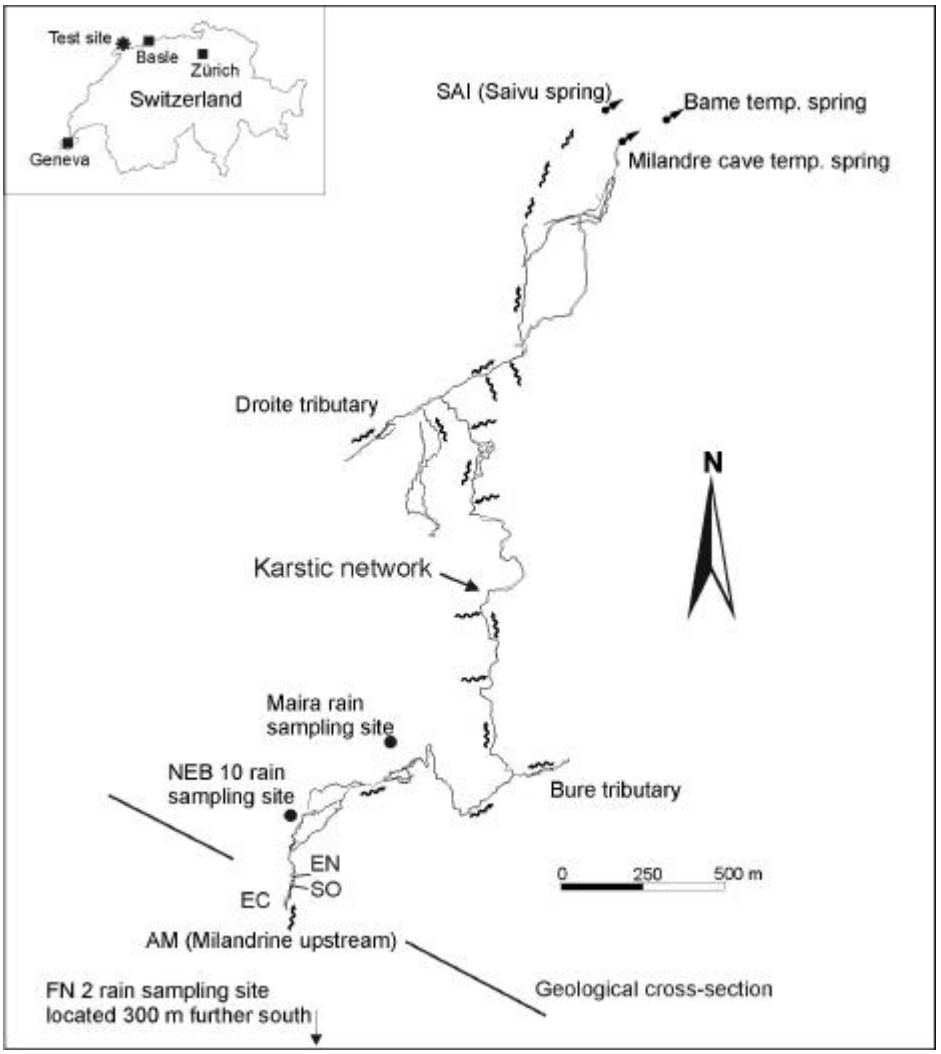

Fig. 1. Milandrine underground stream and its tributaries: location of the sampling points.

2.4.2. Study area

The Milandre test site is part of a karstic aquifer located in the Swiss tabular Jura in the vicinity of Basle, (Fig. 1). It has been intensively studied for the last decade. A thorough knowledge of the hydraulics of the system has been developed using numerous borehole measurements, water levels, discharge and tracing tests (Grétillat, 1996; Jeannin, 1996; Grasso, 1999).

Fig. 2 presents a geological cross-section of the area illustrating the structure of the aquifer: diffuse infiltration recharges the Rauracian limestone overlying the Oxfordian marls, which limit the flow downwards. Piezometric levels are highly variable (Jeannin, 1996). The unsaturated zone is about 40 to 80 metres thick and the saturated zone is limited to a few tens of metres. A well developed karstic network drains the aquifer towards Saivu spring (Fig. 1). Sampling points are located along the drain and include a spring, an underground river and several of its tributaries. The hydraulic behaviour of the sampling points is heterogeneous: seepage flow (SO, EN) showing buffered hydraulic responses, vadose flow (EC) with strong hydraulic reaction to recharge pulse, and conduit flow (AM, SAI) with rapid responses to storm pulses and high discharge

The area receives around 1000 mm annual precipitation that recharges the karst aquifer mainly by diffuse infiltration. Rain samples for isotopic analyses were collected in the middle of the catchment area. The springs of the system consists of the Saivu, with a discharge comprised between 20 and 200 l/s, and the Bame temporary spring with a discharge reaching up to 1500 l/s. The catchment area, defined by numerous tracing experiments and a water budget calculation, is estimated to be on the order of 13 km^2 (Grétillat, 1996; Jeannin, 1996). Land is used as pasture, forestry, tillage, and locally for settlement. Soil thickness varies from nothing to a few metres and consists mainly of silty loam, highly cohesive. Thicker soils are generally colluvial. Perrin et al. (2003) showed the strong relation between land use and spatial variability of the ground water chemistry.

The underground river, as well as several of its tributaries, have been equipped with continuous recording stations measuring parameters such as water levels, specific conductance and temperature.

Tributaries react differently to flood pulses: the drainage axis is very sensitive with frequent floods. The main tributaries (Droite and Bure, Fig. 1) react similarly to the main stream, whereas some small tributaries have delayed responses, and others show completely dampened hydraulic signals.

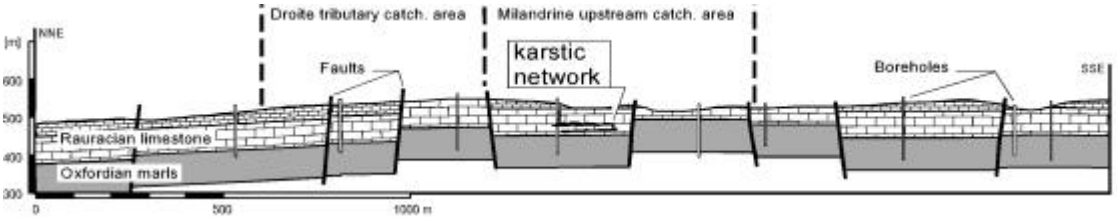

Fig. 2. Geological cross-section showing the aquifer in the Rauracian limestone, the location of the karstic network and selected boreholes.

2.4.3. Sampling and analytical procedures

The Saivu spring and rainfall have been sampled on a weekly basis over two and a half years. Flood events were sampled on a high resolution time scale adapted to expected discharge variations. In addition to rainfall and Saivu spring, other tributaries located in the upstream part of the underground river were also sampled (Fig. 1). These tributaries are, in decreasing order of discharge, AM (the underground river upstream, 20-600 l/s), SO (0.04-0.4 l/s), EN (0.005-0.3 l/s) and EC (0.02-1.5 l/min). These points are located between 40 and 50 metres below the ground surface. Water was collected in 50 ml plastic bottles carefully filled and sealed in order to avoid any degassing or contamination by air.

Stable isotope analyses were carried out at Hydroisotop Gmbh, Germany within six months after sampling. Isotope compositions are reported in the usual δ-scale in parts per thousand (‰):

$$d_{sample} = \left(\frac{R_{sample} - R_{SMOW}}{R_{SMOW}} \right) \cdot 10^3 \quad (1)$$

where *R* is the ratio $^{18}O/^{16}O$ or $^{2}H/^{1}H$. Accuracy is +/- 0.15 ‰ for $^{18}O/^{16}O$ and +/- 1.5 ‰ for $^{2}H/^{1}H$. Regular duplicates confirmed the quality of the analyses.

Continuous water level measurements were carried out with piezometric probes connected to a datalogger. Data were converted into discharge after the determination of the relation water level – discharge from punctual gauging experiments. Discharges values have an accuracy at around 10 %.

Weekly samples were collected by hand at the Saivu spring, and with a funnel-collector at Maira village for rainfall. Additional bulk samples were taken near NEB 10 and FN 2 sites (Fig. 1). Flood events sampling was carried out with the help of autosamplers. Carefully cleaned bottles were collected on a regularly basis at Milandrine upstream (AM), EC percolation water, SO and EN tributaries, Saivu spring (SAI). An autosampler was also installed at the Maira hut (directly above AM) for sampling of rainfall falling on the roof at 10 minutes interval.

Raw isotopic data are available on the web at the following address: www.unine.ch/chyn.

In order to compare correctly input and output concentrations, isotopes fluxes have to be considered (Margrita et al., 1984). In the following, we accounted for fluxes by comparing mean weighted concentrations (C_w) defined as:

$$\overline{C_w} = \frac{\sum Q_i C_i}{\sum Q_i} \quad (2)$$

Where Q_i is the discharge or the rain intensity at time *i*, and C_i is the concentration at time *i.*

2.4.4. Results

Rainfall and spring long-term isotopic observations

1. Input isotopic signal

A bulk sample of rainfall (giving the mean isotopic composition of rainfall) was sampled every week at Maira village. Possible effect of evaporation in the sampling device was checked by cross-analyses of oxygen and hydrogen stable isotopes. Points correlate along a straight line with a correlation coefficient of 0.96 (number of samples = 90) indicating that the evaporation effect can be neglected. Oxygen isotopes show a clear seasonal trend with maximum values in summer (mean value at -6 ‰) and minimum values in winter (mean value at -11 ‰). However the short term variability of the signal is important and is probably due to heterogeneous rainfall intensities, which directly influence the isotopic composition of the rain (Fig. 3).

Point source recharge that can modify the input function (Katz et al., 1998), does not exist at Milandre test site. Moreover no altitude effect is sensitive on the isotopic composition of infiltration water (Perrin et al., 2003). Hence the input function at one point can be considered as representative for the whole basin. This assumption is also confirmed by the similar composition of the bulk samples collected at different sites.

2. Spring isotopic signal

The oxygen isotopic response at the spring is highly buffered. However, the signal has also a strong variability related to the temporally non-linear mixing of infiltrated waters (Fig. 3). The main deviations from the average isotopic ratio occur during important flood events caused by infiltrated waters with a

contrasted isotopic composition (September 1999, March 2000, August 2000, December 2000, March 2001, September 2001).

3. Comparison of the input and output signals

The consistency of both signals has been checked by comparing the mean weighted concentrations. The estimation has been made over the whole observation period: Results give -9.12 ‰ at the Saivu spring and -9.45 ‰ in the rain. The small difference is probably due to evaporation in the initial stage of the recharge process. Other isotopic studies in the unsaturated zone showed a $\delta^{18}O$ enrichment by evaporation up to 1.5 ‰ in the epikarst (Bar-Matthews et al. 1996), and 4.5 ‰ in the soil zone (Hsieh et al., 1998). Hence it appears that for Milandre site evaporation has a limited effect on the isotopic composition. Consequently ^{18}O tracer can be considered as a conservative tracer.

The seasonal variations in the input function are strongly reduced at the spring. Such a dampening illustrates the existence of an important storage component allowing an efficient mixing of the infiltrated water with stored water (Bakalowicz et al., 1974). The transit times through this reservoir should be at minimum equal to the period of the input function, i.e. one year, for a complete disappearance of the input signal.

In case of important recharge, the isotopic composition of spring water deviates from its mean. This results from a significant contribution of fresh infiltrated water to the flood. Transit times of this fresh water are comparable to the sampling pace (i.e. one week). A good example is the important flood event of March 2001, which activated Milandre cave temporary spring that had been dry for years. Over a two weeks period, the Saivu spring showed oxygen isotopic values at around -9.8 ‰. This value is significantly lower than the spring average. Rainfall for the same period has also a lower isotopic signal at around -15 ‰. Hence fresh infiltrated water contributed to discharged water at the spring during this important flood event.

Main results of the weekly sampling are:

- coherence of the input and output signals showing the non reactive behaviour of the tracer
- a strong buffering of the input signal at the spring
- perturbation of the output signal during important flood events. The participation of fresh infiltrated water seems to be the main cause.

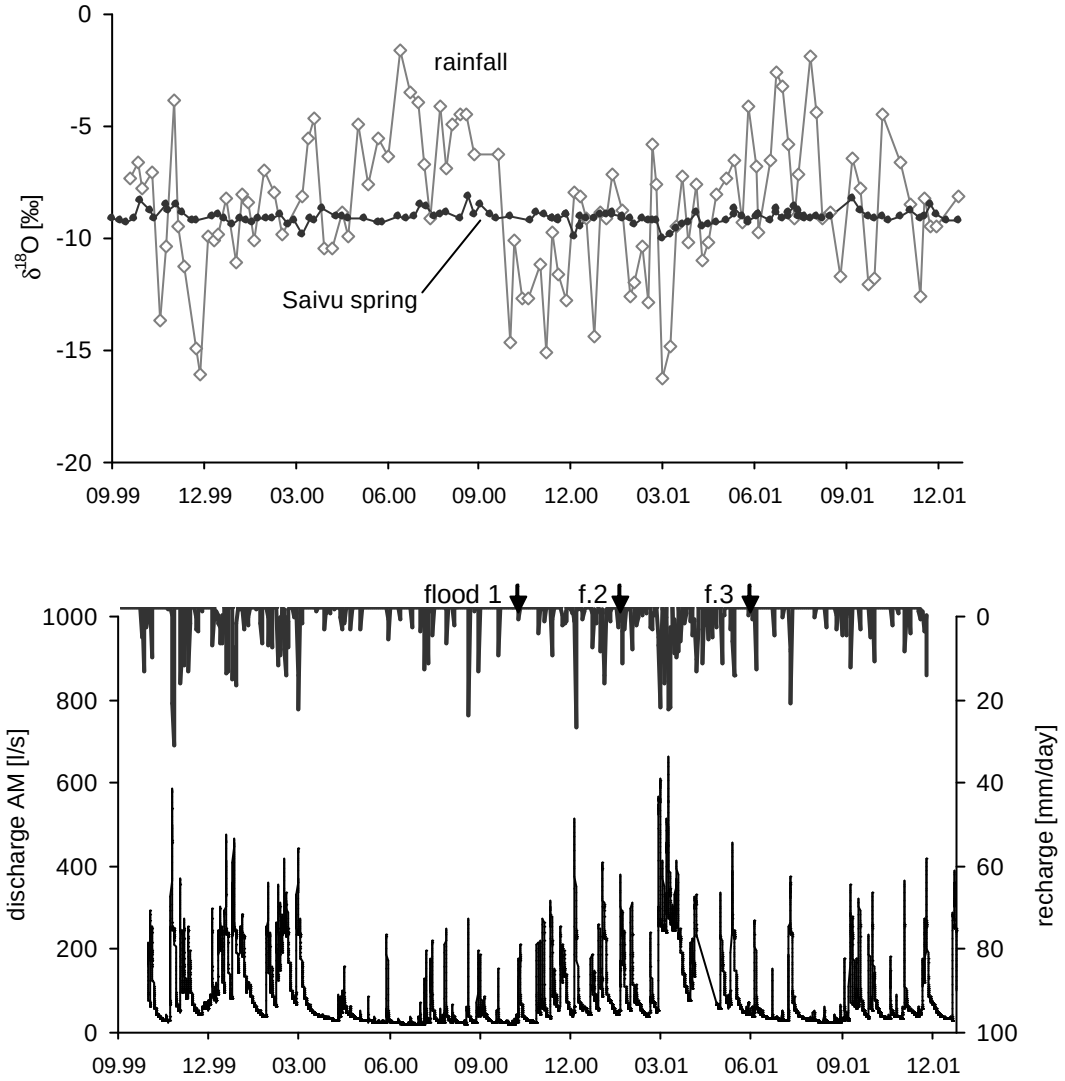

Fig. 3. The upper graph shows the $d^{18}O$ evolution in rainfall (Maira village site), and at Saivu spring. The lower graph presents actual infiltration and discharge at Milandrine upstream (AM) for the same period. Floods 1, 2, and 3 are those which are described in detail later.

Isotopic signal during flood events

Three flood events were sampled in October 2000, January 2001 and June 2001. For each period, water was collected at a sampling point just above the upstream part of the cave system for rainfall, at the Saivu spring (SAI), and in the upstream part of the underground river (AM). Apart from this, some tributaries were sampled on an irregular basis (SO, EC, EN). In the following, data from SAI are not shown as they are comparable to the observations made at AM.

1. October 2000 flood event (Fig. 4)

The flood started after continuous rainfall during the morning of the 11th of October. Daily infiltration calculated by the model of Jeannin and Grasso (1995) is 2.8 mm (13 mm total rainfall). It followed a dry period of about three weeks. Rainfall had already started on the 6th of October, continuing the 8th, the 9th and the 10th. However no recharge occurred, as the soil water moisture deficit was high (no infiltration given by the model and no discharge increase observed in the stream). Discharge at Milandrine upstream (AM) increased about 4 hours after the start of the main rainfall event (October 11). Discharge at SO tributary did not change significantly.

This flood event is relatively small with a maximum discharge in the Bame-Saivu system of less than 450 l/s. The response to infiltration is rapid (a few hours) and the pulse duration is limited (one day).

- Rainfall: Bulk samples before the flood (October 4 to October 9) have an oxygen-18 isotopic composition at -10.07 ‰ (Maira village), -13.01 ‰ (FN 2 site), and -12.48 ‰ (NEB 10 site). Bulk samples of the flood event (October 11, 5 a.m. – 5 p.m.) give -11.18 ‰ (FN 2 site), and -11.24 ‰ (NEB 10 site). Detailed sampling at Maira hut gives the following short term evolution (Fig. 4): the first 8 mm of rain have a weighted average isotopic composition at -9.8 ‰ and the next 5 mm are at -12.5 ‰. The residual rain does not contribute significantly to recharge. These values are in agreement with the samples collected from FN 2 and NEB 10, showing that the signal can be considered representative at basin scale.
- Aquifer: Groundwater isotopic signals show no significant changes with all variations included within the analytical error (± 0.15 ‰). Mean weighted values are -9.25 ‰ for SO, and -9.05 ‰ for AM.

These results show that the fresh water infiltrated during the event does not contribute significantly to the groundwater flowing during the flood pulse.

2. January 2001 flood event (Fig. 5)

This flood started January 24, 1:30 after continuous rain began falling, and lasted till the 29th. The event can be separated in three successive floods of decreasing magnitude, each linked to a rainfall event: calculated daily actual infiltration is 17 mm the 24th, 7 mm the 25th and 7.5 mm the 27th. A small flood had occurred the day before the sampling event (3 mm actual infiltration leading to a slight discharge increase at AM) and, before the hydraulic conditions were stable for about two weeks.

The flood of January 24, following a small flood the day before, started at 112 l/s and reached 400 l/s, a third small flood followed one day later and a last January 27. SO tributary shows a highly buffered hydraulic response with an increase in discharge starting the 24th and a peak occurring on the 28th. EC tributary has strong responses, except for the first flood which is barely visible.

- Rainfall: the isotopic signal shows a strong decrease (Fig. 5). The weighted mean value is -12.19 ‰, which is close to the values found in the bulk samples collected in the vicinity of NEB 10 and FN 2 boreholes (respectively -11.72 ‰ and -11.83 ‰).
- Aquifer: the isotopic evolution in the aquifer (Fig. 5) shows that no significant change occurs for SO. EC first presents a decrease associated with the first flood; it then returns to pre-flood values at the beginning of the 25th and decreases again with the arrival of the second flood. AM shows a slight increase associated with the start of the flood event, and then starts decreasing at around 16:30 the 25th.

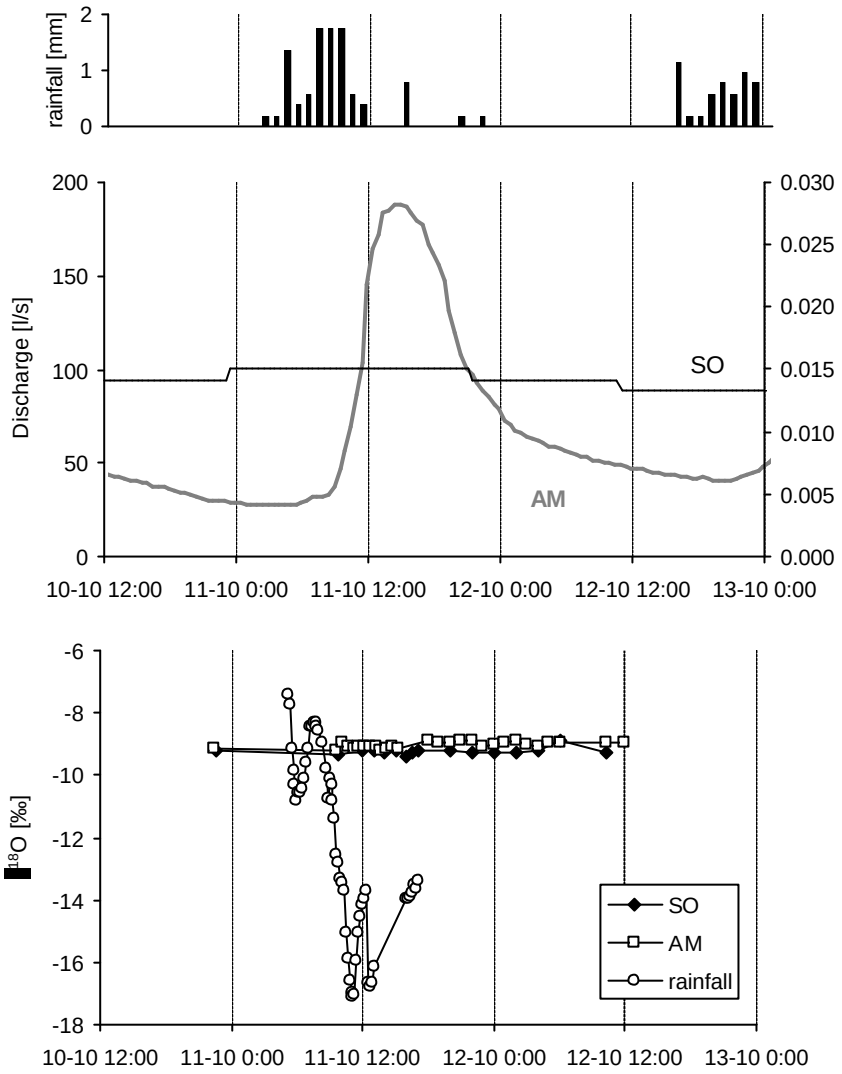

Fig. 4. October 2000 flood event: hourly rainfall height (upper graph), discharge measurements (middle graph); isotopic evolution of groundwater and rainfall (lower graph).

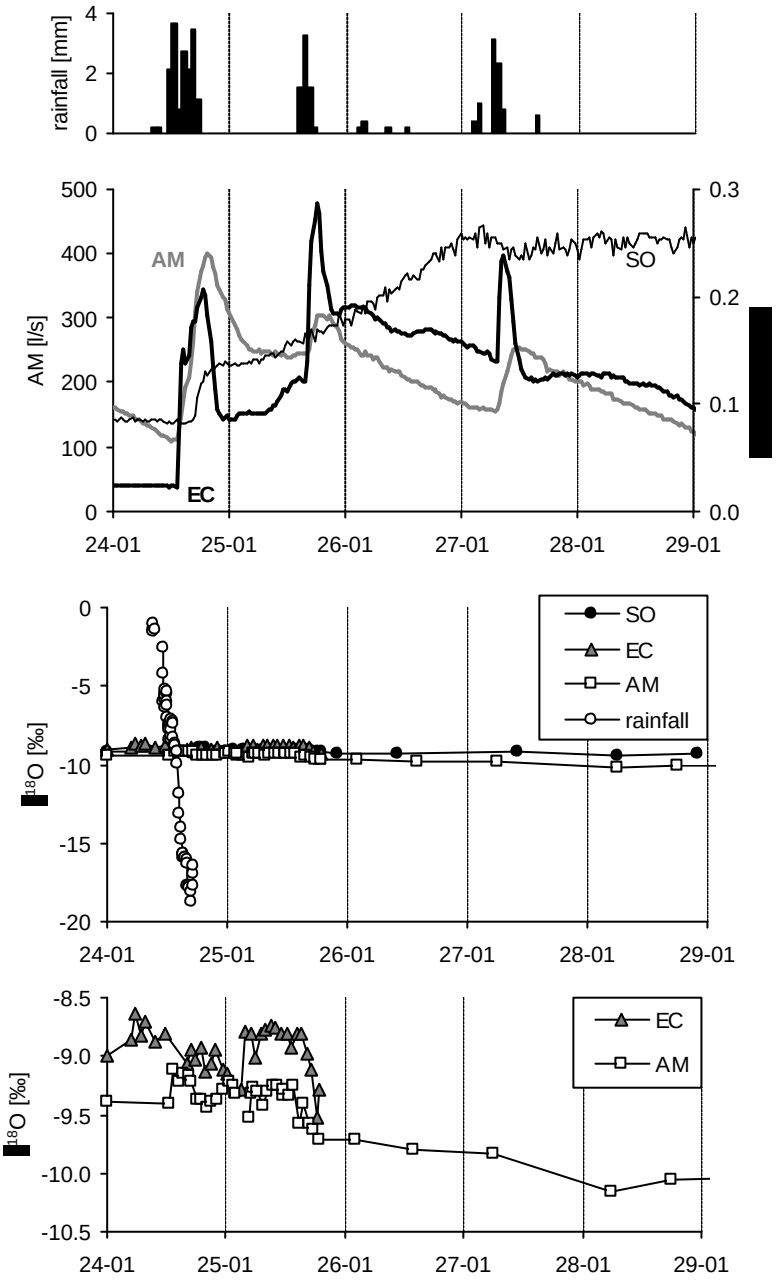

Fig. 5. January 2001 flood event: hourly rainfall height (upper graph), discharge measurements (middle graph); isotopic evolution of groundwater and rainfall (two lower graphs). The lowest graph is a zoom illustrating the slight variations at EC and AM.

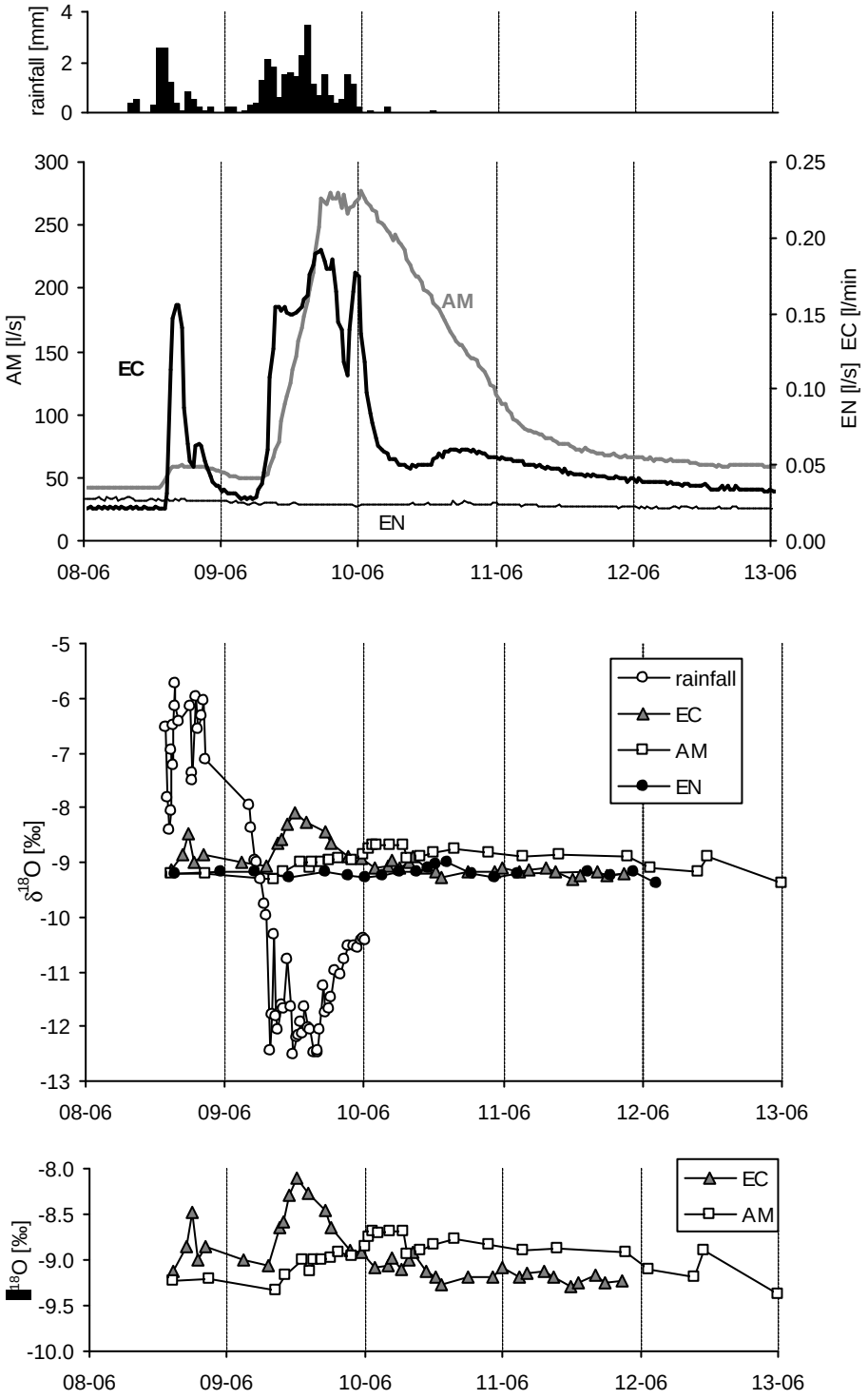

Fig. 6. June 2001 flood event: hourly rainfall height (upper graph), discharge measurements (middle graph); isotopic evolution of groundwater and rainfall (two lower graphs). The lowest graph is a zoom illustrating the slight variations at EC and AM.

3. June 2001 flood event (Fig. 6)

This flood began June 9, after the start of an important rainfall which lasted the whole day. A small rainfall event the previous day already gave a slight increase in discharge. Prior to this, the aquifer was in stable conditions for about two weeks. Calculated daily actual infiltration gives 0.4 mm the 8th and 18.2 mm the 9th. At AM, the flood event started the 9th at 7:30 and peaked at 21:00. EC tributary showed a clear peak the 8th already, but the sampled flood event started at 5:30 the following day reaching a peak discharge at 17:00. EN tributary showed no change in discharge during the recharge event.

- Rainfall: Weekly bulk samples at Maira had $\delta^{18}O$ values of -4.12 ‰ the 1st of June, -6.76 ‰ the 8th and -9.73 ‰ the 11th. The sampled recharge event shows a decreasing isotopic signal with two phases: rain on June 8 had a weighted isotopic ratio of -6.7 ‰ and rain on June 9 had a weighted isotopic ratio of -11.4 ‰.
- Aquifer: There was no significant change in the isotopic composition of EN. EC was the most sensitive: it shows a strong increase during the flood of the 9th, which corresponds to the rain of the day before. The decrease of the 10th and 11th is caused by the second rain event with a more negative isotopic signature. AM has also perturbed isotopic responses, with a more positive signal during the flood. This corresponds to the first event rainfall signature.

4. Summary of the observations

In case of a limited flood event, seepage flow (EN and SO), vadose flow (EC), conduit flow (AM) present no variations in their isotopic response. However the discharge varies strongly for EC and AM.
In case of important flood event, vadose and conduit flows present slight variations in their isotopic signal and strong increase in discharge. Seepage flow shows no significant change in the isotopic ratio, and a buffered response in discharge. The respective behaviors are schematized in Fig. 7.

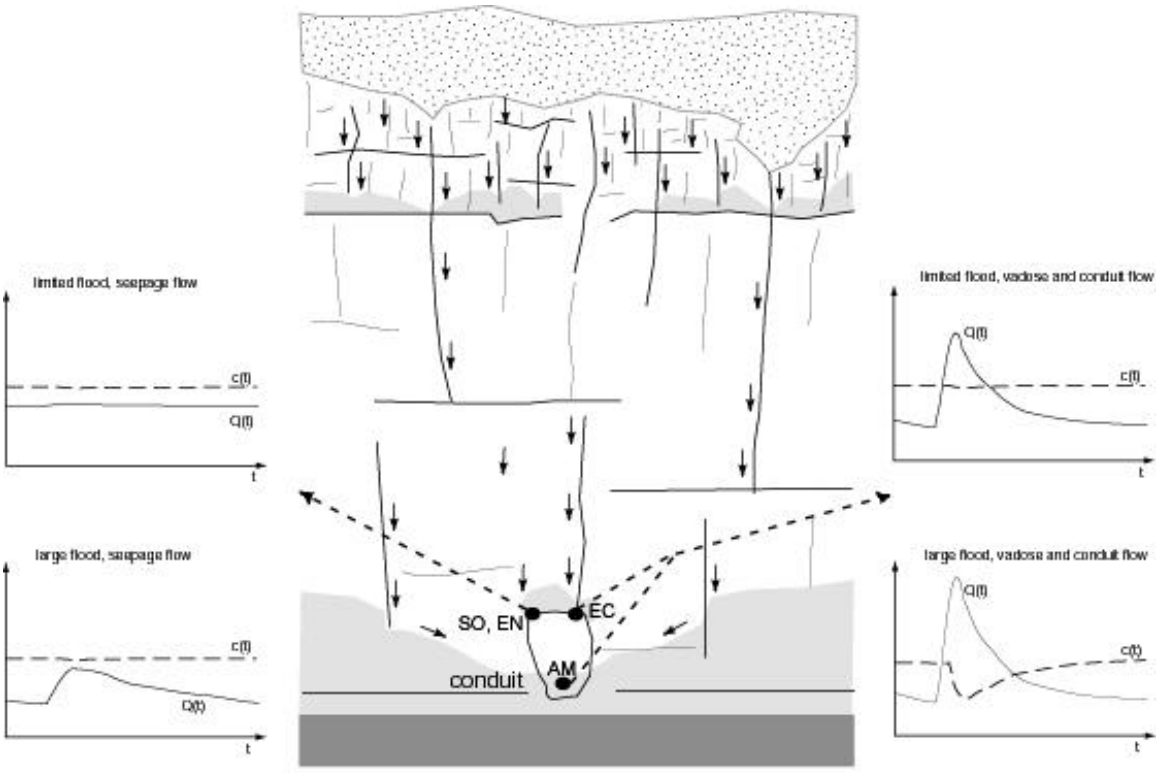

Fig. 7. Schematic representation of the flow and transport responses during flood events for vadose, seepage, and conduit flow.

5. Mixing calculations

For each groundwater sampling sites, the isotopic signal observed in rainfall is strongly buffered. Thus important storage exists already in the unsaturated zone as this zone feeds EN, SO, and EC. The first flood consists of pre-storm water only. During the second flood EC and AM showed a slight influence of fresh infiltrated water. During the last flood event isotopic variations occurred at EC, SAI and AM.

A two components mixing model can be used to estimate the proportions of pre-storm groundwater and fresh infiltrated water participating to the flood pulse (Lakey and Krothe, 1996). The percentage of freshly infiltrated water is given by:

$$F_{fw} = \frac{(d_{flood} - d_{bf})}{(d_{fw} - d_{bf})} \qquad (3)$$

where delta notation represents the ^{18}O composition of the measured groundwater during the event (d_{flood}), the rainwater (d_{fw}), and the pre-storm water (d_{bf}). However this relation is not correct as the transient terms of mixing are neglected. We suggest to compute one global F_{fw} for the whole flood event by integrating the time variations in discharges and concentrations according to (4):

$$F_{fw} = \frac{V_{fw}}{V_{flood}} = \frac{\dfrac{\int Q_{flood}(t) \cdot d_{flood}(t) \cdot dt}{V_{flood}} - \dfrac{\int Q_{bf}(t) \cdot d_{bf}(t) \cdot dt}{V_{bf}}}{\dfrac{\int Q_{fw}(t) \cdot d_{fw}(t) \cdot dt}{V_{fw}} - \dfrac{\int Q_{bf}(t) \cdot d_{bf}(t) \cdot dt}{V_{bf}}} \qquad (4)$$

where Q and V correspond respectively to discharge and water volume. The term d_{bf} is the value measured before the start of the flood pulse. It is considered as constant during the flood event, hence relation (4) simplifies into:

$$F_{fw} = \frac{\dfrac{\int Q_{flood}(t) \cdot d_{flood}(t) \cdot dt}{V_{flood}} - d_{bf}}{\dfrac{\int Q_{fw}(t) \cdot d_{fw}(t) \cdot dt}{V_{fw}} - d_{bf}} = \frac{\overline{C}_{flood} - d_{bf}}{\overline{C}_{fw} - d_{bf}} \qquad (5)$$

For the June 2001 flood event, it was necessary to consider only the first rainfall for C_{fw} as the water of the second rain event did not participate significantly to the flood water.

Results (Table 1) show that seepage flow (SO, EN) does not seem to be influenced by fresh infiltrated water. On the contrary, vadose (EC) and conduit flow (AM) show a fresh water component for important recharge events (January and June 2001). The amount appears to be limited at 30 % for vadose flow and 10 % for conduit flow.

Table 1: Results of the fresh flow percentage calculation

	site	C_{fw}	δ_{bf}	C_{flood}	F_{fw}
flood Oct.00					
	AM	-10.96	-9.14	-9.17	0.02
	SO	-10.96	-9.36	-9.37	0.01
flood Jan.01					
	AM	-12.19	-9.39	-9.42	0.01
	SO	-12.19	-9.36	-9.41	0.02
	EC	-12.19	-8.80	-9.02	0.06
flood Jun.01					
	AM	-6.66	-9.14	-8.90	0.10
	EN	-6.66	-9.37	-9.38	0.01
	EC	-6.66	-8.80	-8.11	0.32

2.4.5. Conceptual model of flow and storage in the infiltration zone

Evidence for significant storage in the Milandre karst system has been provided in the last paragraphs. Storage can occur in different sub-systems of the karst aquifer: soil, epikarst, unsaturated and phreatic zones (Fig. 8). Data from the literature show that the most effective sub-systems are the epikarst (Gouisset, 1981; Williams, 1983; Klimchouk, 2000) and the phreatic zone (Kiraly and Mueller 1979). Our data suggest that the epikarst is the most efficient: the tributaries fed by the unsaturated zone only (EC, SO, EN) present buffered isotopic signal comparable to conduit flow at AM.

Grasso (1999) estimated the dynamic storage of the system based on hydrograph recession analysis of the spring discharge. He found a value of 1.8 million of cubic metres. This storage homogeneously distributed on the whole basin is equivalent to 138 mm (catchment area of 13 km^2). This storage can be located in soils, epikarst, or the phreatic zone. We investigate here if storage in soils and epikarst may be sufficient for explaining part or total of the whole aquifer storage.

Soil thickness over the basin is variable but can be estimated at 1 m on average. Water content in the soil has been estimated at 140 mm by Jeannin and Grasso (1995). However this volume is mainly stored in the soil matrix porosity and does not participate significantly to the dynamic storage, but it can play a role in mixing.

Dynamic storage can be located in the epikarst. A 10 % porosity (e.g. Gouisset, 1981; Williams, 1985) in the epikarst would lead to an epikarst nappe of 138 cm thickness. At Milandre, the epikarst layer is known to be a few metres thick. Hydraulic data directly measured in the epikarst are scarce (7 piezometers) and show a strong heterogeneity: water levels can be measured in some piezometers whereas others stay dry most of the time. However these data can support the existence of important storage in the epikarst. Furthermore, measured tributaries have perennial flow even after long dry periods.

When considering flow and transport simultaneously, our conceptual model (Fig. 8) should reproduce sharp hydraulic responses, but dampened solute concentrations.

- Hydraulics of the conceptual model: The soil reservoir splits rainfall (R_r) into evapo-transpiration (ETR) and actual infiltration (I_a). The epikarst reservoir distributes flow into base flow (Q_b) and quick flow (Q_q). In case of high I_a, infiltrated water in excess bypasses the soil-epikarst reservoirs as fresh water (Q_f).
- Non reactive transport in the conceptual model: Water leaving the epikarst reservoir (Q_b and Q_q) has the solute concentration C_b. C_b is a weighted average of the rain solute concentration (C_r). Soil may partly transform C_r into C_b. Fresh water (Q_f) has the concentration of the rain (C_r). Field data indicate that fresh water (Q_f, C_r) reaches the saturated zone when actual infiltration is over 15 to 20 mm. For lower recharge, solute concentration infiltrating towards the saturated zone is C_b. EC is mainly fed by Q_q, SO and EN by Q_b and the underground river (AM, SAI) by a mixing of Q_q and Q_b.

- Towards numerical modeling: The soil-epikarst reservoir model should account for (1) the progressive concentration of flow in the vertical direction (bottleneck effect described by Williams, 1983), (2) storage and mixing, and (3) piston flow allowing rapid hydraulic pulses (a few hours) and delayed transport response (days). Moreover non-linearity in flow and transport has to be introduced with a temporary outlet functioning when a given hydraulic head is reached.

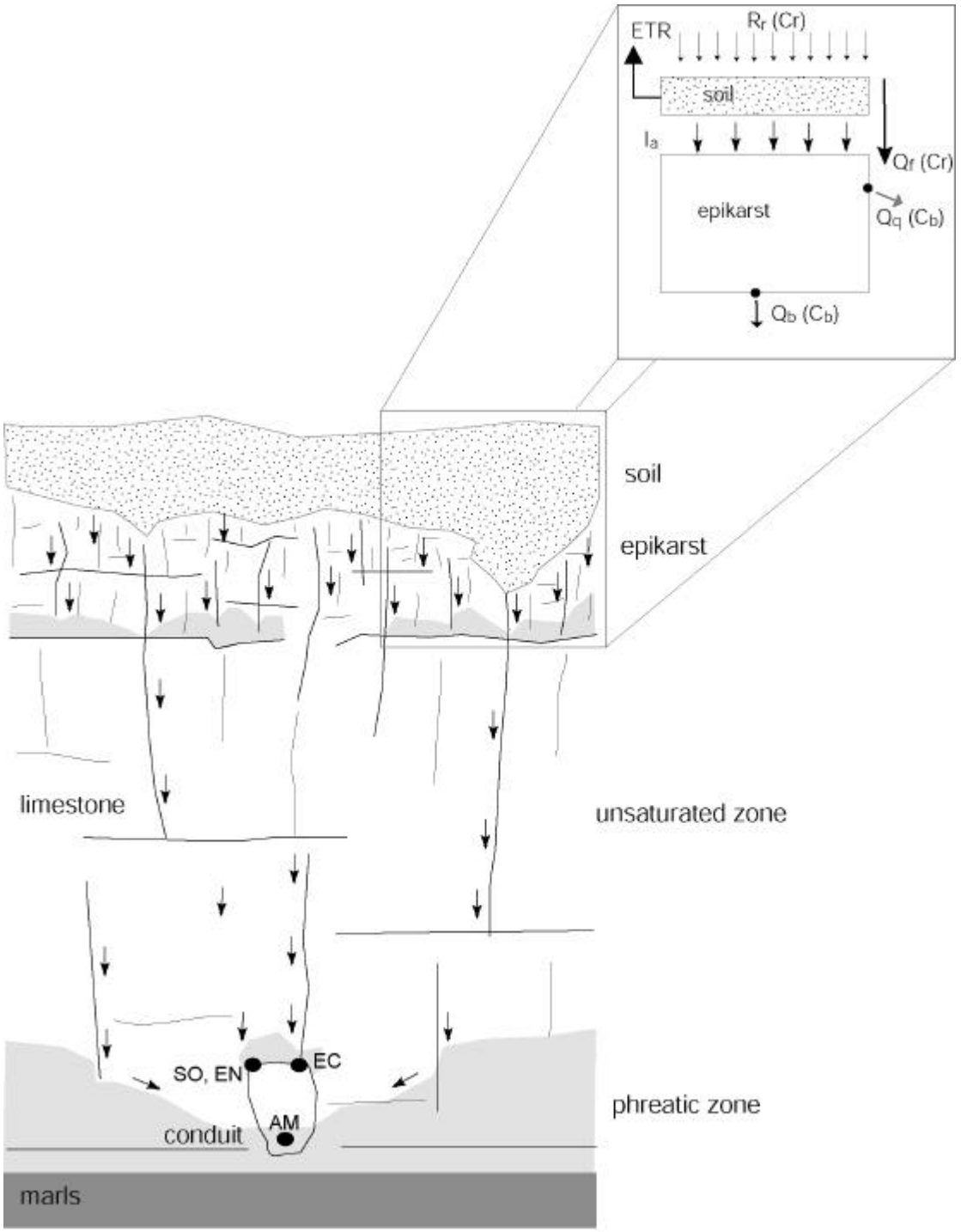

Fig. 8. Schematic vertical cross-section of the Milandre aquifer. Flow is indicated by arrows, and storage by pale grey areas. Water inlets in the conduit are vadose flow (EN), seepage flow (SO, EN) and conduit flow (AM). Conceptual model of flow and storage in the soil/epikarst layer is represented in the upper right part of the figure, see text for explanations.

2.4.6. Numerical modeling

Simulation of flow and transport in epikarst reservoirs should help to define the geometry of the reservoirs in more detail (length, height, location of inflows and outflows), and to estimate the spatial distribution and value of flow and transport parameters.

The numerical model has to be consistent with the proposed conceptual model. The simulation results should reproduce observed discharge and concentration evolution observed at EC: rapid hydraulic responses, and buffered solute concentration variations as schematized in Fig. 7.

The chosen strategy was to start with the simplest model and to progressively add complexity when results did not correspond to observed data. This technique allows to justify the complexity of the final model.

Flow in the infiltration zone is partly non-saturated. The hydraulic parameters are highly heterogeneous, and the processes occur in three dimensions. This situation has been simplified in order to simulate a more classical configuration. Feflow software by Wasy Gmbh, which simulates flow and transport by finite element was selected. The reservoir is modeled as a confined aquifer in a vertical plane (2-D model). It is represented by a rectangle with squares meshing (15 cm by 15 cm dimensions). Inflow is at the upper boundary and outflows are located at the bottom or on the right side of the rectangle.

Firstly, the model was run until stationary conditions were reached (run 1). This run determined the hydraulic head initial distribution. Secondly, a run of 14 or 28 days (1 hour step) was computed under transient flow and transport conditions (run 2).

Calibration of flow and transport parameters (Table 2)

Hydraulic conductivity in the epikarst was estimated at $5 \cdot 10^{-5}$ to 10^{-3} m/s by Jeannin (1996) and 10^{-5} m/s or more by Williams (1985). Its spatial distribution should reproduce the bottleneck effect described in the conceptual model. After several model runs, consistent hydraulic heads in the model were obtained with the following configuration: three horizontal layers of equal thickness with respective vertical hydraulic conductivities of 10^{-4}, 10^{-5} and 10^{-6} m/s from the top to the bottom of the reservoir. An anisotropy factor of 0.1 has been introduced in order to decrease the horizontal conductivity of a factor 10.

Confined storage coefficient (S_c) has been distributed at 10^{-2} m^{-1} over the whole model: higher values gave too small hydraulic heads at the end of a run, and lower values suppressed any hydraulic pulse at the outflow.

Longitudinal dispersivity (D_l) was fixed at 0.5 m, and transverse dispersivity (D_t) at 0.05 m. Small changes in this parameter has only a slight influence on the transport result. Epikarst porosity ranges between 1 % (Smart and Friederich, 1986), 2-10 % (Gouisset, 1981) and 5-10 % (Williams, 1985). Selected value for the model is 10 % in order to get a relatively low flow velocity.

Table 2: Values of the parameters used for the modeling

K_v [m/s]	K_h [m/s]	S_c [m^{-1}]	D_l [m]	D_t [m]	n [%]	C_{ini} [mg/l]
10^{-4}	10^{-5}	10^{-2}	0.5	0.05	10	100
10^{-5}	10^{-6}					
10^{-6}	10^{-7}					

Initial conditions and recharge events

Initial heads were fixed by the run 1 as defined above. Initial concentration was set at 100 mg/l of solute in the whole reservoir. Recharge amount and frequency were defined in the same range as field observed data: during the first day a constant recharge at 5 mm/day was assigned with a concentration at 10 mg/l. This concentration has been chosen in order to be well distinct from the initial. Day 2 to day 6, drought conditions prevailed. Day 7 a constant recharge at 20 mm/day was set with again a concentration at 10 mg/l. Day 8 to day 14, drought conditions were assigned (Fig. 10). The maximum recharge at 20 mm/day was based on the hypothesis that surplus recharge bypasses the reservoir (Q_f of the conceptual model).

Geometry and results of the five models presented below are given in Fig. 9 and 10.

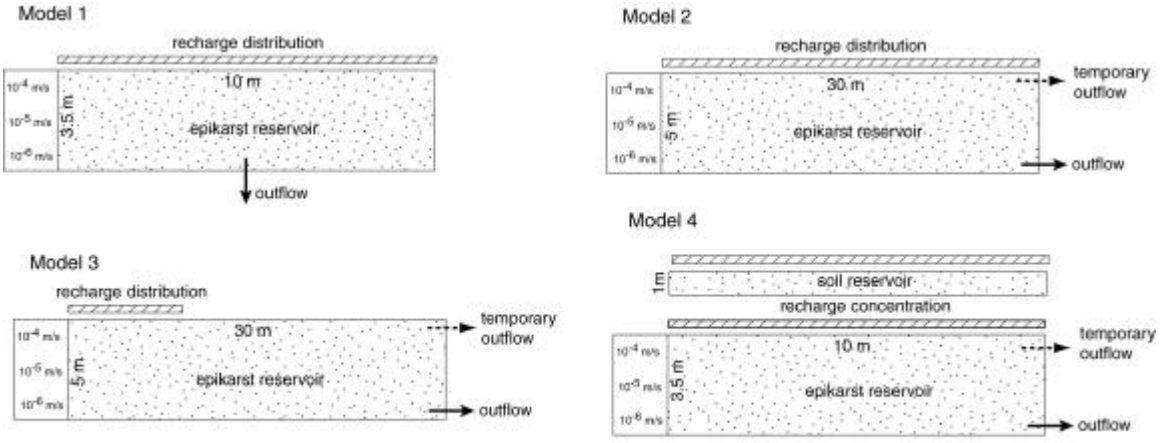

Fig. 9. Geometry of the four epikarst reservoirs modeled with Feflow. The epikarst geometry of model 5 is equivalent to that of model 4.

Model 1

A catchment area of 100 m^2 (size equivalent to EC tributary catchment area) with diffuse recharge was first considered. Recharge is increased by a factor of 10 in order to integrate the catchment size in the 2-D vertical model (which is a vertical cross-section across a square of 10 m side) . The height of the reservoir was fixed at 3.5 m (corresponding to the zone Z1 and Z2 defined by Gouisset, 1981). One outflow (fixed head equal to the outflow altitude) was set at the bottom of the reservoir. Results showed a buffered hydraulic response (very different from that observed in hydrographs from EC and AM) and a strong decrease in solute concentration.

Model 2

In order to obtain a nervous hydraulic response, a second outflow was set on the top of the right side of the reservoir. This outflow is temporary: it activates (fixed head equal to the outflow altitude) when a certain hydraulic head is reached in the reservoir. Residence time was increased by enlarging the reservoir size (30 by 5 m), and by setting the main outflow at the bottom right corner. Results were more consistent with respect to the hydraulics. Discharge rates are drastically increased by the temporary outflow during the recharge events. However, transport is still too fast: solute concentration at the end of the run drops to 63 mg/l and to 19 mg/l at the temporary outflow.

Model 3

The flow path was increased by locating the recharge to the top left corner of the reservoir in order to retard the concentration drop at the outlet . In the simulation, the recharge was concentrated in one third of the initial surface.

The concentration started decreasing at the end of the run. In order to check the influence of further recharge, the model was run for 14 more days with the equivalent number of recharge events as the first run. Concentrations at the outflows continued to drop for reaching 75 mg/l at the main discharge point and 50 mg/l at the temporary outflow. This result showed that transport is mainly by piston flow, and only limited mixing can occur.

Our stable isotopes observations suggest an important mixing effect which cannot be reproduced in the modeled epikarst reservoir. Hence we propose the mixing being made above the reservoir, i.e. in the soil zone. That means we have to recharge a first reservoir (the soil) where mixing is the most efficient. Below, the epikarst will concentrate fluxes and generate characteristic floods by temporary outflows. Some mixing can still occur by dispersion, but transport is mainly by piston flow.

Model 4. Soil reservoir

A first attempt to model the soil reservoir was made using the following conditions: a saturated confined nappe in the vertical dimension, 10 m long and 1 m thick reservoir. Boundary conditions were diffuse recharge at the top and fixed head at 1 m at the bottom. Flow parameters were 10^{-4} m/s for hydraulic conductivity and 10^{-3} m^{-1} for compressibility. Transport parameters were set at 10 % for porosity, 0.1 m and 0.01 m for longitudinal and transverse dispersivity respectively. Initial hydraulic head was set at 1 m and the same recharge scenario as previous models was used. The concentration dropped drastically with the first 20 mm recharge event: the transport appears to be by piston flow only, and no mixing occurs.

Model 5. Analytical instant mixing reservoir

A simple way to generate mixing is to define a reservoir with a given storage capacity and to instantaneously mix recharging water with stored water during each time step.

Hydraulics of the reservoir is given by:

$$Q_{out}(t_i) = KH(t_i)S \quad (6)$$

where

$$H(t_i) = H(t_{i-1}) + \Delta H(t_i) \quad (7)$$

and

$$\Delta H(t_i) = \frac{Q_{out}(t_{i-1}) - Q_{in}(t_{i-1})}{S}\Delta t \quad (8)$$

with Q_{in} and Q_{out} the flow rate entering and leaving the reservoir, K the exhausting coefficient of the reservoir, S the surface area of the reservoir, and H the water level above the reservoir outflow.

Concentration is given by:

$$c(t_i) = \frac{M_{out}(t_i)}{Q_{out}(t_i)\cdot\Delta t} \quad (9)$$

where

$$M_{out}(t_i) = \frac{M_{res}(t_i)}{V_{res}(t_i)}Q_{out}(t_i)\Delta t \quad (10)$$

and

$$M_{res}(t_i) = M_{res}(t_{i-1}) + M_{in}(t_{i-1}) - M_{out}(t_{i-1}) \quad (11)$$

$$V_{res}(t_i) = Sh + SH(t_i) \quad (12)$$

where c is the concentration at the outflow, $M_{out,\ in,\ res}$ are respectively the solute mass in the outflow, the inflow and the reservoir, V_{res} is the volume of water in the reservoir, and h is the depth of the reservoir below the outflow.

The simulation was carried out with h=140 mm (field capacity defined by Jeannin and Grasso, 1995), K=0.009 j^{-1} (large enough in order to get a sharp discharge decrease), and the recharge scenario was the same as before. The model strongly buffered the input concentrations for reservoirs having a

sufficient volume (i.e. an adequate h value). In the simulation, the concentration drop is only 15 mg/l , and the recharge at 150 mg/l is insufficient for reaching the initial concentration of the reservoir.

Solute concentration and discharge at the outflow were used as inputs to the epikarst reservoir. Similar conditions to those in model 1 were applied, except that two outflows were set on the right wall of the model. Concentrations and discharge at the lower outflow (Q_b) were highly dampened. However a slight concentration decrease is visible. This corresponds to the observed response at SO and EN. At the upper outflow (Q_q), discharge responses are sharp and high, whereas concentration responses are visible but highly dampened. This is consistent with observations at EC.

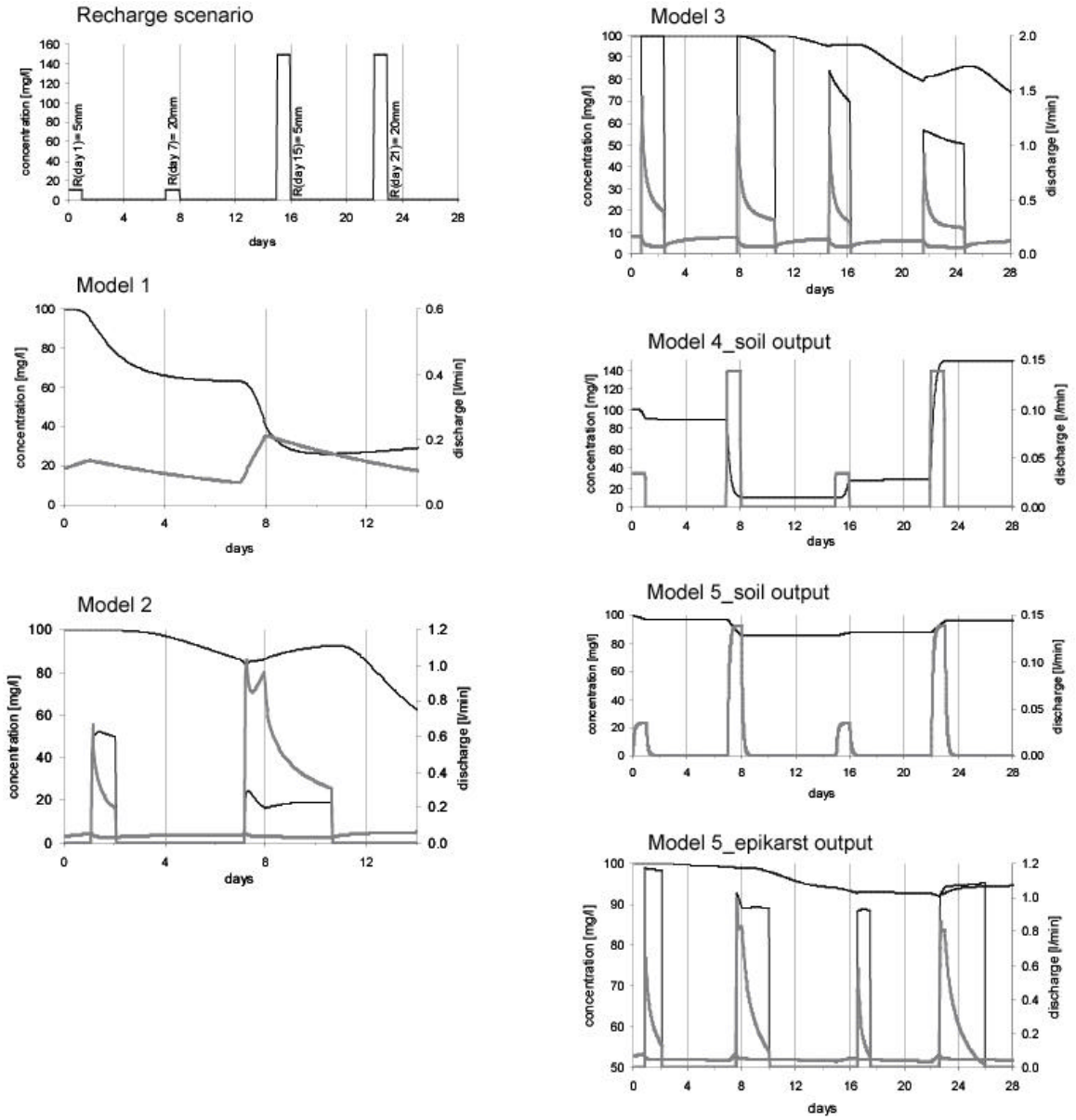

Fig. 10. Results from modeling: Grey lines represent discharge and black lines solute concentration at the outflow. Time limited curves correspond to the temporary outflow.

2.4.7. Discussion

Results of the modeling show the necessity to consider two successive reservoirs; a soil reservoir, which has a mixing function, and an epikarst reservoir, which provides epikarst dynamic storage. Moreover, the epikarst distributes water to the main outflow (Q_b of the conceptual model) and to the temporary outflow (Q_q).

The dimensions of the reservoirs are in agreement with field data. Soil thickness varies between nothing and 5 m. The smallest catchment sizes for measured tributaries are 50 m^2, which is consistent with a 10 m long epikarst reservoir. Smart and Friederich (1986) estimate spacing between shafts at 50 m, which would better correspond to a 30 m long reservoir.

A detailed survey of fissures and shafts in karrenfields or of water inlets in caves (unpublished data) shows that the density of permeable vertical fractures with a significant penetration length is on the order of 30-50 m.

Epikarst recharge has to be concentrated in order to provide enough water for the model. This is probably a consequence of the bottleneck effect, i.e. diffuse infiltration concentrates at one point at the base of the epikarst.

These results confirm hypotheses proposed in the conceptual model and demonstrate the necessity of mixing in the soil. Most field soils exhibits a spatial variability in their structure and hydraulic properties (Flühler et al. 1996, Vogel et al. 2000). At Milandre site, soils present a high clay content. The low permeability soil matrix is cut by macropores of higher permeability. These macropores decrease progressively at depth. Solute transport in such soils has an important lateral mixing component (Flühler et al. 1996).

The simple mixing reservoir used for the soil modeling can be interpreted in the following way: In unsaturated soils, water is mainly stored in the matrix and flow rate is limited. When recharge occurs, especially when field capacity is reached, the hydraulic conductivity increases drastically and part of the fresh water bypasses the soil reservoir through macropores. Matrix water becomes completely mobile and can mix very effectively with fresh water. The reservoir model is clearly a strong simplification of this process, but qualitatively reproduces similar responses.

A detailed study on sandy soil by Rank et al. (2001) supports this conceptual model: repeated 100 mm rainfall simulations lead to rapid hydraulic responses (after 2 hours at 110 cm depth). Isotopic tracers injected in the rain water showed a strong mixing with capillary water already stored in the unsaturated soil zone. 500 mm of repeated simulated rainfall was necessary to recover 90 % of the conservative tracer.

These data confirm that the soil zone cannot be neglected in karst infiltration zone transport processes. It controls flow velocities and mixes solutes efficiently. Epikarst is necessary for dynamic storage and for the distribution of infiltration towards the saturated zone.

The modeling approach should be further refined by accounting for the unsaturated properties of the soil and the epikarst. Use of existing codes simulating flow and transport in soils (Simunek et al. 2003) should allow to test further the mixing processes. More field data should be collected at the base of the soil zone and directly in the epikarst. These data will help to confirm the ideas developed above. Sampling needs to be continued long after a recharge event as flow velocities can be low.

2.4.8. Conclusions and further work

Fresh water infiltrated during rainfall events is mainly stored in the aquifer, although a highly peaky response is observed at the spring with respect to discharge. Thus the isotopic response at the spring is highly buffered when compared to rainfall. Similar results were observed at the catchment scale for three different karstic systems located in the French Pyrenees by Bakalowicz et al. (1974), as well as in many other systems (Lastennet 1994, Stichler et al. 1997, Maloszewski et al. 2002).

In case of important recharge, a fraction of fresh infiltrated water contributes to the flood pulse. The percentage can reach up to 30 % for vadose flow, 10 % for conduit flow but is not significant for seepage flow. Such percentages are in agreement with the study of Lee and Krothe (2001) carried out on a karst system in Indiana. With a mixing model, these researchers estimated at 11 % the contribution of rain water to a flood event.

The soil and epikarst sub-systems at the Milandre test site appear to act as the important groundwater storage element of the karst system, as already illustrated by Yonge et al. (1985), Chapman et al. (1992), and Caballero et al. (1996). Numerical modeling shows that the soil zone has a mixing function, whereas dynamic storage happens mainly in the epikarst. Epikarst separates flow into base flow and quick flow. When recharge exceeds a certain threshold, part of the water may bypass the epikarst sub-system as fresh flow. Water reaching the saturated zone is then transported by the conduit network to the spring. Based on observations and modeling presented above, it appears that storage and mixing in the soil and epikarst are sufficient to explain responses of the whole system. Thus phreatic storage has to be of moderate importance, at least in the Milandre karst system.

More detailed solute transport field work in the soil and epikarst should help to improve the proposed conceptual model. Tracing experiments can be used for validation: a diffuse injection at a low recharge rate will provide information on the residence time in the unsaturated zone. Point injection, meaning a high recharge rate, will strongly reduce the attenuation effect related to mixing in the soil storage and will also activate the epikarst overflow. As a consequence, this type of experiment will mainly test conduit flow velocity. A future challenge will be to adapt the conceptual model to the transport of chemical parameters such as nitrates and hardness. This model should also be tested on other sites in order to determine to what extent it can be generalized.

This study has several important consequences on protection policies applied to karst aquifers: diffuse infiltration seems to increase transit times and dispersion drastically (by orders of magnitude). Thus inputs of degradable contaminants will have more impact if injected at a point source rather than spread over a large surface area. Removal of soil and epikarst (e.g. by quarrying) will suppress an important storage element of the system and could be harmful to groundwater quality and quantity.

Acknowledgements
This project was supported by the Swiss National Science Foundation, Grant n° 20-61717.00. We are indebted to the Jura Caving Club for access to the cave and to Boncourt local authorities for sending numerous samples from the spring. At the Centre of Hydrogeology, T. Ettlin, F. Bourret, B. Wenger and S. Cattin gave us priceless support for the field and the lab work. We thank O. Atteia and P.G. Cook for their valuable comments on the manuscript.

References

Atkinson, T.C., Hess, J.W., Harmon, R.S., 1985. Stable isotope variations in recharge to a karstic aquifer, Yorkshire dales, England. Annales de la Société Géologique de Belgique, 108: 225.

Bakalowicz, M., Blavoux, B., Mangin, A., 1974. Apports du traçage isotopique naturel à la connaissance du fonctionnement d'un système karstique - teneurs en oxygène 18 de trois systèmes des Pyrénées, France. Journal of Hydrology, 23: 141-158.

Bakalowicz, M., Jusserand, C., 1987. Etude de l'infiltration en milieu karstique par les méthodes géochimiques et isotopiques. Cas de la grotte de Niaux (Ariège, France). Bulletin d'Hydrogéologie, Neuchâtel, 7: 265-283.

Bar-Matthews, M., Ayalon, A., Matthews, A., Sass, E. and Halicz, L., 1996. Carbon and oxygen isotope study of the active water-carbonate system in a karstic Mediterranean cave: Implications for paleoclimate research in semiarid regions. Geochimia and Cosmochimia Acta, 60(2): 337-347.

Blavoux, B., 1978. Etude du cycle de l’eau au moyen de l’oxygène 18 et du tritium., Univ. Pierre et Marie Curie, Paris, 333 pp.

Caballero, E., Jimenez de Cisneros, C., Reyes, E., 1996. A stable isotope study of cave seepage waters. Applied Geochemistry, 11(4): 583-587.

Chapman, J.B., Ingraham, N.L., Hess, J.W., 1992. Isotopic investigation of infiltration and unsaturated zone flow processes at Carlsbad Cavern, New Mexico. Journal of Hydrology, 133: 343-363.

Dansgaard, W., 1964. Stable isotopes in precipitation. Tellus, 16: 436-468.

Flühler, H., Durner, W., Flury, M. 1996. Lateral solute mixing processes – A key for understanding field-scale transport of water and solutes. Geoderma, 70: 165-183.

Ford, D. and Williams, P., 1989. Karst geomorphology and hydrology. Chapman & Hall, London, 601 pp.

Gouisset, Y., 1981. Le karst superficiel: genèse, hydrodynamique et caractéristiques hydrauliques., Univ. des Sciences et techniques du Languedoc, France, Montpellier, 218 pp.

Grasso, D.A., 1999. Interprétation des réponses hydrauliques et chimiques des sources karstiques., Neuchâtel, 135 pp.

Gretillat, P.-A., 1996. Les aquifères karstiques et poreux de l'Ajoie (Jura, Suisse)., Neuchâtel, 209 pp.

Harmon, R.S., 1979. An isotopic study of groundwater seepage in the Central Kentucky karst. Water Resources Research, 15(2): 476-480.

Hsieh, J.C.C., Chadwick, O.A., Kelly, E.F. and Savin, S.M., 1998. Oxygen isotopic composition of soil water: Quantifying evaporation and transpiration. Geoderma, 82: 269-293.

Jeannin, P.-Y., 1996. Structure et comportement hydraulique des aquifères karstiques, Neuchâtel, 237 pp.

Jeannin, P.-Y., Grasso, D.A., 1995. Estimation des infiltrations efficaces journalières sur le bassin karstique de la Milandrine. Bulletin d'Hydrogéologie, 14: 83-94.

Katz, B.G., Catches, J.S., Bullen, T.D., Michel, R.L., 1998. Changes in the isotopic and chemical composition of ground water resulting from a recharge pulse from a sinking stream. Journal of Hydrology, 211(1-4): 178-207.

Kiraly, L, Mueller, I., 1979. Hétérogénéité de la perméabilité et de l'alimentation dans le karst : effet sur la variation du chimisme des sources karstiques. Bulletin du Centre d'Hydrogéologie, 3: 237-285.

Klimchouk, A.B., 2000. The formation of Epikarst and Its role in Vadose Speleogenesis. In: A.B. Klimchouk, D.C. Ford, A.N. Palmer and W. Dreybrodt (Editors), Speleogenesis. Evolution of Karst Aquifers. National Speleological Society, pp. 91-99.

Lakey, B., Krothe, N.C., 1996. Stable isotopic variation of storm discharge from a perennial karst spring, Indiana. Water Resources Research, 32(3): 721-731.

Lastennet, R. 1994. Rôle de la zone non saturée dans le fonctionnement d'un aquifère karstique. Approche par l'étude physico-chimique et isotopique du signal d'entrée et des exutoires du massif du Ventoux (Vaucluse), Avignon.

Lee, E.S. and Krother, N.C., 2001. A four-component mixing model for water in a karst terrain in south-central Indiana; USA. Using solute concentration and stable isotopes as tracers. Chemical Geology, 179: 129-143.

Margrita, R., Guizerix, J., Corompt, P., Gaillard, B., Calmels, P., Mangin, A., Bakalowicz, M., 1984. Refléxions sur la théorie des traceurs. Applications en hydrologie isotopique. Proc. Int. Congr. Isotopic Hydrology, IAEA, Vienna : 1-27.

Mueller, I., Schotterer, U., Siegenthaler, U., 1982. Etude des caractéristiques structurales et hydrodynamiques des aquifères karstiques par leurs réponses naturelles et provoquées. Eclogae geol. Helv., 71(1): 65-75.

Perrin, J., Jeannin, P.-Y. and Zwahlen, F., 2003. Implications of the spatial variability of the infiltration water chemistry for the investigation of a karst aquifer. Accepted by Hydrogeology journal.

Rank, D., Papesch, W., Rajner, V., Steiner, K.-H. and Vargay, Z., 2001. Lysimeter study on infiltration processes in the sandy soil of the Great hungarian plain. Beiträge zur Hydrogeologie, 52(Special Issue: Tracer studies in the unsaturated zone and Groundwater): 60-73.

Simunek, J., Jarvis, N.J., van Genuchten, M.T., Gärdenäs, A. 2003. Review and comparison of models for describing non-equilibrium and preferential flow and transport in the vadose zone. Journal of Hydrology, 272: 14-35.

Smart, P.L. and Friederich, H., 1986. Water movement and storage in the unsaturated zone of a maturely karstified carbonate aquifer, Mendip Hills, England. In: D. National Water Well Association, Ohio. (Editor), Proc. Conf. env. problems of karst terrains and their solutions: 59-87.

Stichler, W., Trimborn, P., Maloszewski, P., Rank, D., Papesch, W., Reichert, B., 1997. Isotopic investigations. In: Acta carsologica XXXVI/1: Karst hydrogeological investigations in south-western Slovenia, Ljubljana, pp. 213-235.

Vogel, T., Gerke, H.H., Zhang, R., van Genuchten, M.T. 2000. Modeling flow and transport in a two-dimensional dual-permeability system with spatially variable hydraulic properties. Journal of Hydrology, 238 (1-2): 78-89.

White, W.B., 1988. Geomorphology and hydrology of karst terrains. Oxford University Press, Oxford, 464 pp.

Williams, P.W., 1983. The role of the subcutaneous zone in karst hydrology. Journal of Hydrology, 61: 45-67.

Williams, P.W., 1985. Subcutaneous hydrology and the development of doline and cockpit karst. Zeit. Geomorph. NF., 29: 463-482.

Yonge, C.J., Ford, D.C, Gray, J., Schwarcz, H.P., 1985. Stable isotope studies of cave seepage water. Chemical geology, 58: 97-105.

Appendix to chapter 2.4.

Mass balances of flow and solute (oxygen-18) for the three sampled flood events at Milandre

Introduction

Fluxes of water and Oxygen-18 have been computed for the three sampled flood events at Milandrine upstream (AM). The objective was to test the validity of the interpretations based either on raw concentrations or on mass fluxes. Mass calculations were made for the Milandrine upstream catchment taking a 4.5 km^2 surface area. Oxygen-18 concentration was calculated from the analyses of the isotopic ratio. The conversion formula is the one published by Margrita et al. (1984). Actual infiltration was calculated daily by the model of Jeannin and Grasso (1995).

Method

Water volumes flowing during the flood event are given by:

$$V_{rain} = \sum P_i A \quad (1)$$

for the rain, with P_i corresponding to the total precipitation during the time period i, and A the surface area of the catchment.

$$V_{\inf iltration} = \sum I_i A \quad (2)$$

for the actual infiltration, with I_i corresponding to the total infiltration during the time period i considered by the infiltration model model.

$$V_{AM} = \sum Q_i \Delta t_i \quad (3)$$

for the Milandrine upstream, with Q_i corresponding to the discharge at time i.

The efficiency of the rainfall and the actual infiltration are respectively given by (4) and (5):

$$R_{eff} = \frac{V_{rain}}{V_{AM}} \quad (4)$$

$$I_{eff} = \frac{V_{\inf iltration}}{V_{AM}} \quad (5)$$

The Oxygen-18 mass fluxes are given by:

$$M_{rain} = \sum (P_i A) C_i \quad (6)$$

for the rain with C_i corresponding to the Oxygen-18 concentration at time i.

$$M_{\inf iltration} = \sum (I_i A) C_i \quad (7)$$

However, the model of infiltration calculates I_i on a daily basis and C_i is generally known on a half-hour basis. We decided to take I_i equivalent to P_i at the end of the flood event when it is assumed that all rainfall participate to recharge. The equivalence was kept backwards through the flood until the sum if the P_i was equal to the modelled actual infiltration. Earlier rainfall was considered to be lost by evapotranspiration.

$$M_{AM} = \sum Q_i C_i \Delta t_i \quad (8)$$

for Milandrine upstream with Q_i being the discharge at time *i.*

The mass recovery is defined as:

$$MR_{rain} = \frac{M_{rain}}{M_{AM}} \quad (9)$$

for rainfall, and:

$$MR_{\text{inf}\,iltration} = \frac{M_{\text{inf}\,iltration}}{M_{AM}} \quad (10)$$

Then it is possible to work out the average Oxygen-18 concentration from:

$$\overline{C}_{rain} = \frac{M_{rain}}{V_{rain}} \quad (11)$$

for the rain, and:

$$\overline{C}_{AM} = \frac{M_{AM}}{V_{AM}} \quad (12)$$

The concentrations were then converted into isotopic ratios according to Margrita et al. (1984).

Results

Table 1 presents the results of the calculations for the rainfall and the actual infiltration, whereas table 2 gives the results for Milandrine upstream.

Table 1

	V_{rain} [m^3]	$V_{actual\ infiltration}$ [m^3]	R_{eff} [%]	I_{eff} [%]	M_{rain} [mol]	$M_{actual\ infiltration}$ [mol]	$C_{mean\ rain}$ [‰]
10.00	38'900	12'600	26	80	4'270'737	1'373'802	-10.92
01.01	77'727	76'000	64	65	8'521'280	8'500'000	-12.34
06.01	154'800	67'050	27	63	16'961'016	7'517'552	-12.91

Table 2

	V_{AM} [m^3]	M_{AM} [mol]	MR_{rain} [%]	$MR_{infiltration}$ [%]	$C_{mean\ AM}$ [‰]
10.00	10'086	961'854	23	70	-8.99
01.01	49'654	5'459'248	64	64	-9.49
06.01	42'505	4'675'791	28	62	-8.96

Discussion

Rain efficiency and rain mass recovery are very similar. This is also true for infiltration efficiency and mass recovery infiltration. The reason is that the mass fluxes are largely controlled by the water flow which is much more variable as compared to concentration (Fig. 1). It is clear that the mass fluxes

curves follow closely discharge curves. Hence the similar values in the table are not a surprise. The information contained in the isotopic concentration signal is completely obliterated by the discharge.

Fluxes analysis does not bring more information than a rain vs. discharge analysis. The most informative characteristic is the fact that an input with highly variable concentrations is transformed into an output with almost no variations in concentrations.

When the percentage of fresh water flow is researched, a mixing model using concentrations appears to be more adapted. However the mixing model has to use weighted mean concentrations as those given in tables 1 and 2. Instant concentrations often used in the literature (Lakey and Krothe 1996, Dreiss 1989, Blavoux and Mudry 1983) may lead to erroneous results.

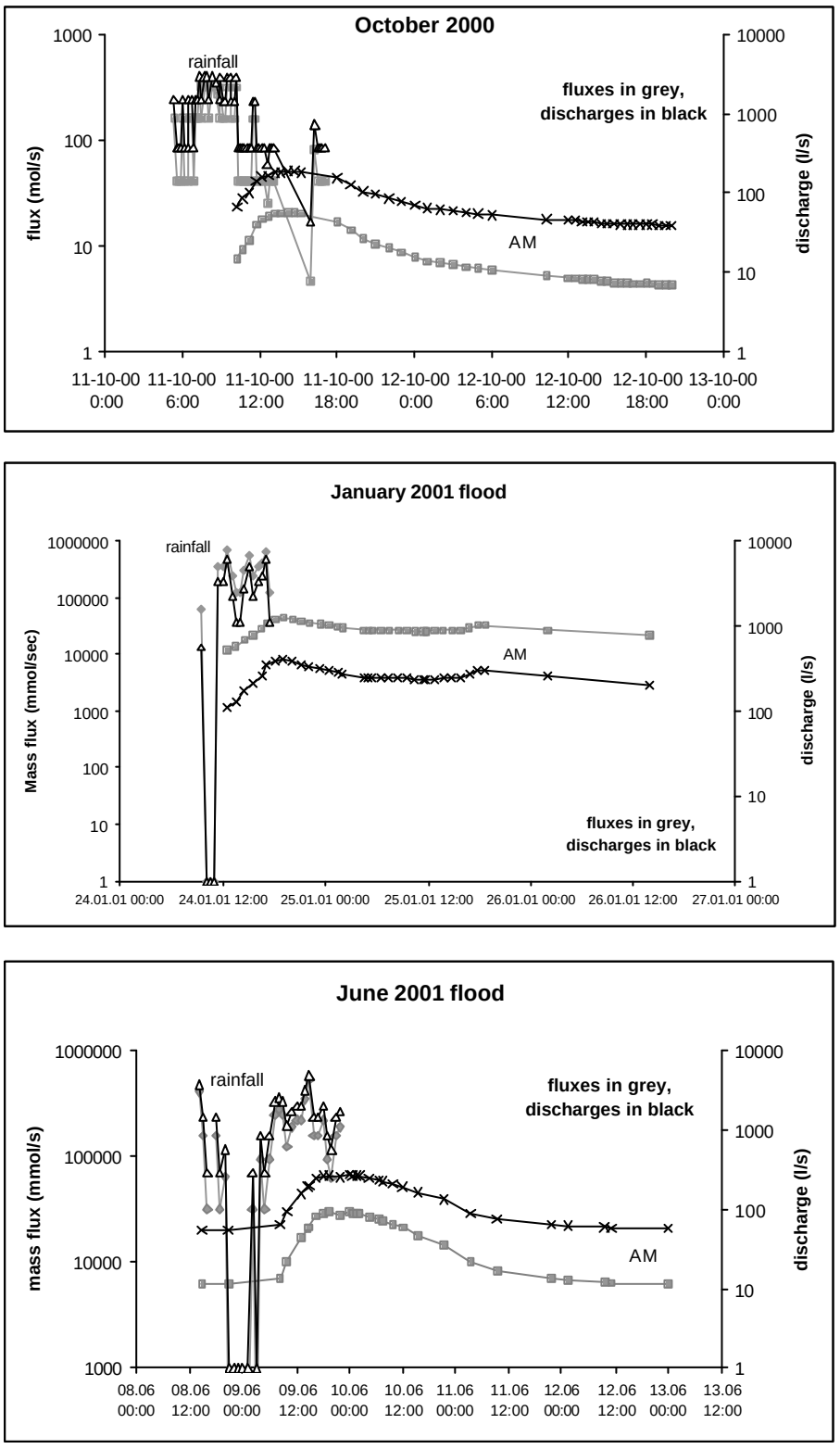

Figure 1: Oxygen-18 mass fluxes and discharge at Milandrine upstream (AM) and in rainfall for the three flood events. Rainfall "discharge" is calculated from the measured rainfall height integrated over the whole catchment (4.5 km^2).

Conclusions

During a flood event, the discharges and rainfall intensities have a strong variability as compared to concentrations. When fluxes are calculated, the information contained in the concentrations signals is lost. In our opinion a two-end mixing model is suitable for estimating the percentage of fresh infiltrated water participating to the flood events. However, the calculation should be made with weighted mean concentrations as presented earlier in chapter 2.4. This approach integrates the total mass flux of the considered tracer.

Literature

Blavoux, B. and Mudry, J., 1983. Décomposition chimique des hydrogrammes du karst. Hydrogéologie-Géologie de l'Ingénieur, 4: 270-278.

Dreiss, S.J., 1989. Regional scale transport in a karst aquifer: 1. Component separation of spring flow hydrographs. Water Resources Research, 25(1): 117-125.

Jeannin, P.-Y., Grasso, D.A., 1995. Estimation des infiltrations efficaces journalières sur le bassin karstique de la Milandrine. Bulletin d'Hydrogéologie, 14: 83-94.

Lakey, B., Krothe, N.C., 1996. Stable isotopic variation of storm discharge from a perennial karst spring, Indiana. Water Resources Research, 32(3): 721-731.

Margrita, R., Guizerix, J., Corompt, P., Gaillard, B., Calmels, P., Mangin, A., Bakalowicz, M., 1984. Refléxions sur la théorie des traceurs. Applications en hydrologie isotopique. Proc. Int. Congr. Isotopic Hydrology, IAEA, Vienna : 1-27.

2.5. The role of mixing in chemical variations at karst springs, Milandre test site, Switzerland

J. Perrin, P-Y. Jeannin, F. Zwahlen

Centre of Hydrogeology, Neuchâtel University, 11 rue E-Argand, 2007 Neuchâtel, Switzerland

Paper submitted to Journal of Hydrology

Abstract
Solute concentration variations during flood events were investigated in detail in a karst aquifer in the Swiss Jura. Observations were made at a spring, and at the three main tributaries feeding an underground river. A simple numerical model was able to reproduce karst spring chemographs and hydrographs by mixing the concentration and discharge of the tributaries through time. The good match between observed and modelled curves indicated that horizontal mixing between tributaries was the main transport process occurring in the saturated zone. Chemical reactions were non-existent, and other mixing components (e.g. phreatic storage) have no significant influence.

Dissolution-related and pollution-related parameters displayed differing behaviour: the former showed limited variations and the later changed during the moderate flood events. In the case of important flood events, both presented chemographs with significant changes. Variations of pollution-related parameters during moderate flood events offer a tool for inferring the drainage structure (presence of tributaries, distance to the spring). The groundwater quality is much more vulnerable during large flood events, when fresh infiltrated flow contributes significantly to spring flow.

Keywords: karst hydrology, groundwater chemistry, solute transport, mixing, numerical model.

2.5.1. Introduction

Water chemistry of karst springs can show significant variations during the hydrological cycle. These variations are generally related to flood events (Kiraly and Mueller 1979, White 1988, Dreiss 1989, Vervier 1990). The changes observed are considered to be related to the organised heterogeneity of karst aquifers schematised by a network of high permeability conduits embedded in a Low Permeability limestone Volume (LPV) (Kiraly 1998). This structure leads to a duality in recharge conditions (concentrated in the conduits, diffuse in the LPV), in storage capacity (high in the LPV, low in the conduits), and in flow velocities (high in conduits, low in the LPV). Time-concentration curves at karst springs are often called chemographs. Their shape is considered as giving information on the degree of karstification of the system (Shuster and White 1971, Ternan 1972): flat chemographs corresponding to fissured aquifer, and contrasted chemographs to well karstified hydrological systems. More specifically, these chemical variations are due to three main processes:

- Non-equilibrium chemical reactions (especially dissolution reactions) under transient flow conditions (i.e. flood event). Examples in the literature are mainly from systems with point source recharge (Hess and White 1988, Groves 1992, Wicks and Engeln 1997).
- Mixing processes under transient flow conditions (including dilution). Mixing can occur in two different ways: classically, a differential contribution of the respective karst sub-systems (i.e. epikarst, phreatic zone, fresh infiltrated water) combine during the flood (Blavoux and Mudry 1983, Lakey and Krothe 1996, Sauter 1992). An alternative mixing model is based on the differential contribution of the sub-catchments, each having a specific flow through time to the spring (Hess and White 1988).
- Seasonal changes in the solute concentrations recharging the aquifer. These changes occur on a long-term scale and are not directly related to hydraulic conditions (i.e. the system is steady-state). Such type of variations are not specific to karst aquifers (Iqbal and Krothe 1995, Coxon 1999, Worrall and Burt 2001).

The present study aims to investigate the extent that mixing processes are responsible for the chemical variations observed at karst springs. This will be achieved by simulating hydrographs and chemographs observed at the spring by using hydrographs and chemographs measured derived from several tributaries within the karst system. A pure mixing model will be used and criticised.

The following issues will be addressed:

1. the extent mixing models can explain karst spring chemographs compared to non-equilibrium dissolution processes or seasonal changes in the chemistry of recharging water
2. the origin of the groundwater participating to mixing
3. inferences concerning the structure of the karst system from chemographs
4. information provided by the mixing model about transit times and karst systems vulnerability

2.5.2. Study area and methods

The Milandre test site forms part of a karstic aquifer located in the Swiss tabular Jura in the vicinity of Basle (Fig. 1). The springs of the system consists of the Saivu spring, which has a discharge ranging between 20 l/s and 200 l/s, and the Bame temporary spring, which has a discharge of up to 1500 l/s. A small part of the total discharge is lost to an alluvial aquifer downstream. The catchment has been defined by numerous tracing experiments and a water budget calculation, and is estimated to be on the order of 13 km^2 (Gretillat 1996, Jeannin 1998). Land is used for pasture, forestry, tillage, and locally for settlement. Soil thickness varies from nothing to a few metres and consists mainly of highly cohesive silty loam. Thicker soils are generally colluvial.

The area receives around 1000 mm of precipitation per year, half of which recharges the karst aquifer mainly by diffuse infiltration. A well developed karstic network, located 50 to 80 m below ground surface, drains the aquifer towards the Saivu and Bame springs (Fig. 1). Water level measured in piezometers located in low permeability volumes away from the drain are systematically higher than levels in karst conduits (Jeannin 1998). Perrin et al. (2003a) showed a strong relation between land use and spatial variability of ground water chemistry.

The main tributaries of the Milandre underground river are Milandrine upstream (AM), the Bure tributary (BU), and the Droite tributary (AF). Water levels were recorded continuously at AM, BU, Saivu spring (SAI), and Bame temporary spring. Discharges were then determined from a rating curve. Specific conductance was continuously measured at AM, BU, AF, and SAI over a period of several years. These recordings were calibrated with regular manual measurements. Nitrate was continuously recorded at AM following the procedure presented by Perrin and Wenger (2001).

During three flood events, groundwater was sampled at AM and SAI (results presented below), and at two small tributaries located in the upstream part of the system. For each sample, specific conductance and temperature were measured directly on site, pH was determined within 12 hours at sampling temperature, bicarbonate within 24 hours by titration and the other parameters were analysed by ionic chromatography after a 0.45µm filtration. For cation preservation, filtered samples were acidified to pH < 2 with HNO_3 suprapur. Nitrate concentrations in samples with or without formol were equivalent, therefore all samples were collected without it. The quality of the analyses has been checked by ionic balances. Raw data are available at the following web address: www.unine.ch/chyn.

The chemical parameters presented in the study have been selected for their contrasting temporal variations at the spring. Three parameters are derived from external sources (fertilisers mainly): that is nitrate, chloride and potassium. These ions are generally present as solute in the soil pore water. Mobility and heterogeneous spatial distribution are the main causes of differences in their respective chemographs. The other parameters (bicarbonate, calcium, specific conductance) are representative of the limestone dissolution process. Specific conductance is also considered as a dissolution related parameter as calcium and bicarbonate account for 85 to 90 % of the measured specific conductance values.

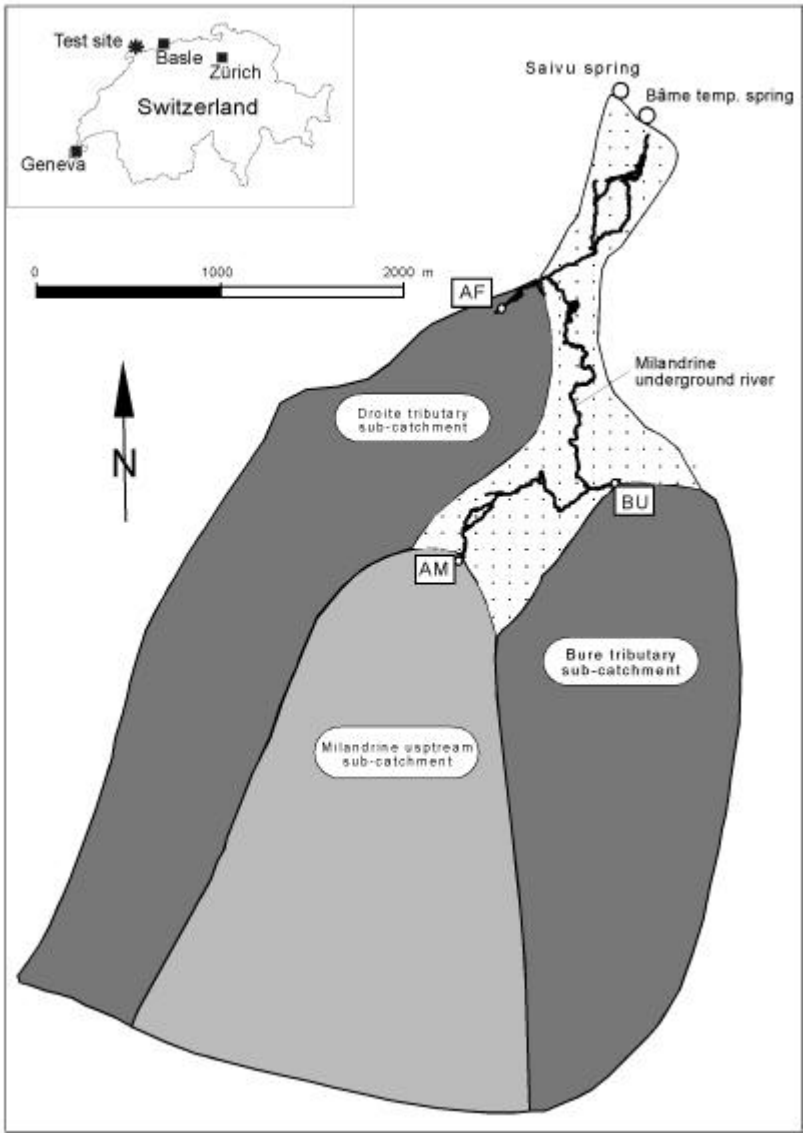

Fig. 1. Location of the Milandre karst aquifer. The conduit network is indicated by the thick black line. The three main sub-catchments (AF, BU, AM) are in gray. The dotted surface represents the part of the basin that is drained by small tributaries (modified after Grasso and Jeannin 1994).

2.5.3. Field data

October 2000 flood event

Hydrographs and chemographs description

Following a three weeks dry period, a flood began on the morning of the 11th of October following the start of continuous rainfall. Daily infiltration calculated by the model of Jeannin and Grasso (1995) is 2.8 mm for that day. Rainfall had already started on the 6th of October, continuing the 8th, the 9th and the 10th. No recharge occurred prior to the 11th, as the soil moisture deficit was high (no infiltration given by the model and no discharge increase observed in the underground stream). The main rainfall event (October 11) started at 4 a.m. Discharge at Milandrine upstream (AM) increased at 8 a.m., and Saivu spring (SAI) about 2 hours later. This flood event was relatively small with a maximum discharge in the Bame-Saivu system of less than 450 l/s (Fig. 2). The response to infiltration is rapid (a few hours) and the pulse duration is limited (one day).

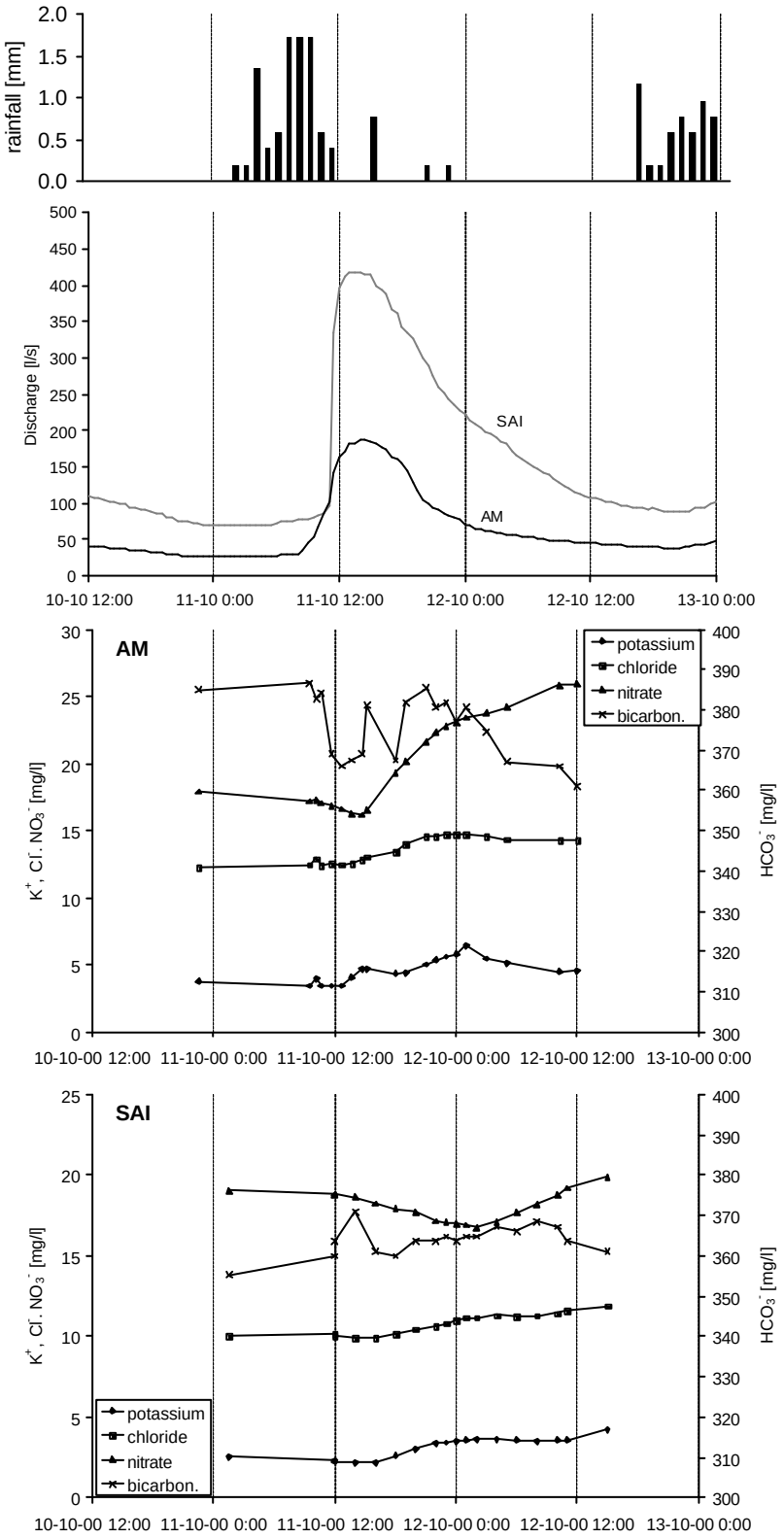

Fig. 2. October 2000 flood event: discharge measurements at AM and SAI (upper graph) and rainfall; chemographs at AM and SAI (lower graphs).

Chemographs were separated in four successive phases: At AM, pre-event water flowed until the 11th at 11:00 –11:30 a.m., i.e. during a large part of the rising limb of the hydrograph. Peak flood water was characterised by lower concentrations in bicarbonates and nitrates and a progressive increase in chloride and potassium beginning at around 1:40 p.m. Decreasing limb water started to arrive at 3:15

p.m. and showed an increase for all ions until midnight. Recession water was characterised, from the 12th onwards, by a slight decrease in bicarbonate. Nitrates still increased but chloride and potassium stabilised.

At Saivu spring, pre-event water showed stable parameters until the 11th at 2 p.m., when Bame temporary spring reached its flood maximum. Peak flood water occurred between 2 p.m. and 5 p.m. when nitrates and potassium showed a slight decrease in concentration. The decreasing limb lasted from 5 p.m. to 6 a.m. on the 12th of October: chloride and potassium showed an increase in concentration, but nitrates continued to decrease. Recession water was characterised by an increase in nitrates and a stabilisation of other parameters at values slightly higher than pre-event water. Bicarbonate remained fairly stable throughout the flood event, except for a short positive peak at the beginning of the flood event.

Qualitative interpretation

Significant concentration changes appear clearly in pollution-related parameters namely NO_3^-, Cl^-, K^+. A decrease in NO_3^- started at 11:15 a.m. at AM, and two hours forty-five minutes later at SAI, that is about four hours later than the arrival of the flood pulse. Increase in Cl^-, K^+ started at 1:40 p.m. at AM, and three hours twenty minutes later at SAI. Finally NO_3^- increase started at 3:15 p.m. at AM, and at 6 a.m. the following day at SAI.

These variations can be interpreted as a consequence of the differential contributions from the tributaries: the first four hours correspond to the piston phase of flow where the water stored in the conduit between the more downstream tributary (AF) and the spring is flushed. The volume of the flushed water is 4000 m^3 and the distance between AF tributary and the spring is 1400 m. Hence the flooded conduit section is on the order of 2.8 m^2. Initial variations at the spring cannot be caused by AM waters as the travel time ranges between 6 and 15 hours depending on the discharge (Maréchal 1994). It is most probable that nitrate dilution at the spring originates from the preferential contribution of AF tributary, which has low nitrate concentration (Perrin et al. 2003a). Increases in chloride and potassium can be linked to the preferential contribution of BU tributary, which is more polluted than AF. AM is the tributary which is the most heavily contaminated with nitrate. The increase in nitrate at the spring corresponds to that observed at AM with a time lag of 14:45, giving a flow velocity of 330 m/h. This velocity falls in the range of the measured velocities in the Milandre underground stream (Jeannin and Maréchal 1995).

January 2001 flood event

Hydrographs and chemographs description

This flood started January 24, one and a half hours after continuous rain began falling, and lasted until the 29th. The event can be separated in three successive floods of decreasing magnitude (A, B, C in Fig. 3), each linked to a rainfall event: calculated actual daily infiltration is 17 mm the 24th, 7 mm the 25th and 7.5 mm the 27th. Prior to the flood, the hydraulic conditions were stable for about two weeks. The first flood (A) at Milandrine upstream started January 24 and had a discharge of 112 l/s rising to 400 l/s a few hours later. The small flood of January 25 (B) started at 240 l/s and reached 300 l/s, then a third flood (C) followed two days later. The hydraulic response at Saivu spring followed the same pattern and reached a maximum discharge of 1000 l/s.

Only flood A was sampled in detail. Chemographs were separated into three successive phases (1, 2, 3 in Fig. 3): At AM, pre-event water (1) lasted until 3:30 p.m. on the 24th, thus two and a half hours after the discharge started to increase. Peak flood water (2) showed concentrations that decreased in bicarbonate and chloride from 3:00 p.m. onwards. Nitrates started to decrease 2:30 later. Decreasing limb water (3) was characterised by a concentration increase in chloride, bicarbonate and nitrate starting early on the 25th. The recovery was quite complete for nitrate and bicarbonate by the 27th. In contrast, chloride remained to lower concentrations. At Saivu spring, pre-event water (1) lasted until 5 p.m., that is four hours later than the start of the increase in discharge. Peak flood water (2) lasted from 5 p.m. to 6 a.m. the following day, and was characterised by a decrease in nitrate, bicarbonate, and chloride. For chloride, a secondary peak is visible. Decreasing limb water (3) showed concentrations that recovered progressively with time. For both AM and SAI, potassium showed no clear change during the whole event.

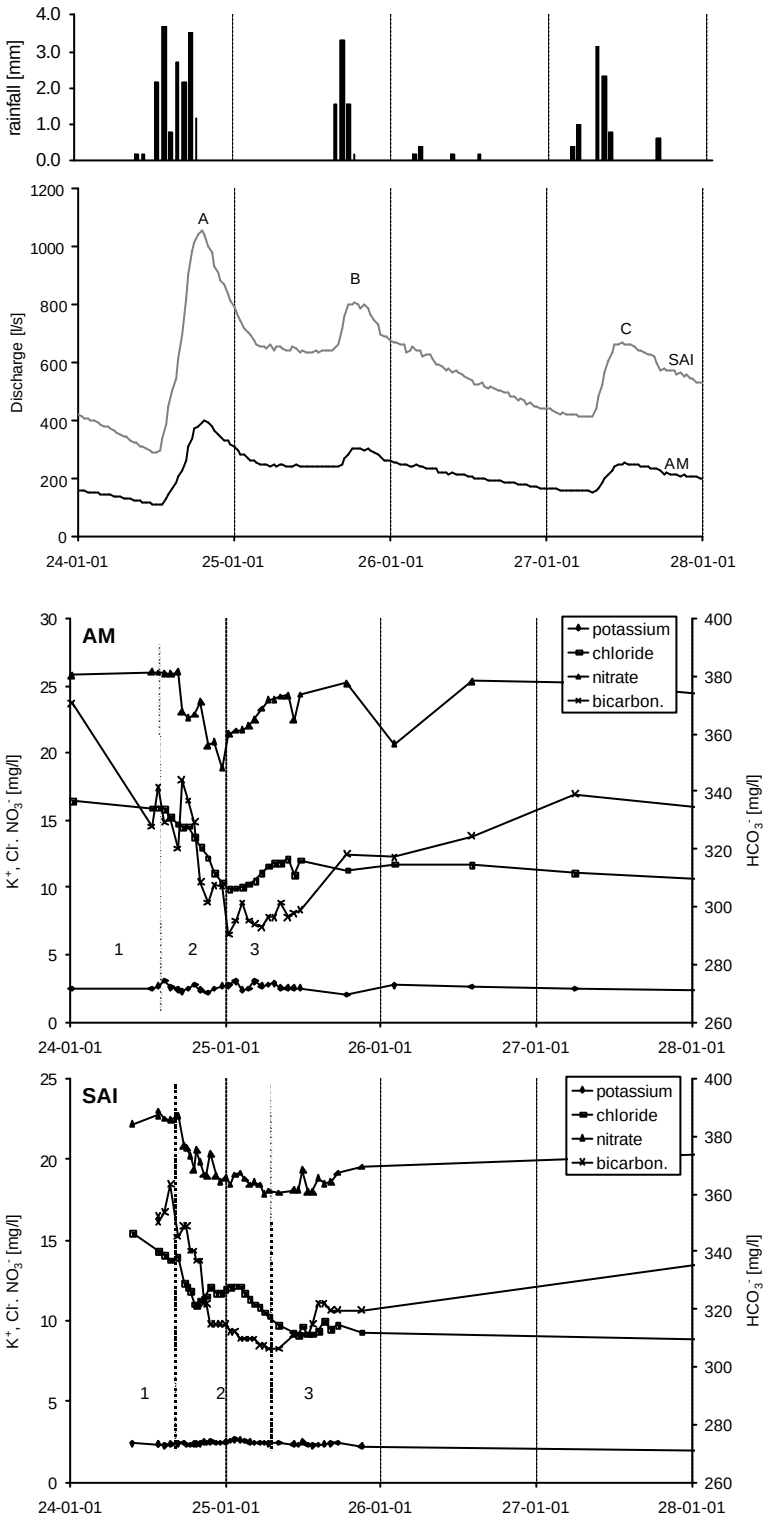

Fig. 3. January 2001 flood event: discharge measurements at AM and SAI (upper graph) and rainfall; chemographs at AM and SAI (lower graphs).

Qualitative interpretation

The overall trend is towards a decrease in concentration during the peak discharge. The major difference between AM and SAI is the existence of a peak in chloride at SAI during the flood maximum. At the spring, the piston phase lasted 4 hours, which corresponds to a volume of 5000 m^3, higher than for the October 2000 flood event as discharge at the beginning of the flood is more important. Consequently, preferential contribution by the AF tributary causes a general dilution. During the flood

peak, the influence of more contaminated tributaries (BU and AM) results in a peak in chloride, followed by a dilution corresponding to the arrival of the AM diluted waters. For all ions except bicarbonate, minimum concentrations at AM and SAI are the same (within 1 mg/l). For bicarbonate, the minimum concentration increased from 290 mg/l at AM to 305 mg/l at the spring. This change may indicate a possible dissolution along the horizontal flow path towards the spring.

June 2001 flood event

Hydrographs and chemographs description

This flood began on June 9th, after the start of a rainfall event continuing the whole day. A small rainfall event the previous day already caused a slight increase in discharge. Prior to this, the aquifer was stable for about two weeks. Calculated daily actual infiltration was 0.4 mm on the 8th of June, and 18.2 mm on the 9th of June. At AM, the flood event started on the 9th at 7:30 a.m. and peaked at 7 p.m. (Fig. 4). At SAI, the flood event also started at 7:30 a.m., and reached a maximum discharge of 700 l/s at 11 p.m.

Chemographs can be separated in three successive phases: At AM, pre-event water showed stable concentrations until 12 a.m. on the 9th, four hours later than the discharge. Peak flood water lasted 24 hours until 12 a.m. on the 10th. Nitrate and chloride increased continuously, bicarbonate decreased, and potassium peaked at midnight. Decreasing limb water displayed a decrease in chloride, nitrates and potassium, and a progressive increase in bicarbonate.

At the Saivu spring, pre-event water flowed until 12 a.m. on the 9th (equivalent to AM). Peak flood water occurred for 16 hours, until 6 p.m. on the 10th. Nitrate and chloride increased continuously, bicarbonate showed an initial peak followed by a decrease in concentration; potassium peaked at around 8 a.m. the 10th. Decreasing limb water was characterised by a progressive decrease in chloride, nitrates and potassium, and an increase in bicarbonate. At the end of the sampling period, concentrations were still higher than in pre-event waters, except for bicarbonate which returned to its initial concentration.

Qualitative interpretation

The June 2001 flood event showed a clear increase in pollution-related parameters together with a slight decrease in bicarbonate. The major difference between AM and SAI is the presence of a secondary peak in bicarbonate on the rising limb at SAI (confirmed by specific conductance measurements). Bicarbonate decreased during the flood maximum, but the decline was more important at AM. At the spring, the piston phase lasted four hours. This is similar to the two previously analysed flood events. Consequently an increase in bicarbonate was caused by more mineralised waters issued by either AF or BU. The chemical evolution after the flood peak is strongly linked to variations observed at AM. The nitrate curve followed the same pattern with a 6 hour delay, corresponding to a flow velocity of 750 m/h.

Conclusions

For the three flood events, concentrations are systematically lower at SAI compared to AM. This difference is caused by a dilution effect due to the mixing of the less contaminated tributaries BU and AF (Perrin et al. 2003a).

The three floods analysed illustrate that the spring chemographs can be explained by the preferential contribution of the respective tributaries through the flood (horizontal mixing). In the following section, we test a numerical model that attempts to simulate the observed chemographs by mixing the three main tributaries.

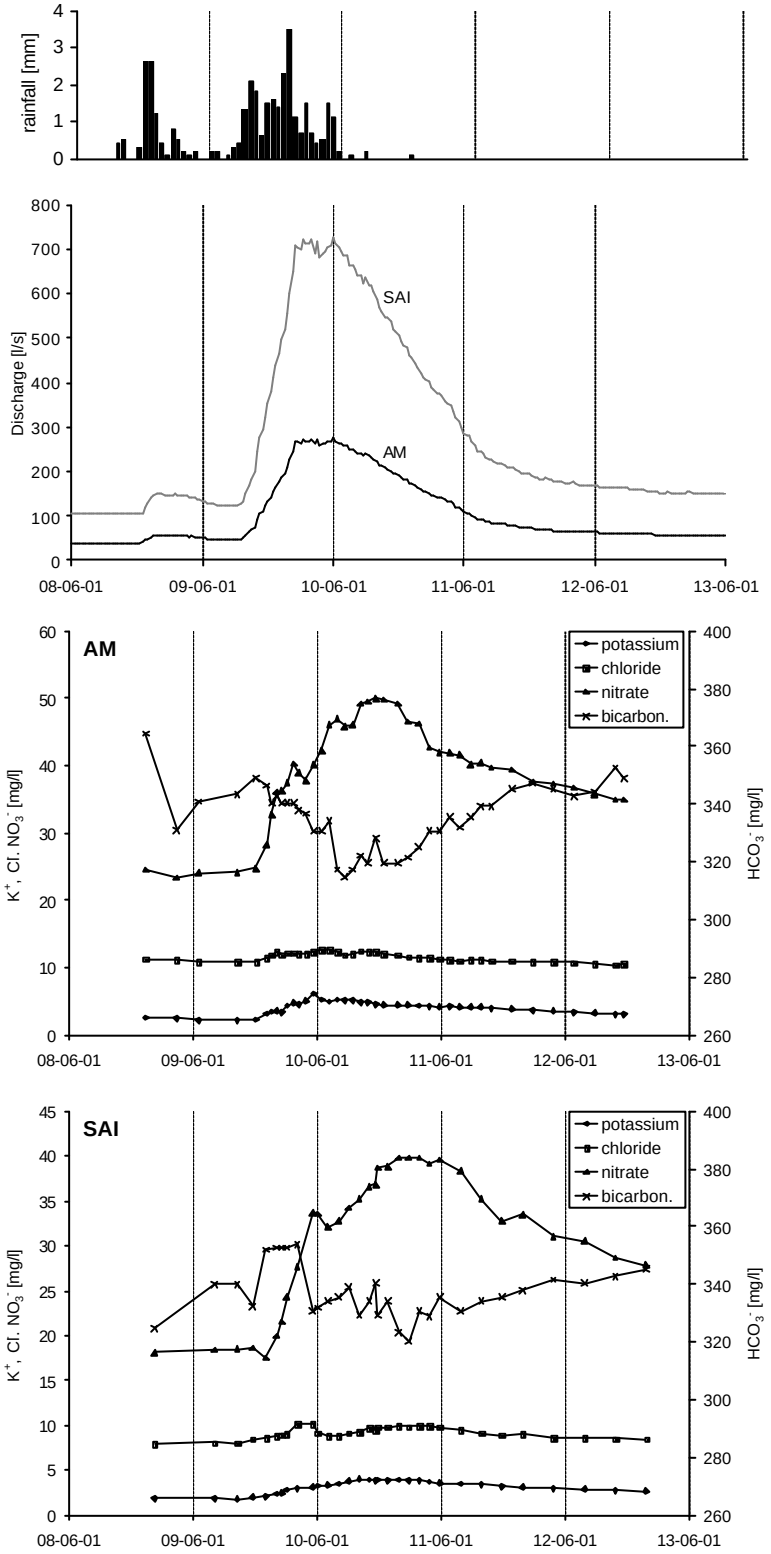

Fig. 4. June 2001 flood event: discharge measurements at AM and SAI (upper graph); chemographs at AM and SAI (lower graphs).

2.5.4. Numerical modelling

A numerical mixing model was used in order to simulate hydraulic and chemical responses at the Saivu spring. It considers the following three tributaries: Milandrine upstream (AM), Bure (BU), and Droite (AF). These tributaries are hydraulically connected and their combination should reproduce the spring response (SAI). Low discharge tributaries were not integrated as they can, at best, contribute to less than 1 % of the change in the chemical response (Perrin et al. 2003a).

Characteristics of the numerical model

Simulations were carried out using a 1-D transient flow and transport finite element numerical model developed at the Hydrogeology Centre, University of Neuchâtel . Well-type boundary conditions are used for discharge, and Dirichlet-type boundary conditions for fixed head and concentrations. The geometry is based on the Milandre conduit network (Fig. 5). A main conduit of 4766 m length is meshed with 2383 two-noded elements (nodes 1 to 2384) with 2 m size. Node 1 is AM where a flow and transport boundary condition is assigned. Node 2384 is SAI where the head is fixed to 0 m. At nodes 783 and 1699, corresponding to BU and AF tributaries respectively, boundary conditions of flow and transport are assigned.

Results of the modelling are fitted to the observed spring hydrographs and chemographs. Hydraulic heads are not considered as they have no real meaning in the system. An important limitation of the model is that it is based on darcian flow in pipes (constricted), where the relationship between flow velocity and discharge is linear. In real karst systems, this is rarely the case.

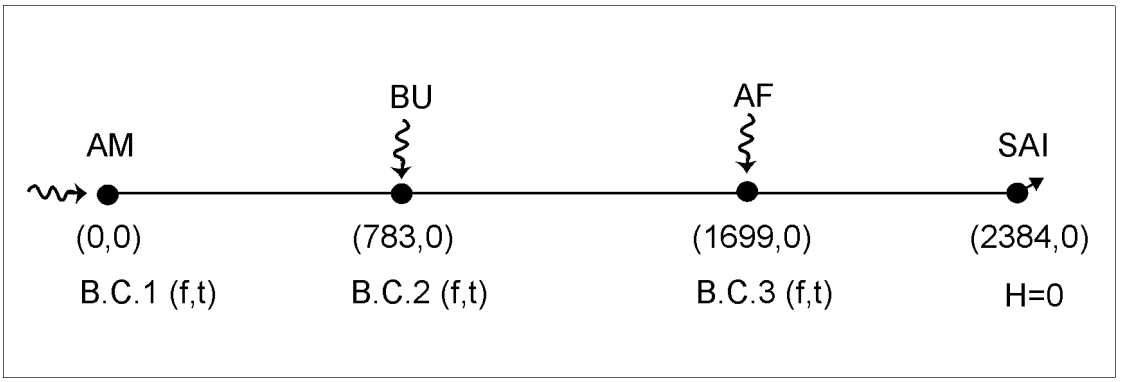

Fig. 5. Geometry of the numerical model.

Calibration of flow and transport parameters

Several simulations were carried out to test the sensitivity of the model to hydraulic and transport parameters. The most realistic results were obtained using the following values: Hydraulic conductivity between 0.5 and 10 m/s, a specific storage of 0.001, a porosity of 100 %, and a dispersivity of 0.1 m. These values are consistent with previous studies: Cornaton and Perrochet (2002) used a hydraulic conductivity of 10 m/s and a specific storage of 0.005 for an analytical modelling of karst spring hydrographs. Jeannin (2001) also used an effective hydraulic conductivity of 10 m/s for modelling head and flow distribution in the Hölloch cave system.

The flow velocity changes between the upstream part of the conduit and the spring. Based on tracing tests, Jeannin and Maréchal (1995) found the following velocities for a discharge of 50 l/s at AM: 500 m/h between AM and BU, 300 m/h between BU and AF, and 500 m/h from AF to the spring. These changes are reproduced in the model by distributing the hydraulic conductivity. We assigned a hydraulic conductivity of 0.5 m/s for the slower velocity section, and of 2 m/s for the two other sections.

Initial values of zero flow and head are attributed to all nodes in the model. The model is then run for 80 hours with constant flow and concentration imposed at the three tributaries in order to reach steady-state conditions.

Theoretical case

In these scenarios, discharge rates are the same at the three tributaries and concentration is kept constant at each of the tributaries. The only difference is the absolute concentration assigned to the respective tributaries. Three sets of fixed concentrations have been calculated (Fig. 6). The first two curves show that the model can reproduce temporal variations in concentration at the spring even if the concentrations are kept constant but different at the three tributaries. The two curves are asymmetric as the concentrations of AF and AM are reversed. Thus from real data, it could be possible to predict the existence of tributaries with different chemistries. Moreover their relative distance to the spring could be inferred.

Curve 3 is obtained with fixed concentrations at AF and AM, and changing concentrations at BU (curve 1 as boundary condition for transport). The result is close to curve 1, hence it appears difficult to ascertain if the tributaries have a constant or a varying chemistry based on the spring chemograph.

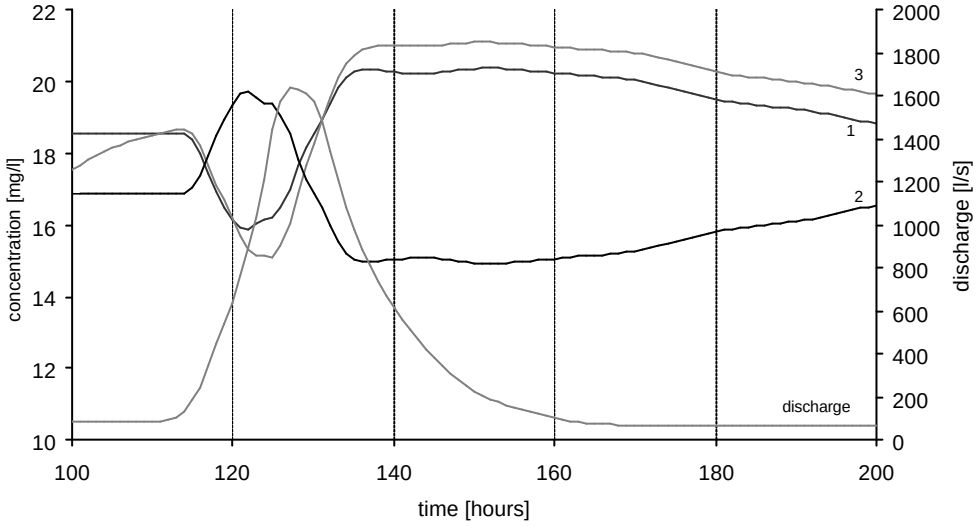

Fig. 6. Model response to theoretical boundary conditions. An equivalent discharge is assigned to the three tributaries. Curve 1 results from fixed concentrations of 25 mg/l at AM, 18 mg/l at BU, and 10 mg/l at AF. Curve 2 is obtained with fixed concentrations of 10 mg/l at AM, 18 mg/l at BU, and 25 mg/l at AF. Curve 3 results from fixed concentrations of 25 mg/l at AM, 10 mg/l at AF, and curve 1 at BU.

Modelling of the observed chemographs

In the following section, the nitrate chemographs of the three analysed flood events were modelled. This choice is based on the observed contrasted response at the spring, on the contrasted concentration of the three tributaries (Perrin et al. 2003a), and on the conservative behaviour of the tracer in the conduit network.

The discharge at AF was not continuously measured, nor were chemographs at BU and AF . Hence, boundary conditions at the three tributaries were fixed as follows: Measured nitrate and discharge at AM, measured discharge and fixed concentration at BU (based on monthly analyses), equivalent discharge to BU and fixed concentration at AF (based on monthly analyses). Discharge at AF is known to differ little from that of BU based on 10 discharge measurements. Selected concentrations for BU and AF are the mean annual values calculated from 14 samples. These are 17 mg/l at BU, and 16 mg/l at AF. For the October 2000 flood event, the fitting was improved by using the slightly different concentration of 21 mg/l at BU, and 20 mg/l at AF.

October 2000 flood event

The simulated discharge provides a good fit to the observed hydrograph (Fig. 7). The flood peak is sharper, but this difference can be due to uncertainties in the observed data (existence of losses in the phreatic zone). The simulated chemograph reproduces a slight decrease in concentration, but 7 hours later than the observed one. If this decrease is due to AM tributary, then flow velocity is underestimated

by the model. However, it is also possible that concentration decreases occurred in the other tributaries (data not available).

Total discharge at SAI spring is subdivided into three hydrographs corresponding to the volume of water issued from each tributary (Fig. 7, below). The relative contribution of the tributaries through the flood is clearly illustrated: AF water predominates during the rising limb, BU water during the decreasing limb, and the end of the flood is made up of AM water largely. The secondary peak of AM water after the flood starts is attributed to the piston effect: at low stage preceding the flood, AM water is more abundant than water from AF and BU . This secondary peak also occurs for the two flood events presented below.

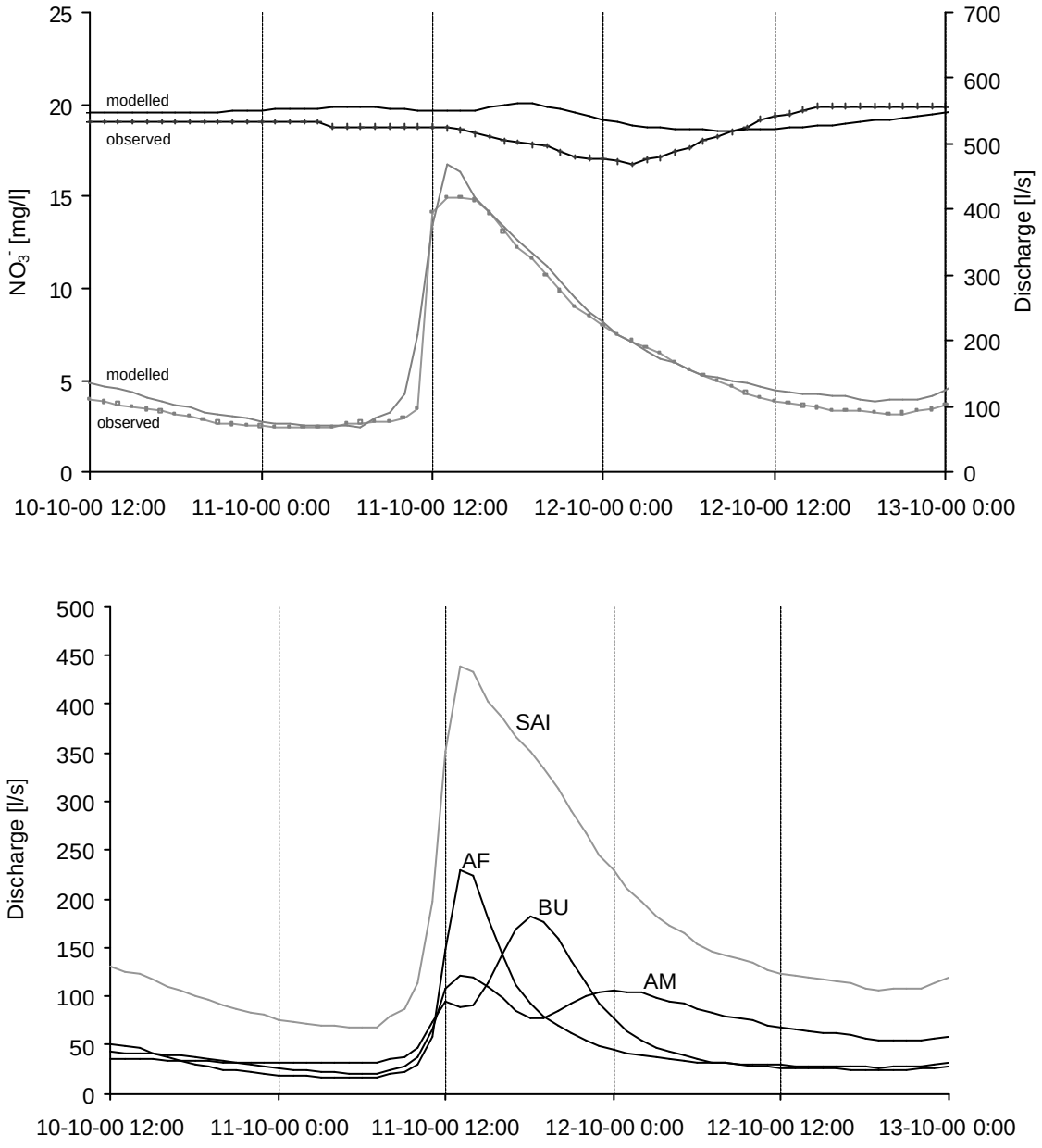

Fig. 7. Simulation of the October 2000 flood event. The upper graph compares the modelled curves (in plain) with the observed curves (line with symbols). Chemographs are in black and hydrographs in grey. The lower graph shows the respective contribution of the AM, BU, AF tributaries to the spring discharge SAI throughout the flood.

January 2001 flood event

Peak flood discharge is overestimated by the model, and the decreasing limb is retarded (Fig. 8). These differences could be partly a result of the uncertainties of AF's discharge rates, or of underestimates in the springs discharge (losses in the phreatic zone). The modelled chemograph closely matches that observed, even if the negative peak is slightly accentuated.

The successive preferential contribution of waters from AF, BU, and AM is adequate. The lag between AF and BU peaks is 2 h only. Hydrograph recession is largely dominated by AM's water.

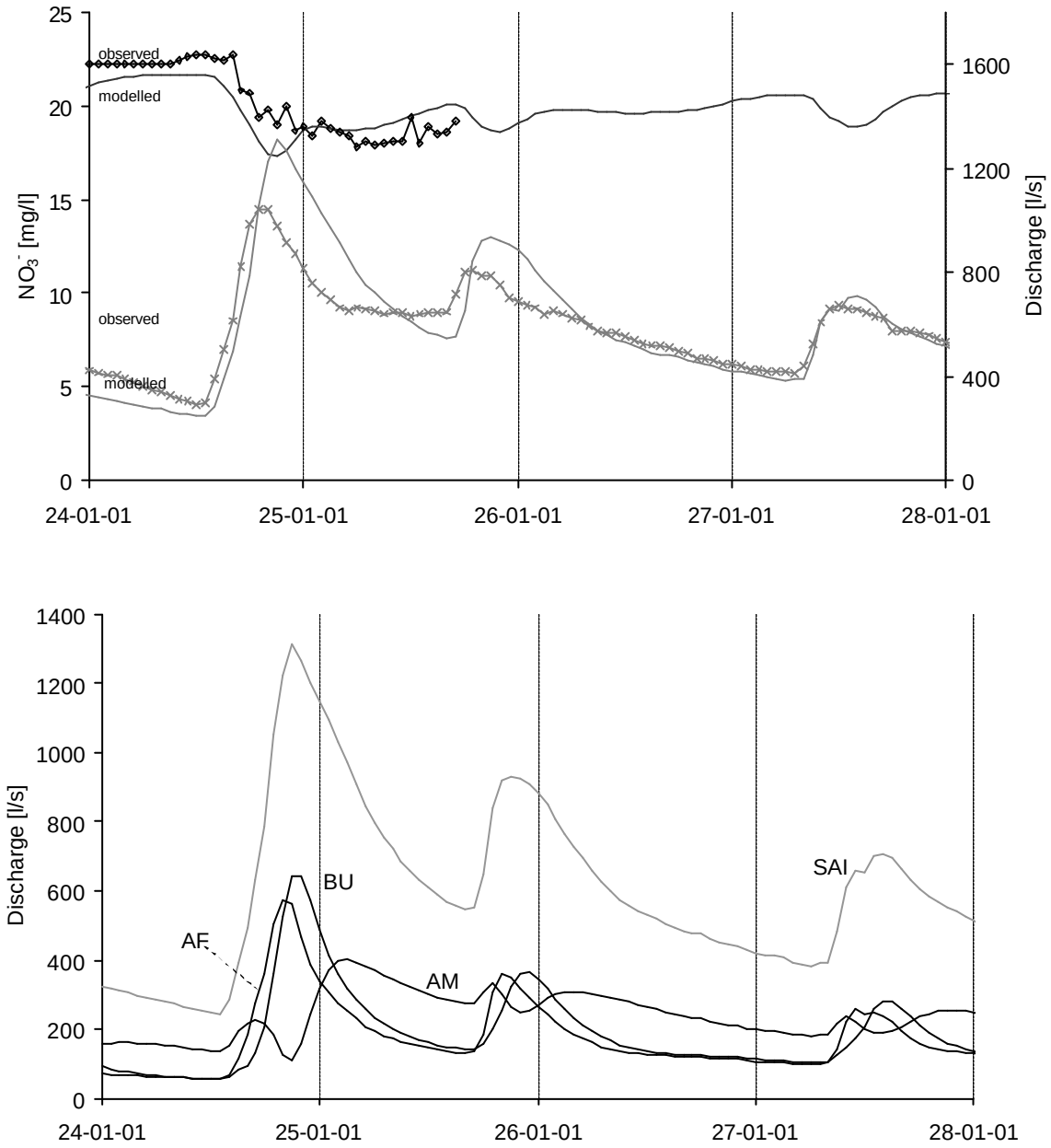

Fig. 8. Simulation of the January 2001 flood event. The upper graph compares the modelled curves (in plain) with the observed curves (line with symbols). Chemographs are in black and hydrographs in grey. The lower graph shows the respective contribution of the AM, BU, AF tributaries to the spring discharge SAI throughout the flood.

June 2001 flood event

The modelled hydrograph corresponds closely to that observed (Fig. 9). The major difference between the simulated and the observed chemograph lies in the retarded increase in concentration for the simulated curve (about 7 hours delay). The peak in nitrate concentration seems mainly to be due to the observed peak at AM. Hence the model underestimates flow velocities.

AF water predominates for a short duration when the flood starts, and BU water is the more dominant during the flood peak. The recession flow is mainly made up of AM water .

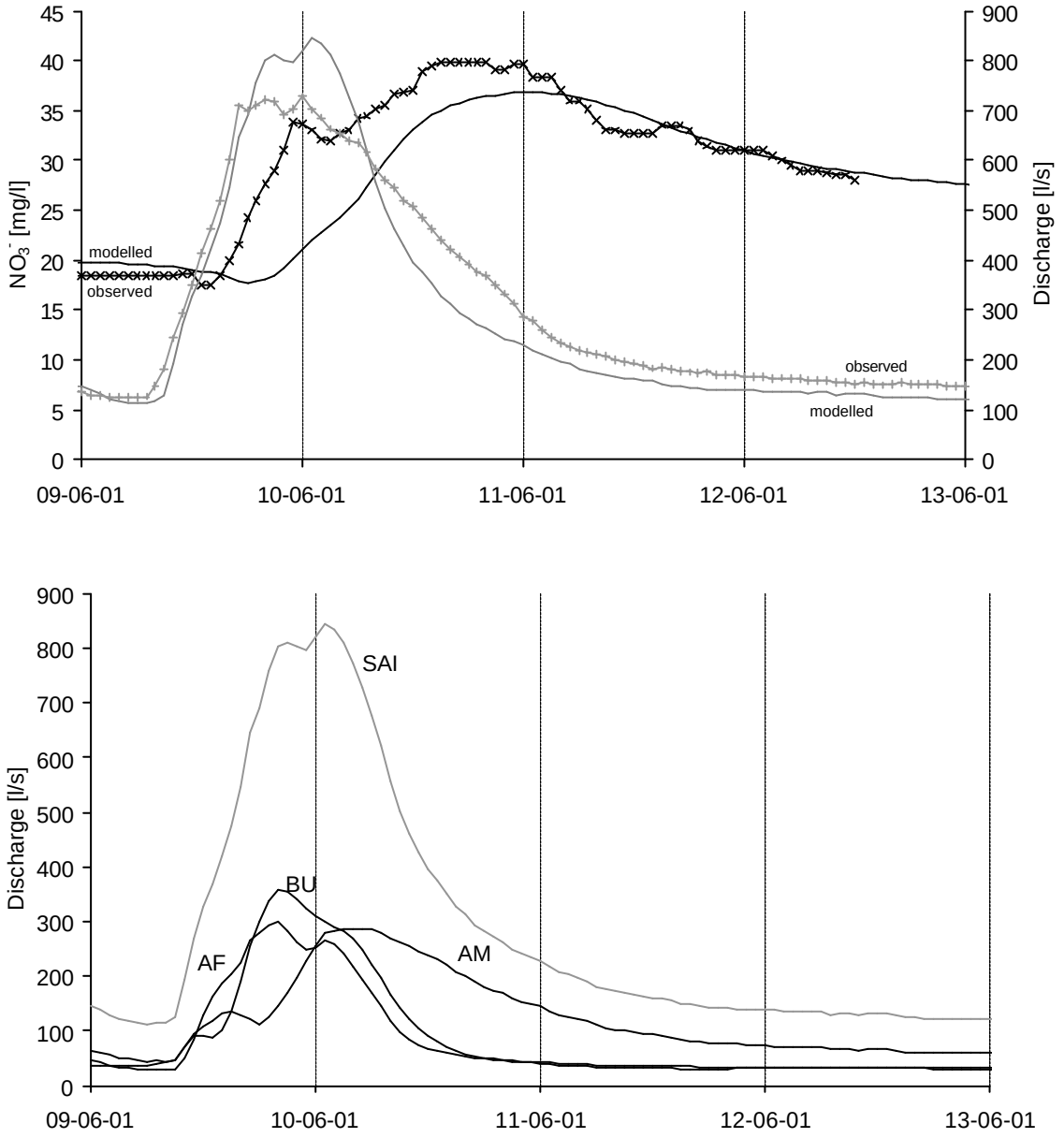

Fig. 9. Simulation of the June 2001 flood event. The upper graph compares the modelled curves (in plain) with the observed curves (line with symbols). Chemographs are in black and hydrographs in grey. The lower graph shows the respective contribution of the AM, BU, AF tributaries to the spring discharge SAI throughout the flood.

Conclusions

The fit between modelled and observed hydrographs and chemographs is satisfactory, especially when considering the simplicity of the used flow and transport model and the approximated flow and chemographs at BU and AF tributaries. From a qualitative perspective, the observations are reproduced. Two major differences appear however. Hydraulically, peak discharge is higher in the simulation, and chemically, changes in concentration are delayed in the simulation. This delay seems to be due to an underestimation of flow velocities. The use of a turbulent flow model could allow more realistic velocities to be obtained, and to better reproduce lag times in the chemographs.

Specific conductance curves

Specific conductance offers the advantage of being continuously recorded on the three tributaries. It is mainly related to dissolution parameters and hence allows verification of possible dissolution effects during the transit through the conduit network. During the three flood events presented above, the recording of specific conductance was incomplete at BU and non-existent at AF. Hence it was necessary to look for previous data in order to test the mixing on the whole system. Between 1992 and 1996, the three major tributaries and the spring were periodically measured. However time overlaps where all the data are available are limited. Two characteristic results are described below:

In February 1995, missing data are discharge at Saivu spring and discharge at AF. We assigned the discharge of BU at AF as an approximation. The modelled specific conductance curve closely matches the observed one (Fig. 10). The first peak is due to a NaCl tracing experiment carried out at AM. It is reproduced with a 7 hour delay, similar to those indicated in the nitrate modelling. Other peaks (negative or positive) coincide more closely: they originate at AF which is closer to the spring.

The only missing data for the February 1996 flood event is discharge at AF. For the simulation, we used the same discharge as BU. The modelled specific conductance is similar to the observed one (Fig. 11). Specific conductance measurements were not accurately calibrated; This may explain the shift between the two curves.

The mixing model accurately reproduces the measured specific conductance curves at the spring. As this parameter is mainly a result of dissolution related parameters, and, as the mixing model does not take this process into account, it is clear that dissolution is reduced in the conduit network, even during important flood events.

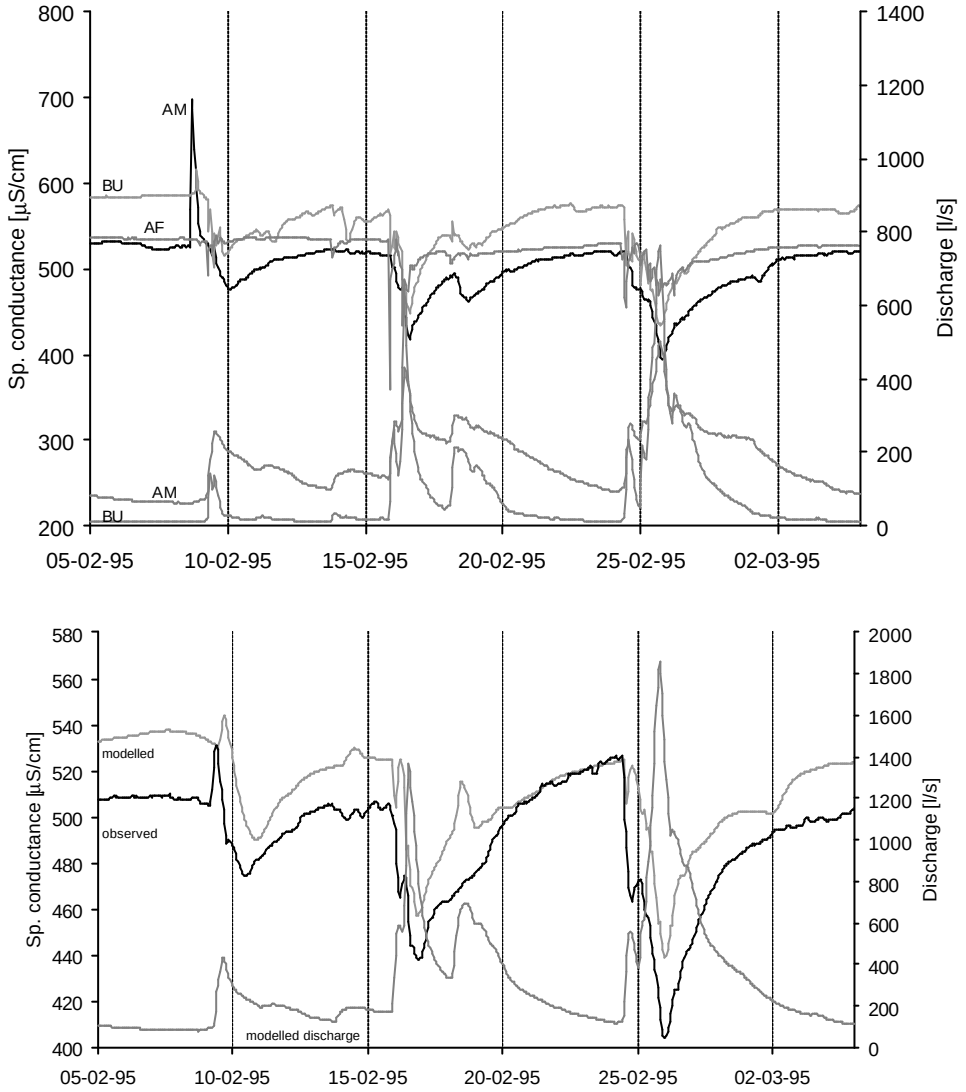

Fig. 10. The upper graph presents the observed data, used as boundary conditions for the simulation. The lower graph compares the results of the simulation with the observed specific conductance at the spring. No discharge data are available at the spring for this period.

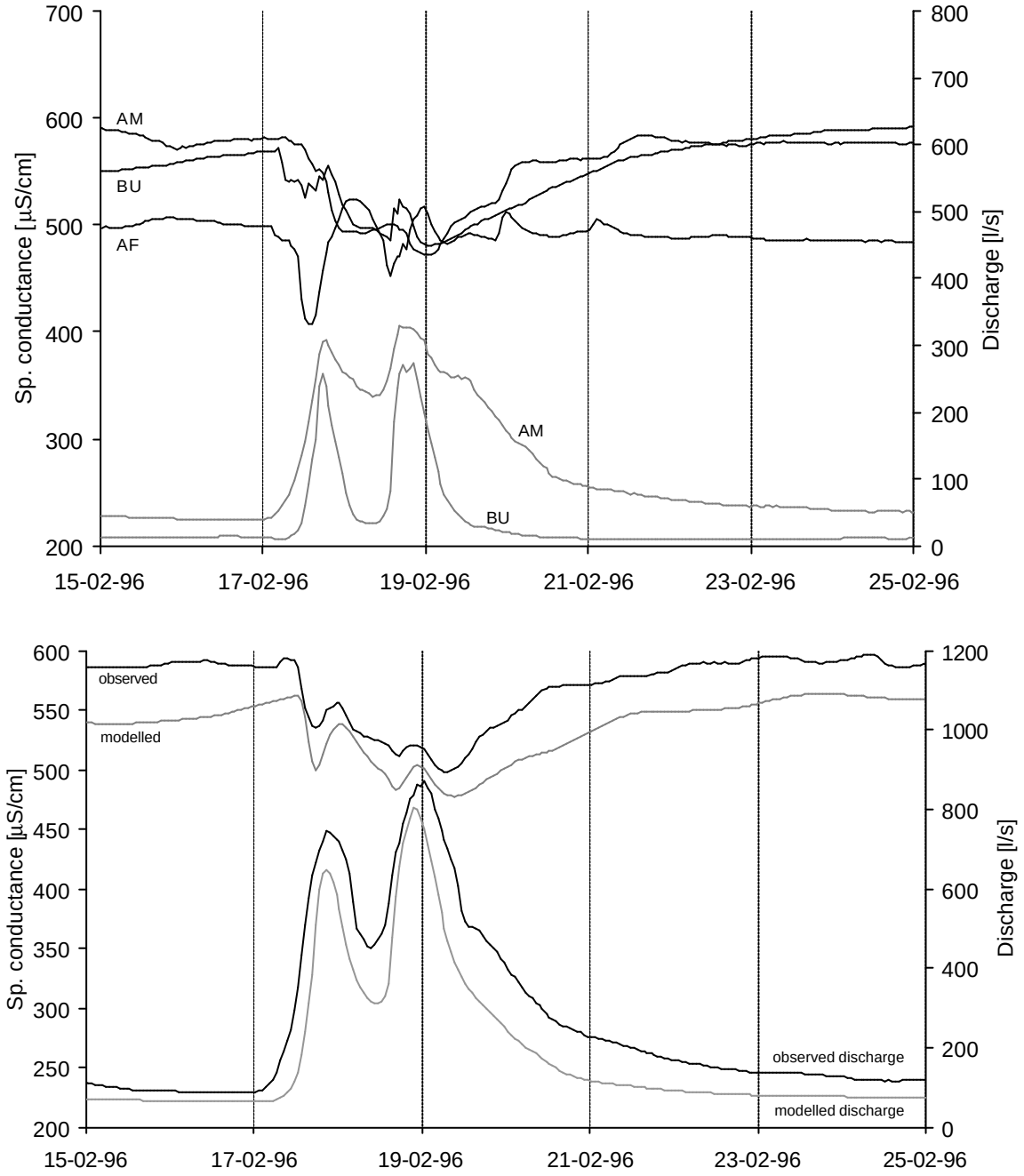

Fig. 11. The upper graph presents the data used as boundary conditions for the simulation. The lower graph compares the results of the modelling with the observed specific conductance and discharge at the spring.

2.5.5. Discussion

Sensitivity analysis

As shown in Fig. 12, results are not very sensitive to inflow boundary conditions, i.e. strong modifications in flow boundary conditions are necessary to produce significant changes in the chemographs. Increasing discharge at AF by a factor 4 or 8 accentuate the first negative peak but not much the other part of the curve. Moreover, by assigning the AM flow rate instead of BU at the AF tributary only has a slight influence on the resulting chemograph. Hence uncertainties about AF's discharge have limited consequences for the simulated chemographs.

Modifications on transport boundary conditions are more sensitive: The first negative peak disappears if AF or BU are kept at a constant concentration. The last peak is absent and the dilution effect is shortened if AM's concentration is fixed.

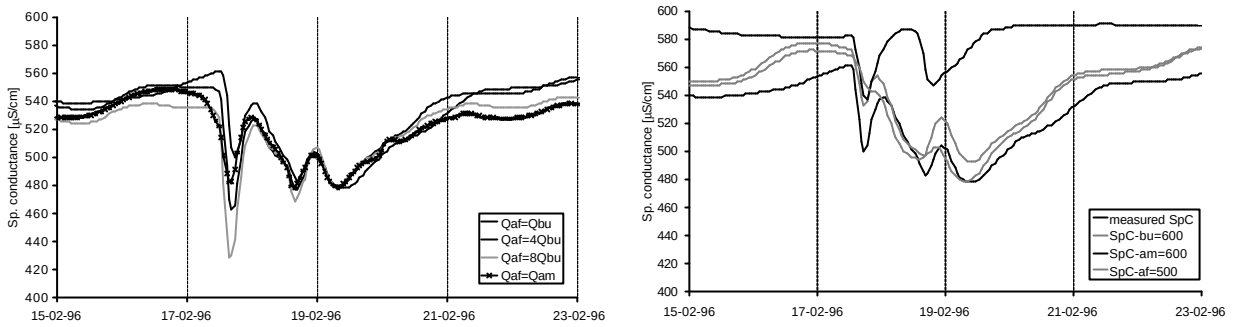

Fig. 12. Sensitivity analysis for the February 1996 flood events: on the right, specific conductance is fixed at a constant value (600 µS/cm for AM and BU, 500 µS/cm for AF) successively for each tributary. On the left, AF discharge is progressively increased by a factor 4, and 8. A last simulation is run by assigning AM discharge at AF instead of BU.

The role of mixing at Milandre karst system

The use of a simple mixing model allows spring chemographs to be reproduced from the chemographs and hydrographs of the main tributaries feeding the phreatic zone. This important result shows that chemical reactions (especially dissolution) are non-existent or limited in the horizontal conduit network feeding the spring. Moreover, mixing of waters with differing chemistries can lead to temporal variations in the spring chemistry during flood events. This is especially true for parameters showing an important spatial variability in the spring catchment. At Milandre, pollution-related parameters fall into this category as they are directly linked to land use in the sub-catchments (Perrin et al. 2003a). In contrast, dissolution-related parameters are spatially more homogeneous as they are acquired within the system.

At Milandre, the mixing poles are the three main tributaries of the underground river. Their chemistries are acquired in the unsaturated zone of the system. Thus most of the mixing models proposed in the literature are not adapted to this test site, as they generally do not consider tributary mixing (except Hess and White 1988), but attribute a mixing pole to phreatic storage (Blavoux and Mudry 1983, Dreiss 1989, Vervier 1990, Lee and Krothe 2001, Maloszewski et al. 2002).

A conceptual model of flow and transport for the Milandre karst system

We can summarise the hydraulic and transport behaviour of the Milandre karst system by the conceptual model presented in Fig. 13:

Diffuse infiltration occurs in different sub-catchments having differing land-uses. Land-use controls groundwater chemistry to a large extent for pollution related parameters. Water is stored in reservoirs located in the upstream part of the sub-catchment (probably in the soil and the epikarst), and becomes saturated with respect to calcite. At low water stage, this "perched" groundwater is continuously released as base flow (Q_b) and feeds the tributaries. These base flows mix together in the phreatic zone to yield the spring water chemistry.

In case of moderate flood events (e.g. October 2000 flood event), quick flow (Q_q), which is an overflow of the perched reservoirs and has the same chemical composition ($C_{1, 2, 3}$) as base flow, contributes to the spring discharge. No clear changes occur in dissolution-related parameters as they have similar concentrations in the sub-catchments. In contrast, pollution-related parameter chemographs vary at the spring due to the horizontal mixing of the tributaries. Their flow-through times are proportional to the distance from the spring (L1, L2, L3). This case is illustrated by the hydrograph A (Fig. 13).

In the case of important flood events (e.g. January 2001 flood event), reservoir thresholds (h) are fed by water infiltrated as fresh flow (Q_f) having the chemistry C_f. This water is undersaturated with respect to

calcite and dilutes the base flow and quick flow components. Hence both dissolution-related parameters and pollution-related parameters vary at the spring (hydrograph B, Fig. 13).

This overall behaviour is illustrated by the two successive flood events of October 2001 (Fig. 14). The first flood is characterised by significant variations for the pollution related parameter (nitrate) and only slight changes for the dissolution related parameter (specific conductance). Hence, this flood event consists only of base flow and quick flow. Horizontal mixing explains the nitrate variations. The second flood, with higher discharge rates, presents an important dilution for both parameters. The specific conductance decrease is caused by the participation of fresh flow, which also accentuates the decrease in nitrate concentrations. Participation of base flow, quick flow, and fresh flow to flood events has also been observed by temporal variations of water stable isotopes at different points in the Milandre karst system (Perrin et al. 2003b).

This aquifer's behaviour has two important consequences:

- Moderate flood events could be used to detect the existence of tributaries with a contrasting chemistry. Moreover it should be possible to infer their respective location with respect to the spring.
- Vulnerability of the karst system becomes more elevated during important flood events, when fresh flow by passes the reservoirs and can reach the spring in hours. In contrast, flow-through times of base flow and quick flow are of the order of weeks or months.

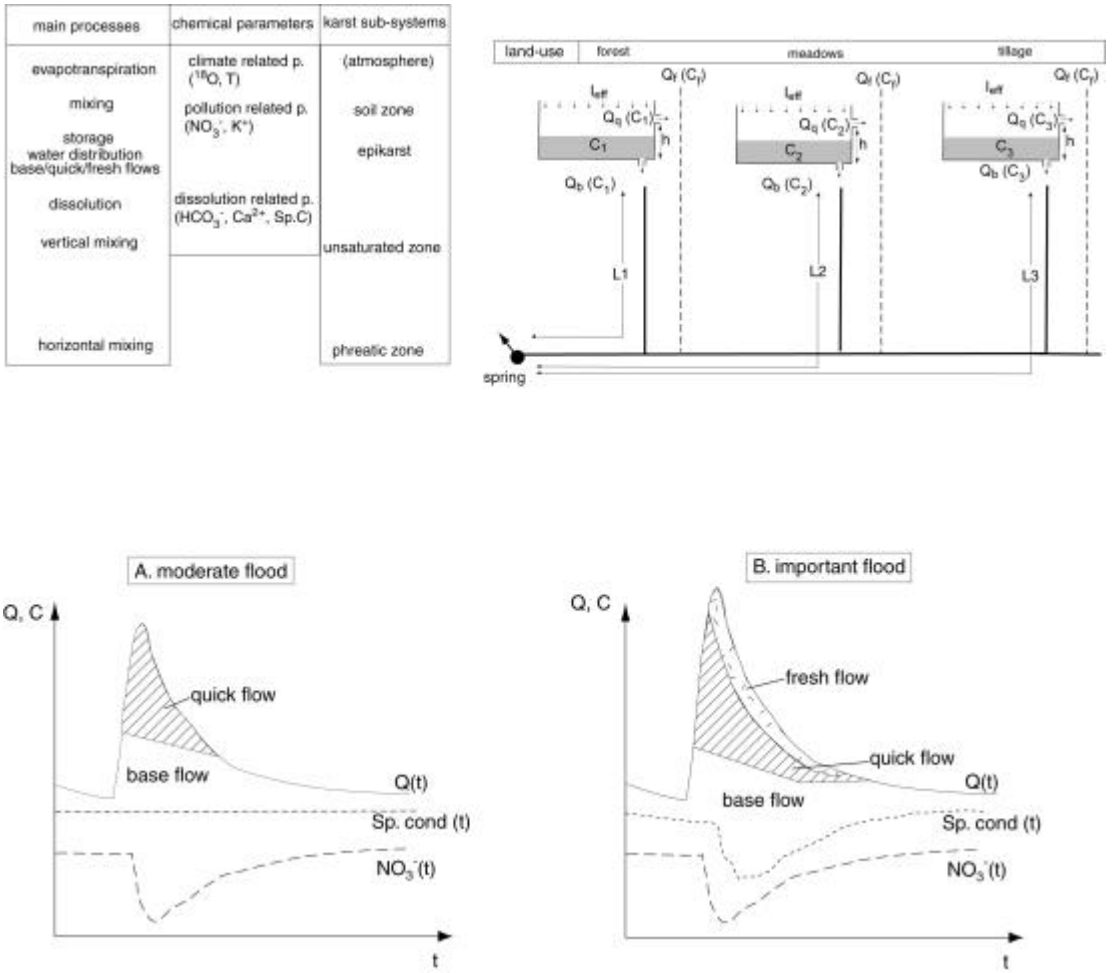

Fig. 13. Conceptual model of flow and transport in the Milandre karst aquifer. Three sub-catchments are schematised: the first, mainly forested, could correspond to AF, the second occupied by meadows approximates BU, and the last, cultivated, could represent AM. The two lower graphs schematically represent the hydrograph decomposition into base (Q_b), quick (Q_q) and fresh (Q_f) flows from chemographs for nitrate concentrations and specific conductance. A. corresponds to a moderate flood event (no fresh flow), and B to a flood event with a higher discharge rate.

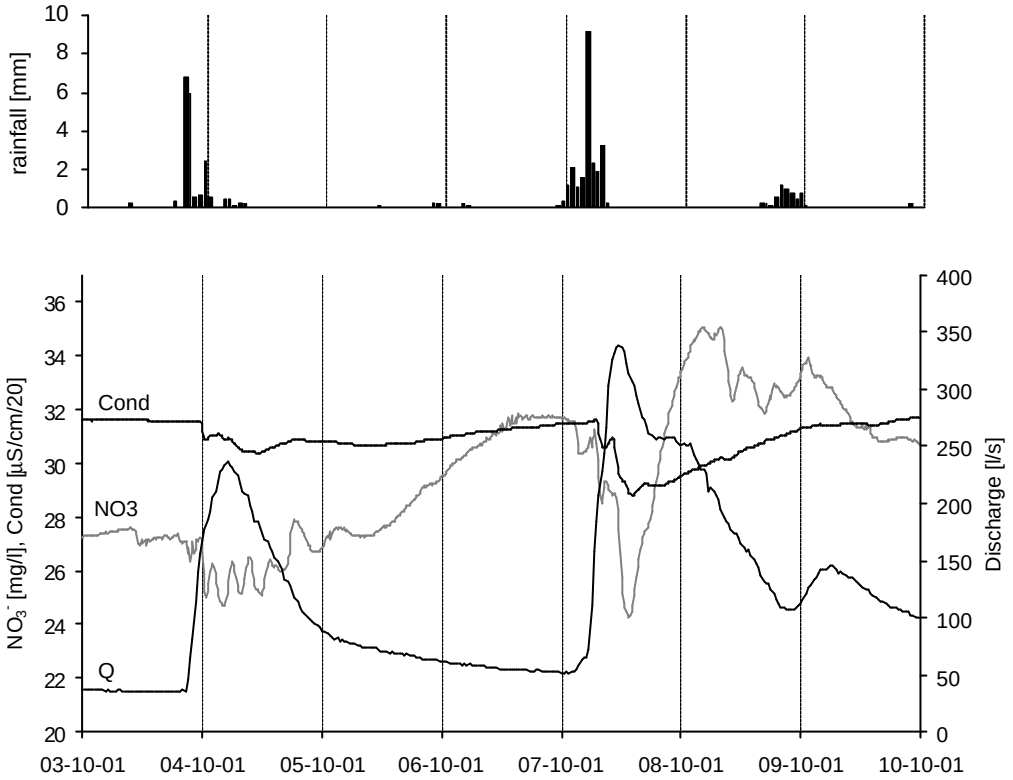

Fig. 14. Evolution of the specific conductance and the nitrates concentration at Milandrine upstream (AM), in October 2001.

2.5.6. Conclusions

The proposed mixing model, which only consider the relative contribution of the three main tributaries of the system, can reproduce karst spring chemographs. This has two important consequences for the transport in the conduit network:

- transport is mainly non-reactive even during flood events
- no other mixing component exists in the conduit network

Hence, chemical reactions (e.g. limestone dissolution) occur in the unsaturated part of the system, most probably in the soil and epikarst zones. It means that the chemistry of the mixing tributaries is determined in the upstream part of the system.

Two types of natural tracers can be defined: dissolution related parameters, which have similar concentrations in the sub-systems, and pollution related parameters, which are spatially heterogeneous due to contrasted land-use in the sub-systems. Observations of their respective chemographs allow two types of flood events to be distinguished:

- Floods of moderate importance: Only the concentrations of the pollution-related parameters vary significantly at the spring because of the non linear mixing of the tributaries during floods (horizontal mixing). A detailed description of the chemograph can lead to the detection of tributaries with a distinct chemistry. Their distance to the spring and their relative importance can be assessed, allowing some information to be inferred on the karst systems drainage structure.
- Important flood events: Both types of natural tracers present important concentration variations at the spring. The general trend results in a decrease in the concentration of dissolution-related parameters due to the participation of fresh infiltrated water.

The fresh water component mixes with the pre-existing groundwater present in the unsaturated zone of the system. This mixing process is complicated by dissolution processes occurring in the mean time. This topic must be studied in more detail in the future. With respect to the vulnerability of the aquifer, it is clear that important flood events threaten much more the water quality as transit times are shortened to a large extent.

Acknowledgements
This project was supported by the Swiss National Science Foundation, Grant n° 20-61717.00. We are indebted to the Jura Caving Club for access to the cave. At the Centre of Hydrogeology, T. Ettlin, F. Bourret, B. Wenger and S. Cattin gave us priceless support for the field and the lab work. F. Cornaton provided great help for the modelling part of the study.

References

Blavoux, B. and Mudry, J., 1983. Décomposition chimique des hydrogrammes du karst. Hydrogéologie-Géologie de l'Ingénieur, 4: 270-278.

Cornaton, F. and Perrochet, P., 2002. Analytical 1 D dual-porosity equivalent solutions to 3D discrete single-continuum models. Application to karstic spring hydrograph modelling. Journal of Hydrology, 262: 165-176.

Coxon, C., 1999. The nature of human impacts on karst waters: agriculturally induced impacts. In: IAH (Editor), Karst hydrogeology and human activities. International contribution to hydrogeology: 37-63.

Dreiss, S.J., 1989. Regional scale transport in a karst aquifer: 1. Component separation of spring flow hydrographs. Water Resources Research, 25(1): 117-125.

Grasso, D-A. and Jeannin, P-Y. 1994. Estimation des pertes dans la partie aval du réseau karstique de la Milandrine: bilan hydrique au sein d'un aquifère karstique. Bulletin d'Hydrogéologie, 13: 115-128.

Gretillat, P.-A., 1996. Les aquifères karstiques et poreux de l'Ajoie (Jura, Suisse), Neuchâtel, Neuchâtel, 209 pp.

Groves, C.G., 1992. Geochemical and kinetic evolution of a karst flow system: Laurel creek, West Virginia. Groundwater, 30(2): 186-191.

Hess, J.W. and White, W.B., 1988. Storm response of the karstic carbonate aquifer of south-central Kentucky. Journal of Hydrology, 99: 235-252.

Iqbal, M.Z. and Krothe, N.C., 1995. Infiltration mechanisms related to agricultural waste transport through the soil mantle to karst aquifers of southern Indiana, USA. Journal of Hydrology, 164: 171-192.

Jamier, D., 1976. Interprétation des essais de traçage des eaux karstiques. Proc. 2nd Conf. On limestone hydrology. Ann. Sci. Univ. Besançon, 25: 229-240.

Jeannin, P-Y., 2001. Modeling flow in phreatic and epiphreatic karst conduits in the Hölloch cave (Muotatal, Switzerland). Water Resources Research, 37(2): 191-200.

Jeannin, P.-Y., 1998. Structure et comportement hydraulique des aquifères karstiques, Neuchâtel, Neuchâtel, 237 pp.

Jeannin, P.-Y. and Grasso, D.A., 1995. Estimation des infiltrations efficaces journalières sur le bassin karstique de la Milandrine. Bulletin d'Hydrogéologie, 14: 83-94.

Jeannin, P.-Y. and Maréchal, J.-C., 1995. Lois de pertes de charge dans les conduits karstiques: Base théorique et observations. Bulletin d'Hydrogéologie, 14: 149-176.

Kiraly, L. and Mueller, I., 1979. Hétérogénéité de la perméabilité et de l'alimentation dans le karst : effet sur la variation du chimisme des sources karstiques. Bulletin du Centre d'Hydrogéologie, 3: 237-285.

Kiraly, L., 1998. Modelling karst aquifers by the combined discrete channel and continuum approach. Bulletin d'Hydrogéologie, 16: 77-98.

Lakey, B. and Krothe, N.C., 1996. Stable isotopic variation of storm discharge from a perennial karst spring, Indiana. Water Resources Research, 32(3): 721-731.

Lee, E.S. and Krothe, N.C., 2001. A four-component mixing model for water in a karst terrain in south-central Indiana; USA. Using solute concentration and stable isotopes as tracers. Chemical Geology, 179: 129-143.

Maloszewski, P., Stichler, W., Zuber, A. and Rank, D., 2002. Identifying the flow systems in a karstic-fissured-porous aquifer, Scheealpe, Austria, by modelling of environmental 18O and 3H isotopes. Journal of Hydrology, 256: 48-59.

Maréchal, J-C., 1994. Etude et modélisation de l'hydraulique et du transport dans les drains karstiques. MSc. Thesis Hydrogeology Centre, Neuchâtel University. 128 pp.

Perrin, J. and Wenger, B., 2001. Continuous measurement of nitrates concentrations, lab tests and field results in a karstic aquifer. In: J. Mudry and F. Zwahlen (Editors), 7th Conference on Limestone hydrology and Fissured media. Univ. de Besançon: 277-280.

Perrin, J., Jeannin, P.-Y. and Zwahlen, F., 2003a. Implications of the spatial variability of the infiltration water chemistry for the investigation of a karst aquifer. Accepted by Hydrogeology journal.

Perrin, J., Jeannin, P.-Y. and Zwahlen, F., 2003b. Epikarst storage in a karst aquifer : a conceptual model based on isotopic data. Milandre test site, Switzerland. Submitted to Journal of Hydrology.

Sauter, M., 1992. Quantification and forecasting of regional groundwater flow and transport in a karst aquifer (Gallusquelle, SW Germany), Tübingen, Tübingen, 151 pp.

Shuster, E.T. and White, W.B., 1971. Seasonal fluctuations in the chemistry of limestone springs: A possible means for characterizing carbonate aquifers. Journal of Hydrology, 14: 93-128.

Ternan, J.L., 1972. Comments on the use of a calcium hardness variability index in the study of carbonate aquifers; with references to the central Pennines, England. Journal of Hydrology, 16: 317-321.

Vervier, P., 1990. Hydrochemical characterization of the water dynamics of a karstic system. Journal of Hydrology, 121: 103-117.

White, W.B., 1988. Geomorphology and hydrology of karst terrains. Oxford University Press, Oxford, 464 pp.

Wicks, C.M. and Engeln, J.F., 1997. Geochemical evolution of a karst stream in Devils Icebox Cave, Missouri, USA. Journal of Hydrology, 198: 30-41.

Worrall, F. and Burt, T.P., 2001. Inter-annual controls on nitrate export from an agricultural catchment - how much land-use change is safe ? Journal of Hydrology, 243: 228-241.

2.6. Chemical reactions vs. mixing in the unsaturated zone of karst aquifers

Abstract
Chemical variations at karst springs during flood events are interpreted as the result of the mixing of waters from different origins, or as the arrival of undersaturated waters with respect to calcite. In order to describe the actual processes in more details, the present observations have been made at a local scale: i.e. within the unsaturated zone of karst systems located in the Swiss Jura. Sampling points were percolation waters arriving at the roof of natural caves, between 15 m and 50 m below ground surface. Significant recharge events were sampled in details: observed natural tracers were major ions, specific conductance, and Oxygen stable isotopes. The hydraulic response was also recorded. Three sites were selected, each having their own specificity: Brandt site has no soil cover and percolation water was sampled in a cave 15 m below ground surface, Grand Bochat has a thin soil cover and percolation water is sampled 18 m below ground surface, EC percolation (Milandre test site) is located at the base of the unsaturated zone, 35 m below ground surface, in a catchment of thicker soil cover.

Results showed that, during flood events, vadose flow is a mixing of waters from different origins: base flow water mainly issued from the epikarst, soil water, and fresh infiltrated water. Their respective proportion is changing between sites, but, when present, soil water appears to be dominant. Base flow water recovers rapidly to 100 % participation at the end of the flood. Epikarst water is at saturation with respect to calcite. Fresh water and soil water are undersaturated and dissolve limestone during their transit in the unsaturated zone. These waters can reach the base of the vadose zone still undersaturated with respect to calcite. The soil zone, even of limited thickness, contributes largely to the flood flow, and mixes fresh infiltrated water. The epikarst reservoir has to be of an important size in order to keep a stable chemistry. During flood events, it distributes soil (and fresh) water to the fissures downwards. At steady-state flow conditions, it sustains base flow. Karst spring chemographs are the results of the transport processes occurring in the unsaturated zone mainly.

2.6.1. Introduction

Rain water recharging a karst aquifer acquires a typical calcium-bicarbonate chemistry during its flow path through the system (White 1988). In steady-state conditions, karst spring water is generally equilibrated with respect to calcite and keeps a stable chemistry. During flood events, spring water chemistry presents variations. In the literature, two distinct models are applied to explain these variations: The first is based on the mixing of different types of water (Blavoux and Mudry 1983, Dreiss 1989, Williams 1983, Vervier 1990, Sauter 1992, Hess and White 1988, Plagnes 2001). The second is based on the disequilibrium between dissolution kinetics and flow velocity: during flood events, water flows too quickly for reaching thermodynamic equilibrium (Shuster and White 1971, Ternan 1972, Grasso 1999). Most of these studies were carried out at the basin scale in studying the chemical response at the spring.

In the present study, three sites located in the Swiss Jura have been used: Milandre, Brandt, and Grand Bochat (Fig. 1). The first allows observations at the base of the unsaturated zone and within the phreatic zone. The two others are percolation waters within the unsaturated zone.

The objectives of the study are the following:

1. what are the respective role of mixing and chemical reactions in the unsaturated zone?
2. what are the origin of the waters participating to the flood?
3. what are the proportions and transit times of these waters during the flood?
4. to what extent can we interpret karst spring chemographs?

2.6.2. Study areas and methods

The Milandre test site is a karst aquifer with a 13 km^2 catchment area (Gretillat 1996, Jeannin 1998). The springs have a total discharge comprised between 40 and 2000 l/s. Specific conductance in base flow conditions is around 600 µS/cm, and can decrease to 530 µS/cm at high discharge rate. Sampling sites (EC, EN, SO) are located in the upstream part of the Milandre underground river. EC occurs at the cave ceiling as vadose flow (mean discharge is 0.07 l/min), SO and EN feed the underground river as secondary tributaries (mean discharge is 6 l/min for SO, 2.4 l/min for EN). They are situated at the base of the unsaturated zone that is 35 m to 45 m below ground surface. The unsaturated zone comprises a cohesive soil of 1 m thickness, an epikarst of variable thickness (probably 1-5 m) and a fissured media connected to the base of the unsaturated zone. Piezometric levels measured apart from the underground river show that the river is the lowest part of the phreatic zone.

Fig. 1: Geographical location of the sites

Brandt and Grand Bochat sites are small caves located high in the unsaturated zone of the Areuse karst system (Gigon 1976). The total thickness of the unsaturated zone is about 300 m and the catchment size is on the order of 130 km^2. Mean discharge of Areuse spring is 4.5 m^3/s. Specific conductance is 370 µS/cm at low stage, and can decrease to 230 µS/cm during flood events.

At Brandt site, sampled water is vadose flow issued from a fissure at the cave roof. It is located 15 m below ground surface; the discharge at low stage is 0.4 l/min, corresponding to a basin of 100 m^2.

At Grand Bochat site, sampled water is vadose flow issued from a small conduit located 20 m below ground surface. Discharge is 0.1 l/min at low stage. For both sites, brown soils are less than 1 m thickness. They cover the epikarst zone which is drained by a fissured media connected to the caves where observations were done. The sampled flood event at Brandt site was carried out when the soil cover was artificially removed from the sampled inlet catchment.

At each site, flood events caused by important precipitation were sampled in detail (Oxygen-18, major ions, discharge, specific conductance). Water specific conductance and temperature were measured directly on site. Water samples were collected by an automatic sampler at regular time spacing. pH was determined within 12 hours at sampling temperature, bicarbonate within 24 hours by titration and the other ions were analysed by ionic chromatography after a 0.45µ filtration. For cation preservation, filtered samples were acidified to pH < 2 with HNO_3 suprapur. Nitrate concentrations in samples with or without formol were equivalent, therefore most samples were taken without it.

The quality of the analyses has been checked by ionic balances, which have to be comprised between 0 and 5 %. Oxygen-18 analyses have been carried out by the lab Hydroisotop Gmbh with the standard method of CO_2 equilibration and purification. The analytical precision is ± 0.15 ‰.

The Saturation Index (S.I.) is calculated with the Phreeqc code (Parkhurst et al. 1980, Parkhurst and Appelo 1999). The S.I. for calcite is given by:

$$S.I. = \log\left[\frac{IAP(T)}{K(T)}\right] \quad (1)$$

Where *IAP(T)* is the ion activity product and *K(T)* the equilibrium solubility product (both as functions of the sample temperature) for the reaction:

$$CaCO_3(s) = Ca^{2+} + CO_3^{2-} \quad (2)$$

The values of S.I. determines whether the solution is undersaturated (S.I.< 0), supersaturated (S.I.> 0), or in equilibrium (S.I.= 0) with respect to calcite.

The sensitivity of S.I. to changes in pH, Ca, and HCO_3 concentrations is given in table 1. The "true" S.I. was calculated for a sample of Brandt site (sample) at base flow conditions. The pH was decreased and increased by 0.1 unit corresponding to the measure uncertainty (<pH, >pH). Then Ca was increased by 10 mg/l (>Ca), and HCO_3 was decreased by 10 mg/l (<HCO_3). The results show that S.I. is very sensitive to pH. As most samples were collected by autosamplers, the pH measurement precision is at maximum $\pm$ 0.1, meaning the same precision for S.I. Error bars are used accordingly for each S.I. graph.

Table 1: sensitivity analysis of the S.I. parameter

	pH	Ca	HCO_3	calcite S.I.
sample	7.3	76.33	261.08	**-0.10**
< pH	7.2	76.33	261.08	-0.20
> pH	7.4	76.33	261.08	0.00
> Ca	7.3	86.33	261.08	-0.05
< HCO_3	7.3	76.33	251.08	-0.11

2.6.3. Calcite saturation index under base flow conditions

At Milandre site, 16 observations points (percolation waters, tributaries, spring) issued from the unsaturated and the phreatic zones were collected on a monthly basis during one year. Sampling was mainly carried out at low stage (Perrin et al. 2003c). All the samples are saturated with respect to calcite (data available on the web site: www.unine.ch/chyn, karst hydrogeology).

At Grand Bochat site, base flow water is supersaturated with S.I. values at around 0.4 (Madec 1999). At Brandt site, base flow water is close to saturation with S.I. values at -0.1 (see 2.6.4.).

Hence at low water stage, groundwater dissolves limestone in the epikarst, and then flows through the unsaturated zone at saturation with respect to calcite.

2.6.4. Calcite saturation index during flood events

Observations in the phreatic zone
Samples were taken at Milandre site in the upstream part of the underground river (AM) and at Saivu spring (SAI) for three flood events. Results (figure 2) show that groundwater stays mainly at saturation during the whole event.

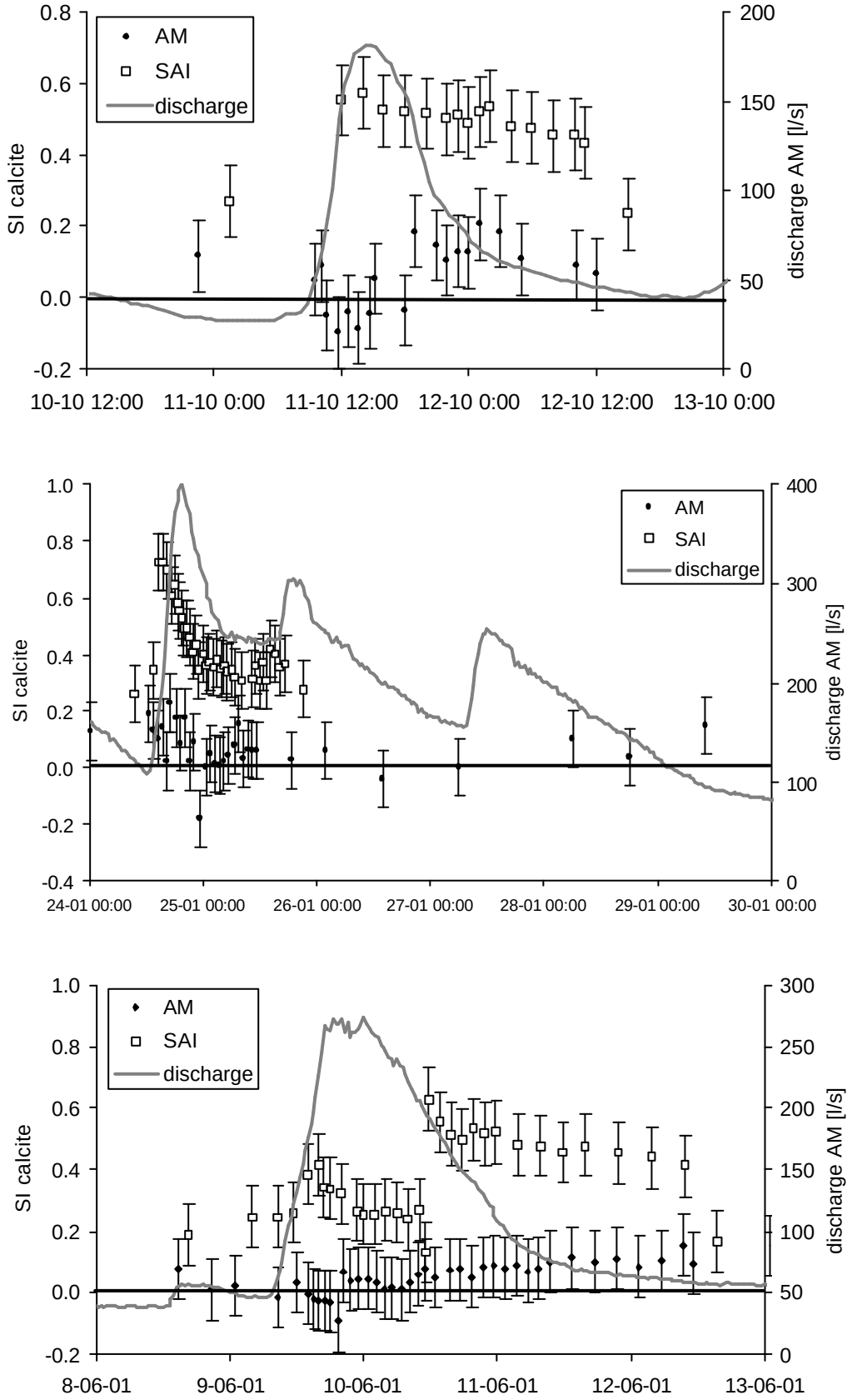

Fig 2: Evolution of the saturation indices at SAI and AM during three flood events (October 2000, January 2001, June 2001). The horizontal black line splits the undersaturated and supersaturated domains.

Observations in the unsaturated zone

One flood was sampled at Grand Bochat site in October 1999 (Madec 1999), another flood was sampled at Brandt site in October 2001, and the EC percolation water at Milandre site was sampled during the January 2001 and June 2001 floods (same floods as those presented for SAI and AM). Results (Fig. 3) show that at Brandt site groundwater becomes significantly undersaturated during the flood maximum. At Grand Bochat, groundwater is supersaturated at the beginning, and then reaches the saturation line during the discharge peak. The January 2001 flood event at EC presents slightly undersaturated waters during the flood. The June 2001 flood event at EC is constituted by saturated waters, but at the end of the flood undersaturated groundwater is observed.

These results show first that during floods the discharge of slightly undersaturated water with respect to calcite is an indication of rapid flow for part of the water, which has short residence times. Second, the fact that water is generally oversaturated with respect to calcite is a consequence of a CO_2 degassing, i.e. a flow path in a well aerated part of the aquifer (two phases flow in the infiltration zone, and/or flow in an open channel). Therefore the time evolution of calcite S.I. must be related to variations in CO_2 partial pressure of water (pCO_2), which will be high for low S.I. and inversely. These variations in pCO_2 and S.I. should then be associated with Ca and HCO_3 variations.

The S.I. vary much more in the unsaturated zone than in the phreatic zone. Hence the respective roles of dissolution and mixing on the observed groundwater chemistry will be assessed further by data limited to the unsaturated zone. The following tracers will be used:

- Oxygen-18 is considered as a perfect conservative tracer and the best indicator of fresh infiltrated water.
- Nitrate and chloride are conservative tracers in oxidizing conditions (as it is the case in the unsaturated zone). Their origin is the soil zone (and anthropogenic sources for Milandre site).
- Bicarbonate, calcium, and specific conductance are tracers related to limestone dissolution processes.

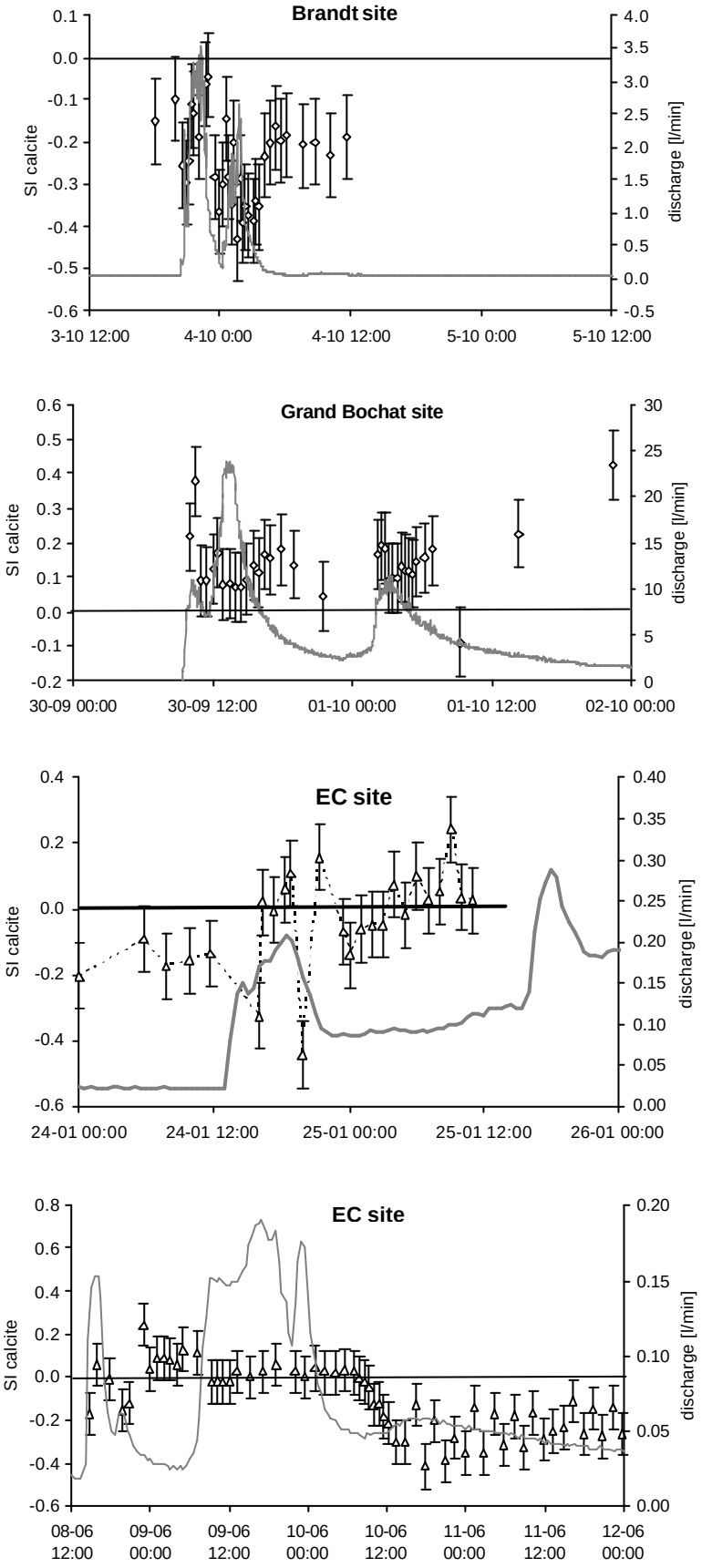

Fig 3: Evolution of the saturation indices at Brandt, Grand Bochat, and EC sites. The horizontal black line splits the undersaturated and supersaturated domains. The grey curves represent discharge.

2.6.5. Temporal variations of the tracers during flood events

Brandt flood event, October 2001

This flood event was sampled when the 1 m thick brown soil covering the karst was artificially removed from the catchment of the percolation water. The flood was caused by a total rainfall of about 24 mm occurring in two main phases (Fig. 4) during the night of the 3rd to the 4th of October. The second rain wave created spectacular surface runoff in the fields surrounding the Brandt cave entrance. At rainfall maximum, a brook of 2 l/s was swallowed by the entrance, which is generally dry all the year round. The last rainfall events occurred 4 days before (10 mm at La Brévine meteorological station), and 11 days before (11 mm). Rainfall started at 7 p.m. (6.8 mm in 1 hour), but strong intensity was recorded between 8 and 8:15 p.m. (7 mm). Flood started in the cave at 8:25 p.m. First peak flood occurred at 10 p.m., intermediate minimum discharge at 0:15 a.m. the 4th. The second flood, associated with the next rain event, peaked at 1:50 a.m., and recession started at 4:10 a.m. Specific conductance is closely anti-correlated to discharge, with a delay comprised between 10 and 20 minutes. Stable oxygen isotopes in percolation water followed the same pattern as in the rainfall. However the signal is dampened and the peaks occurred with a 15 minutes delay. Nitrates followed the same evolution as specific conductance, with peaks arriving at the same time (Fig. 5). On the contrary, chloride started decreasing 35 minutes later than nitrates, and then kept lower concentrations through the whole flood event, recovering only to half of its initial concentration. Limestone dissolution related parameters (bicarbonate and calcium) followed closely the specific conductance pattern, and recovered their initial concentrations at 4:30 a.m.

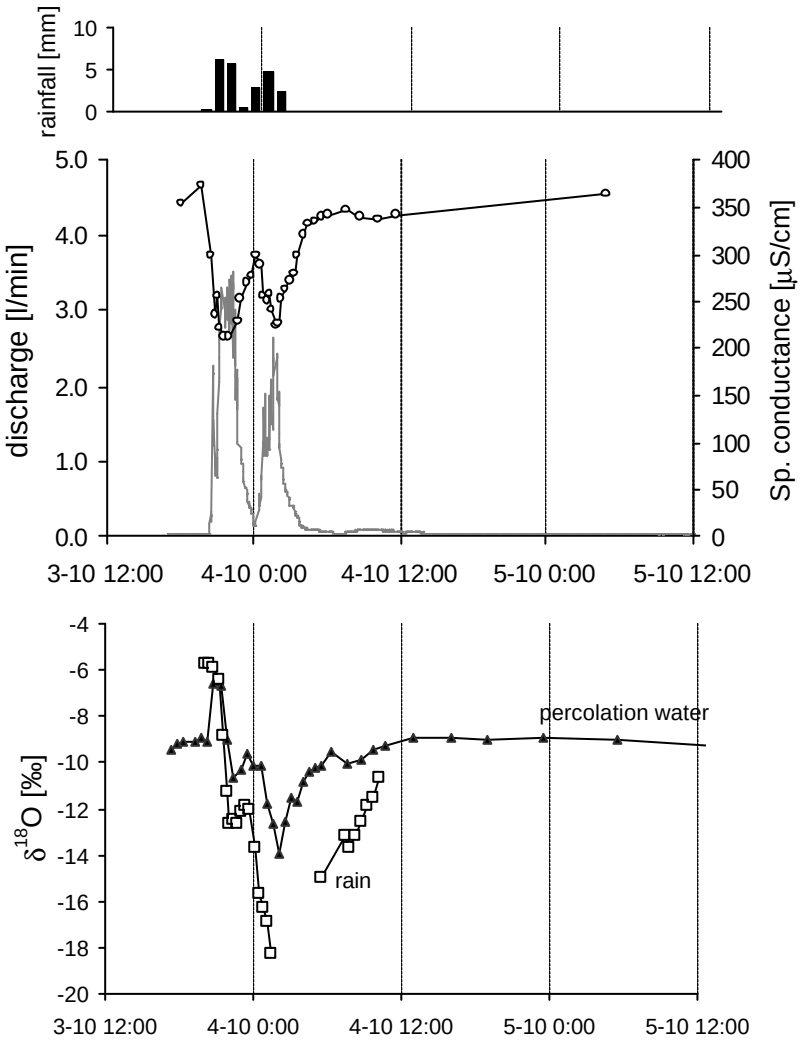

Fig 4: Rainfall (La Frétaz meteorological station), discharge, and stable isotopes evolution during the October 2001 flood event, Brandt test site.

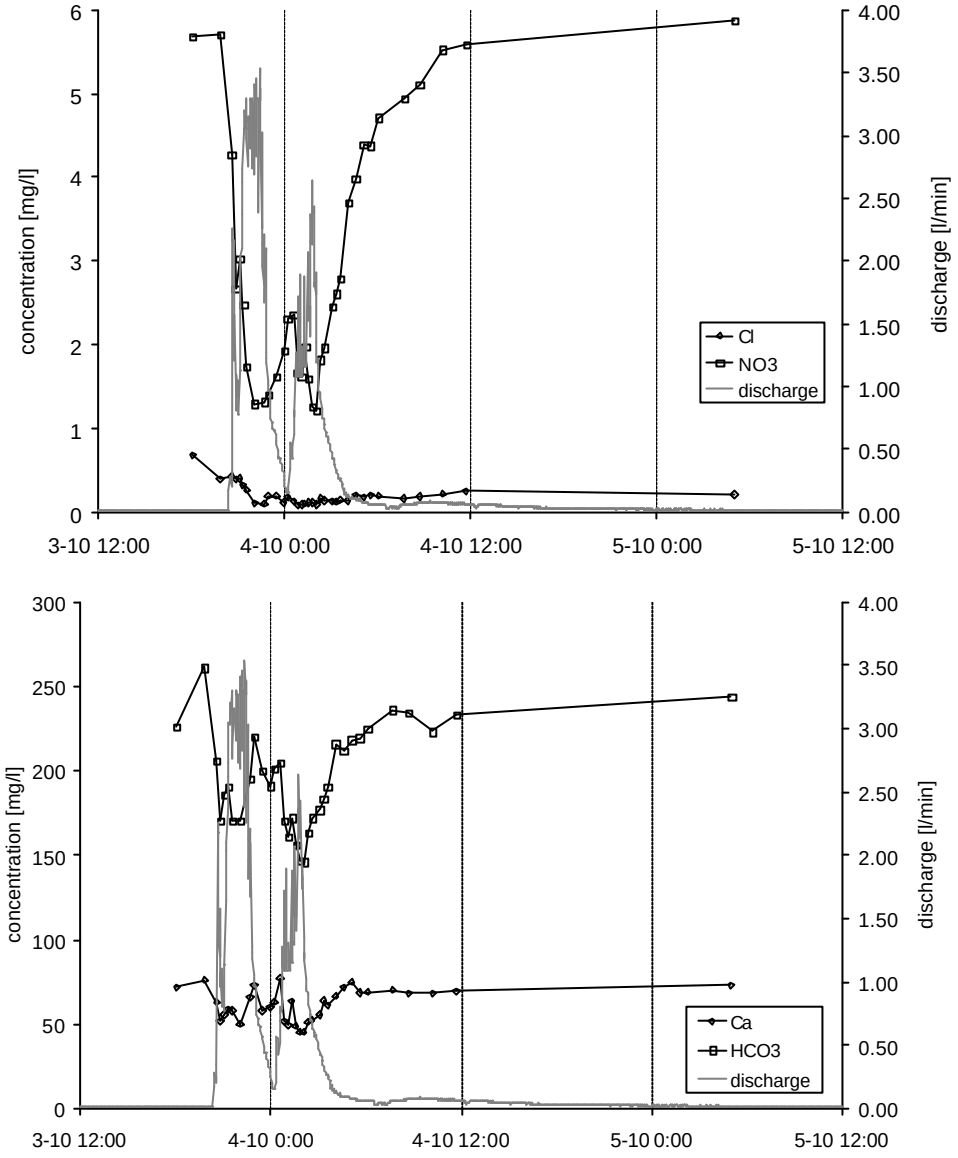

Fig 5: Evolution of soil related parameters (upper graph), and limestone dissolution related parameters (lower graph), Brandt flood event of October 2001.

Grand Bochat flood event, October 1999

The flood started the 30th of September at 10:24 a.m. Rainfall data was recorded at La Chaux-de-Fonds meteorological station (hourly measurements) located 15 km to the NE. Therefore values of rainfall are qualitative. Total rainfall recorded during the first flood (until 7 p.m. the 30th) is 20 mm, with a first phase of intense rain at 10 a.m. The last important rainfall occurred on the 25th with 42 mm at La Brévine station (located 7 km to the W, and giving only daily measurements). A first discharge peak occurred at 11:20 a.m., and a second at 2:45 p.m. (Fig. 6). Flow then decreased until 2:45 a.m. the 1st of October when a second flood peaked at 4:15 a.m. This second flood was caused by a rainfall event of 10 mm.

Specific conductance followed closely the discharge evolution, with decreases at each flow increase. Mineralisation decreases are retarded of 12 minutes as compared to flow changes. Values were 547 µS/cm in pre-event water, 521 µS/cm at the end of the first recession, and 538 µS/cm at the end of the second recession (at 3 a.m. the 3rd of October). Hence the system need about 20 hours for recovering. Oxygen isotopes in percolation water started to change before 11 a.m. with a sudden increase from –8.8 ‰ (pre-event value) to –8.1 ‰. Increase was then progressive, peaking at –7.5 ‰, followed by a decrease to –8.4 ‰. The second flood was also characterised by an increase to –7.8 ‰, and a decrease to –8.4 ‰. This evolution has no correlation with the isotopic signal in the first rainfall which

was systematically less than –8 ‰. The second rainfall averaged at around –7.4 ‰, and may explain the second increase in percolation water.

Chloride and nitrates concentrations started to change between 10:30 and 11 a.m. (Fig. 7). Chloride doubled its concentration (peak on the recession limb of the hydrograph), and then decreased until the next flood which generated a second increase. Nitrates decreased from 1.3 mg/l in pre-event water to 0.4 mg/l, and kept low concentrations until the second flood where values showed a multi-peaked variation. Concentrations then recovered progressively.

Dissolution related parameters decreased all during the two flood events (first decrease between 10:30 and 11 a.m.) High concentration in magnesium is due to the presence of dolomitic limestone in the rocks above the cave. The ratio Ca/Mg increases during both floods, in agreement with the more rapid kinetic of calcite dissolution, as compared to dolomite.

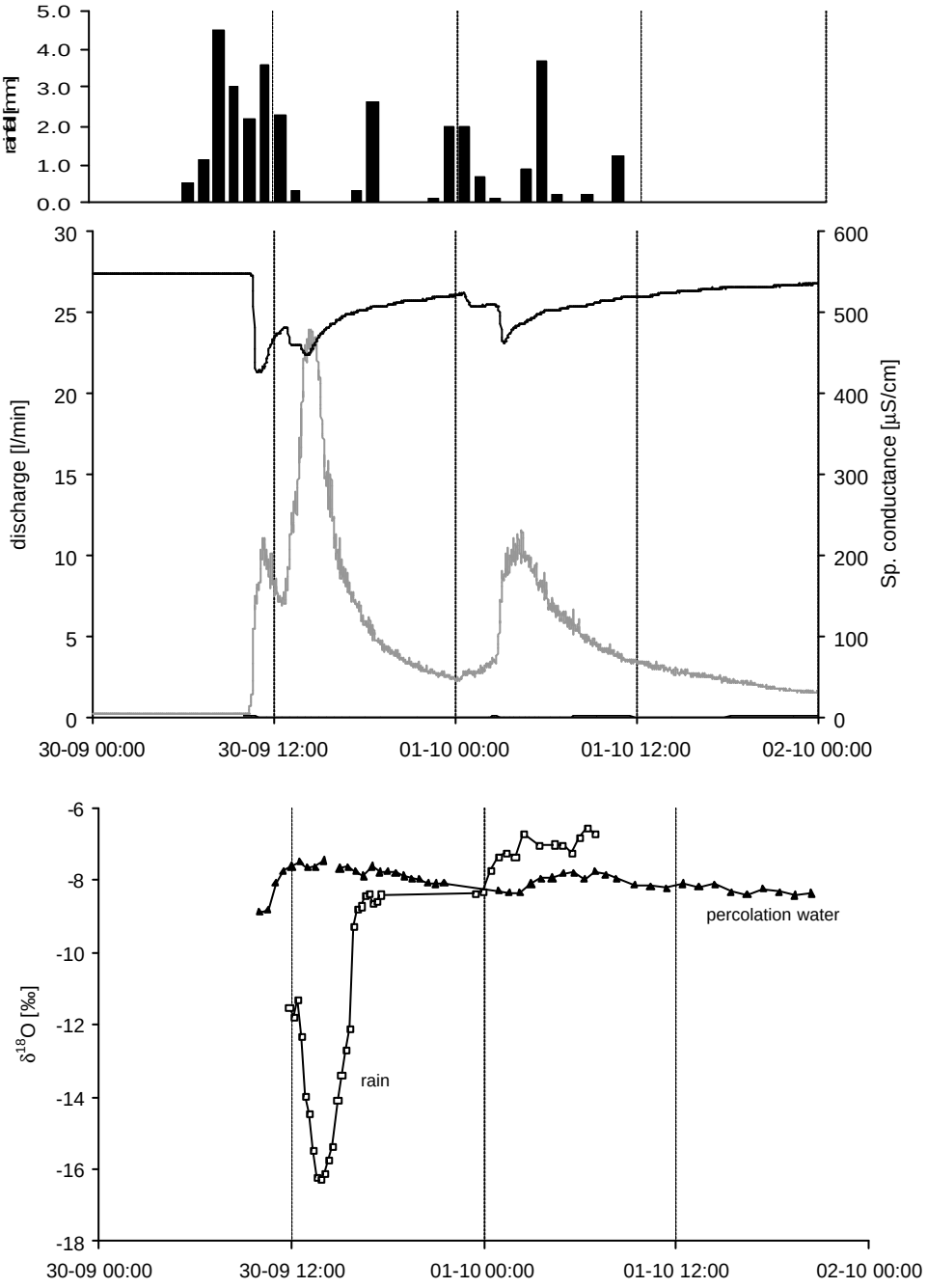

Fig 6: Rainfall (La Chaux-de-Fonds meteorological station), discharge, and stable isotopes evolution during the October 1999 flood event, Grand Bochat test site.

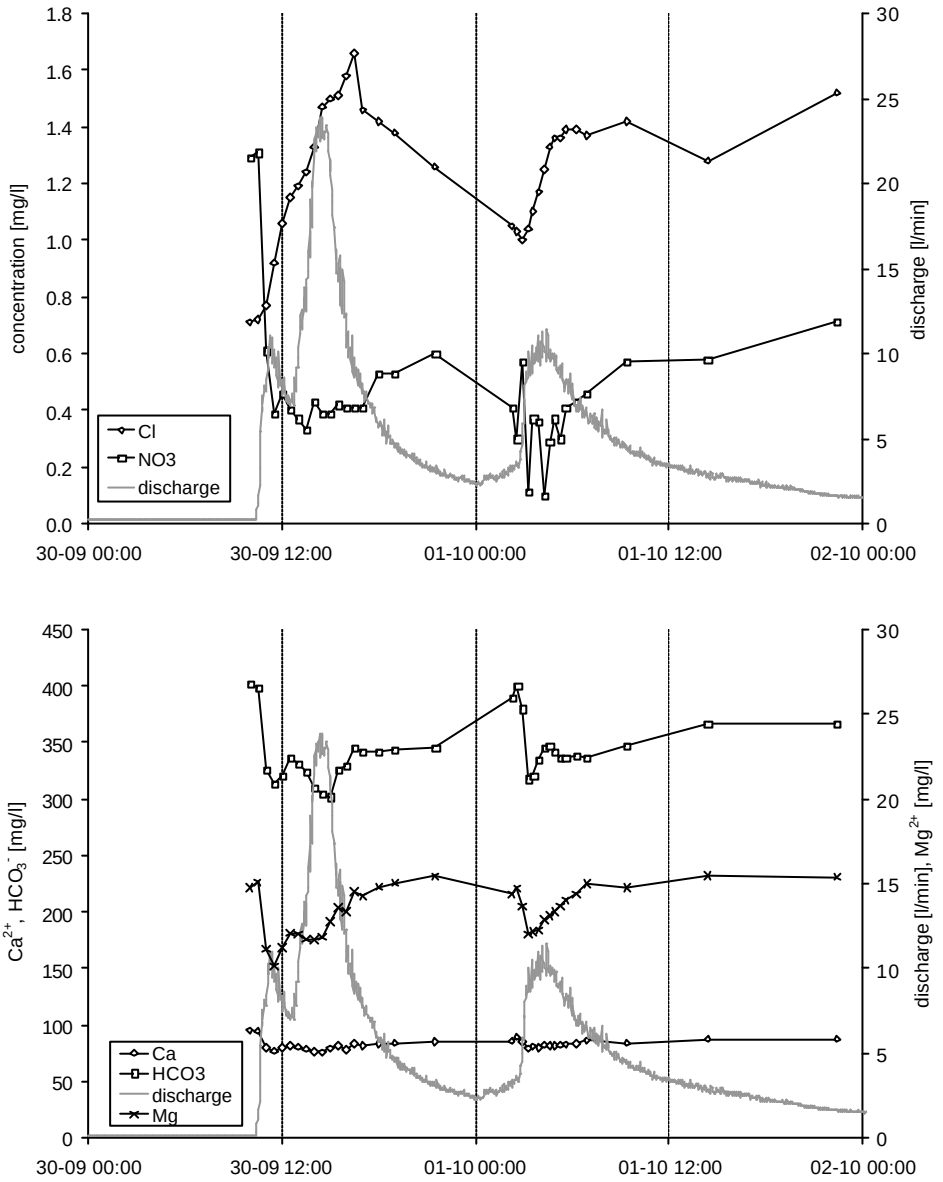

Fig 7: Evolution of soil related parameters (upper graph), and limestone dissolution related parameters (lower graph), Grand Bochat flood event of October 1999.

EC (Milandre site) flood event, January 2001

This flood event started January 24, 1:30 after continuous rain began falling, and lasted till the 29th. The event can be separated in three successive floods of decreasing magnitude, each linked to a rainfall event: calculated daily actual infiltration is 17 mm the 24th, 7 mm the 25th and 7.5 mm the 27th. Sampling was carried out on the first flood only (Fig. 8). A small flood had occurred the day before the sampled event (3 mm actual infiltration) and, before the hydraulic conditions were stable for about two weeks. Specific conductance showed a small positive peak on the increasing limb of the hydrograph. It then decreased slightly to a minimum before the top of the discharge peak, and increased to values less than recorded in pre-event water. The second flood was preceded by a positive peak. The isotopic signal in percolation water presented a progressive decrease associated to the first flood; it then returns to pre-flood values at the beginning of the 25th and decreases again with the arrival of the second flood. The isotopic signal in rainfall showed a strong decrease; its weighted mean is –12.2 ‰. It can explain the decrease recorded during the first flood at EC by an effective contribution of rainwater to EC discharge.

Pollution related parameters followed a similar evolution: a first decrease on the increasing limb of the hydrograph was followed by a positive peak before flood maximum (Fig. 9). A negative peak occurred during the recession limb, and the concentrations recovered partly for chloride and entirely for nitrates before the next flood.

Dissolution related parameters increased during the flood peak (30 mg/l increase for bicarbonate, 5 mg/l for calcium) and decreased to values under pre-event water concentrations during the recession (25 mg/l less for bicarbonate, 10 mg/l less for calcium). Bicarbonate increased then significantly before the next flood started.

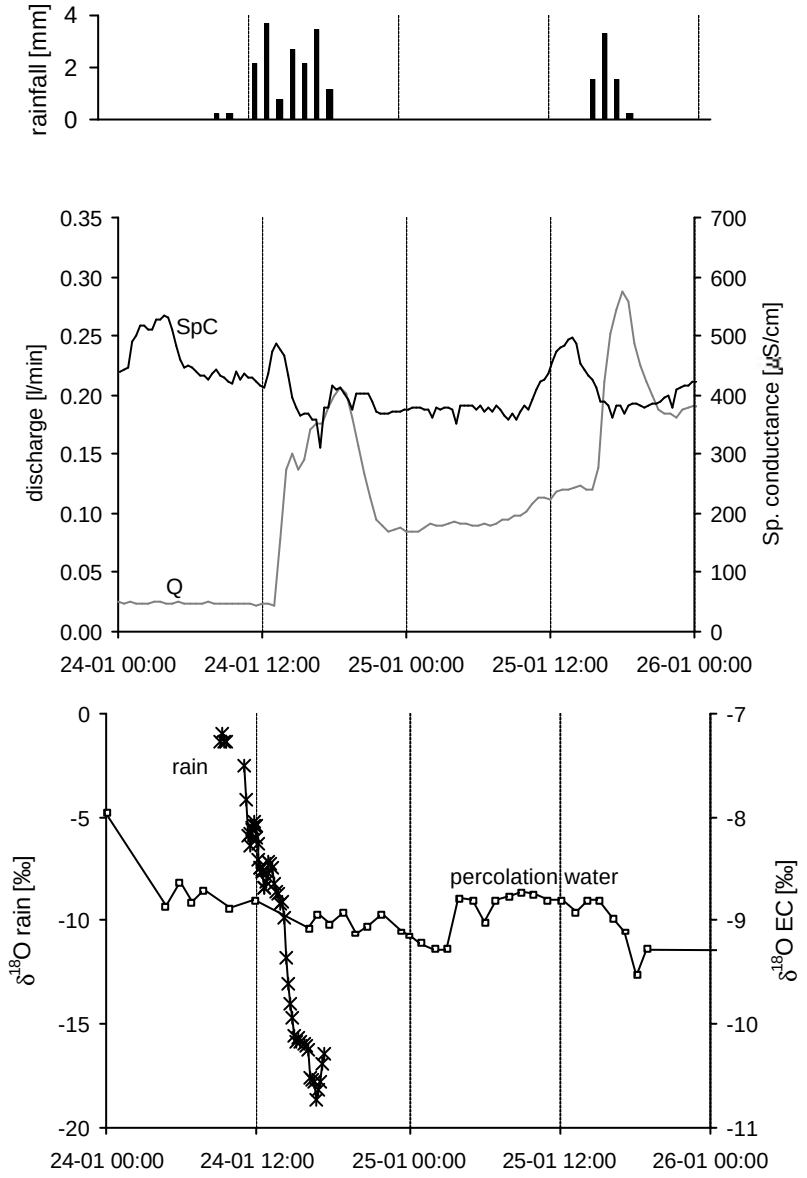

Fig 8: Rainfall, discharge, and stable isotopes evolution during the January 2001 flood event, EC vadose flow.

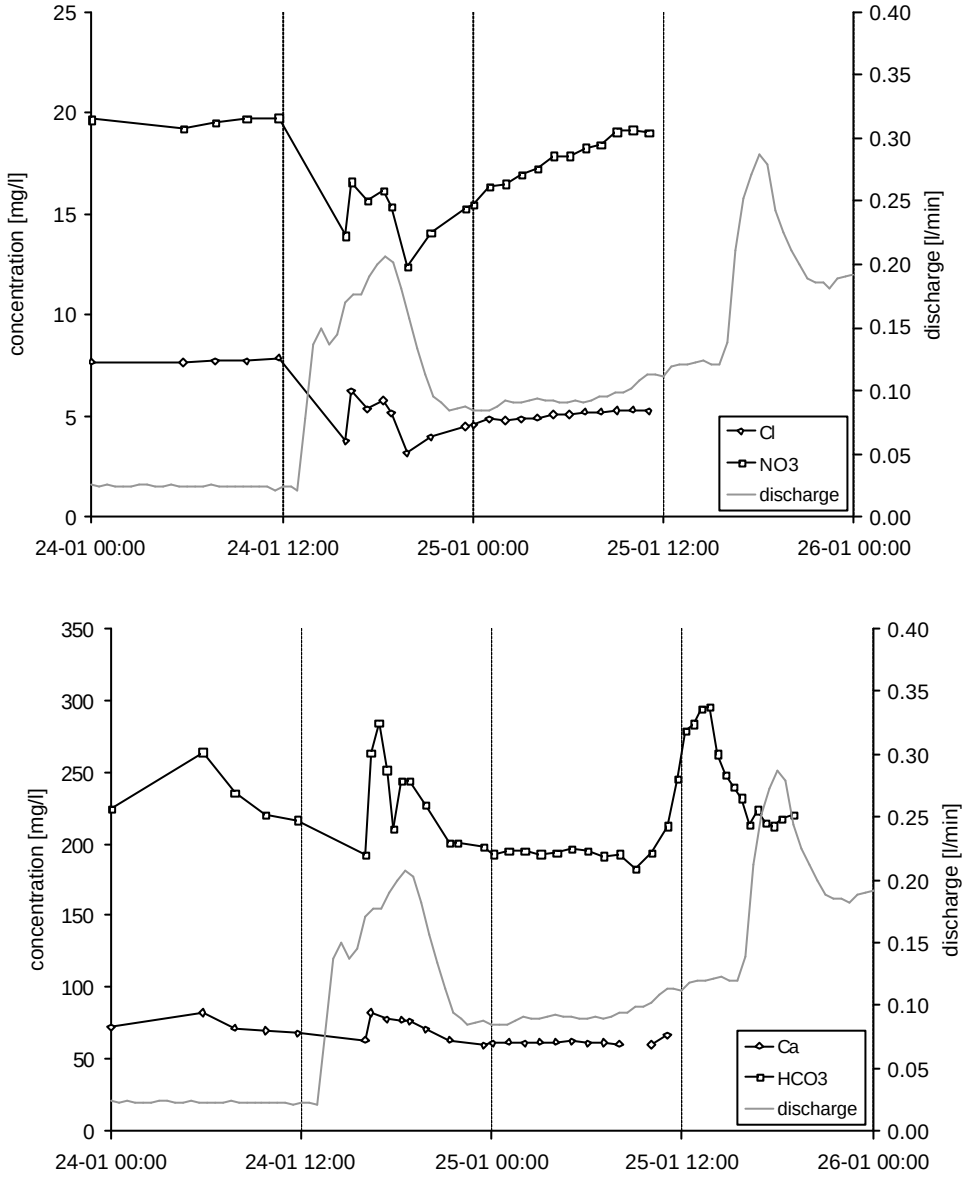

Fig 9: Evolution of pollution related parameters (upper graph), and limestone dissolution related parameters (lower graph), EC flood event of January 2001.

EC (Milandre site) flood event, June 2001

The main flood event began June 9, after the start of an important rainfall which lasted the whole day (Fig. 10). A small rainfall event the previous day already generated a first flood. Prior to this, the aquifer was in stable conditions for about two weeks. Calculated daily actual infiltration gives 0.4 mm the 8th and 18.2 mm the 9th. EC tributary showed a clear peak the 8th already, but the sampled flood event started at 6 a.m. the following day reaching a peak discharge at 5 p.m. Specific conductance decreased only slightly during the flood (20 µS/cm), but decreased strongly during the recession limb (150 µS/cm less than pre-event water). The isotopic signal in percolation water showed a strong increase during the flood of the 9th, corresponding to the influence of the rain of the day before (weighted mean at –6.7 ‰ for rainfall). The decrease of the 10th and 11th was caused by the influence of the second rain event with a more negative isotopic signature (weighted mean at –11.4 ‰).

Pollution related parameters decreased slightly during the flood of the 8th (Fig. 11), and were strongly diluted during the flood of the 9th (16 to 9.3 mg/l for nitrate, 4.3 to 2.2 mg/l for chloride). The decrease started between 7 and 9 a.m., hence more than 1 hour later than discharge rise started. The concentration recovery was completed at the end of the flood, two days after the discharge peak.

Dissolution related parameters were only slightly influenced by the flood of the 8th. During the next flood, concentrations increased (55 mg/l for bicarbonate, 20 mg/l for calcium). Then on the recession limb, concentrations decreased significantly (135 mg/l for bicarbonate, 45 mg/l for calcium), and water became undersaturated with respect to calcite (Fig. 3).

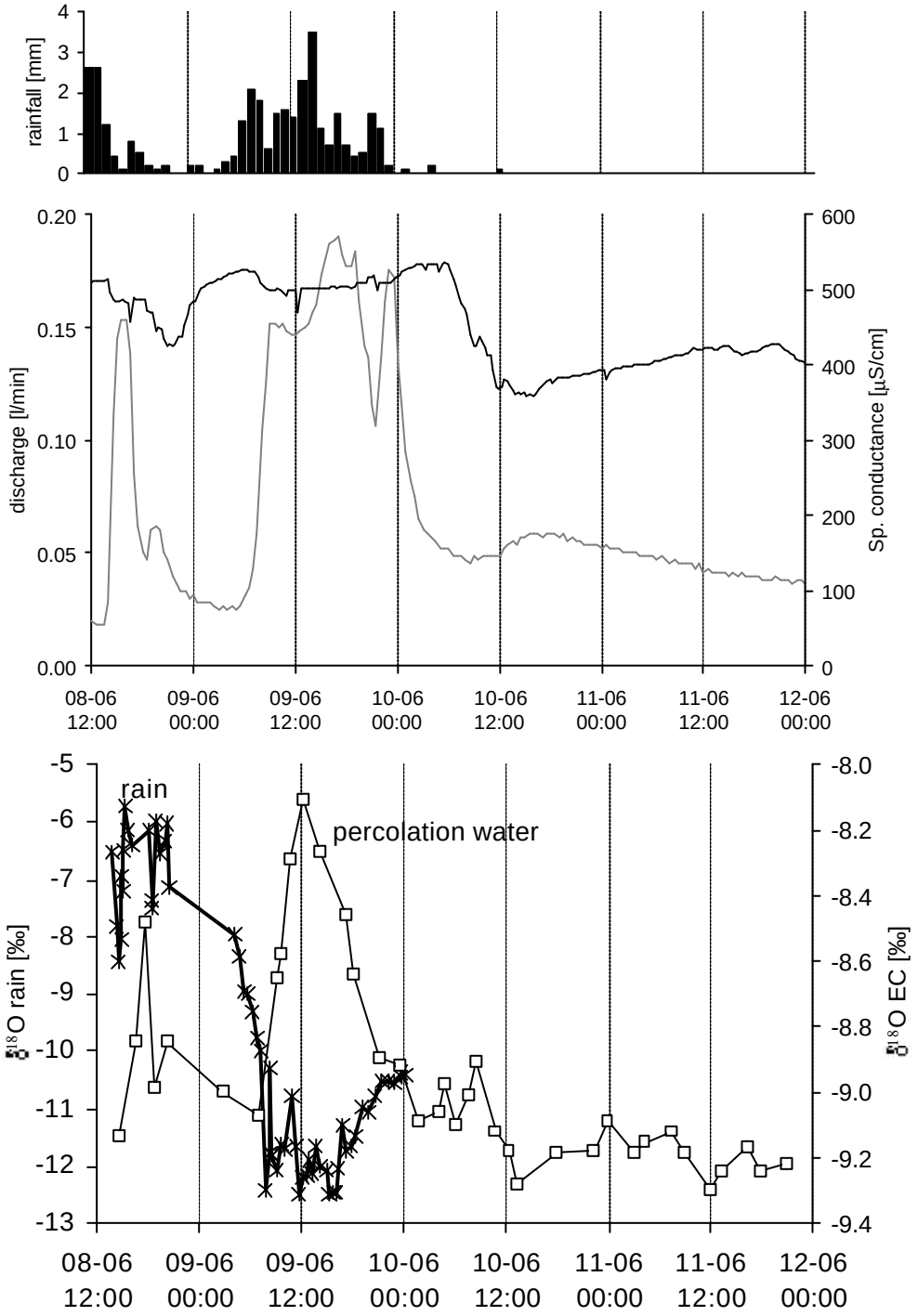

Fig 10: Rainfall, discharge, and stable isotopes evolution during the June 2001 flood event, EC vadose flow.

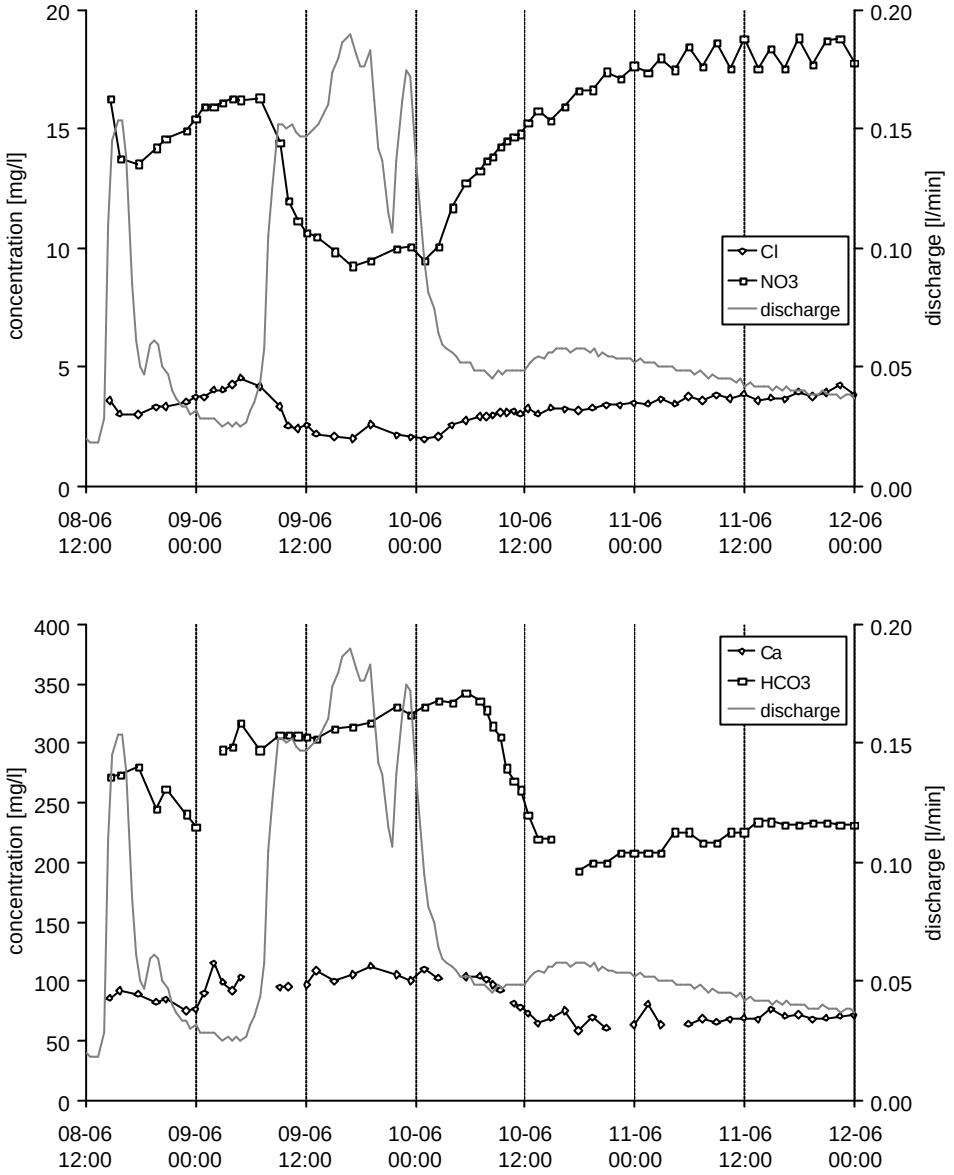

Fig 11: Evolution of pollution related parameters (upper graph), and limestone dissolution related parameters (lower graph), EC flood event of June 2001.

2.6.6. Interpretation

Specific conductance and chemical parameters vary with discharge changes. These variations occur generally with no or limited lag times as compared to hydraulics (except for EC). The dissolution related parameters (calcite, bicarbonate, specific conductance) follow similar patterns for each flood and each site. On the contrary chloride and nitrates can present very different evolutions.

The isotopic signal in percolation water does not match the signal in rainfall, except for Brandt site. It is the only site without soil, suggesting that important mixing occurs in the soil zone: the rain isotopic signal is highly buffered when reaching the unsaturated zone below the soil.

The observed chemographs are generated by the combination of two processes: mixing and calcite dissolution. We propose to use the non-reactive tracers to assess the role of mixing. Then it is possible to remove the effects of mixing and estimate the role of calcite dissolution correctly on the rapid flow component.

Determination of the waters participating to the flood

Flood water is a mixing of base flow water, soil water, and fresh infiltrated water. The representative tracers for each water component are stable isotopes for fresh water, pollution-related parameters for soil water, dissolution-related parameters for base flow (waters saturated with respect to calcite) (see chapter 2.3). In the following paragraph the water components are assessed for each sampled flood event.

Brandt site

All the parameters are diluted during the flood event, and the percolation water isotopic evolution follows closely that of rainfall, although with some buffering. This suggests a mixing of two waters: base flow water stored in the unsaturated zone (most probably in an epikarst reservoir), and fresh infiltrated water having the chemical composition of rainfall. Dilution by fresh water is less marked for dissolution related parameters as dissolution occurs during the flow path to the cave. The different behaviour of chloride may be due to variable concentrations in rainfall.

Grand Bochat site

The soil was already saturated by heavy rainfall fallen 4 days before. Base flow water originates from an epikarst reservoir and has a constant chemistry (supersaturated with respect to calcite, Fig. 3). First flood water has no contribution from rainfall as shown by isotopes. Hence the main contribution should come from soil water pushed by fresh infiltrated water: In the catchment, decarbonated brown soils of 15-40 cm thickness overlay homogeneous strata of dolomitic limestone.

This soil water is enriched in Oxygen-18 and chloride, less mineralised, and less concentrated in nitrates. Such a soil water chemistry is in agreement with data found in the literature: Dalla Piazza (1996) collected 14 samples (over 32 months) of soil water in a lysimeter under a forested area of the Swiss Jura. Concentration spans are the following: 36-68 mg/l for Ca^{2+}, 0.3-0.7 mg/l for Mg^{2+}, 0.4-4.4 for NO_3^-, 0.7-1.8 for Cl^-. This soil water is undersaturated with respect to calcite (absence of limestone fragments in the soil matrix), and dissolution occurs along the flow path to the cave. It is well illustrated by the increase of the Ca^{2+}/Mg^{2+} ratio during the flood. More rapid dissolution kinetics for calcite than for dolomite leads to a respective enrichment in calcium in the flood water component originating from the soil zone. The dolomite saturation index becomes strongly negative during the flood (-0.6 computed by Phreeqc). Two main components participate to the flood event: base flow water from the epikarst, and flood water issued from the soil zone.

For the second flood event, it is possible that rain water participates also to the flood (no incompatibility with isotopic values in rainfall). However the increase in chloride indicates again a large participation of soil water.

EC (Milandre site) flood event, January 2001

For this site, the soil is thicker (up to 1 m). This can explain the more complex responses observed. The isotope signal in percolation water indicates a participation of fresh infiltrated water. However the increase in calcium and bicarbonate should be linked to another water source, issued from the soil or epikarst zones. Pollution related parameters indicate the successive participation of different waters. Hence observed percolation water during the flood is a mixing of base flow water (issued most probably from the epikarst reservoir) with a constant chemistry, fresh infiltrated water, and different waters stored in the soil or the epikarst. The absolute variations are limited, indicating that the contribution of base flow water is predominant throughout the flood.

EC (Milandre site) flood event, June 2001

The first flood on the 8^{th} has limited effect on the chemistry and will not be discussed. Water of the second flood is a mixing of base flow water, rainfall water from the day before (as indicated by Oxygen-18), and more mineralised water issued from the soil or the epikarst. During the flow recession, a surprising arrival of undersaturated water occurs (Fig. 3). Isotopes indicate that it is partly rain water fallen about 20 hours before. Other components should be issued from the soil zone where absence of

limestone keeps water less concentrated in dissolution related parameters. This zone should also be more contaminated, leading to an increase in nitrates and chloride.

Dissolution and transit times

The dissolution model should be applied to the non-equilibrated component(s) of flow. That is fresh infiltrated water mainly, and soil water. A prerequisite to the dissolution model is to suppress the participation of the base flow component which is already equilibrated with respect to calcite.

Method: theoretical presentation

First, flood water is divided into its fresh water and base flow water components. This separation is done by a two-end members mixing model. Such a model is particularly valid in case of small systems where the existence of other mixing end-members is unlikely (e.g. base flow components issued from another part of the system). However this model has been used at the basin scale (Blavoux and Mudry 1983, Dreiss 1989).

$$C_{bf}\left(Q_{bf}+Q_{qf}\right)+C_{ff}Q_{ff}=C_{flood}Q_{flood} \tag{3}$$

where *C* are concentrations and *Q* discharges. Subscripts *bf*, *qf*, and *ff* correspond to base flow, quick flow, and fresh flow respectively.

as

$$Q_{bf}+Q_{qf}=Q_{flood}-Q_{ff} \tag{4}$$

it comes

$$\Phi_{ff}=\frac{Q_{ff}}{Q_{flood}}=\frac{\left(C_{flood}-C_{bf}\right)}{\left(C_{ff}-C_{bf}\right)} \tag{5}$$

which gives the percentage of fresh infiltrated water participating to the flood event.

However this relation is correct under steady-state conditions only. Under transient flow conditions, we suggest to compute one global Φ_{ff} for the whole flood event by integrating the time variations in discharges and concentrations according to (6):

$$\Phi_{ff}=\frac{\dfrac{\int Q_{flood}(t)\cdot C_{flood}(t)\cdot dt}{V_{flood}}-\dfrac{\int Q_{bf}(t)\cdot C_{bf}(t)\cdot dt}{V_{bf}}}{\dfrac{\int Q_{ff}(t)\cdot C_{ff}(t)\cdot dt}{V_{ff}}-\dfrac{\int Q_{bf}(t)\cdot C_{bf}(t)\cdot dt}{V_{bf}}} \tag{6}$$

where *Q* and *V* correspond respectively to discharge and water volume. The term C_{bf} is the value measured before the start of the flood pulse. It is considered as constant during the flood event, hence relation (6) simplifies into:

$$\Phi_{ff}=\frac{\dfrac{\int Q_{flood}(t)\cdot C_{flood}(t)\cdot dt}{V_{flood}}-C_{bf}}{\dfrac{\int Q_{ff}(t)\cdot C_{ff}(t)\cdot dt}{V_{ff}}-C_{bf}} \tag{7}$$

Concentrations of a non-reactive tracer have to be used. Stable isotopes are most suitable as they are generally distinct in the rain and in base flow.

Second, the percentage of each component allows to work out the true chemical composition of the fresh infiltrated water (C_{FIW}).

$$C_{FIW} = \frac{C_{flood} - [(1 - \Phi_{ff})C_{bf}]}{\Phi_{ff}} \quad (8)$$

Third, the kinetics 1-D dissolution model of Palmer (2000) is used:

$$\Delta C_x = \frac{2k}{w_x}\left(1 - \frac{C}{C_s}\right)^n \Delta t_x \quad (9)$$

where k is the reaction coefficient, n the reaction order, Dt_x the residence time within the passage segment, C the calcium concentration of dissolved bedrock and C_s the calcium concentration at saturation, C_x the increase in C within the passage segment, w_x the passage width.

Proposed values by Palmer (2000) for karst systems are the following: k=0.01 and n =2 for C/Cs<0.7, k=0.1 and n=4 for C/Cs>0.7.

Concentration is then given by:

$$C(t) = C(t-1) + \Delta C(t-1) \quad (10)$$

Initial conditions are determined by mean concentrations found in rainfall. C_s is chosen as the prevailing base flow concentration before the flood event started. This choice is supported by calcite S.I. presented in Fig. 2 and Fig. 3. C is the concentration in the fresh water component feeding the vadose flow.

This model allows to determine at each time step the ratio C/Cs. The ratio C_{FIW} / C_{bf} determined from (8) is compared to the ratio C/ C_s calculated with the model. The best correspondence gives the transit time of the fresh infiltrated water component of the flood event.

A theoretical example is given in Fig. 12. An initial concentration of 1 mg/l, a base flow concentration of 120 mg/l, and a fissure width of 0.1 cm were used for the simulation. Two scenarios are showed: the first considers a flood concentration at 100 mg/l, the second a flood concentration at 80 mg/l. The percentage of fresh flow participating to the flood (Φ_{ff}) is progressively increased. The concentrations of the fresh infiltrated water (C_{FIW}) increase, and the transit times increase also as a consequence. For low Φ_{ff}, transit times become very short. In scenario 2, the transit times are strongly reduced as compared to scenario 1.

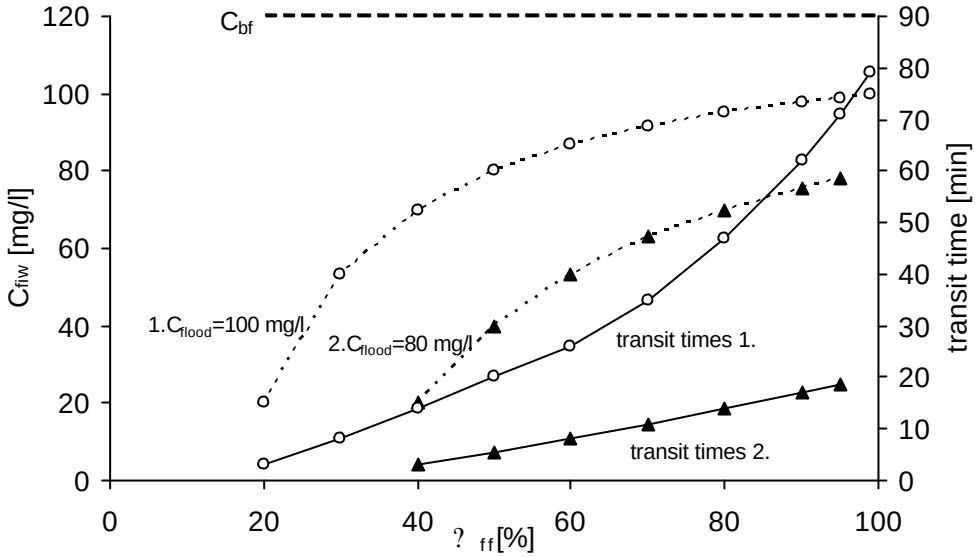

Fig. 12: Theoretical example of the evolution of C_{fiw} and transit times under different percentages of fresh infiltrated water (F_{ff}). Two scenarios are given.

Fresh flow percentage estimation

In order to use equation (7), C_{ff} has to be known. The corresponding water can be issued from the rain or from the soil zone. At Brandt site, stable isotopes are well suited for separating fresh infiltrated water and base flow water. At Grand Bochat site, C_{ff} from the soil zone is unknown. At EC site, both floods are constituted of a mixing of three components. For both sites, relation (7) cannot be used.

At Brandt test site we have clearly the mixing of two components. The base flow isotopic ratio is -9.15 ‰. Mean values for flood water and fresh water are respectively -10.02 ‰ and -11.51 ‰. The calculated percentage of the fresh and base flow components are respectively 40 % and 60 %. The average concentrations in flood water (C_{flood}) were 55.5 mg/l for Ca^{2+}, and 174 mg/l for HCO_3^-. Base flow concentrations (C_{bf}) are those of the pre-event water (table 2). Rainfall concentrations (C_{ff}) are those of Madec (1999). Fresh infiltrated water (C_{FIW}) concentrations are calculated with equation (6).

Table 2: Concentrations in bicarbonate and calcium for the different components of flow at 1.35 a.m.

	C_{bf} [mg/l]	C_{flood} [mg/l]	C_{ff} [mg/l]	C_{FIW} [mg/l]
Ca^{2+}	75	55.5	2	26.3
HCO_3^-	225	174	5	97.5

The ratio C_{FIW} / C_{bf} is 0.35 for calcium and 0.43 for bicarbonate.

Neighbouring ratios calculated with the dissolution model (relations 7 and 8) are given in table 3 together with the corresponding transit times. Initial concentrations for the model are those of rainfall. Different fissure widths (w) were used.

Calculation of the transit time at Brandt site

Table 3: Estimation of transit times at Brandt test site from the dissolution model

C/Cs	w = 0.5 cm	w = 1 cm	w = 10 cm
0.3	14 min	26 min	4.3 hr
0.4	21 min	41 min	6.7 hr
0.5	31 min	63 min	10.1 hr

The transit times found with a 0.5 cm fissure width are consistent with Oxygen-18 data presented above: delays between peaks in rainfall and in the percolation water averaged at 15 minutes. The same transit time was found by a tracing experiment (iodide, rhodamine, lithium) under natural infiltration conditions, i.e. by reproducing a rain of normal intensity (Perrin et al. 2002).

The dissolution model can give an idea on the residence time of the base flow component. With a 0.5 cm fissure width, the *C/Cs* ratio reaches 0.95 after 5.8 days, and 0.97 after 27 days. As observed calcite saturation indices indicate nearly saturation, the residence time in the epikarst (baseflow) is on the order of several weeks.

2.6.7. Discussion

A conceptual model of flow and transport in the unsaturated zone
Flow and transport time variations from the unsaturated zone can be synthesized into four phases: a reaction phase where rain has started and discharge has not started changing, a piston phase where base flow water (stored in the epikarst) is pushed by the fresh water pressure, a phase of mixing of waters of different origin (base flow, fresh water, soil water mixing), and a recovery phase where concentrations of base flow water are progressively reached (Fig. 14).

1. Reaction phase: The lag time between rainfall start and flood start is variable and depends on the degree of saturation of the soil as shown by Puech and Jeannin (1997).
2. Piston phase: it is defined by the duration where discharge increases but concentrations do not vary. At Brandt site, the piston lasted 15 minutes corresponding to a total water volume of around 15 litres. Taking a unique conduit of 0.5 cm diameter (as given by the dissolution modelling), the length necessary for this volume would be 190 m. At Grand Bochat site, the piston duration is 12 minutes. At Milandre site, the piston is more than 1 hour for the June 2001 flood, and is difficult to estimate for the January 2001 flood because of the limited variations in the tracer concentrations. The vertical distance between the surface and the groundwater sampling point is 15 m for Brandt site, 20 m for Grand Bochat, and 35 m for EC. Therefore transit velocities for the flood water is about 60 m/h at Brandt site, 100 m/h at Grand Bochat, and less than 35 m/h at Milandre site.
3. Mixing phase: the flood water is a mixing of waters of different origins. At Brandt site, the mixing is made of base flow water and fresh infiltrated water. The respective contributions are changing during the flood (Fig. 13). At Grand Bochat, the mixing is made of base flow water and soil water mainly. At Milandre, the mixing is made of base flow water, soil water of variable composition, and fresh infiltrated water.
4. Recovery phase: the system recovers more or less rapidly to the concentrations of base flow water. Duration is 2.7 hours at Brandt site, 20 hours at Grand Bochat site, and 12 hours at Milandre site for the January 2001 flood event. The June 2001 flood event presents undersaturated waters during the recession which are not in agreement with our model.

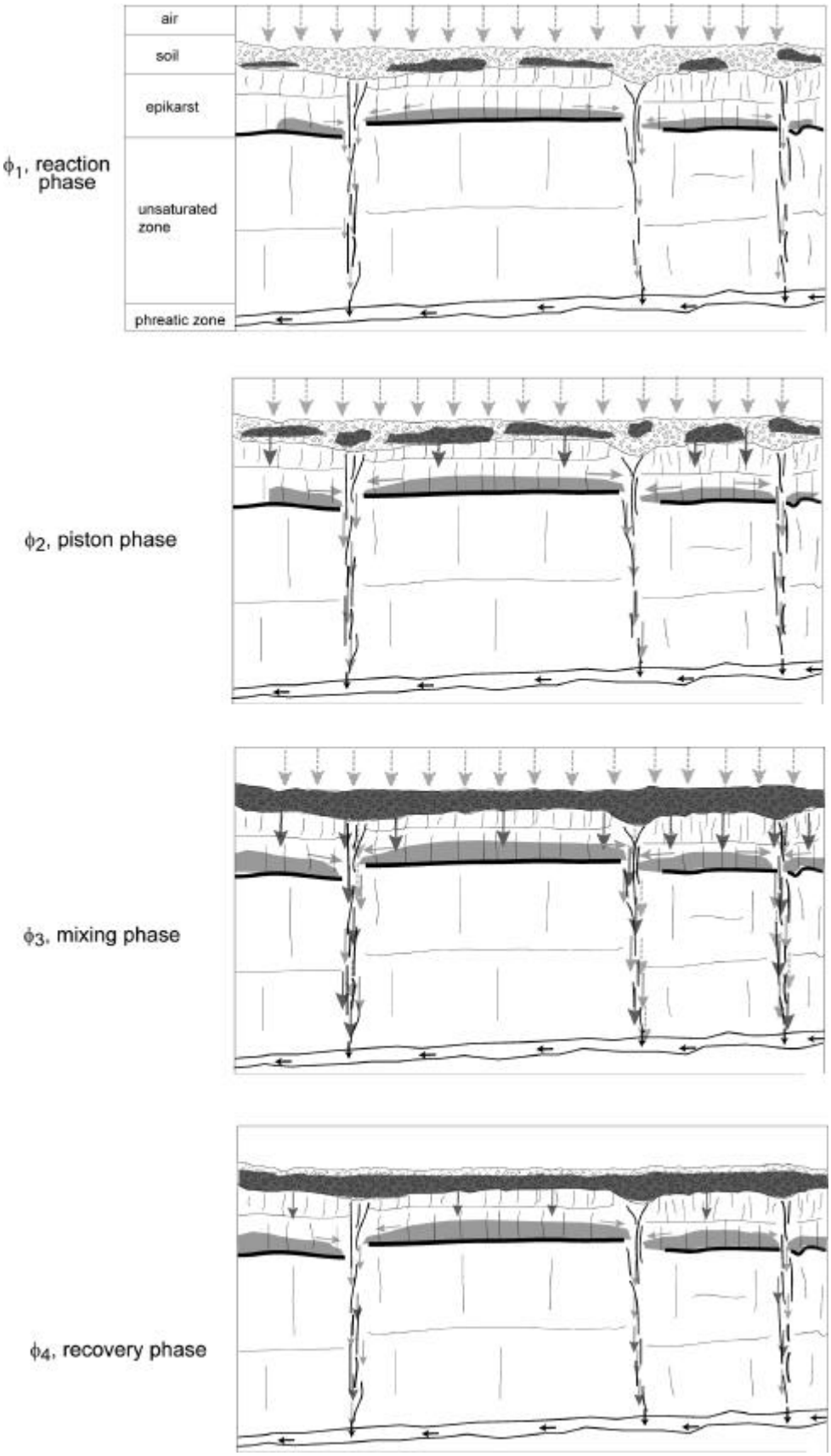

Fig 14: conceptual model of flow and transport in the unsaturated zone. Dark grey represents soil water, pale grey epikarst water, and dashed arrows fresh infiltrated water.

This schematic functioning of flow and transport in the unsaturated zone leads to several remarks:

- The reservoirs feeding the waters of different composition should be separated in order to preserve their specific chemistry. Hence the mixing occurs below the reservoirs (i.e. in the unsaturated zone below the epikarst).
- The rapid recovery to concentrations corresponding to base flow water indicates a large reservoir for base flow. This reservoir is mainly the epikarst where water is equilibrated with respect to calcite. It should be replenished by slow percolation from the soil zone.
- Even thin soils (e.g. Grand Bochat) contribute greatly to the dampening of the isotopic rain signal, and can store significant volumes of water. The soil is a source for several ions like chloride, sulfate or potassium. Tracers transit times through the soil are much larger than in the zone below: a tracing experiment carried out at Grand Bochat (Pochon, pers. comm.) showed a first arrival of the tracer after 40 minutes (simulated rainfall intensity of 30 mm/h). From our data, it is possible to estimate the transit time below the soil at about 10 minutes (lag time between flow increase and specific conductance decrease). The transit time in the soil should then be of about 30 minutes. With an average soil thickness of 30 cm, the velocity is 60 cm/h. This value is in agreement with those of Pochon (1978) for a brown soil of the Swiss Jura: 43 to 110 cm/h for a simulated rain of 20 mm on a 4 hours duration.
- Dissolution processes are active during the transit of fresh infiltrated water and soil water through the unsaturated zone. Even if these waters mix with saturated water from the epikarst, the resulting water can be still undersaturated with respect to calcite when reaching the base of the unsaturated zone.
- Soil water can be undersaturated with respect to calcite, especially in brown soils poorly drained, as already shown by Aubert and Pochon (1977). Hence a mineralisation decrease does not necessarily means the arrival of fresh infiltrated water.

Consistency of the model with data from other sites

At Milandre site, two other small tributaries were sampled during the flood events: SO tributary during the January 2001 flood, and EN percolation water during the June 2001 flood. They are located in the upstream part of the Milandrine river, about 45 m below ground surface. Both have an intermediate hydraulic behaviour with no marked flood during the summer season, and dampened floods in winter (Perrin and Kopp 2003). EN percolation water showed no variations in discharge and tracers during the whole flood. SO tributary showed slight changes (Fig. 15) except for Oxygen-18 which kept a constant value. Such a constant evolution is interpreted as indicative of a large reservoir allowing efficient mixing and feeding both tributaries with base flow water all the year round. SO tributary has important concentrations in Rn-222 (Savoy 2002). The main source of Radon being the soil (Surbeck and Medici 1990, Climent 1996, Savoy 2002), it seems probable that the SO tributary reservoir is located mainly in the soil zone or at its base. The Rn source could also be situated below the soil, in a zone where soil leaching occurred (e.g. important fault crossing the SO catchment area).

These data from other tributaries show that tracer responses to flood pulses can differ greatly in tributaries located closely. The karst spring chemograph is the sum of all these different responses.

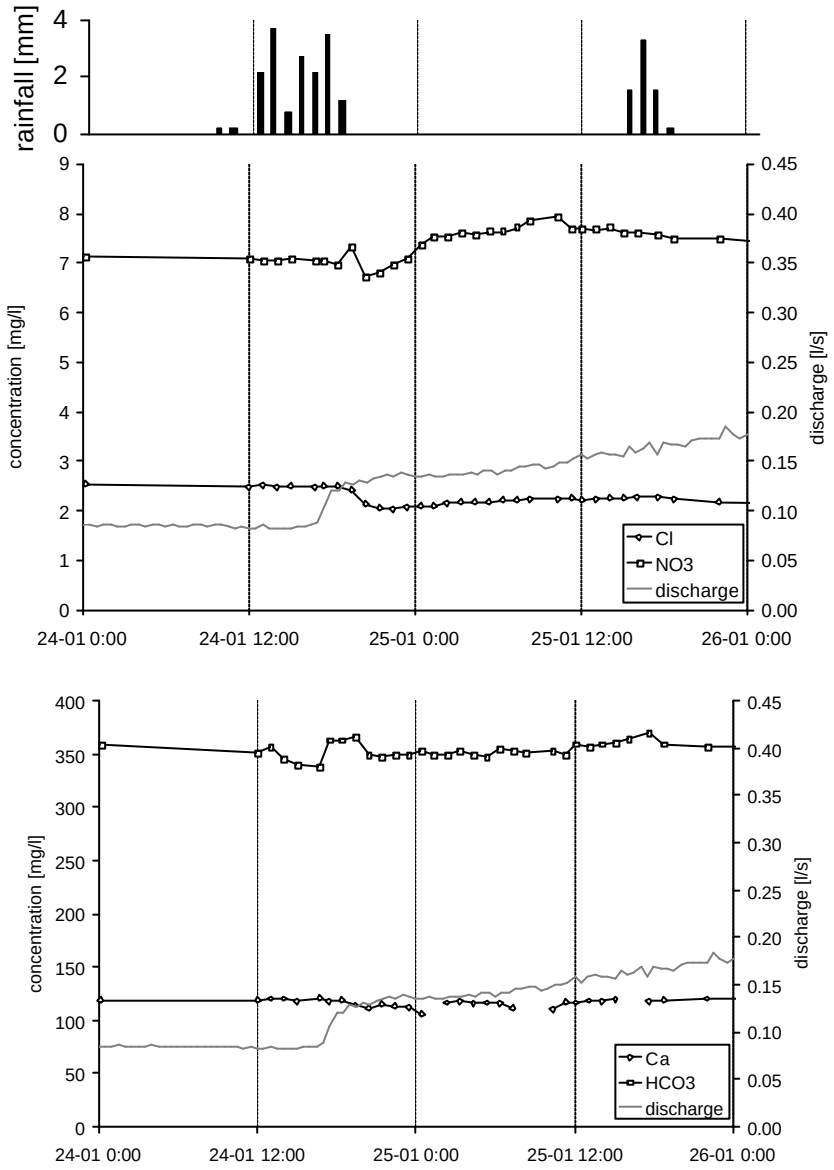

Fig 15: Rainfall, and chemical evolution of SO tributary during the January 2001 flood event, Milandre test site.

The role of soil in recharge processes, a literature review

Our data have shown the prominent role of the soil cover in transport processes in the unsaturated zone of karst aquifers. A literature review on soil types of the Jura mountains offers interesting insights on flow and transport. Gaiffe and Bruckert (1990) showed that pedogenesis in the Jura mountains is controlled by the underlying bedrock, and hence soil and bedrock have to be considered together (functional unity). Two types of soil cover a large part of the area: brown soils and humo-calcic soils.

Brown soils develop on solid limestone with a limited fissure density (e.g. dolomitic limestone, marly limestone, dip slope strata). These soils have no limestone fragment due to the compactness of the underlying strata, and thus are decarbonated. They are poorly drained because of the low density of fissures in the rock below and keep a high humidity level.

On the contrary, humo-calcic soils develop on fissured limestone allowing an efficient drainage. Thus the soil has a low storage capacity and moreover desiccation cycles enhance the soil permeability. Presence of rock fragments is a source of calcium.

The degree of limestone fissuring depends on the limestone composition (Gaiffe and Bruckert 1990), and on the structural position (Aubert and Pochon 1977). These last authors showed that brown soils are located on the strata dip, and humo-calcic soils develop in the steps between strata. This soil distribution has been an important factor of the Jura karst geomorphology evolution. They also compare the soil water chemistry in these two soils: mean concentrations of calcite and bicarbonate range respectively between 12.5 mg/l and 21.7 mg/l for brown soils, between 47.2 mg/l and 126.3 mg/l for calco-humic soils.

Our test sites are all covered by brown soils. It means that the storage is efficient, the permeability reduced, and the water weakly mineralised. At Milandre site, fractured limestone is theoretically unfavorable to brown soils. However, these soils have developed from important loess deposits which limited the drainage role of the underlying fractures.

Experiments conducted on sites with humo-calcic soils would probably lead to rather different results. Such soils exist in the Jura mountains at higher elevation on anticlinal ridges, and in Alpine karsts.

2.6.8. Synthesis and conclusions

During flood events both mixing of different waters and limestone dissolution occur in the unsaturated zone of the studied karst systems. Pure mixing models (Blavoux and Mudry 1983, Dreiss 1989) or pure dissolution models (Grasso et al. 2003) simulating karst spring chemographs are both too simple.

Mixing poles are base flow water mainly issued from the epikarst, soil water, and fresh infiltrated water. In base flow conditions, mixing is non existent and groundwater base flow is issued from the epikarst. This water is saturated with respect to calcite due to sufficient storage time. In flood conditions, mixing is most effective and both fresh and soil waters can dissolve limestone during their transit towards the phreatic zone. Hence the mixed water reaching the base of the unsaturated zone can be still undersaturated with respect to calcite. However, it is near to saturation and only limited dissolution can occur in the phreatic zone. In this zone, horizontal mixing will mostly influences the chemical variations observed at the spring (see chapter 2.5).

Decarbonated soils (i.e. brown soils) are the most effective at providing undersaturated water. The presence of such a soil cover in the catchment may lead to a mineralisation decrease at a karst spring during flood events due to the arrival of soil water. Hence a decrease in mineralisation does not necessarily mean the arrival of fresh infiltrated water as often described in the literature (Blavoux and Mudry 1983, Williams 1983, Sauter 1992).

The epikarst reservoir appears to be of an important size in order to keep a stable chemistry. During flood events, it distributes soil (and fresh) water to the fissures downwards. At steady-state flow conditions, it sustains base flow.

The mixing proportions are variable depending on the geological context. With no soil cover (Brandt site), fresh infiltrated water can reach up to 40 % of the total discharge. At Grand Bochat, the 15-40 cm soil reservoir can participate for 60 to 70 % of the total flow, and fresh water between 0 and 10 %. At Milandre site, the mixing appears to be more complex, but isotopic variations indicate a maximum of 30 % of fresh water participating to the flood events. The soil appears to limit efficiently the participation of fresh infiltrated water to flood pulses.

The presented mixing and limestone dissolution model is one-dimensional. It should be adapted into a two-dimensional vertical numerical model of flow and transport as used in chapter 2.4. This model was created for reproducing the hydraulic and stable isotope responses observed at the base of the unsaturated zone at Milandre site. Reactive transport should be implemented in a fracture network of variable openings, and the results could then be compared to the simple 1-D model shown in the present chapter. The interest of a 2-D model is that it would give more information on the structural properties of the soil and epikarst reservoirs.

In the future, it would be of interest to investigate other sites with different soil covers. It is also necessary to detail more the sampling at small scale (i.e. within the soil and the epikarst). Other tracers like radon or CO_2 should lead to complementary information.

References

Aubert, D. and Pochon, M., 1977. Géochimie de la surface et formes du relief. VIII. Aplanissement karstique dans le Jura. Sci. Géol. Bull., 30, 4: 297-302.

Blavoux, B. and Mudry, J., 1983. Décomposition chimique des hydrogrammes du karst. Hydrogéologie-Géologie de l'Ingénieur, 4: 270-278.

Climent, H., 1996. Transport du Radon à l'interface sol-air: étude de l'influence des paramètres externes. PhD thesis, Univ Montpellier: 234 p.

Dalla Piazza, R., 1996. Géochimie des altérations dans trois écosystèmes sol tempérés - application à l'acquisition des caractéristiques chimiques des solutés, Thèse EPF, Lausanne, N° 1483, 237 p.

Dreiss, S.J., 1989. Regional scale transport in a karst aquifer: 1. Component separation of spring flow hydrographs. Water Resources Research, 25(1): 117-125.

Gaiffe, M. and Bruckert, S., 1990. Origine paléoécologique de l'aptitude des calcaires jurassiques à la fracturation. Conséquences tectoniques, pédogénétiques et écologiques. Bull. Soc. Neuch. Sci. Nat., 113: 191-206.

Gigon, R. 1976. Inventaire spéléologique de la Suisse, 1: canton de Neuchâtel. Comm. Spéléo. Soc. Helv. Sc. Nat., Neuchâtel: 223 p.

Grasso, D.A., 1999. Interprétation des réponses hydrauliques et chimiques des sources karstiques., PhD thesis, Neuchâtel: 135 p.

Grasso, D.A., Jeannin, P-Y., Zwahlen, F. 2003. A deterministic approach to the coupled analysis of karst spring hydrographs and chemographs. Journal of Hydrology, 271: 65-76.

Gretillat, P.-A., 1996. Les aquifères karstiques et poreux de l'Ajoie (Jura, Suisse), Neuchâtel, Neuchâtel: 209 p.

Hess, J.W. and White, W.B., 1988. Storm response of the karstic carbonate aquifer of south-central Kentucky. Journal of Hydrology, 99: 235-252.

Jeannin, P.-Y., 1998. Structure et comportement hydraulique des aquifères karstiques. PhD thesis, Neuchâtel, 237 pp.

Lee, E.S. and Krothe, N.C., 2001. A four-component mixing model for water in a karst terrain in south-central Indiana; USA. Using solute concentration and stable isotopes as tracers. Chemical Geology, 179: 129-143.

Madec, G., 1999. Etude des écoulements dans l'épikarst. Approche géophysique, hydraulique et hydrochimique sur le site de Grand Bochat. MSc thesis, Centre of Hydrogeology, Neuchâtel.

Palmer, A.N., 2000. Digital modeling of individual solution conduits. In: A.B. Klimchouk, D.C. Ford, A.N. Palmer and W. Dreybrodt (Editors), Speleogenesis. Evolution of Karst Aquifers. National Speleological Society: 194-200.

Parkhurst D.L., Thorenston D.C. & Plummer N.L. (1980): PHREEQE - A computer program for geochemical calculations. U.S. Geological Survey Water Resource Investigations 80-96 210 pp.

Parkhurst D.L., Appelo C.A.J. (1999): User's guide to PHREEQC (version 2) - A computer program for speciation, batch reaction, one-dimensional transport, and inverse geochemical calculations. U.S. Geological Survey Water-Resources Investigations Report 95-4227, Denver, Colorado. http://gwrp.cciw.ca/gwrp/software/software.html

Perrin, J., Pochon, A., Jeannin, P.-Y. and Zwahlen, F., 2002. Vulnerability assessment in karstic areas: validation by field experiments. Proceedings of the 32nd IAH Congress, Mar del Plata, Argentina.

Perrin, J., and Kopp, L. 2003. Hétérogénéité des écoulements dans la zone non saturée d'un aquifère karstique (site de Milandre, Jura suisse). Bulletin d'Hydrogéologie, Neuchâtel.

Perrin, J., Jeannin, P.-Y. and Zwahlen, F., 2003a. Epikarst storage in a karst aquifer : a conceptual model based on isotopic data. Milandre test site, Switzerland. Submitted to Journal of Hydrology.

Perrin, J., Jeannin, P.-Y. and Zwahlen, F., 2003b. The role of mixing in chemical variations at karst springs, Milandre test site, Switzerland. Submitted to Chemical Geology.

Perrin, J., Jeannin, P.-Y. and Zwahlen, F., 2003c. Implications of the spatial variability of the infiltration water chemistry for the investigation of a karst aquifer. Accepted by Hydrogeology journal.

Plagnes, V. and Bakalowicz, M., 2001. May it propose a unique interpretation for karstic spring chemographs? In: J. Mudry and F. Zwahlen (Editors), 7th Conference on Limestone Hydrology and Fissured Media. Franche-Comté University, Besançon, pp. 293-298.

Pochon, M., 1978. Origine et évolution des sols du Haut-Jura suisse. Mém. Soc. Helv. Sci. Nat., 90: 162 p.

Puech, V. and Jeannin, P-Y. 1997. Contribution à la compréhension du fonctionnement hydraulique de l'épikarst ; expériences d'arrosage sur le site de Bure. Proceedings of the 12th Int. Congress of Speleology, La Chaux-de-Fonds. Vol 1 : 293-296.

Sauter, M., 1992. Quantification and forecasting of regional groundwater flow and transport in a karst aquifer (Gallusquelle, SW Germany), Tübingen, Tübingen, 151 pp.

Savoy, L., 2002. Caractérisation du temps de transit et du stockage de l'eau dans la zone non saturée des systèmes karstiques. MSc thesis, Centre of Hydrogeology, Neuchâtel.

Shuster, E.T. and White, W.B., 1971. Seasonal fluctuations in the chemistry of limestone springs: A possible means for characterizing carbonate aquifers. Journal of Hydrology, 14: 93-128.

Surbeck, H. and Medici, F. 1990. Rn-222 transport from soil to karst caves by percolating water. IAH Memoires, 22, 1: 348-355.

Ternan, J.L., 1972. Comments on the use of a calcium hardness variability index in the study of carbonate aquifers; with references to the central Pennines, England. Journal of Hydrology, 16: 317-321.

Vervier, P., 1990. Hydrochemical characterization of the water dynamics of a karstic system. Journal of Hydrology, 121: 103-117.

White, W.B., 1988. Geomorphology and hydrology of karst terrains. Oxford University Press, Oxford, 464 pp.

Williams, P.W., 1983. The role of the subcutaneous zone in karst hydrology. Journal of Hydrology, 61: 45-67.

Introduction to Chapter 2.7.

In the previous chapters, responses of natural tracers under various flow conditions have been presented. These results were the basis of the proposed conceptual model of flow and transport. Part of this model is supported by simplified numerical simulations.

In the following chapter, a new topic is addressed: the vulnerability assessment. This theme has been the focus of important European projects over the past 15 years (COST actions). The major issues were vulnerability mapping tools like the PI or the EPIK methods. In this chapter, we look at the agreement of our conceptual model with these existing vulnerability mapping methods. Additionally artificial tracing experiments were carried out in order to validate the proposed vulnerability assessment. The conclusions present some new ideas on the vulnerability and possible future work.

This chapter has been published in the Proceedings of the 32nd Congress of the IAH, and a revisited version should be integrated in a special issue of Environmental Geology.

2.7. Vulnerability assessment in karstic areas: validation by field experiments

Jérôme Perrin, Alain Pochon, Pierre-Yves Jeannin, François Zwahlen.
Hydrogeology Centre, Neuchâtel University, 11 rue E-Argand, 2007 Neuchâtel, Switzerland.
jerome.perrin@unine.ch

Abstract
Several methods have been developed for vulnerability mapping in karstic areas. These methods need additional validation by field experiments. Several tests have been carried out in the Swiss Jura with both natural and artificial tracers. The protective role of some intrinsic properties of the system, such as glacial deposits covering karst, epikarst storage, and system dilution effect have been clearly demonstrated. Use of three tracers in parallel showed the reactivity of the epikarst: all tracers arrived at the same time but their relative concentration stayed clearly different. A classification of contamination scenarios into four classes is proposed. It is shown that the relevance of some intrinsic properties depends on the considered scenario class. The hydrodynamic state of the aquifer influences greatly flow velocities and can strongly modify contaminant concentrations at the output of the system. The spatial repartition (point vs. diffuse) and the quantity of contaminant entering the system will also influence the output response. Hence results from tracing experiments cannot be used straightforward for getting a representative value of flow velocity, dispersion or recovery rate.

Keywords: karst aquifer, vulnerability, contamination scenario, tracing test.

Introduction and objectives of the study

Assessment of groundwater vulnerability in karst aquifers has to be carried out with methods especially adapted. These methods should account for the strong heterogeneity of karst systems: point or diffuse recharge, rapid flow through high permeability conduits or slow flow in low permeability volume (Doerfliger et al. 1999).

Resource vulnerability assessment implies the characterization of the pathway between the surface and the limit of the saturated zone. It has to be differentiated from *source vulnerability assessment* which is the characterization of the pathway between the surface of a catchment area and a well or a spring. Resource vulnerability maps are mainly generated for general groundwater management and land use planning, while source vulnerability maps are more detailed and mainly used as a tool to delineate protection zones. Vulnerability discussed in this paper deal with the latter approach.
Vulnerability will be considered at three different levels: intrinsic vulnerability, specific vulnerability and contamination scenario. Definitions of these terms are as follows (Daly et al. 2002):

- *Intrinsic vulnerability* takes account of the inherent geological, hydrological and hydrogeological characteristics of an area, but it is independent of the nature of contaminants.
- *specific vulnerability* is used to define the vulnerability of groundwater to a particular contaminant or group of contaminants. It considers the properties of the contaminant in the different sub-systems of the karstic aquifers.
- A *contamination scenario* is defined by the temporal evolution and the spatial distribution of the input function of a given contaminant.

In Switzerland, the EPIK method has been developed for intrinsic vulnerability mapping of a karst system catchment area (Doerfliger et al. 1999). For each sub-system of the investigated catchment (epikarst, protective cover, infiltration and karstic network), areas of contrasted vulnerability are mapped (e.g. soil thickness will be the criteria for protective cover mapping based on the principle that thicker the soil, lower the vulnerability). These four maps are then combined into a vulnerability map giving “protection index values”. In EPIK, these values depend mainly on the epikarst and infiltration sub-systems, but less on protective cover and karstic network sub-systems. This vulnerability map can be easily converted into protection zones for a drinking water supply. The main drawback of this method is the weighting of the parameters which is completely qualitative, with no physical basis.
Recent developments within the framework of the European program COST-620 lead to the definition of intrinsic vulnerability using a physically based approach (Brouyère et al. 2001). The idea is to consider the aquifer impulse response to a contaminant pulse. Vulnerability can be defined by three questions: (1) when does the pollution start, (2) to which maximum level, (3) for how long. A 1-D dual porosity analytical dispersive-advective

transport model called VULK has been developed in order compute the transfer function of the system (Jeannin et al. 2001). Five layers are considered: topsoil, subsoil, epikarst, unsaturated karst, karst phreatic zone (Figure 1). For each, flow velocity, distance (or thickness), dispersivity and dilution should be entered into the model. Thickness is determined by geological mapping and geophysics, while dilution is simply the ratio of the output to input discharges. Velocity and dispersivity can be estimated by tracing tests.

For example Smart and Friederich (1986), Bottrell and Atkinson (1992) carried out tracing experiments in the unsaturated zone of karstic systems and were able to estimate tracers transit times. Goldscheider et al. (2001) made a multitracing experiment aiming at testing EPIK mapping at the catchment scale. The present study uses in the same way artificial and natural tracers for checking some theoretical hypotheses of vulnerability methods. These field experiments should help to improve existing models.

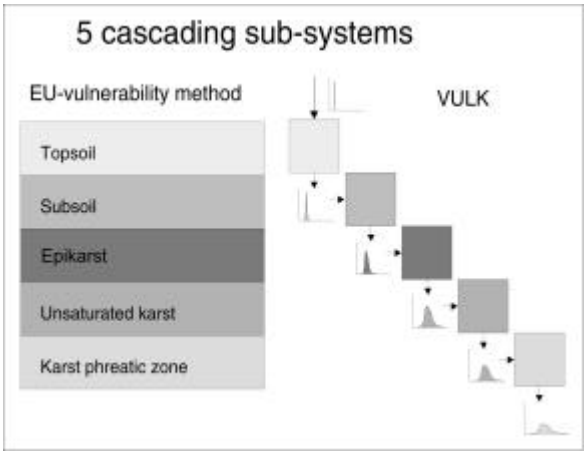

Fig. 1 *Principle of the VULK model according to Jeannin et al. (2001).*

Field experiments

The three test sites are located in the Jurassic limestone of the Swiss Jura mountains (Figure 2). Lionne test site belongs to the folded part of the chain. The Lionne karstic spring drains a catchment of 20 km^2 situated between 1000 and 1400 m elevation (annual recharge is about 1000 mm). The area is mainly covered by forests and pastures. The principal contaminant is faecal bacteria due to the presence of cattle (Perrin and Zwahlen 2002). The Brandt site is also located in the folded Jura at an elevation of 1160 m (comparable annual recharge) in an area of pasture and forests. It consists of a cave of 260 m length draining a stream fed by several tributaries. The studied tributary is equipped for continuous recording of discharge. It is situated in the upstream part of the cave, 15 m under the surface (Blant and Puech 2001). The Milandre site is located in the tabular Jura at an elevation of 450 m (annual recharge is about 600 mm). The Saivu karstic spring drains the Milandre catchment (13 km^2), which has a contrasted land-use: forests, meadows, pasture, cultures and urbanised areas (Perrin et al. 2000).

Discharge data are obtained by continuous recording of water levels by a pressure gauge. The conversion of water levels into discharge is given by an extrapolation from several punctual discharge measurements. Fluorescent tracers are analysed at the lab with a spectrofluorimeter (LS-50 B by Perkin-Elmer). Detection limits are 0.05 µg/l for uranine, 0.1 µg/l for sulforhodamine G and 0.1 µg/l for rhodamine B01. Continuous data are measured at four minutes interval with a field fluorimeter and recorded data are calibrated with samples analysed in the lab (Schnegg and Doerfliger 1997). Lithium is analysed by Ionic chromatography (Dionex DX 20) with a detection limit of 10 µg/l. Iodide is analysed by a specific electrode with a detection limit at 5 µg/l.

Fig. 2 Map of Switzerland with the location of the field test sites.

Lionne catchment: intrinsic vulnerability and effect of the contamination scenario

The vulnerability of the Lionne spring catchment area has been mapped by the EPIK method (Perrin and Zwahlen 2002). Two successive tracing experiments were then carried out in the medium part of the catchment in order to test the vulnerability map. The tested area is located partly in a high vulnerability zone (mainly karrenfield with thin soils) and partly in a lower vulnerability zone (karst covered by thick glacial deposits). Objectives were:

- to check the protection effect of the protective cover
- to assess and compare different contamination scenario by generating point infiltration and at the same time diffuse infiltration

Experiment of the 13.07.2000

Two tracers were injected on the karrenfield area: 400 g of sulforhodamine G diluted and flushed with 680 litres of water was injected directly into a fissure, simulating a point contamination. 315 g of uranine diluted in 700 litres of water was sprinkled over a 35 m^2 surface area in order to generate a diffuse pollution. Infiltration was rapid and thus

possible photo-degradation limited. Breakthrough curves at the spring are given in Figure 3. Maximum velocity (calculated with the time of first arrival) are comparable with 49 m/h for sulforhodamine and 41 m/h for uranine. Mean velocity (calculated with the time of maximum concentration) is respectively 47 and 20 m/h and recovery rate of the tracer 40 % and 16 %. Diffuse pollution leads to lower maximum concentration and lower recovery rate, however first arrival is not different than point pollution and the pollution lasts for a longer time.

Experiment of the 08.08.2000

Sulforhodamine G was injected at the same location than the previous month and uranine was injected a few metres apart, on top of glacial deposits of 5 m thickness. Flush was obtained with 1000 litres of water for sulforhodamine and 1900 litres for uranine. The low permeability of glacial deposits lead to surface runoff on a few metres. Again rapid infiltration limited the effect of photo-degradation. Breakthrough curve is illustrated on Figure 3. Uranine was never detected: the concentrations were under the detection limit or the transit time was more than one month (velocity less than 45 m/day). First arrival of sulforhodamine gives a maximum velocity at 6 m/h and maximum concentration gives a mean velocity of 5 m/h. Estimated recovery rate is 50 %. Low water gives flow velocities ten times less important than the previous month. The protective role of glacial deposits is clearly illustrated with no detection of uranine.

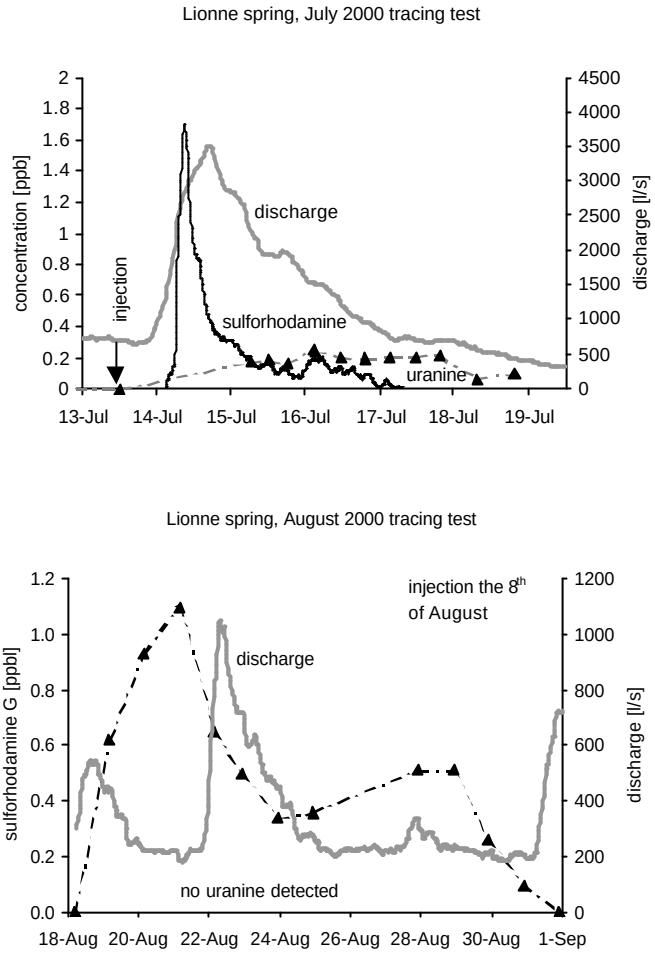

***Fig. 3**: Breakthrough curves of the tracing experiments carried out on the Lionne spring catchment area.*

Brandt site: specific vulnerability testing

This site is suitable for studying hydraulics and transport in the epikarst. Percolation water inside the Brandt cave corresponds to the drainage of the epikarst. It is equipped for continuous measurement of discharge. For the experiment, an autosampler and a field fluorimeter was installed. The catchment area, with a surface estimated at 100 m^2, is located 15 m above in a pasture. Soil (average thickness of 1 m) was removed in a square of 10 m corresponding to a large part of the catchment. This precaution allows to focus the experiment on the epikarst sub-system. A sprinkling system was installed inside the square in order to generate artificial rainfall. Sprinkled water was previously traced with three chemicals (iodide, lithium, rhodamine) homogeneously dissolved in pools of 4 m^3 volume. Tracers were chosen for their chemical properties: iodide is an anion, lithium a cation and rhodamine an organic compound. A total of 6 pools were emptied on a 18.5 hours duration, corresponding to a recharge intensity of 12 mm/h. Such a heavy rainfall was chosen with the aim to completely renew the hanging reserve of the epikarst. The chemistry of the sprinkled water was

also analyzed in order to compare it with the recovered groundwater.

The hydraulic response to sprinkling occurred with 20 minutes delay. Water percolation discharge increased from 0.4 L/min to 5 L/min in 1.3 hour. The discharge stayed then constant except for short periods corresponding to the pools changes at the surface.

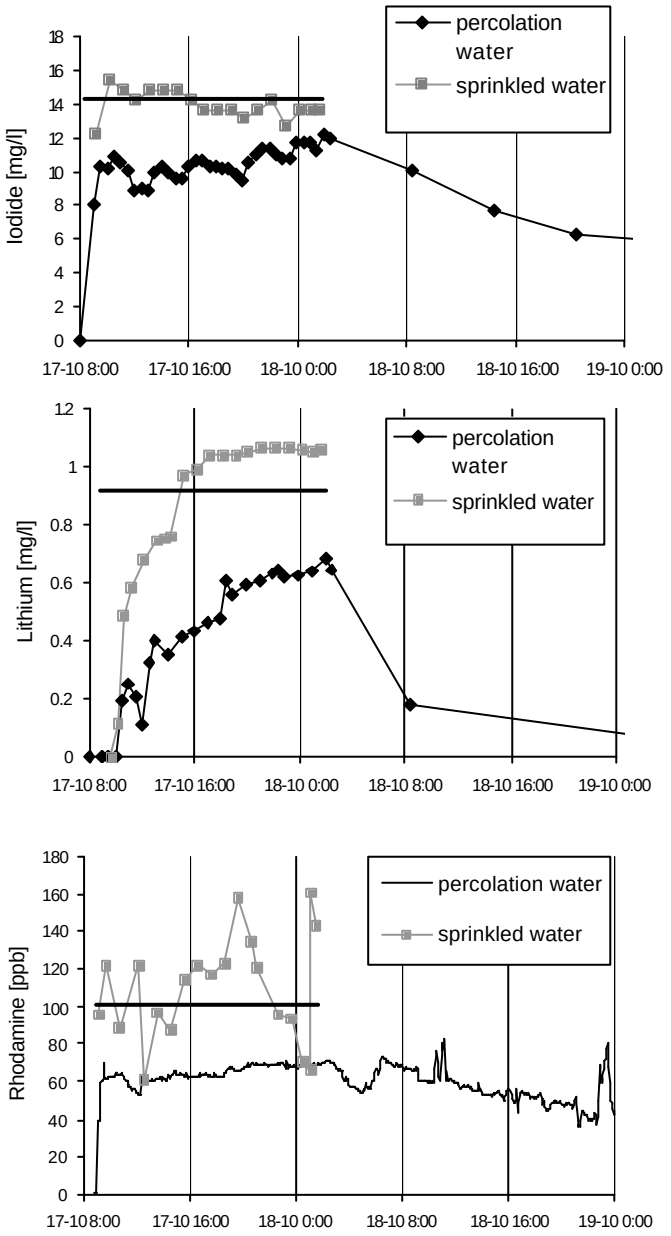

***Fig. 4**: Concentration evolution of the three tracers used for the Brandt sprinkling experiment, October 2001. Points are values obtained by lab analyses. Continuous measurement for rhodamine B01 was recorded with a field fluorimeter. Thick lines indicate the mean concentration of the sprinkled tracers.*

Expected result was a progressive concentration increase in the percolation water up to the sprinkled concentration. Figure 4 gives the observed data: an increase occurs but none of the tracers reaches its input concentration. This result illustrates important storage of traced water in the epikarst and the existence of a large spectrum of flow velocity in this zone. Moreover the specific behaviour of the tracers is different: the most mobile is iodide with a strong increase in concentration about 15 minutes after the start of sprinkling at the surface. At the end of the experiment, the concentration gets close to the injected water.

Rhodamine is intermediate with a first arrival 15 minutes after the start of the experiment and concentration stabilizing at 60 µg/l after. However this value stays lower than the injected water at 100 µg/l. The difference is partly due to adsorption as illustrated by the continuous release of tracer after the sprinkling stopped. The variability of the injected concentration is probably due to a poor homogenisation of rhodamine in the pools.

Lithium is the less mobile: its first arrival occurred 20 minutes after the sprinkling started and maximum concentration reached half the concentration of the injected water. Concentration decreases rapidly after the end of sprinkling.

Milandre site: contamination scenarios

The catchment of this karst system is drained by an underground river fed by several tributaries (Jeannin 1996, Perrin et al. 2000). Many chemical and stable isotopes data have been collected from groundwater at different location within the karst system. These natural tracers can be used to test contamination scenarios.

Example 1: nitrates

The catchment area of the Milandre karst system has contrasted land-use with forests, pasture, cultivated land and urbanized areas. Thus nitrates inputs are spatially highly heterogeneous with elevated inputs in cultivated areas and natural background in forests. Outputs responses show high concentrations for tributaries fed by a cultivated catchment (e.g. CA), low concentrations for tributaries fed by a forested catchment (e.g. SO) and average concentration at the spring (Figure 5). No clear temporal evolution is visible, indicating that the inputs can be considered as constant. Slight short term variations on the output signal might be caused by changes in hydraulic conditions (e.g. dilution during a flood event). Mitigation of a contamination by dilution from less contaminated tributaries is called “system dilution effect”.

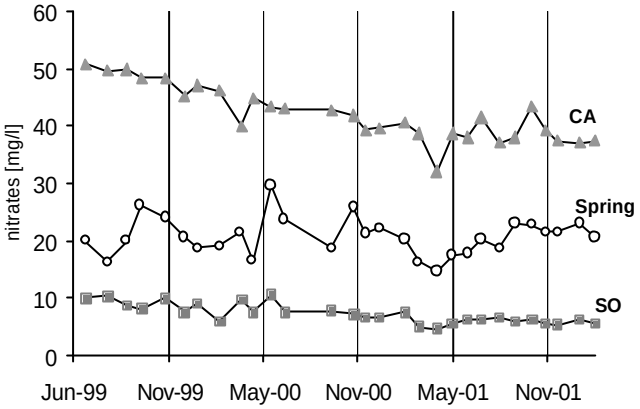

Fig. 5*: Monthly nitrates measurements at two tributaries (CA, SO) and the spring of Milandre karst system.*

Example 2: stable isotopes

On an annual basis oxygen 18/16 isotopic ratio can be considered as an homogeneous input both spatially and temporally: the input function is simply the annual mean isotopic ratio found in rainfall (Figure 6). When entering the system, this function is degraded by evaporation and then should be reproduced at the spring. It corresponds to the annual mean ratio represented by the dashed line on Figure 6.

Weekly samples taken at the spring deviate significantly from the annual mean. Such deviations have two main causes: first, the input signal is not constant but shows a strong seasonal cycle with high values in summer and low values in winter. Second, input signal during a rainfall event is far from constant. Hence an important recharge event will modify the output signal. These perturbations are called “flood dilution effect”.

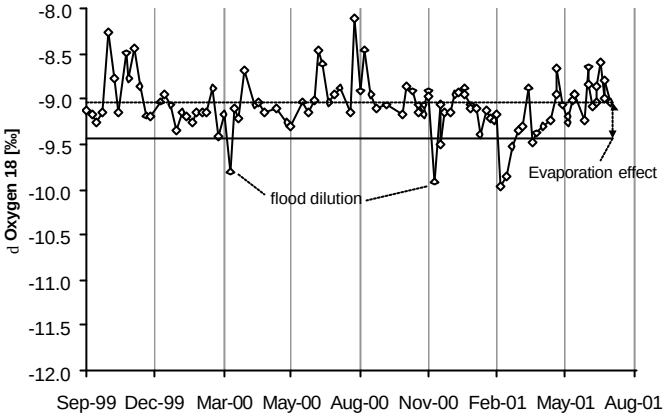

Fig. 6*: Evolution of oxygen stable isotopes ratio in the Milandre karst system spring water. The thick line indicates the annual mean ratio in rainfall and the dashed line corresponds to the mean ratio at the spring.*

Discussion

Experiments on the Lionne catchment area

Tracing experiments on the Lionne catchment show the efficiency of low permeability glacial deposits in the retardation of a contaminant. This protective cover is mapped under the attribute P by the EPIK method. The thickness is considered as the discriminating factor in the EPIK method. This assumption seems valid as the tested protective cover has a thickness of 5 metres determined by geophysics (RMT method).

The type of infiltration (diffuse or concentrated) plays an important role on the shape of the contaminant breakthrough curve. First arrivals at the spring are similar but the maximum concentration is much higher in the case of a point injection. However diffuse contamination shows a longer duration. The result of this experiment shows the necessity to differentiate point and diffuse pollution.

Strong dilution effects associated to flood events can be seen on Figure 3. This effect is not taken into account by the EPIK method but can favour contamination attenuation. Its importance is dependant on the ratio between contaminant input flux and discharge at the spring (i.e. proportional to the size of the catchment area, intrinsic to the system) and to the hydraulic conditions during the contamination (which can be considered in the pollution scenario phase). This intrinsic property is integrated in the VULK approach as the model needs a dilution factor for each sub-system.

Experiment at Brandt test site
Experiment of Brandt site illustrates the strong reactivity of the epikarst sub-system: first arrival of the three tracers is similar but the recovery is clearly different with iodide as the more mobile and lithium as the less mobile.

Soil was removed before injection in order to avoid retardation and soil storage, and to test epikarst only. It appears that retardation is efficient in the epikarst also. This can be due to the presence of organic matter and clays in the fissured media. Retardation can be caused also by the structure of the epikarst: thin fissures and capillary tubes allowing a high storage capacity. It is clear that the epikarst structure can play a protective role by retardation of the flow velocity.

The use of a tracer like tritium would help to discriminate between transport delay caused by structural properties or by chemical adsorption.

Data from Milandre test site
The intrinsic properties of the system (system dilution, dispersion, transit time) are relevant only for some contamination scenarios. Nitrates concentrations will undergo system dilution as inputs are not spatially homogeneous at Milandre test site. But neither transit time nor dispersion will influence the output concentrations as inputs are temporally constant. Long term stable isotopes input can only be modified by evaporation (reactive effect specific to the tracer). The input is spatially homogeneous and no system dilution effect will be possible. Modifications of the output signal are mainly caused by changes in the hydraulic state of the system.
By and large we can schematised the different contamination scenarios by four end-members characterised by the shape and the distribution of the input function (Figure 7). In a previous study, Teutsch and Sauter (1998) proposed also a classification in four “problem classes”, but they limited their scenario at the spatial dimension.
The output functions are first considered under steady-state conditions: possible effects of degradation (specific vulnerability) is a decrease in output concentrations. Second, modifications of the output functions under transient conditions are given. General remarks are given in the Table below.

Contamination scenarios have to be described at three levels:

1) the shape and spatial distribution of the input function will directly determine the output function under steady-state conditions.

2) The hydrodynamic state of the aquifer for a given pollution will influence greatly the contaminant output. Velocity can increase of more than one order of magnitude between base flow and flood conditions (results from the Lionne catchment and other unpublished data) and thus reduce Δt into $\Delta t'$. Karst spring discharge have typical variations of one to two orders of magnitude (e.g. Lionne spring discharge varies from 100 to 10’000 l/s). Such changes in fluxes will lead to flood dilution. Such an effect is illustrated by Figure 3: Sulforhodamine is diluted by the flood event occurring during breakthrough. Concentration changes can also be caused by a differential contribution of the sub-catchments through the flood duration. As an example, we can imagine a catchment covered by forests in the downstream part and by cultivated land in the upstream part. If we look at nitrates, we can expect a decrease in concentration in the first part of the flood followed by an increase in the second part.

3) Last but not least, the quantity of spread pollutant will be of major importance on the outputs. Figure 7 illustrates only cases where the quantity will significantly influence the system. However, we can imagine scenarios where limited amount of pollutant will lead to output at background levels. Such a case is illustrated by the tracing experiment on glacial deposit at Lionne site. No response was obtained even if the input function is described by case d. A second example is given by short time scale stable isotope data at Milandre site. A strong signal in the rain is transmitted to the spring only if the recharge is greater than 20 mm. Such a threshold value is an indicator of the storage capacity of the soil and epikarst sub-systems. Signal at the spring will occur only if the tracer (or pollutant) exceeds this threshold value.

	Input	Steady-state output	Transient output
Case a	short-term pollution spread over the entire catchment. Stable isotopes changes during a rainfall event can be a representative tracer.	transit time and dispersion are relevant but no system dilution is possible.	Flood can decrease concentration by dilution. Transit time is reduced.
Case b	long-term pollution spread over part of the catchment. That is the nitrates example at Milandre site.	Transit time and dispersion are not relevant. System dilution can mitigate pollution.	Concentration changes are mainly caused by differential temporal contributions of the sub-catchments.
Case c	long-term pollution spread over the entire catchment. That is the stable isotopes example at Milandre site.	Transit time, dispersion and system dilution are not relevant.	Flood dilution possible if variations in the input occur on a short time scale.
Case d	short-term pollution spread on a limited area. It corresponds to the tracing experiments at Lionne site.	Transit time, dispersion and system dilution will influence the output.	Flood dilution will occur. Transit time is reduced.

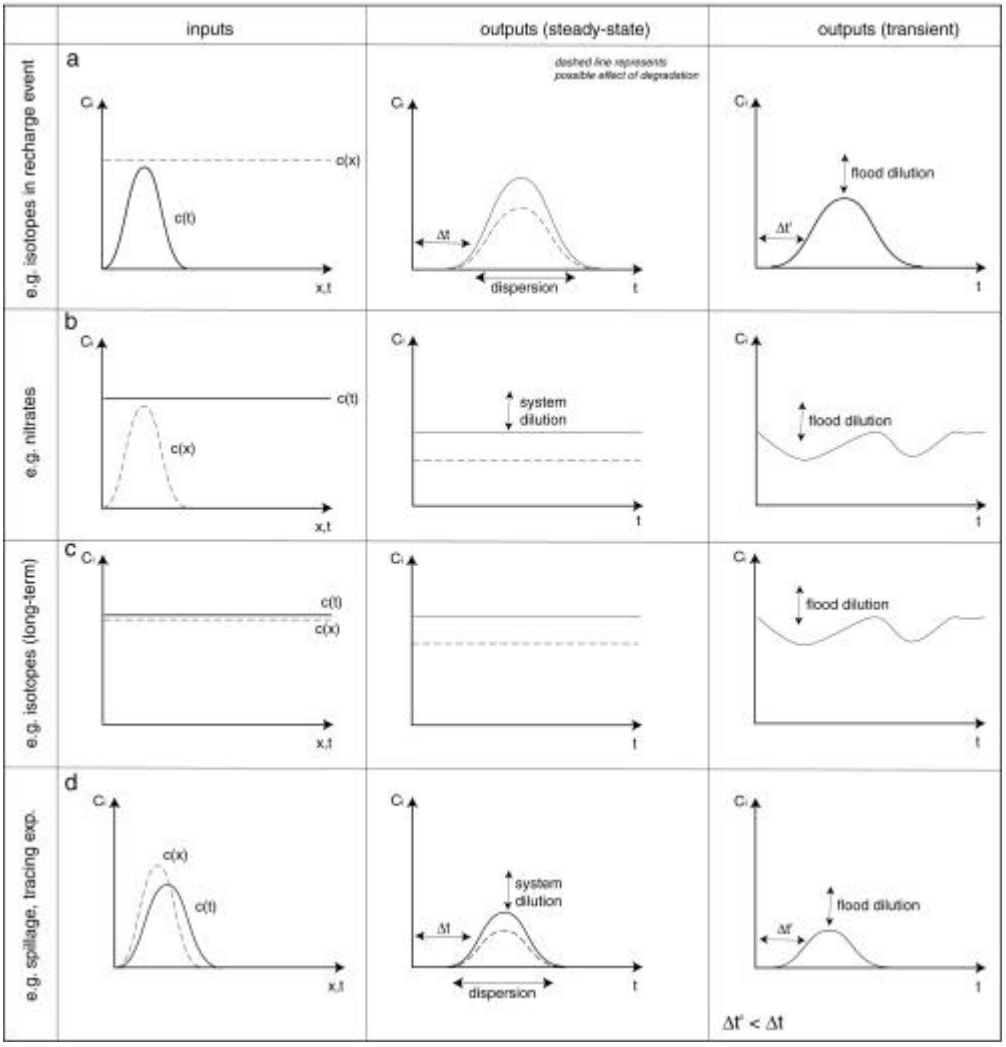

Fig. 7*: Schematic representation of the four end-members contamination scenarios. Inputs are characterised by their spatial repartition (space is represented by x) and their duration (time represented by t). Ci corresponds to concentration of a given contaminant i. Outputs are theoretical breakthrough curves.*

To summarise, the response to these contamination scenarios are dependant on:

- the structure of the aquifer (intrinsic vulnerability): system dilution, dispersion, flow velocity field given a certain retardation (Δt) and threshold of the soil-epikarst storage capacity
- The shape and spatial distribution of the input function, the volume of pollutant, the hydrodynamic state of the aquifer (contamination scenario)
- The degradation of a given pollutant (specific vulnerability)

Major issues for vulnerability assessments

Intrinsic vulnerability

- Role of glacial deposits: Moraine covering karstic rocks plays a clear protective role as indicated by the Lionne tracing experiments.
- Role of epikarst: Epikarst can have an important storage capacity and limit flow velocity.
- Role of the karstic network: Dilution related to the size of the catchment can decrease drastically output concentrations.

Specific vulnerability

- Role of the epikarst: Presence of clay materials and organic matter can limit significantly the mobility of certain contaminants.

Pollution scenarios

- Role of the contamination scenario: Input function shapes and flux of contaminant will determine to a large extent the output function shape. Intrinsic vulnerability parameters (flow velocity, dispersion, system dilution) will be relevant only for some scenarios.
- Role of the hydrodynamic state of the aquifer: Changes in hydraulic conditions have an important effect on the concentrations at the output: a flood event can decrease transit time of one order of magnitude.

Conclusions

Our field experiments showed the adequacy of the sub-systems conceptual model which is used by the EPIK method: the possible protective role of the soil, the epikarst and the type of infiltration has been clearly illustrated. However, weighting factors of the sub-systems would need to be adapted. Protective cover need a higher weight than proposed by the method and the possible protective role of the epikarst has to be integrated. The main difficulty lies in the absence of tools for epikarst mapping. More work has to be done on the infiltration sub-system: the spatial distribution of true diffuse infiltration, surface runoff or subcutaneous flow is still not clear.

An important point, which is not considered by EPIK is the system dilution directly dependant on the catchment size. However recent developments have integrated this parameter (e.g. VULK model).

It has to be kept in mind that classical tracing tests (point injection of a few cubic metres of traced water) carried out for delineation of catchment areas cannot be used straightforward for getting information on vulnerability of the system (e.g. flow velocity). In most cases, such experiments bypass the “soil-epikarst filter” and can only give information on flow velocity and dispersion in the karstic network. The only way to get the flow parameters of soil and epikarst is small scale experiments using realistic recharge intensities.

It is clear that the contamination scenario will influence to a large extent the breakthrough curve at the output. In order to optimise the protection of karst groundwater quality, it is necessary to adapt the vulnerability mapping to the most probable contamination scenario.

Acknowledgements

We are indebted to R. Le Fanic, V. Puech, F.Bourret and T. Ettlin for field work and analyses in the lab. We also thank the L’Abbaye local authorities for giving us the opportunity to study in details the Lionne karstic spring.

R. Hirata made useful comments which improved the readability of the paper.

References

Blant D, and Puech V. 2001. La grotte de Vers chez le Brandt et cavités alentours. Cavernes n°1, 7-11.

Bottrell S H, and Atkinson T C. 1992. Tracer study of flow and storage in the unsaturated zone of a karstic limestone aquifer. In: H. Werner (Editor), Tracer Hydrology. Balkema, Rotterdam, pp. 207-211.

Brouyère S, Jeannin P-Y, Dassargues A, Goldscheider N, Popescu I-C, Sauter M, Vadillo I, Zwahlen F. 2001. Evaluation and validation of vulnerability concepts using a physically based approach. In: F. Zwahlen and J. Mudry (Editor), 7th Conference on Limestone Hydrology and Fissured Media. Univ. de Franche-Comté, mém. hors-série n°13, Besançon, pp. 67-72.

Daly D, Dassargues A, Drew D, Dunne S, Goldscheider N, Neale S, Popescu I-C, Zwahlen F. 2002. Main concepts of the "European approach" to karst-groundwater-vulnerability assessment and mapping. Hydrogeology Journal, 10: 340-345.

Doerfliger N, Jeannin P-Y, Zwahlen F. 1999. Water vulnerability assessment in karst environments: a new method of defining protection areas using a multi-attribute approach and GIS tools (EPIK method). Environmental Geology, 39(2): 165-176.

Gogu, R C, and Dassargues A. 2000. Current trends and future challenges in groundwater vulnerability assessment using overlay and index methods. Environmental Geology, 39(6): 549-559.

Goldscheider N, Hötzl H, Fries W, Jordan P. 2001. Validation of a vulnerability map (EPIK) with tracer tests. In: F. Zwahlen and J. Mudry (Editor), 7th Conference on Limestone Hydrology and Fissured Media. Univ. de Franche-Comté, mém. hors-série n°13, Besançon, pp. 167-170.

Jeannin P-Y. 1996. Structure et comportement hydraulique des aquifères karstiques, PhD thesis, Neuchâtel, 237 pp.

Jeannin P-Y, Cornaton F, Zwahlen F, Perrochet P. 2001. VULK: a tool for intrinsic vulnerability assessment and validation. In: F. Zwahlen and J. Mudry (Editor), 7th Conference on Limestone Hydrology and Fissured Media. Univ. de Franche-Comté, mem. hors série 13, Besançon, pp. 185-188.

Perrin J, Jeannin P-Y, Zwahlen F. 2000. Spatial variability of groundwater chemistry within a karst aquifer (Milandre test site, Swiss Jura)., Karst 2000: New trends in karst studies., Marmaris.

Perrin J, and Zwahlen F. 2002. Protection zones of the Lionne spring catchment area. Unpublished report, Hydrogeology Centre Neuchâtel.

Schnegg P-A, and Doerfliger N. 1997. An inexpensive flow-through field fluorimeter. Proceedings of the 12th International Congress of Speleology, 2: 47-50.

Smart P L, and Friederich H. 1986. Water movement and storage in the unsaturated zone of a maturely karstified carbonate aquifer, Mendip Hills, England. In: D. National Water Well Association, Ohio. (Editor), Proc. Conf. env. problems of karst terrains and their solutions, pp. 59-87.

Teutsch G, and Sauter M. 1998. Distributed parameter modelling approaches in karst-hydrological investigations. Bulletin d'Hydrogéologie 16, Neuchâtel University: 99-109.

3. Conclusions

Main results for each topic (hydraulics, isotopes, pollution-related solutes, dissolution-related parameters) are synthesized in paragraph 3.1. Then, the new ideas developed in the project are confronted to existing conceptual models (3.2). The generalization of the ideas to other systems is discussed in paragraph 3.3. The practical issues of the proposed conceptual model are presented in paragraph 3.4. Finally, proposition are made for further studies aiming at improving the proposed conceptual model (3.5.)

3.1. Synthesis of the project's main results

3.1.1. Hydraulics in the unsaturated zone, Milandre test site

Two types of hydraulic responses are characteristic at the base of the unsaturated zone: a vadose flow response with strongly marked floods, and a seepage flow response with dampened responses on an annual cycle. The combination of both flows allows to reproduce the main characteristics of the hydraulics of the underground river and its tributaries. Hence the hydraulic behaviour of the system is already established in the unsaturated zone, and the phreatic zone appears to plays a limited role (chapter 2.2.) The distribution of infiltrated water into seepage or vadose flows seems to occur in the epikarst sub-system.

3.1.2. Stable isotopes: spatially homogeneous non-reactive tracers

At Milandre test site, the Saivu spring isotopic signal is fairly constant throughout the year under steady-state flow conditions despite clear seasonal variations in the rainfall isotopic signal. The complete dampening of this signal in the aquifer indicates an important mixing and storage in the system.

During flood events, stable isotopes are the best natural tracers for estimating the fresh infiltrated water (i.e. rain water) component, as they vary strongly in rainfall. Detailed sampling showed a limited contribution of fresh water in vadose flow, and in several tributaries of the underground river. This contribution is comprised between nothing for a recharge of 3 mm to 15-20 % for a recharge of 20 mm.

The relevant processes of mixing and storage occur in the unsaturated zone. Numerical modelling of the epikarst reservoir showed the role of water storage and distribution of this sub-system. It was however necessary to buffer the variations in the input concentrations in order to reproduce the observed responses (chapter 2.4). The soil zone is likely to act as a buffer by mixing infiltration water with water stored in the soil. This role was confirmed by flood sampling at Grand Bochat site and Brandt site (chapter 2.6). The former is covered by a thin soil which buffers efficiently the rain isotopic signal. The latter is not covered by soil, and the rain isotopic signal was accurately reproduced in the percolation water.

The buffering of rain isotopic variations within the unsaturated zone has already been illustrated for different aquifer systems by Clark and Fritz (1997). In surface hydrology, hydrograph separation of flood events showed also a limited participation of rain water (e.g. Ladouche et al. 2001).
This buffer effect is still present in karst systems, even if the hydraulic response is more direct and strongly marked than for other aquifers (Bakalowicz et al. 1974, Lastennet 1994, Stichler et al. 1997, Maloszewski et al. 2002).

The numerical modeling of flow and transport in the unsaturated zone suggests that mixing is very effective in the soil zone. Most field soils exhibits a spatial variability in their structure and hydraulic properties (Flühler et al. 1996, Vogel et al. 2000). The soils of our test sites present a high clay content. The low permeability soil matrix is cut by macropores of higher permeability (figure 1). These macropores decrease progressively at depth. They can favour a rapid hydraulic response but the fresh infiltrated water should be mixed efficiently with pre-event water. This apparent paradoxal situation could be overcomed by the following model:

Let imagine n capillary tubes of different length crossing the soil. Even if flow velocities are similar, breakthrough times ($t_1, \ldots, t_n$) are different. Hence, if the discharge rate of the n capillary tubes is similar, we can write:

$$c_{out}(t_i) = \sum_{k=1}^{n} \frac{1}{n} c_{in}(t_i - t_k)$$

where c_{out} and c_{in} are respectively the solute concentration leaving the soil and entering the soil. If the c_{in} function has some periodicity (which is the case for stable isotope) and the t_k have a time span covering at least a period of the input function, c_{out} will be highly buffered. Rapid hydraulic response can be guaranteed by piston flow in the capillary tubes when recharge occurs.

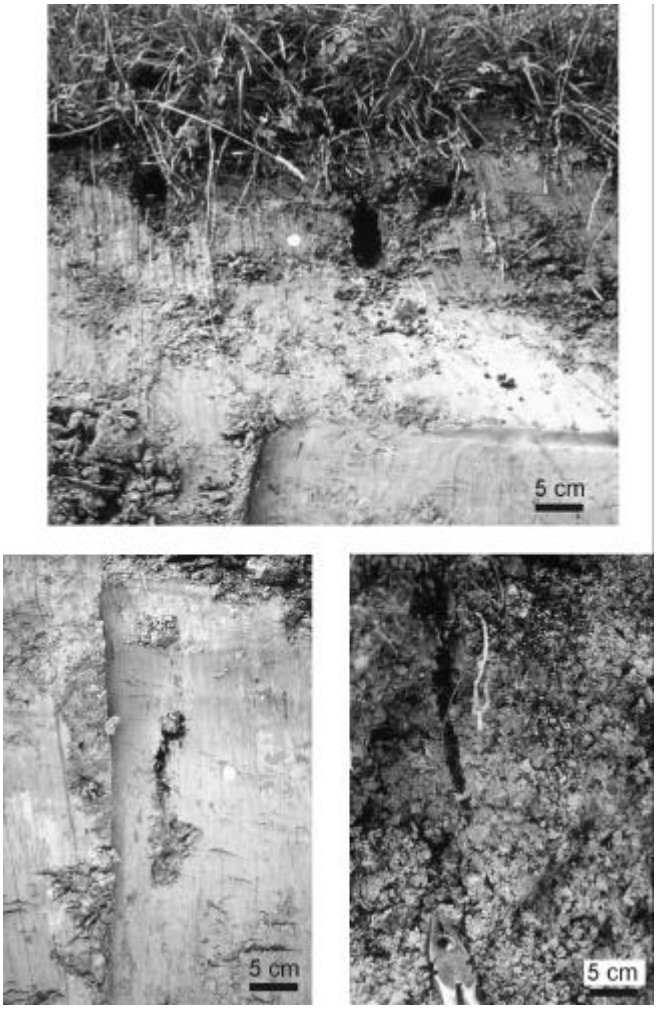

Figure 1: Soil profiles at Brandt site. The higher picture illustrates the existence of mole holes. The lower pictures show root holes embedded in a compact soil (left) and a granular soil (right). (Pictures courtesy V. Puech).

3.1.3. Pollution-related solutes: spatially heterogeneous non-reactive tracers

At Milandre site, pollution-related parameters (nitrates, sulfates, chloride, potassium, magnesium) have contrasted concentrations in the tributaries feeding the Saivu karst spring. This variability is strongly controlled by land use in the different sub-basins: contaminated waters are issued from cultivated sub-basins, pristine waters from forested sub-basins (chapter 2.3). The spring chemistry reflects the mixing of these different waters. This type of mixing is called “horizontal mixing”, as it occurs in the sub-horizontal conduit network. During flood events, it induces changing chemographs for pollution-related solutes, and nearly flat chemographs for homogeneously distributed solutes (stable isotopes, dissolution related parameters). Existence of horizontal mixing gives an insight on the structure of the conduit network: presence of contaminated tributaries, and distance to the spring (chapter 2.5).

During flood events, variations of pollution-related parameters in the underground river are either a decrease in concentrations (up to 20 %) or an increase (up to 100 %). These differences are due to seasonal fluctuations in the chemical composition of the reservoirs located in the unsaturated zone (epikarst and soil mainly). They are controlled by the timing of fertilisers inputs, the intensity of the vegetation activity, and leaching depending on climatic conditions.

Main chemical reactions occur in the soil and epikarst reservoirs: hydration, cationic exchange, oxidation of nitrogen compounds, and ionic enrichment by evapotranspiration. Traces of nitrites could be detected in the underground river during important floods only.

Long-term evolution in concentrations is illustrated in Appendix 3e over a three years period (monthly sampling). Some tributaries kept stable concentrations, whereas others varied significantly for pollution-related parameters (VI, CA, ST). These changes are probably related to modifications in land-use and fertilizers inputs. However no further investigations were carried out in order to test this hypothesis. Such water chemistry long-term changes due to agriculture are also a possible reason for the existence of fresh corrosion trenches on speleothems in the upstream part of the Milandre cave. Speleothems grew when the catchment area was still preserved. Later, use of the catchment for agriculture modified the chemical properties of percolation water. Speleothems were fed by aggressive waters and started to be dissolved.

In preserved systems, the soil zone can also be a main source of chloride and sulfate as illustrated by the Grand Bochat site (chapter 2.6).

Samples for pesticides analyses (sulcotrione, metazachlore, isoproturon) were collected on ST, EG, VI, EN, AM tributaries and at Saivu spring during a flood event (29^{th} and 31^{st} of May 2000). Only AM showed traces of isoproturon. Thick cultivated soils may explain the efficient degradation of the pesticides and their metabolites.

3.1.4. Dissolution-related parameters: spatially homogeneous reactive tracers

In steady-state conditions, tributaries can have distinct mineralisation even if they are all saturated with respect to calcite. Such differences are due to the spatial variability of soil pCO_2, which gives groundwater its corrosive properties (see Appendix 7). However the spatial variability is not as important as for pollution-related parameters (chapter 2.3). Stored soil water can be undersaturated with respect to calcite, especially in brown decarbonated soils (chapter 2.6). Mineralisation occurs mainly in the epikarst zone, and water reaching the phreatic zone is close to saturation.

During important flood events, part of the infiltrated water can reach the phreatic zone slightly undersaturated with respect to calcite. This water is issued from the soil or the rain and bypasses the epikarst reservoir. Water reaching the phreatic zone is then a mixing of base flow and quick flow (both

issued from the epikarst and having the same chemical composition), as well as fresh water (issued from rainfall or the soil zone, and being unsaturated with respect to calcite). In the phreatic zone, mixing of the respective tributaries ("horizontal mixing") explain most of the dissolution-related parameters variations (chapter 2.5). Chemical reactions and contribution of phreatic storage seem to be limited or absent.

3.2. New lights on the existing conceptual models

3.2.1. The proposed conceptual model

The conceptual model is based on the observations made at Milandre test site. It should be emphasized that this system is fed by diffuse infiltration only.

The considered cascading sub-systems of the conceptual model are (figure 2): the soil, the epikarst, the unsaturated zone, the phreatic zone (as presented in figure 3a up, steady-state conditions scenario). Representative tracers for the soil are: CO_2, NO_3^-, Cl^-, Na^+, K^+, SO_4^{2-}, and for the epikarst are: Ca^{2+}, HCO_3^-, (and Mg^{2+} if presence of dolomitic limestone). The stable isotopes source is the atmosphere.

Important processes controlling flow and transport occurring in the sub-systems are:

- mixing, storage, and evapotranspiration in the soil,
- dissolution, storage, and funnelling in the epikarst,
- vertical mixing and in some cases dissolution in the unsaturated zone,
- horizontal mixing in the phreatic zone.

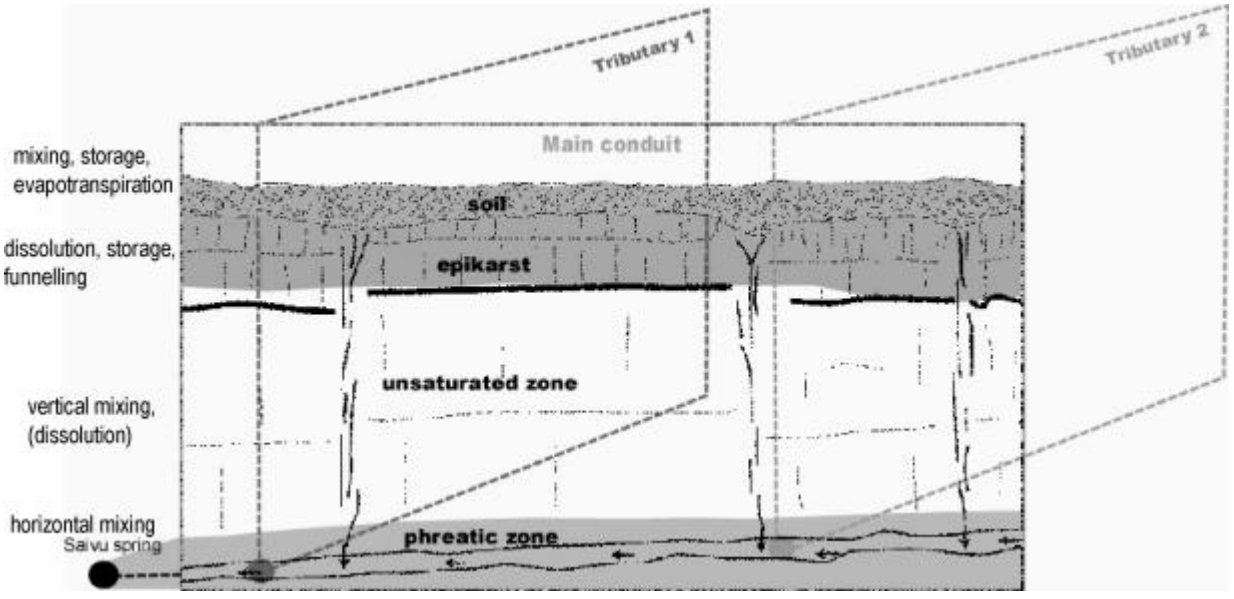

Figure 2: The conceptual model of Milandre karst aquifer.

Figure 3 presents a schematic evolution during a flood event based on the proposed conceptual model. The resulting hydrograph and chemographs are sketched in figure 3b. The whole flood corresponds to an important recharge event, more frequent floods, with less recharge, will not reach configurations ϕ_3 or even ϕ_2 and follow directly the recession configuration (ϕ_4).

In steady-state conditions (ϕ_0), the system is fed by waters stored in the epikarst. Discharge and chemistry are stable at the spring. Water is stored in the soil zone but hold by the capillary barrier.

During phase ϕ_1, rainfall has started, soil water is pushed into the epikarst nappe, and the hydraulic stress on the epikarst causes a discharge increase in the system. The system is fed by epikarst water mainly. Discharge rises at the spring, but chemistry does not change.

During phase ϕ_2, rainfall continues, more soil water is pushed into the epikarst nappe. Part of the soil water bypasses the epikarst reservoir and reaches directly the phreatic zone. The system is fed by epikarst and soil waters. Discharge still rises at the spring. Pollution-related parameters vary due to horizontal mixing, and dissolution-related parameters may also vary if the soil water is undersaturated with respect to calcite, but stable isotopes do not vary because soil water has a constant concentration.

During phase ϕ_3, rainfall continues, the soil is entirely at field capacity. Some fresh water bypasses the soil reservoir and reaches the phreatic zone. The system is fed by a mixing of fresh water, soil water, and epikarst water. Discharge is near maximum at the spring. Stable isotopes vary at the spring if the isotope signal in rainfall is significantly different from the system background.

During phase ϕ_4, rainfall has stopped, the soil releases water into the epikarst reservoir. The system is mainly fed by epikarst water, but soil water can still be present. At the spring, the discharge decreases and the chemical parameters return to their pre-event concentrations (recession phase).

In this conceptual model, the storage is mainly located in the soil and epikarst zones. The role of phreatic storage is neglected, as it is not necessary for explaining the observed hydraulic and chemical responses. The unsaturated zone and phreatic conduits are mainly seen as transmissive zones, with high flow velocity and limited storage.

Flow velocities are very different under steady-state or transient conditions: In Milandre, when the system is at steady-state (low water), no flow is present in the soil, flow velocity in the epikarst should be low, and velocity in the unsaturated and phreatic zones is on the order of 100 m/h (value from artificial tracing experiments). During flood events, flow velocity in the soil zone is about 0.5 m/h, 50 m/h in the unsaturated zone, and 400-500 m/h in the phreatic zone.

The contributions of the different components to vertical mixing during flood events are between 0-20 % for fresh water, up to 60-70 % for soil water, and the rest comes from the epikarst. If the soil zone is non-existent, the part of the fresh water may become preponderant.

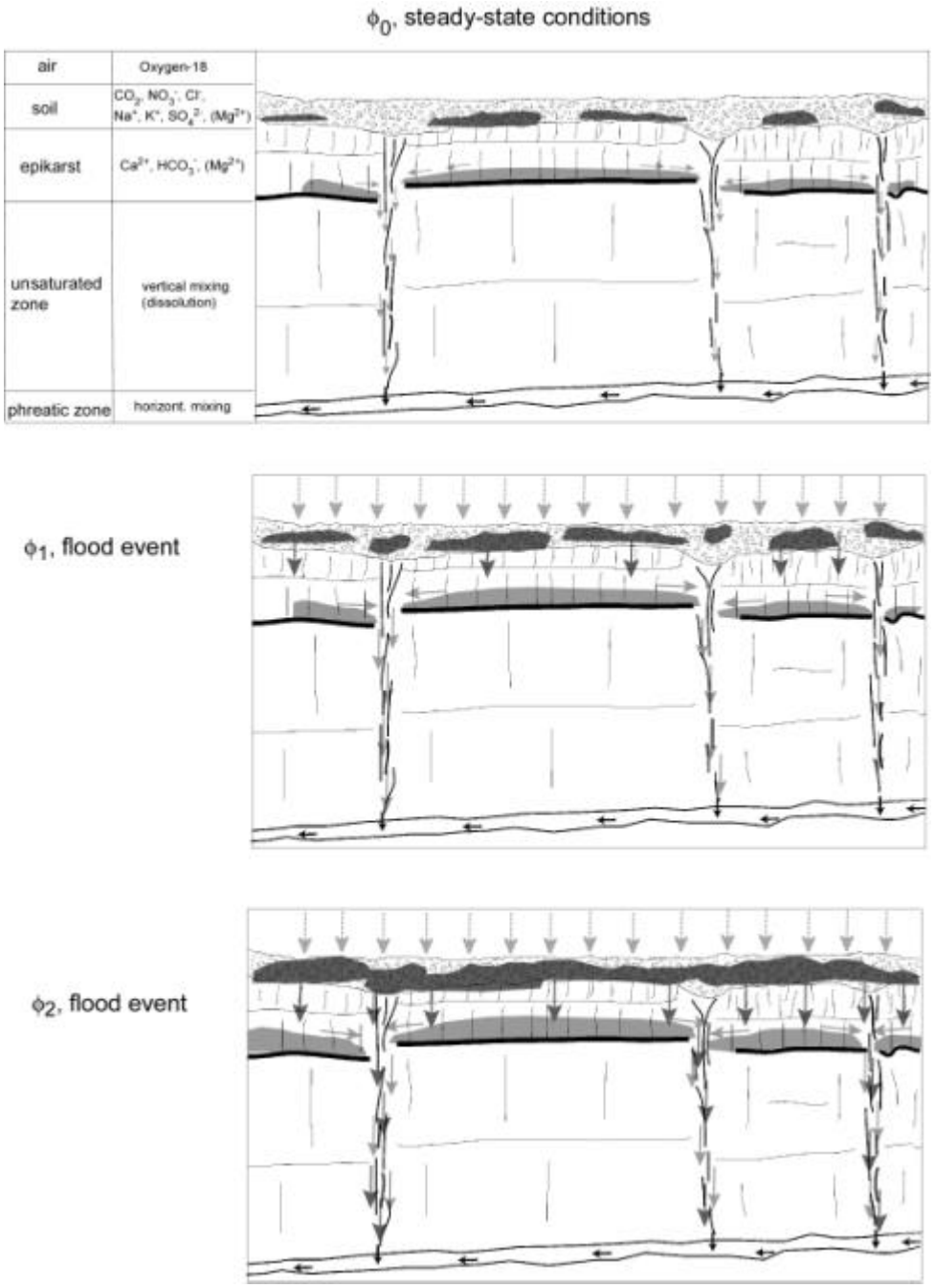

Figure 3a: Evolution during a flood event based on the proposed conceptual model.

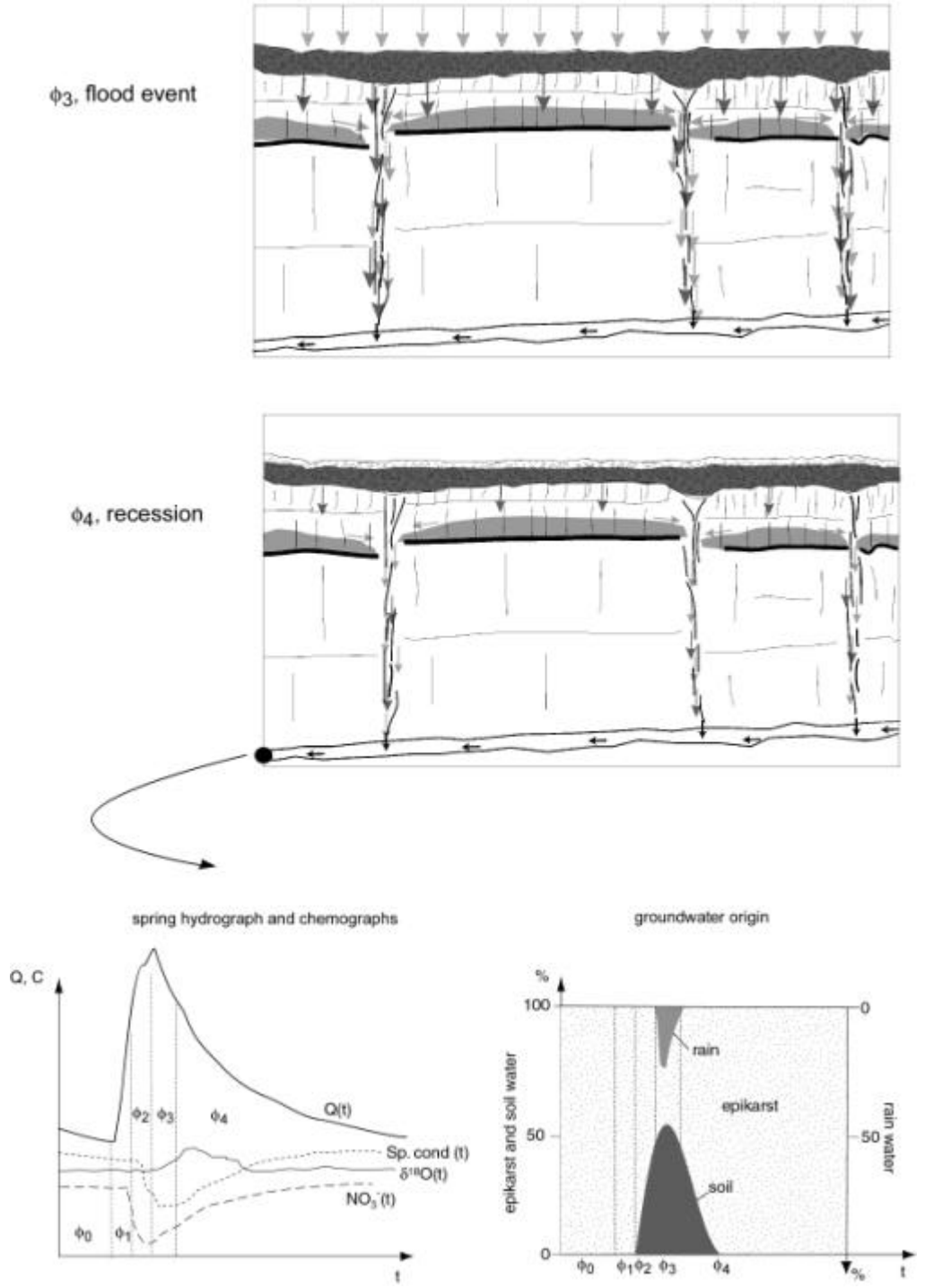

Figure 3b: Evolution during a flood event based on the proposed conceptual model. A schematic representation of the karst spring hydrograph and chemographs is shown, as well as a diagram illustrating the percentage of each component of the spring discharge.

3.2.2. Comparison with existing models

a) Hydrochemical models

Chemograph variations at karst springs during flood events are generally explained by mixing. Models consider different end-members participating to the flood event: concentrated infiltration, diffuse infiltration and phreatic water stored in the low permeability volumes (LPV) (Vervier 1990), phreatic water and fresh infiltrated water (Kiraly and Mueller 1979, Blavoux and Mudry 1983), epikarst storage, conduit storage, and fresh infiltrated water (Williams 1983, Sauter 1992), mixing of several tributaries (Hess and White 1988), rapid delayed infiltration water and phreatic water (Plagnes 2001). At Milandre site, mixing occurs first “horizontally” between groundwater issued from the different sub-catchments (mixing of Hess and White 1988). If the recharge event is important, soil water and even fresh water can participate to the flood water.

In some studies (Shuster and White 1971, Ternan 1972, Grasso 1999, Grasso and Jeannin 2002, Grasso et al. 2003), dilution of dissolution-related parameters during floods is explained by the calcite dissolution kinetics: flood water flows too quickly as compared to base flow, and does not reach the thermodynamic equilibrium with respect to calcite. Such models seem relevant for systems mainly fed by concentrated infiltrations. At Milandre site, we showed that groundwater reaches the bottom of the unsaturated zone at saturation with respect to calcite. Hence tributary mixing is much more important for shaping the spring chemograph. In order to assess correctly the role of dissolution for various contexts, we suggest to separate the different components of the flow, and then to apply a dissolution model to the undersaturated component (as it was done in chapter 2.6. for Brandt test site).

b) Karst aquifer conceptual models

Jeannin (1998) proposed a conceptual model of Milandre aquifer based on hydrodynamic observations (discharges in the conduits, piezometers levels). This model integrates a significant contribution of water from the low permeability volumes (LPV) of the phreatic zone: approximately 50 % of the infiltration was supposed to recharge the LPV and to be then slowly released into the conduits. Our model reduces drastically the role of the LPV. These LPV are not necessary for explaining and simulating the observations. However storage in the LPV exists (as shown by piezometers level variations), but the actual water fluxes may be limited, and the actual porosity lower than expected.

Simulation of shallow karst systems by Kiraly (1998) showed a Faraday cage effect in the epikarst, which limits the recharge of the LPV. This concept is in agreement with our model: infiltrated water is mainly stored in the soil and the epikarst. It is then released into the conduits and short-circuits the LPV of the phreatic zone.

Classical models of karst systems by Mangin (1975) or Drogue (1992) give an important role to the LPV or Annex to Drain System (ADS) which are functionally equivalent (see paragraph 1.1.3). These models are not adequate to describe the Milandre karst system. They were built from observations on karst systems presenting a thick phreatic zone (deep phreatic karst system, see below).

Existing conceptual models of the epikarst are in agreement with our model. Williams (1985), Smart and Friederich (1986), Klimchouk (2000) proposed an important storage in this sub-system and a funnelling of the flow towards the conduits (see paragraph 1.2.3).

To summarize, the principal characteristics of our model are:

- Limited role of phreatic storage for both hydraulics and transport.
- Tributary mixing is a prominent process that shapes spring chemographs during flood events.

- The importance of the recharge events (actual infiltrated water) controls the respective percentages of the mixing components (epikarst, soil, fresh waters) participating to the spring water discharge.
- Possible existence of undersaturated water with long residence times in the soil zone.
- Base flow is mainly sustained by the epikarst reservoir.
- Residence times are very different in the respective sub-systems: months in the soil and the epikarst, hours in the unsaturated zone and the phreatic conduits.

3.3. Extension of the model to other karst systems

An important question is to know to what extent the proposed conceptual model (chapter 3.2.) can be applied to other karst systems. In order to illustrate the specificity of the Milandre aquifer, Saivu spring characteristics are compared to other well-studied springs in Table 1. Main conclusions are:

- The Milandre aquifer is of modest size. Larger karst systems are frequent all over the world.
- The discharge ratio (Q_{max}/Q_{min}) is comparable to other "well karstified" aquifer.
- The epikarst dynamic storage is important for a karst system of reduced catchment area.
- The mineralisation variations (specific conductance, SpC_{max}/SpC_{min}) are modest.

Strong hydraulic responses are due to the well-developed and organised conduit network, and a limited extension of the phreatic zone. Modest chemical variations are due to the absence of point source recharge and limited amount of fresh infiltrated water participating to floods (soil and epikarst buffer).

Milandre aquifer is typically a shallow karst system as represented in figure 4, model 2. Other types of systems discharging at karst springs are deep phreatic systems (model 1, figure 4), and allogenic fed systems (model 3, figure 4).

In model 3 (allogenic karst systems), spring chemographs are strongly influenced by the contribution of allogenic streams during flood events (Vervier 1990, Groves 1992, Wicks 1997, Wicks and Engeln 1997). Such systems should be characterised by elevated specific conductance ratio (e.g. Verneau system) and discharge ratio, as well as by low dynamic storage. They are clearly different to the shallow karst system configuration of Milandre.

Table 1: Saivu spring characteristics compared to other karst systems studied in details. The response time is $1/\alpha$, with α equal to the exhaustion coefficient. The dynamic storage is obtained by the recession curve analysis of the hydrograph (Stor.=Q_0/α). The data are taken from White (1988), Tripet (1973), Mangin (1975), Bakalowicz (1979), Plagnes (2000), Bonacci (2001), Tissot and Tresse (1978), Smart (1988), Grasso (1999), Sauter (1992).

Spring	Country	Basin area [km²]	Q_{max} [m³/s]	Q_{min} [m³/s]	Q_{max}/Q_{min} [m³/s]	Response time [days]	Dyn. storage [m³]	S_pC_{max} [µS/cm]	S_pC_{min} [µS/cm]	S_pC_{max}/S_pC_{min}
Verneau	France	13.9	8	0.01	800.0	135.1	170'000	400	250	1.60
Areuse	Switz.	130	50	0.4	125.0	38.5	4'150'000	370	230	1.61
Baget	France	13.2	9	0.1	90.0	333.3	1'800'000	350	250	1.40
Lison	France	104.5	40	0.5	80.0	62.5	4'000'000	400	300	1.33
Espérelle	France	99	23.5	0.35	67.1	156.3	4'580'000	506	403	1.26
Saivu	**Switz.**	**13**	**2**	**0.04**	**50.0**	**400.0**	**1'838'500**	**610**	**530**	**1.15**
Maligne	Canada	730	45	1	45.0	-	2'280'000	-	-	-
Durzon	France	117	38.3	1.02	37.5	250.0	24'658'000	456	412	1.11
Gallusqu.	Germany	45	2.5	0.08	31.3	550	7'000'000	580	520	1.12
Vaucluse	France	1115	100	3.7	27.0	-	80'000'000	400	250	1.60
Cernon	France	16.5	4.3	0.16	26.9	270.3	5'730'000	453	394	1.15
Ras-el-Ain	Syria		40	33	1.2	2070.0	-	-	-	-

The following discussion focuses on the differences and similitudes between models 1 and 2.

a) The unsaturated zone (including soil and epikarst)

In both configurations, the unsaturated zone is comparable. Brandt and Grand Bochat sites are located in the subsurface of a model 1 karst system (Areuse aquifer). Observed hydraulic and solutes responses are comparable to that of the unsaturated zone at Milandre (chapter 2.6). All these sites belong to the same geographical and climatic area. In another environment (e.g. alpine or Mediterranean climates), soils may be absent and the epikarst may present a different structure. The role of the soil and the epikarst will surely be different in such geographical contexts.

b) The phreatic zone

During flood events, fresh water should recharge the Low Permeability Volumes (LPV) because of the hydraulic gradient inversion between conduits and LPV. This inversion will stop the contribution of phreatic storage to spring discharge (Kiraly 1998). This can be true for models 1 and 2. Hence groundwater participating to flood events is mainly issued from the reservoirs of the unsaturated zone.

Under steady-state conditions, models of type 1 (deep phreatic systems) assume an important role to the storage in the phreatic zone. This storage is in the LPV (Drogue 1971, Kiraly 1975), or in annex-to-drains systems (ADS, Mangin 1975). These models are based on observations at the spring and in piezometers. However the actual contribution of phreatic storage to spring flow was never clearly demonstrated. At Milandre site, Jeannin (1998) suggests also an important contribution of water from the LPV at low water stage. From our observations, it is not necessary to consider a contribution from the LPV and we conclude that the fluxes from the LPV, although present, seem to be limited, at least in shallow karst systems.

This may also be true for deep phreatic systems: observed water fluxes in the unsaturated zone (vertical caves) may be sufficient to sustain base flow discharge. This was suggested by Lastennet and Mudry (1997) for the N-D-des Anges karst system. Moreover speleological observations in the unsaturated zone prove the reality of flow in this sub-system even at base flow conditions (Gunn 1983, Klimchouk 2000, Jeannin 1990, Perrin 1997).

The dynamic storage (i.e. the volume of water stored in the phreatic zone above the spring elevation) in models 1 and 2 is of comparable water volume. Hence hydraulically, the role of storage in the phreatic zone can be similar for both models.

For transport parameters, the situation is different. Model 1 presents an important volume of water stored below the spring elevation, which is absent in model 2. This volume can play a direct role on solute transport by mixing. This role was already illustrated by Vaute et al. 1997, or Martin and Dean 2001.

More detailed investigations are necessary for testing the actual significance of the phreatic zone in both flow and transport in deep phreatic configuration systems. Numerical modelling seems the most promising method. Long-term tracing experiments with injection into the LPV would be another method, but they are difficult to carry out. Water budgets in the unsaturated zone and at the end of system (i.e. the spring) would be another way, but they may be not accurate enough in order to quantify the actual fluxes from the LPV.

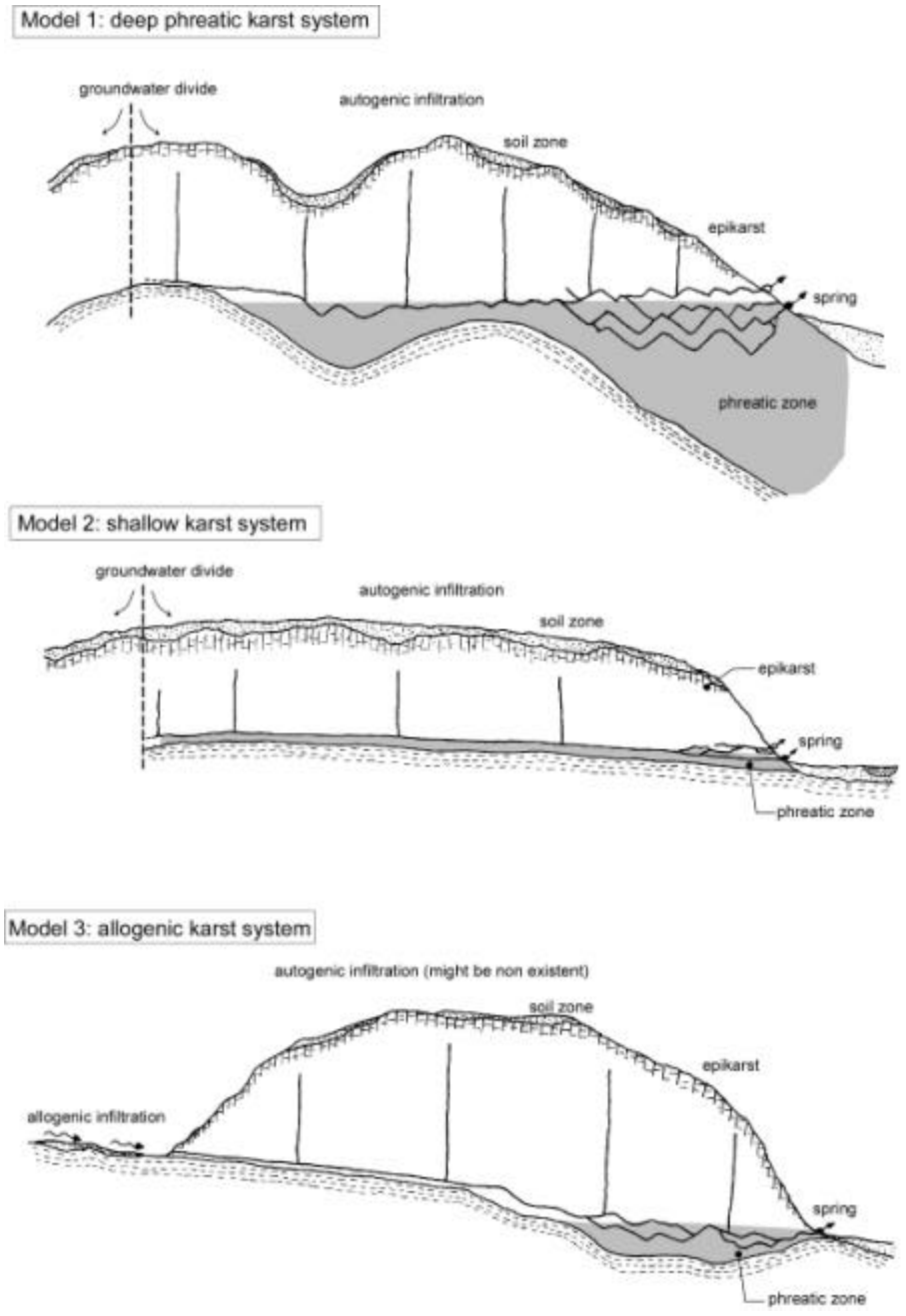

Figure 4: Schematic representation of the three main geometrical models of karst systems discharging at springs. Milandre site is typically a shallow karst system, model 2.

3.4. Practical issues of the model

3.4.1. Vulnerability assessment of karst aquifers

The protective role of the soil and epikarst sub-systems has been clearly demonstrated (chapters 2.6 and 2.7). Their storage function reduces drastically flow velocity and concentrations of contaminants. The presence of organic matter and clays minerals limits the mobility of certain contaminants. This protective role was already integrated in existing vulnerability assessment methods: the EPIK method (Doerfliger et al. 1999), the PI method (Daly et al. 2002), the VULK method (Brouyère et al. 2001, Jeannin et al. 2001). Hence removal of soil and epikarst (e.g. by quarrying) will suppress an important storage element of the system and could be harmful to groundwater quality and quantity.

The system dilution effect, derived from horizontal mixing, has important consequences on the contaminant concentrations at the spring. Pristine water tributaries will efficiently dilute a contaminated tributary. The larger the spring catchment area, the more the system dilution will be efficient. This effect has been integrated in the VULK model (Jeannin et al. 2001, Brouyère et al. 2001).

These existing vulnerability assessment methods aim at defining an intrinsic vulnerability spatially. The main drawback is that the contamination intensity of a spring (or the resource) is strongly dependant on the pollution scenario (chapter 2.7). It appears therefore difficult to end up with a similar vulnerability map if the main risk is a point source contaminant (e.g. hydrocarbons spillage), or a diffuse contaminant (e.g. nitrate).

The numerical models of the soil (chapter 2.4), the epikarst (chapter 2.4), and mixing in the phreatic zone (chapter 2.5) offer the opportunity to better quantify a vulnerability assessment. A pollution scenario may be used as input in the first sub-system of the studied aquifer (i.e. the soil or the epikarst) and the output entered in the next sub-system. This should allow to test more accurately the respective roles of each sub-system. A similar approach has been developed with the VULK model (Jeannin et al. 2001), but the simulation is strongly simplified (only 1-D) and the parameters (hydraulic and transport) are chosen on a theoretical basis.

In chapters 2.4 and 2.6, we have seen that the flood water is issued from different sub-systems depending on the recharge height. It means that the vulnerability will change with increasing recharges. Generally the vulnerability is worse with important recharge events when polluted waters from the soil and fresh water enter the aquifer. However, if we imagine a point source contamination in the epikarst, the worst case will be small recharge events when only epikarst water participates to the flood (limited dilution of the pollutant).

3.4.2. Investigation of karst aquifers with tracers

Generalities

A combined study of hydraulics and transport of a karst aquifer can lead to general but useful information on the system structure and vulnerability. However, the study requires generally numerous data (discharges and several independent tracers variations on a few flood events) in order to carry out a detailed interpretation. For physico-chemical parameters and stable isotopes, the sampling frequency has to be adapted to the studied karst system, and discharge should always be measured in parallel. For well-karstified systems, the study of flood events with hourly measurements (or even less) will give the more information. Continuous measurements of discharge, specific conductance, ions like nitrate are especially suited. The main drawback of such detailed analyses is the elevated cost generated by the large amount of analyses required.

Analysis of spring hydrographs and chemographs

A combined analysis of the hydrographs and chemographs at a karst spring may lead to useful information about the karst aquifer. Figure 5 presents two different responses. The curves should be parameterized by their amplitude of variation (A), and their characteristic times (minima, maxima, recovery, duration). These parameters should be collected for flood events of increasing intensity, and for non-dependant chemical parameters (e.g. nitrate, mineralisation, stable isotopes). Then it would be possible to extract information such as:

- Presence of point recharge (high A2 as compared to A1 for mineralisation)
- Critical discharge when fresh infiltrated water participates significantly to the flood event in a diffuse recharged system (A2 for floods of increasing intensity)
- Existence of polluted tributaries (secondary peaks of a pollution related parameter as shown in the complex response, figure 5)
- Distance to the spring of the contaminated tributaries (based on the time arrival of the secondary peaks)

Main specificities of the tracers

- **Specific conductance** curves allow to separate a flood hydrograph into a pre-event component and a flood component. Care is needed in the interpretations on the origin of these waters. Pre-event water is issued from the epikarst and/or the phreatic zone, flood water from the soil zone and/or the rain. Especially a significant specific conductance decrease is an indication of point source recharge by surface streams. Evolution of the **dissolution-related parameters** in the system can be simulated with a dissolution model. Results give a rough estimate of the groundwater transit times.
- Measurements of major ions allow to investigate the horizontal mixing. The most adequate tracers are those, which are spatially heterogeneous (i.e. **pollution-related tracers**). At Milandre site, nitrate proved to be particularly adapted. The presence of undersaturated water with respect to calcite at the spring is an indicator of point source recharge by surface streams issued from non-carbonated areas.
- **Stable water isotopes** (oxygen-18, deuterium) are adequate for determining the amount of fresh water participating to the flood event. When the aquifer is at steady state, the isotope mean value gives an estimate of the mean elevation of the catchment area.
- **Artificial tracers** are efficient tools for testing flow velocities in the system. Point injection with high discharge rates will by-pass the soil and epikarst filters. Hence observed tracer velocities are representative of the unsaturated and phreatic conduits. Diffuse injection by sprinkling informs on velocities in the soil and the epikarst mainly. The sprinkling intensity should match closely natural rainfall intensities in order to obtain realistic interpretations.

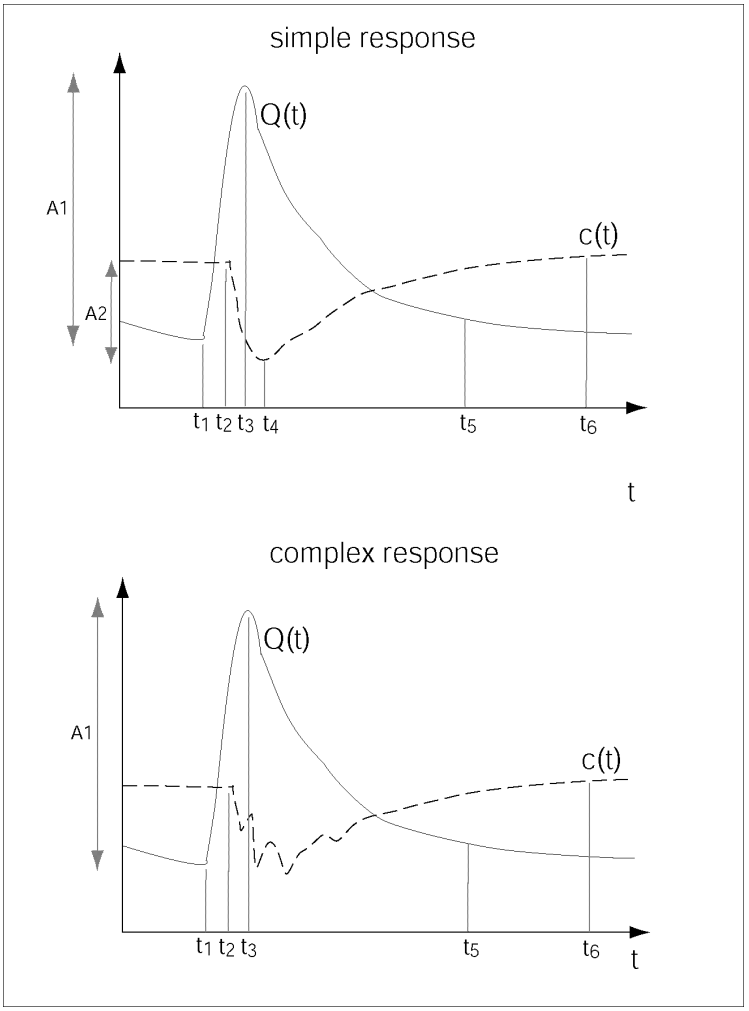

Figure 5: Two different hydrograph and chemograph theoretical responses at a karst spring.

Phreatic storage

At Milandre, phreatic storage exists (Jeannin 1998) but the water fluxes from this reservoir may be less than expected. However, natural tracers are not a well adapted tool for investigating the role of the LPV. The LPV of the phreatic zone are recharged at each flood event by water from the soil and the epikarst. Hence the waters stored in the phreatic zone and in the epikarst should have the same chemical signature, and no distinction can be made at the karst spring.

Other investigations could be made for testing the role of the LPV: in the field, water balance from the unsaturated zone could be compared to the water balance at the karst spring. By a numerical modelling, scenario with increasing LPV could be constructed. Resulting responses at the spring could then be compared to the observations.

3.5. Further work

3.5.1. Investigated sites

Numerical simulation
The presented models of the soil and the epikarst have to be improved. Soil scientists have developed several models of flow and transport for the soil zone. The more complex models account for the heterogeneities of the flow field. The epikarst should be modelled as a partly unsaturated media; its mixing properties would then be increased. The role of the LPV in the phreatic zone could be efficiently tested by numerical simulations.

Detailed field studies on the soil and the epikarst
The conceptual model of flow and transport shows the prominent role of the soil and the epikarst. These sub-systems still need to be studied in more details. Water sampling should be made in soil lysimeters and epikarst boreholes. Such data should confirm mixing processes, the presence of undersaturated water, and the effect of preferential flow paths within the soil zone. The chemical homogeneity of the epikarst reservoir would also be observed.

Use of other tracers in the field
Complementary natural tracers should allow to refine the conceptual model. Significant changes in the load and type of bacteria (coliforms, enterococci, total cultivable bacteria) were observed during a flood event at Milandre test site (Perrin et al. 2001). Such experiments should be conducted further as these “natural tracers” appear to be even more sensitive than more classical ones. It is probable that each reservoir contributing to the flood is traced by a different association of bacteria. Modern techniques of analyses such as molecular analyses on bacterial population offer interesting perspectives. The main drawback is the time-consuming analyses.

Gas natural tracers like Radon and CO_2 are of peculiar interest as they originate from the soil zone mainly. The former is radioactive (decay constant of 3.82 days), the latter is stable. Hence their respective evolution should provide insights on the contribution of the soil zone and the groundwater transit times (Savoy 2002).

Reactive tracers such as natural dissolved organic carbon (DOC) and ^{13}C labelled organic compounds are adequate to study the biodegradation in the unsaturated zone of karst systems. Little is known on the topic so far, and our test sites are well suited for such investigations. A future project at CHYN will focus on these aspects.

Sprinkling experiments with artificial tracers are adapted for testing the unsaturated zone. Inputs are well controlled and the interpretation can then be carried out in a more quantitative way. The uses of different tracers at the same time are efficient for testing the reactivity of the system.

Use of the current engineering works at Milandre test site
Pollution-related parameters should be studied further in the upstream part. A motorway under construction will soon cross part of the upstream basin. Land use will become radically different, and groundwater chemistry should account for these changes. These important civil engineering works are a great opportunity for testing the inertia of the pollution-related transport in the unsaturated zone of the system. Some tributaries (ST, CA) are polluted by agriculture, and with land use modifications one can expect an improvement of their quality.

3.5.2. Complementary sites

Detailed investigations from local to catchment scale should be carried out on other sites corresponding to deep phreatic systems and allogenic fed systems (models 1 and 3, figure 2). Many studies exist at the basin scale that interpret spring responses. However more detailed investigations, within the systems, are still lacking. Such detailed field studies are a promising way of testing conceptual models of flow and transport.

For the soil and the epikarst zone, sites with no soil (e.g. Alpine systems) and soils issued from various origins (e.g. humo-calcic soils in the Jura) should be selected. Previous studies showed that soils can lead to very different hydraulic and chemical responses. However, these data were limited to the soil zone and never extended to the basin scale. Sites in other geological environments (e.g. fissured limestone, dolomitic limestone) should allow to test the efficiency of phreatic storage.

3.6. References

Bakalowicz, M., 1979. Contribution de la géochimie des eaux à la connaissance de l'aquifère karstique, Pierre et Marie Curie, Paris, 257 pp.

Bakalowicz, M., Blavoux, B., Mangin, A., 1974. Apports du traçage isotopique naturel à la connaissance du fonctionnement d'un système karstique - teneurs en oxygène 18 de trois systèmes des Pyrénées, France. Journal of Hydrology, 23: 141-158.

Blavoux, B. and Mudry, J., 1983. Décomposition chimique des hydrogrammes du karst. Hydrogéologie-Géologie de l'Ingénieur, 4: 270-278.

Bonacci, O., 2001. Analysis of the maximum discharge of karst springs. Hydrogeology Journal 9: 328-338.

Brouyère S, Jeannin P-Y, Dassargues A, Goldscheider N, Popescu I-C, Sauter M, Vadillo I, Zwahlen F., 2001. Evaluation and validation of vulnerability concepts using a physically based approach. In: F. Zwahlen and J. Mudry (Editor), 7th Conference on Limestone Hydrology and Fissured Media. Univ. de Franche-Comté, mém. hors-série n°13, Besançon: 67-72.

Clark, I., and Fritz, P., 1997. Environmental isotopes in hydrogeology. CRC Press, Lewis publ., 328 pp.

Daly D, Dassargues A, Drew D, Dunne S, Goldscheider N, Neale S, Popescu I-C, Zwahlen F., 2002. Main concepts of the "European approach" to karst-groundwater-vulnerability assessment and mapping. Hydrogeology Journal, 10: 340-345.

Doerfliger, N., Jeannin, P.-Y., Zwahlen, F., 1999. Water vulnerability assessment in karst environments: a new method of defining protection areas using a multi-attribute approach and GIS tools (EPIK method). Environmental Geology, 39(2): 165-176.

Drogue, C., 1971. Coefficient d'infiltration ou infiltration efficace, sur les roches calcaires, Actes colloque d'hydrologie en pays calcaire, Besançon : 121-131.

Flühler, H., Durner, W., Flury, M. 1996. Lateral solute mixing processes – A key for understanding field-scale transport of water and solutes. Geoderma, 70: 165-183.

Grasso, D.A., 1999. Interprétation des réponses hydrauliques et chimiques des sources karstiques., PhD thesis, Neuchâtel, 135 pp.

Grasso, D.A., Jeannin, P-Y. 2002. A global experimental approach of karst springs'hydrographs and chemographs. Groundwater, 40 (6): 608-618.

Grasso, D.A., Jeannin, P-Y., Zwahlen, F. 2003. A deterministic approach to the coupled analysis of karst spring hydrographs and chemographs. Journal of Hydrology, 271: 65-76.

Groves, C.G., 1992. Geochemical and kinetic evolution of a karst flow system: Laurel creek, West Virginia. Groundwater, 30(2): 186-191.

Gunn, J., 1983. Point recharge of limestone aquifers - a model from New Zealand karst. Journal of Hydrology, 61: 19-29.

Hess, J.W. and White, W.B., 1988. Storm response of the karstic carbonate aquifer of south central Kentucky. Journal of Hydrology, 99: 235-252.

Jeannin, P.-Y., 1998. Structure et comportement hydraulique des aquifères karstiques, PhD thesis, Neuchâtel, 237 pp.

Jeannin, P-Y., 1990: Températures dans la zone vadose du karst. Bull. d'Hydrogéologie, Neuchâtel, 9: 89-102.

Jeannin, P-Y, Cornaton, F, Zwahlen, F, Perrochet, P., 2001. VULK: a tool for intrinsic vulnerability assessment and validation. In: F. Zwahlen and J. Mudry (Editors), 7th Conference on Limestone Hydrology and Fissured Media. Univ. de Franche-Comté, mem. hors série 13, Besançon: 185-188.

Kiraly, L., 1975. Rapport sur l'état actuel des connaissances dans le domaine des caractères physiques des roches karstiques. In: A. Burger and L. Dubertet (Editors), Hydrogeology of karstic terrains. International Union of Geological Sciences: 53-67.

Kiraly, L., 1998. Modelling karst aquifers by the combined discrete channel and continuum approach. Bulletin d'Hydrogéologie, 16: 77-98.

Kiraly, L., Mueller, I., 1979. Hétérogénéité de la perméabilité et de l'alimentation dans le karst : effet sur la variation du chimisme des sources karstiques. Bulletin du Centre d'Hydrogéologie, 3: 237-285.

Klimchouk, A.B., 2000. The formation of Epikarst and Its role in Vadose Speleogenesis. In: A.B. Klimchouk, D.C. Ford, A.N. Palmer and W. Dreybrodt (Editors), Speleogenesis. Evolution of Karst Aquifers. National Speleological Society, pp. 91-99.

Ladouche, B., Probst, A., Viville, D., Idir, S., Baqué, D., Loubet, M., Probst, J.-L., Bariac, T., 2001. Hydrograph separation using isotopic, chemical and hydrological approaches (Strengbach catchment, France). Journal of Hydrology, 242: 255-274.

Lastennet, R. 1994. Rôle de la zone non saturée dans le fonctionnement d'un aquifère karstique. Approche par l'étude physico-chimique et isotopique du signal d'entrée et des exutoires du massif du Ventoux (Vaucluse), Avignon.

Lastennet, R. and Mudry, J., 1997. Role of karstification and rainfall in the behavior of a heterogeneous karst system. Environmental Geology, 32(2): 114-123.

Mangin, A., 1975. Contribution à l'étude hydrodynamique des aquifères karstiques. Thèse Univ. Dijon. Annales de spéléologie, 29/3: 283-332, 29/4: 495-601, 30/1: 21-124.

Martin, J.B. and Dean, R.W., 2001. Exchange of water between conduits and matrix in the Floridan aquifer. Chemical Geology, 179: 145-165.

Maloszewski, P., Stichler, W., Zuber, A., Rank, D., 2002. Identifying the flow systems in a karstic-fissured-porous aquifer, Scheealpe, Austria, by modelling of environmental 18O and 3H isotopes. Journal of Hydrology, 256: 48-59.

Perrin, J., 1997. Géologie et géochimie des eaux dans le réseau du Grand Cor. In: P.-Y. Jeannin (Editor), 6th Conference on limestone hydrology and fissured media., La Chaux-de-Fonds, pp. 99-102.

Perrin J., Tomasi N., Aragno M., Rossi P., 2001. Evolution of inorganic (nitrates) and faecal bacterial contaminants in the water of a karstic aquifer, Milandre test site (Swiss Jura). Proceedings of the 7th conference on Limestone Hydrology and Fissured Media, Besançon: 273-276.

Plagnes, V., 2000. Structure et fonctionnement des aquifères karstiques. Caractérisation par la géochimie des eaux. Documents du BRGM, 294. BRGM, 352 pp.

Plagnes, V. and Bakalowicz, M., 2001. May it propose a unique interpretation for karstic spring chemographs? In: J. Mudry and F. Zwahlen (Editors), 7th Conference on Limestone Hydrology and Fissured Media. Franche-Comté University, Besançon: 293-298.

Sauter, M., 1992. Quantification and forecasting of regional groundwater flow and transport in a karst aquifer (Gallusquelle, SW Germany), Tübingen, Tübingen, 151 pp.

Savoy, L., 2002. Caractérisation du temps de transit et du stockage de l'eau dans l'eau de la zone non saturée des systèmes karstiques. Utilisation des gaz du sol (radon, CO_2) comme traceurs naturels. Unpublished MSc. Thesis, Neuchâtel University.

Smart, C.C., 1988. Quantitative tracing of the Maligne karst system, Alberta, Canada. Journal of Hydrology, 98: 185-204.

Smart, P.L. and Friederich, H., 1986. Water movement and storage in the unsaturated zone of a maturely karstified carbonate aquifer, Mendip Hills, England. In: D. National Water Well Association, Ohio. (Editor), Proc. Conf. env. problems of karst terrains and their solutions, pp. 59-87.

Shuster, E.T. and White, W.B., 1971. Seasonal fluctuations in the chemistry of limestone springs: A possible means for characterizing carbonate aquifers. Journal of Hydrology, 14: 93-128.

Stichler, W., Trimborn, P., Maloszewski, P., Rank, D., Papesch, W., Reichert, B., 1997. Isotopic investigations. In: Acta carsologica XXXVI/1: Karst hydrogeological investigations in south-western Slovenia, Ljubljana, pp. 213-235.

Ternan, J.L., 1972. Comments on the use of a calcium hardness variability index in the study of carbonate aquifers; with references to the central Pennines, England. Journal of Hydrology, 16: 317-321.

Tissot, G. and Tresse, P., 1978. Etude des systèmes karstiques du Lison et du Verneau, région de Nant-sous-St-Anne (France). PhD thesis, Besançon University, 134 pp.

Vaute, L., Drogue, C., Garrelly, L. and Ghelfenstein, M., 1997. Relations between the structure of storage and the transport of chemical compounds in karstic aquifers. Journal of Hydrology, 199: 221-238.

Tripet, J-P. 1973 : Etude hydrogéologique du bassin versant de la source de l'Areuse. Matér. Géol. Suisse, Sér. hydrol., 183 pp.

Vervier, P., 1990. Hydrochemical characterization of the water dynamics of a karstic system. Journal of Hydrology, 121: 103-117.

Vogel, T., Gerke, H.H., Zhang, R., van Genuchten, M.T. 2000. Modeling flow and transport in a two-dimensional dual-permeability system with spatially variable hydraulic properties. Journal of Hydrology, 238 (1-2): 78-89.

White, W.B., 1988. Geomorphology and hydrology of karst terrains. Oxford University Press, Oxford, 464 pp.

Wicks, C.M., 1997. Origins of Groundwater in a Fluviokarst Basin: Bonne Femme Basin in Central Missouri, USA. Hydrogeology Journal 5(3): 89-96.

Wicks, C.M. and Engeln, J.F., 1997. Geochemical evolution of a karst stream in Devils Icebox Cave, Missouri, USA. Journal of Hydrology, 198: 30-41.

Williams, P.W., 1983. The role of the subcutaneous zone in karst hydrology. Journal of Hydrology, 61: 45-67.

Williams, P.W., 1985. Subcutaneous hydrology and the development of doline and cockpit karst. Zeit. Geomorph. NF., 29: 463-482.

4. Appendices

Appendix 1: discharge rating curves
- Appendix 1a: Bure tributary (BU)
- Appendix 1b: EN tributary
- Appendix 1c: SO tributary
- Appendix 1d: Milandrine upstream (AM)
- Appendix 1e: FA tributary
- Appendix 1f: Saivu spring (SAI)
- Appendix 1g: RO tributary

Appendix 2: pH and bicarbonate reproducibility tests

Appendix 3: Major ions analyses
- Appendix 3a: monthly samples (data on the web site: www.unine.ch)
- Appendix 3b: October 2000 flood event (data on the web site)
- Appendix 3c: January 2001 flood event (data on the web site)
- Appendix 3d: June 2001 flood event (data on the web site)
- Appendix 3e: monthly samples in the upstream part (3 years)

Appendix 4: Stable isotopes analyses
- Appendix 4a: monthly samples (data on the web site)
- Appendix 4b: October 2000 flood event (data on the web site)
- Appendix 4c: January 2001 flood event (data on the web site)
- Appendix 4d: June 2001 flood event (data on the web site)
- Appendix 4e: weekly samples in the rain and at the spring (2 years), (data on the web site)

Appendix 5: Isotope duplicates and correlation oxygen-deuterium

Appendix 6: Calibration curves of specific conductance continuous measurements
- Appendix 1a: Bure tributary (BU)
- Appendix 1b: EN tributary
- Appendix 1c: EC tributary
- Appendix 1d: Milandrine upstream (AM)

Appendix 7: Measurements of pCO_2 in soils and in Milandre cave

Appendix 8: Continuous measurements of nitrate

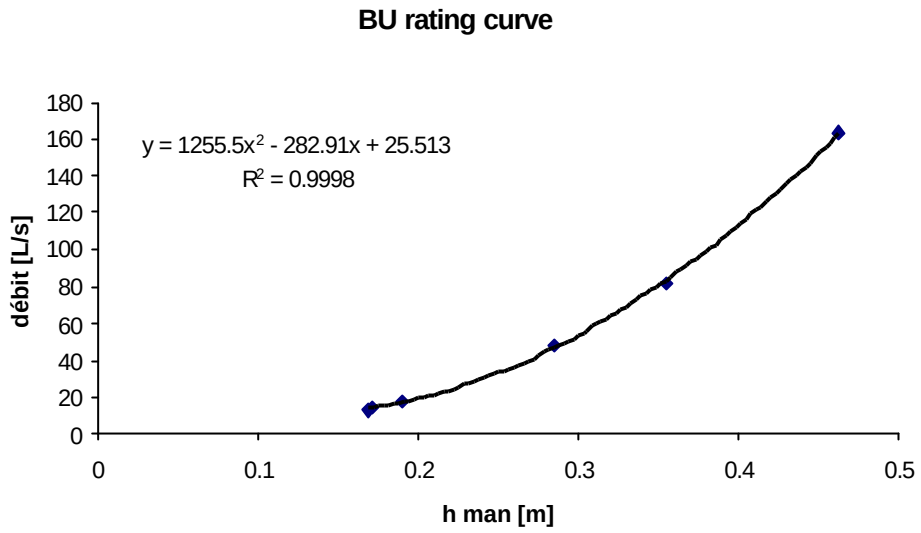

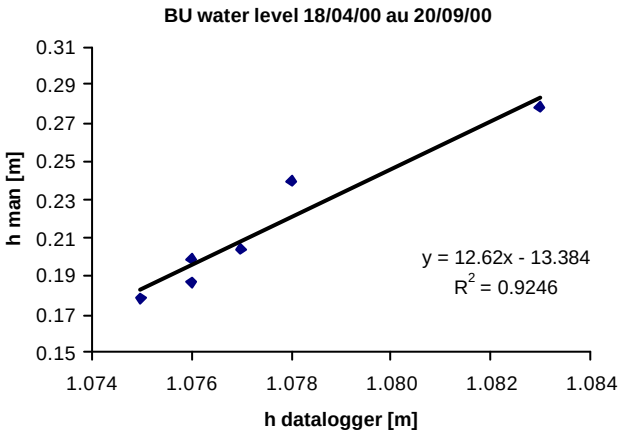

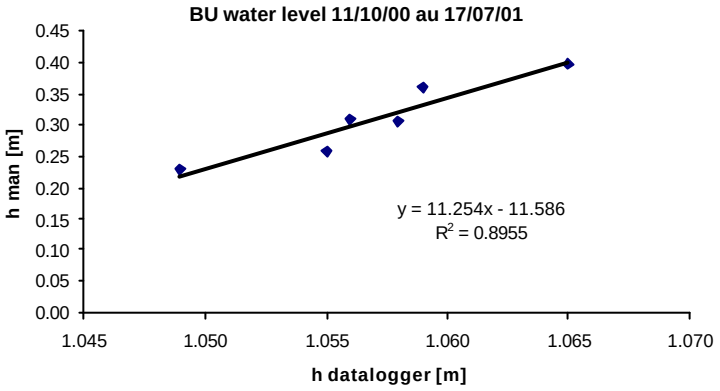

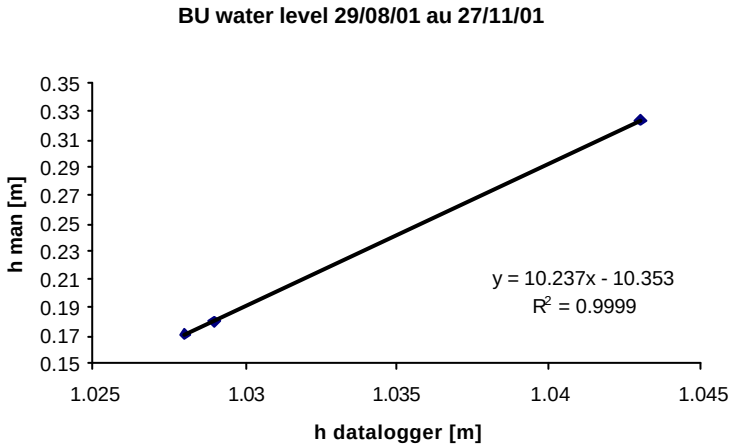

Appendix 1a: Bure tributary discharge rating curve

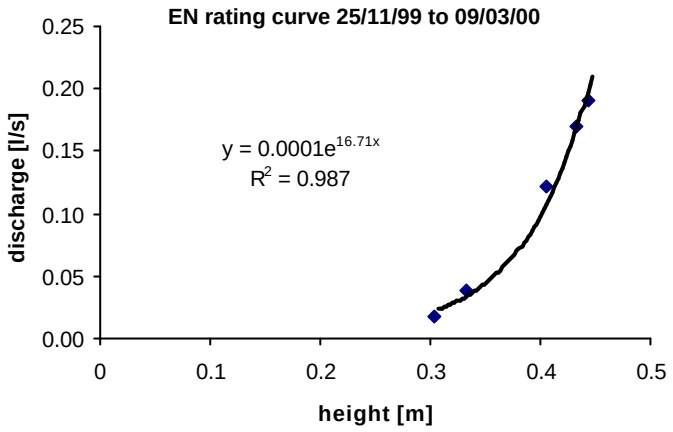

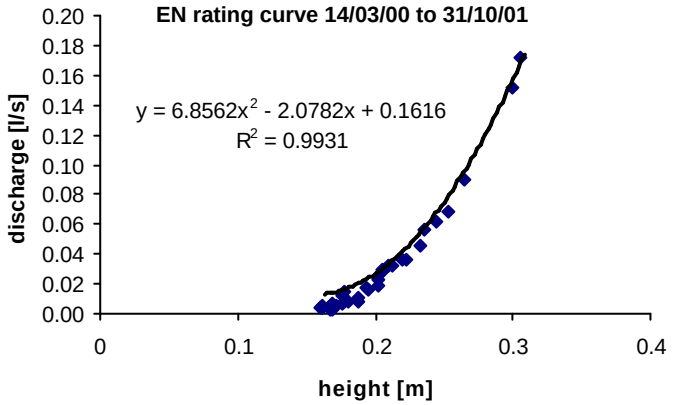

Appendix 1b: EN percolation water discharge rating curves

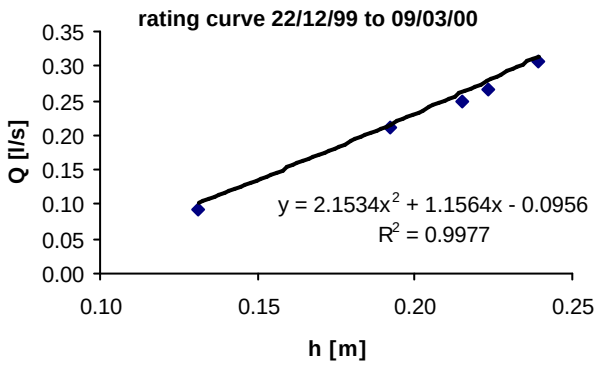

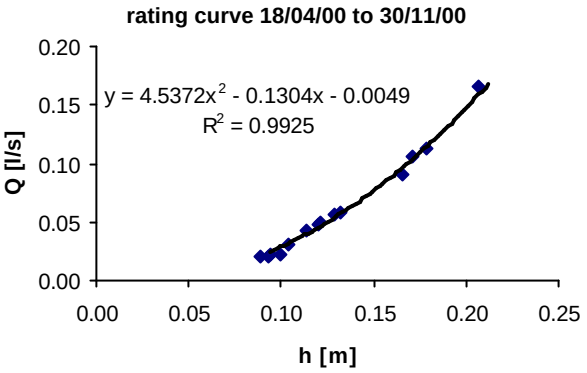

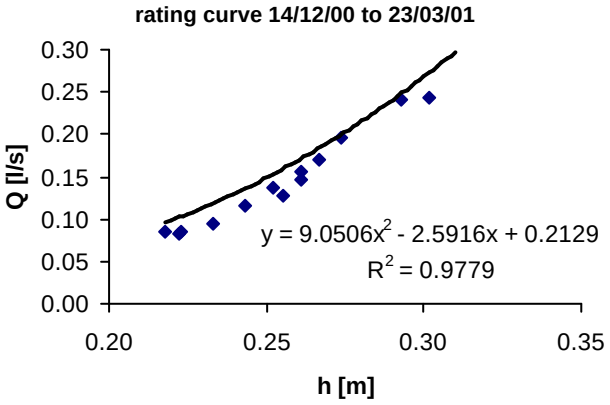

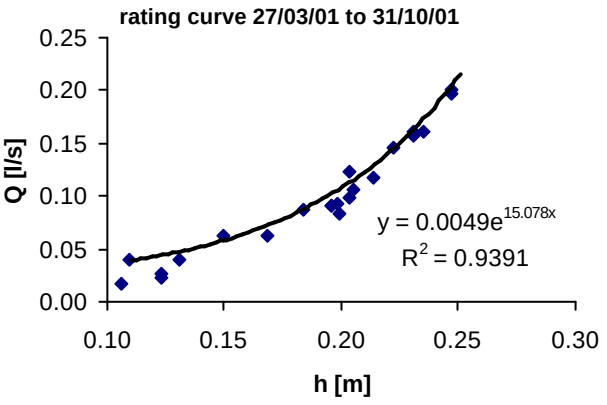

Appendix 1c : SO tributary discharge rating curves

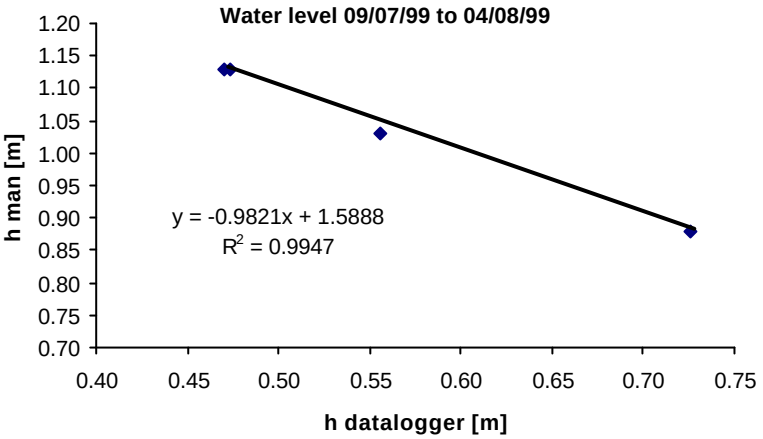

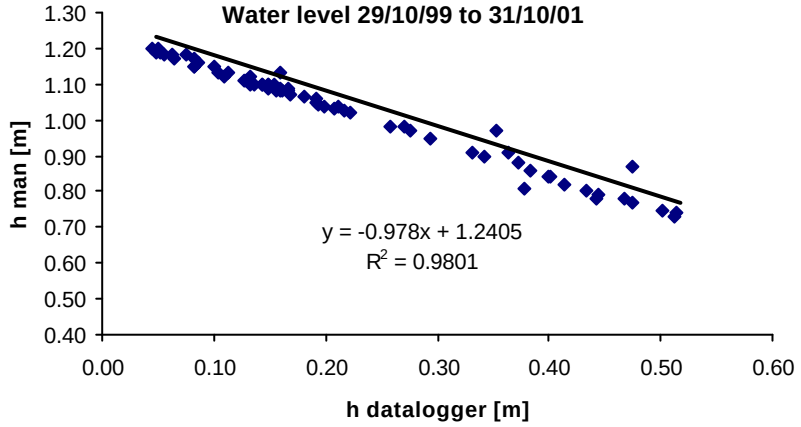

Appendix 1d : Milandrine upstream (AM) water level correlation. The used discharge rating curve is that of MFR-Geology SA : Q=1993.4-3747.1*h+2337.3*h^2-486.94*h^3

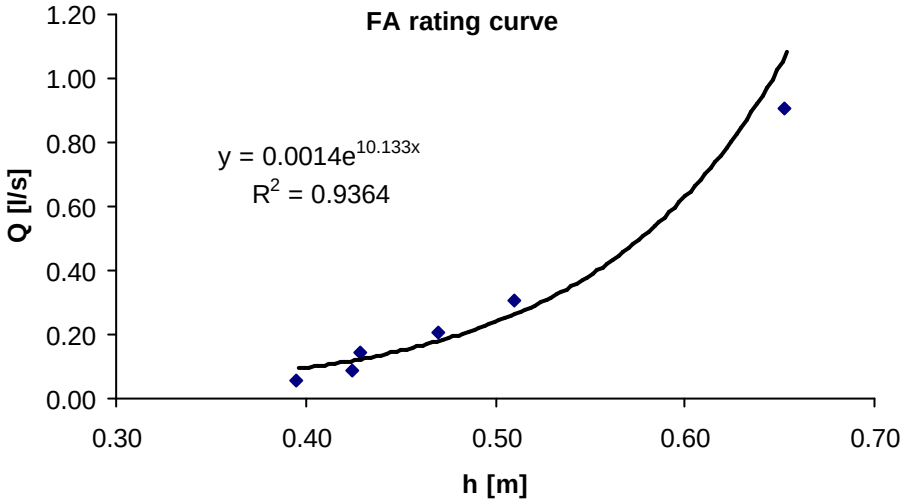

Appendix 1e : FA tributary discharge rating curve

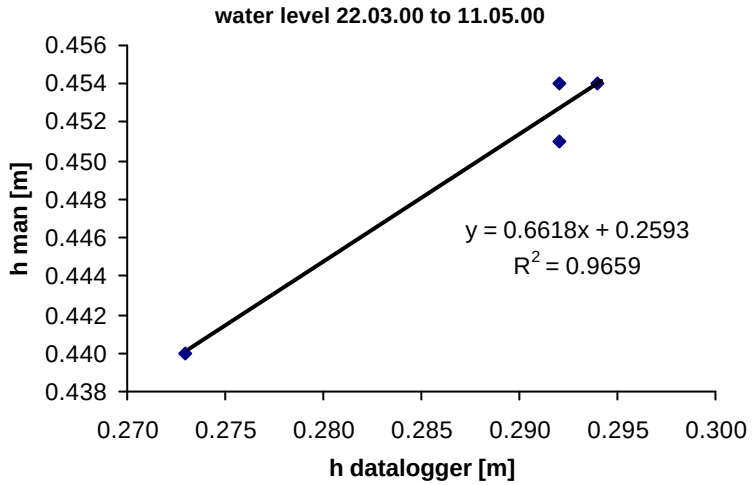

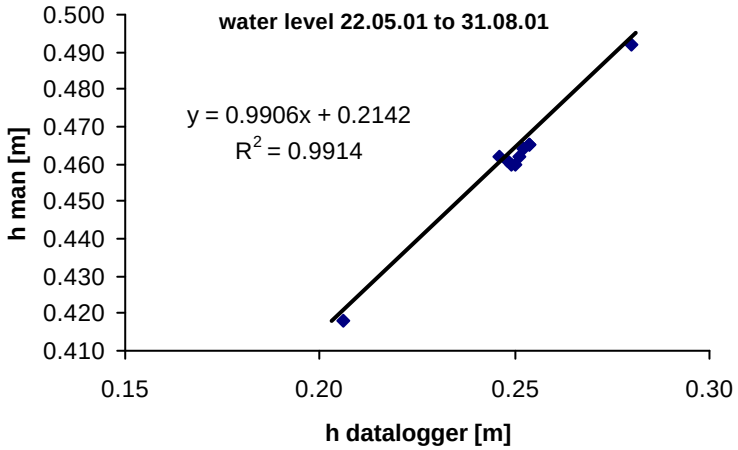

Appendix 1f : Saivu spring (SAI) water levels correlation. The used discharge rating curve is that of MFR-Geology SA . Q=284.9-2306.5*h+5046.4*h^2-2070*h^3

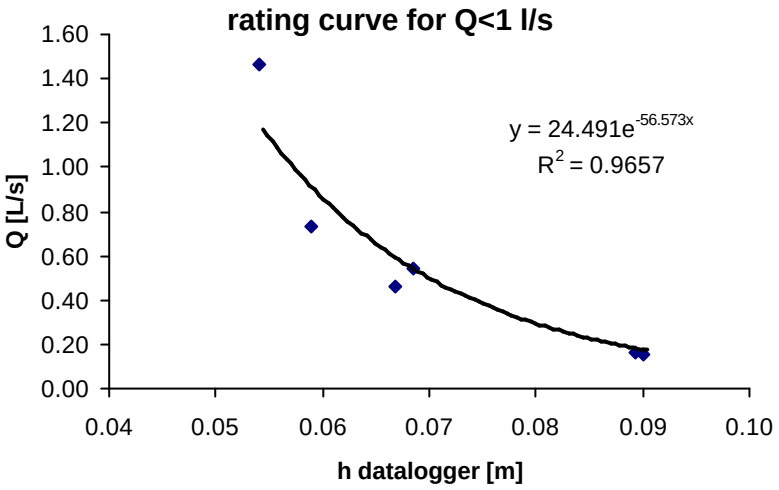

Appendix 1g : Source rouge (RO) tributary discharge rating curve. For Q> 1 l/s the following relationship has been used : Q = -30.376.h + 2.7233

Table 1: **pH** tests. Δt is the elapsed time between sampling and measurement. T changes means that the temperature of the sample was voluntary changed during the experiment. Syringe means that sampled water was stored in the piston of a 100 ml syringe. In bold, values that are in the tolerance limits. It signifies that samples have to be kept at sampling temperature in sealed bottles without air for less than 19 hours. Chosen maximum storage time was 12 hours.

Δt	sampled water	sealed without air	sealed with air	open	syringe
0 (tap water)	7.89				
18h30				8.18	7.98
0 (tap water)	7.83				
12h00				8.40	7.94
0 (tap water)	**7.97**				
19h00		**7.96**	8.04		7.99
19h00 (with T changes)		**7.95**	8.04		8.01
0 (Bure tributary)	7.90	7.39			
27h30					
0 (Saivu spring)	7.02				
33h00		7.14			
33h00 (with T changes)		7.26			
0 (Bame spring)	7.12				
33h00 (with T changes)		7.20			

Table 2: **bicarbonate** tests: Δt is the elapsed time between sampling and measurement. T changes means that the temperature of the sample was voluntary changed during the experiment. Syringe means that sampled water was stored in the piston of a 100 ml syringe. In bold, values that are off the accepted range of deviation. It means that samples have to be kept at sampling temperature in sealed bottles without air for less than 47 hours. Chosen maximum storage time was 24 hours.

Δt	sampled water	sealed without air	syringe
0 (tap water)	226		
18h30			229
0 (Saivu spring)	327		
33h00		326	
0 (Bame spring)	335		
33h00 (with T changes)		337	
47h00 (with T changes)		**351**	
47h00		**346**	
0 (Milandrine upstream)	329		
24h30		332	
38h30		329	

Appendix 2: Lab tests on pH values and bicarbonate concentration reproducibility

Saivu spring

Site	Date	Flow	pH	T(Wa)	Cond	Na	K	Mg	Ca	Cl	SO4	NO3	HCO3	E	TDS	Calcite_si
		[l/s]		[°C]	[µS/cm]	[mg/l]	[mg/l]	[mg/l]	[mg/l]	[mg/l]	[mg/l]	[mg/l]	[mg/l]	[%]	[mg/l]	
SAI	6/24/99 0:00		7.74	9.8	594	3.40	1.90	2.4	121	8.90	9.2	20.1	351	1.1	518	0.66
SAI	8/4/99 0:00		7.01	9.9	613	3.00	1.80	2.3	125	9.60	8.6	16.1	390	3.9	556	-0.01
SAI	9/9/99 0:00	81	7.17	9.8	618	3.30	1.40	2.4	125	9.60	8.5	20.1	359	0.7	529	0.12
SAI	10/8/99 0:00	210	7.07	9.9	640	2.95	2.10	2.3	125	9.12	9.7	26.4	384	4.7	562	0.04
SAI	11/25/99 0:00	135	7.60	9.8	630	5.72	2.23	2.7	132	16.30	9.0	24.1	355	1.4	547	0.56
SAI	12/30/99 0:00	750	7.22	9.7	580	2.73	1.61	1.8	117	9.60	9.4	20.7	337	1.8	500	0.11
SAI	1/26/00 0:00	120	7.34	9.9	600	3.71	1.10	2.1	114	10.96	9.3	18.9	334	2.2	494	0.22
SAI	3/9/00 0:00	261	7.33	9.8	578	2.07	1.15	2.1	119	7.60	9.0	19.0	340	0.8	500	0.24
SAI	4/18/00 0:00	240	7.27	9.8	576	3.25	2.16	2.1	120	10.58	11.4	21.6	329	0.3	500	0.16
SAI	5/11/00 0:00	81	7.29	9.9	579	2.34	1.38	2.5	118	8.02	8.3	16.7	356	2.4	513	0.21
SAI	6/14/00 0:00	66	7.24	10.0	598	2.95	1.70	2.3	116	12.28	12.5	29.7	342	4.8	519	0.14
SAI	7/11/00 0:00	240	7.27	10.4	574	5.62	4.75	3.1	104	11.81	10.1	23.8	310	2.2	473	0.09
SAI	10/11/00 12:00	114	7.61	10.1	605	3.72	2.22	3.1	122	10.05	8.6	18.8	364	1.7	532	0.55
SAI	11/21/00 8:30	168	7.39	10.1	636	3.01	2.06	2.7	128	9.47	9.5	26.0	357	0.3	538	0.34
SAI	12/15/00 10:50	191	7.33	9.9	616	2.86	2.01	2.6	122	8.17	8.7	21.1	360	2.0	527	0.27
SAI	1/10/01 10:00	323	7.28	10.0	606	2.85	1.78	2.2	119	8.04	9.0	22.2	350	2.2	515	0.20
SAI	2/27/01 11:30	217	7.58	10.0	601	4.99	1.90	2.7	117	11.58	8.8	20.2	338	0.7	505	0.48
SAI	3/27/01 9:30	546	7.25	9.7	572	2.72	1.66	2.0	113	5.88	9.0	16.2	338	1.8	489	0.13
SAI	5/1/01 14:40	210	7.38	9.9	582	2.57	1.37	2.1	117	5.60	8.0	14.6	342	0.1	493	0.28
SAI	5/31/01 10:00	155	7.18	10.0	588	2.62	1.02	1.9	121	6.55	9.1	17.4	343	0.2	503	0.10
SAI	6/28/01 15:00	124	7.57	9.9	555	2.95	2.17	2.5	114	7.79	8.4	17.7	301	3.6	457	0.41
SAI	7/23/01 9:15	144	7.25	10.1	607	3.02	2.07	2.3	122	8.51	9.8	20.2	354	1.2	522	0.18
SAI	8/29/01 0:00	72	7.53	10.0		2.98	1.57	2.4	128	8.69	9.1	18.6	345	2.6	516	0.47
SAI	9/27/01 0:00	167	7.40	10.0	626	2.80	1.98	2.4	123	9.05	9.5	23.1	356	1.9	528	0.34
SAI	10/31/01 0:00	105	7.10	10.2	614	2.38	2.42	2.1	124	9.39	9.6	22.8	356	1.6	529	0.05
SAI	11/27/01 0:00	500	7.64	10.0	620	3.75	2.33	3.0	123	9.42	9.0	21.5	365	1.6	537	0.58
SAI	12/20/01 11:00	105	7.92	10.0	594	2.90	1.33	2.7	136	7.38	8.6	21.5	353	4.3	533	0.88
SAI	1/31/02 14:00	155	8.01	10.0	603	3.63	1.84	2.4	121	10.96	10.2	23.2	357	3.0	530	0.93
SAI	2/27/02 14:00	815	7.38	9.9	574	3.67	2.22	2.4	115	9.51	9.6	20.5	326	0.4	488	0.26
SAI	4/10/02 14:10		7.53	10.0	580	2.67	1.14	2.4	130	6.54	8.4	17.6	338	4.7	507	0.47
SAI	5/14/02 17:00		7.30	9.9	580	2.63	1.29	2.0	123	6.89	9.3	15.5	332	2.7	492	0.21

Milandrine upstream (AM)

Site	Date	Flow	pH	T(Wa)	Cond	Na	K	Mg	Ca	Cl	SO4	NO3	HCO3	E	TDS	Calcite_si
		[l/s]		[°C]	[µS/cm]	[mg/l]	[mg/l]	[mg/l]	[mg/l]	[mg/l]	[mg/l]	[mg/l]	[mg/l]	[%]	[mg/l]	
AM	5/11/99 18:00		7.12	9.5	621	3.20	2.20	2.8	108	11.70	12.2	18.2	346	6.1	504	-0.01
AM	5/27/99 14:00		7.08	9.5	612	2.70	1.50	2.8	110	11.00	10.5	19.4	354	6.4	512	-0.03
AM	6/24/99 18:30		7.12	9.6	622	4.10	2.70	3.0	124	10.90	9.0	24.5	359	1.2	537	0.06
AM	8/4/99 19:30	177	6.97	9.6	525	3.20	2.30	2.9	126	11.30	8.0	18.7	381	2.6	553	-0.06
AM	9/9/99 16:50	26	7.07	9.8	640	3.10	1.70	3.0	129	11.00	7.6	18.2	359	1.2	533	0.03
AM	10/8/99 19:00	59	7.11	10.7	625	3.20	2.00	2.5	126	8.40	8.3	20.8	377	2.2	548	0.09
AM	11/25/99 12:54	59	7.09	9.8	645	5.15	2.45	2.6	126	16.30	8.7	26.7	362	2.2	550	0.04
AM	12/30/99 22:30	170	7.27	9.4	567	4.21	1.79	2.1	118	12.40	9.2	25.1	322	0.2	495	0.14
AM	1/26/00 19:00	40	7.37	10.2	602	3.99	1.42	2.3	120	14.13	8.5	23.9	344	2.2	518	0.29
AM	3/9/00 18:30	81	7.30	9.6	611	2.68	1.44	2.5	119	10.30	9.4	26.1	348	3.0	519	0.21
AM	4/18/00 12:00	72	7.07	9.7	599	3.72	2.55	1.7	125	10.36	9.0	22.5	339	1.2	514	-0.01
AM	5/11/00 16:30	27	7.30	10.2	608	2.98	1.78	3.0	120	10.46	7.7	22.3	356	2.2	525	0.23
AM	6/14/00 17:30	22	7.12	9.9	636	4.21	2.94	1.8	123	12.94	9.2	28.5	350	2.3	533	0.05
AM	7/11/00 18:20	32	7.19	9.8	645	6.76	5.53	3.6	112	15.52	11.5	33.3	326	2.6	514	0.05
AM	10/11/00 9:30	38	7.06	10.0	651	4.31	3.41	3.6	129	12.47	8.1	17.2	387	1.2	565	0.05
AM	11/21/00 18:00	56	7.14	9.8	657	3.38	2.12	3.0	133	10.71	9.6	29.5	365	0.2	556	0.11
AM	12/15/00 10:50	64	7.31	10.0	635	3.18	2.01	2.9	125	9.92	8.7	26.3	366	2.3	544	0.26
AM	1/10/01 12:00	108	7.13	9.8	630	3.13	1.85	2.6	124	9.91	9.2	27.4	359	2.2	537	0.07
AM	2/27/01 11:30	72	7.13	9.9	625	4.55	2.05	3.2	124	12.19	9.3	25.4	348	0.4	528	0.06
AM	3/27/01 10:30	182	7.18	9.5	586	3.19	2.09	3.8	115	7.56	9.1	21.2	332	0.0	494	0.06
AM	5/1/01 12:30	70	7.40	9.9	610	2.98	1.80	2.7	131	8.35	9.3	20.3	353	2.7	529	0.36
AM	5/31/01 13:10	52	7.11	10.0	610	3.01	1.56	2.8	123	8.53	8.2	22.4	362	1.7	531	0.06
AM	6/28/01 14:00	41	7.50	9.7	614	3.40	3.24	3.6	123	10.99	11.1	25.8	348	0.6	529	0.42
AM	7/23/01 10:15	48	7.52	10.0	631	3.36	2.63	3.0	124	10.44	9.7	21.2	362	1.3	537	0.46
AM	8/29/01 0:00	24	7.34	10.0		3.71	2.16	3.1	131	11.15	8.4	22.3	342	3.6	523	0.28
AM	9/27/01 0:00	56	7.31	10.0	649	3.08	2.03	2.6	127	11.19	10.0	26.5	365	2.0	547	0.27
AM	10/31/01 0:00	35	7.22	10.0	643	2.93	2.14	2.7	127	10.73	9.5	27.0	367	2.1	549	0.18
AM	11/27/01 0:00	167	7.49	10.0	644	4.38	2.53	3.4	124	11.42	9.6	23.7	376	2.9	555	0.45
AM	12/20/01 14:00	35	7.31	10.0	618	3.19	1.46	3.1	138	9.09	8.1	22.9	366	3.2	552	0.30
AM	1/31/02 16:00	52	7.42	10.0	629	3.97	1.89	2.7	126	13.14	10.5	26.3	362	2.3	546	0.37
AM	2/27/02 14:00	272	7.38	9.7	597	4.63	2.54	2.5	118	12.94	10.5	23.1	338	1.6	512	0.28
AM	4/10/02 11:30		7.09	10.0	611	2.65	1.13	2.5	119	8.94	7.9	22.6	342	1.4	506	0.00
AM	5/14/02 14:00	48	7.15	9.9	606	3.38	1.88	2.7	127	10.11	9.0	22.0	325	4.3	501	0.06

EC percolation water

Site	Date	Flow	pH	T(Wa)	Cond	Na	K	Mg	Ca	Cl	SO4	NO3	HCO3	E	TDS	Calcite_si
		[l/s]		[°C]	[µS/cm]	[mg/l]	[mg/l]	[mg/l]	[mg/l]	[mg/l]	[mg/l]	[mg/l]	[mg/l]	[%]	[mg/l]	
EC	11/21/00 18:20	0.00078	7.14	9.9	570	22.52	0.25	0.7	104	15.83	5.4	18.7	337	1.8	504	-0.01
EC	12/15/00 10:50	0.00063	8.21	9.1	294	16.91	0.31	0.3	43	7.75	5.4	18.0	160	6.3	251	0.39
EC	1/10/01 12:00	0.00130	7.10	9.7	587	22.54	0.39	0.7	105	6.85	4.8	18.9	355	1.7	514	-0.03
EC	2/27/01 11:30	0.00045	7.25	9.5	581	23.57	0.36	0.7	101	7.27	5.2	21.0	337	0.8	496	0.08
EC	3/27/01 10:15	0.00108	7.24	9.6	556	26.04	0.38	0.6	98	4.66	4.9	20.5	288	6.2	443	0.00
EC	5/1/01 12:30	0.00055	7.60	10.0	495	18.51	0.47	0.6	64	4.40	5.1	16.9	214	0.0	323	0.08
EC	5/31/01 14:50	0.00037	7.24	9.9	433	23.36	0.35	0.5	75	4.59	5.0	18.8	260	0.4	389	-0.14
EC	6/28/01 14:20	0.00078	7.89	10.0	327	16.00	0.32	0.3	55	4.09	5.1	17.1	189	2.6	287	0.26
EC	7/23/01 10:00	0.00047	7.11	10.1	479	19.74	0.34	0.5	89	4.88	4.9	18.4	295	0.7	433	-0.15
EC	8/29/01 0:00	0.00008	7.23	10.0		21.07	0.31	0.5	88	5.87	5.4	18.1	304	2.2	444	-0.02
EC	9/27/01 0:00	0.00072	7.25	10.0		20.56	0.31	0.5	80	4.99	4.6	16.7	285	2.8	414	-0.06
EC	10/31/01 0:00	0.00037	7.36	10.0	362	16.95	0.30	0.3	58	4.05	5.4	17.3	201	2.6	304	-0.22
EC	11/27/01 0:00	0.00033	7.40	10.0	346	18.77	0.27	0.4	54	4.98	6.1	15.9				
EC	12/20/01 14:00	0.00028	7.50	10.0	502	26.72	0.23	0.5	99	3.91	5.0	14.7	325	2.7	474	0.32
EC	1/31/02 17:00	0.00058	7.46	10.0	377	22.29	0.24	0.4	58	4.07	5.3	15.0	218	2.1	324	-0.09
EC	2/27/02 14:00		7.27	10.0	426	17.92	0.31	0.5	74	2.72	3.9	11.3	260	1.2	371	-0.11

SO tributary

Site	Date	Flow	pH	T(Wa)	Cond	Na	K	Mg	Ca	Cl	SO4	NO3	HCO3	E	TDS	Calcite_si
		[l/s]		[°C]	[µS/cm]	[mg/l]	[mg/l]	[mg/l]	[mg/l]	[mg/l]	[mg/l]	[mg/l]	[mg/l]	[%]	[mg/l]	
SO	5/27/99 14:00	0.40	7.14	9.8	538	1.80	0.40	1.1	101	4.40	9.6	7.4	318	3.9	444	-0.04
SO	6/24/99 18:15	0.12	7.27	9.6	547	2.40	0.30	1.1	117	3.90	8.4	9.9	348	0.9	491	0.18
SO	8/4/99 19:30	0.05	7.11	9.6	480	2.20	0.30	1.2	122	4.10	8.2	10.3	360	0.6	508	0.05
SO	9/9/99 14:30	0.03	7.10	9.8	578	2.10	0.30	1.2	123	4.10	8.1	8.7	351	1.2	499	0.03
SO	10/8/99 19:00	0.10	7.14	10.6	560	2.00	0.30	1.1	119	3.10	7.2	8.2	383	4.1	524	0.11
SO	11/25/99 13:00	0.07	7.15	9.6	575	1.30	0.29	1.2	129	3.70	7.9	9.9	365	1.4	518	0.11
SO	12/30/99 22:30	0.27	7.27	9.4	536	1.87	0.32	0.9	118	2.80	6.9	7.5	354	0.9	492	0.19
SO	1/26/00 19:00	0.92	7.41	10.1	548	2.09	0.31	1.4	136	3.79	8.6	8.9	345	7.1	507	0.38
SO	3/9/00 18:20	0.21	7.33	9.6	553	1.74	0.40	1.2	115	2.65	7.0	5.9	344	0.1	478	0.23
SO	4/18/00 12:00	0.06	7.21	9.7	593	1.87	0.22	0.9	117	3.93	10.8	9.7	342	0.6	486	0.11
SO	5/11/00 16:30	0.05	7.23	10.1	556	1.83	0.49	1.4	115	3.47	8.1	7.6	349	1.6	486	0.14
SO	6/14/00 17:30	0.03	7.25	9.8	563	2.14	0.32	1.4	114	4.71	11.6	10.5	345	2.3	490	0.15
SO	7/11/00 18:20	0.02	7.29	9.8	568	1.85	0.32	1.3	108	3.34	7.6	7.6	346	4.0	477	0.17
SO	10/11/00 12:00	0.02	7.08	9.9	560	2.11	0.00	1.2	118	2.89	6.7	7.8	348	0.4	487	0.00
SO	11/21/00 18:00	0.11	7.11	9.8	564	1.88	0.01	1.0	116	2.41	6.8	7.2	356	1.9	491	0.03
SO	12/15/00 10:50	0.13	7.41	9.8	561	2.01	0.31	1.1	118	2.27	6.9	6.6	370	2.4	507	0.35
SO	1/10/01 12:00	0.24	7.15	9.8	561	1.96	0.30	1.0	117	2.01	6.7	6.5	360	1.5	495	0.08
SO	2/27/01 11:30	0.09	7.32	9.9	563	2.22	0.34	1.2	119	2.89	7.8	7.6	355	0.5	496	0.25
SO	3/27/01 11:50	0.16	7.27	9.7	552	2.17	0.33	1.1	116	1.98	7.4	5.0	355	1.1	489	0.19
SO	5/1/01 12:30	0.15	7.40	9.9	552	1.88	0.25	1.1	120	1.99	7.3	4.7	345	1.8	482	0.32
SO	5/31/01 13:10	0.12	7.09	9.9	552	2.03	0.27	1.1	118	2.37	8.3	5.7	346	0.8	485	0.01
SO	6/28/01 14:00	0.06	7.29	9.7	560	2.18	0.33	1.2	121	2.80	8.9	6.4	354	0.8	497	0.22
SO	7/23/01 10:15	0.09	7.22	9.9	571	2.01	0.32	1.2	122	2.54	8.4	6.3	368	0.7	511	0.17
SO	8/29/01 0:00	0.03	7.26	9.9		2.04	0.27	1.2	124	2.68	8.4	6.5	337	4.1	482	0.18
SO	9/27/01 0:00	0.06	7.35	9.9	566	1.97	0.42	1.1	117	2.24	7.0	5.9	359	1.1	495	0.28
SO	10/31/01 0:00	0.04	7.33	9.9	561	1.67	0.47	0.9	118	2.00	7.7	6.1	353	0.5	489	0.25
SO	11/27/01 0:00	0.11	7.39	10.0	561	2.00	0.34	1.1	118	1.81	7.1	5.7	365	1.4	501	0.33
SO	12/20/01 14:00	0.05	7.38	10.0	551	1.94	0.12	1.1	131	1.58	7.0	5.2	361	4.0	509	0.35
SO	1/31/02 16:00	0.05	7.33	9.9	547	1.88	0.36	1.0	114	1.83	7.1	6.2	344	0.6	476	0.23
SO	2/27/02 14:00	0.21	7.30	9.8	537	1.84	0.35	0.9	114	1.56	6.8	5.8	343	0.1	475	0.20
SO	4/10/02 12:30		7.21	9.7	545	1.93	0.22	1.0	113	1.83	7.8	6.0	338	0.2	470	0.10
SO	5/14/02 14:00	0.09	7.30	9.9	544	1.99	0.25	1.1	120	1.84	7.8	6.2	334	3.0		0.21

VI percolation water

Site	Date	Flow	pH	T(Wa)	Cond	Na	K	Mg	Ca	Cl	SO4	NO3	HCO3	E	TDS	Calcite_si
		[l/s]		[°C]	[µS/cm]	[mg/l]	[mg/l]	[mg/l]	[mg/l]	[mg/l]	[mg/l]	[mg/l]	[mg/l]	[%]	[mg/l]	
VI	5/27/99 14:40	0.0012	7.22	9.8	615	3.10	0.20	2.7	112	14.30	12.7	32.3	338	6.8	515	0.10
VI	9/9/99 16:30	0.0012	7.17	10.2	556	3.40	0.20	2.4	125	13.50	11.3	37.6	329	1.1	522	0.08
VI	10/8/99 18:40	0.0012	7.12	10.8	609	3.20	0.20	2.3	121	13.30	11.2	37.7	333	3.2	522	0.04
VI	11/25/99 13:20	0.0012	7.12	10.0	627	2.41	0.27	2.6	129	13.60	11.4	41.8	332	0.6	533	0.05
VI	12/30/99 22:15	0.0013	7.24	9.6	630	3.16	0.21	2.5	129	13.90	11.7	45.5	318	0.3	524	0.14
VI	1/26/00 13:15	0.0013	7.67	10.5	572	4.72	0.39	3.0	144	13.33	11.5	43.9	318	6.6	539	0.62
VI	3/9/00 18:10	0.0014	7.44	9.7	627	2.88	0.39	2.6	120	13.30	10.9	45.0	323	3.3	519	0.32
VI	4/18/00 12:15	0.0012	7.13	9.8	629	3.21	0.16	2.0	125	14.98	13.2	52.6	317	2.8	529	0.02
VI	5/11/00 16:30	0.0009	7.34	10.5	626	2.99	0.42	2.7	122	12.44	10.7	44.6	326	2.7	521	0.25
VI	6/14/00 17:15	0.0008	7.26	10.2	622	3.28	0.25	3.6	120	12.29	10.0	43.6	326	2.3	519	0.15
VI	7/11/00 18:00	0.0008	7.24	10.0		2.90	0.25	2.5	123	12.63	10.8	42.8	323	1.8	518	0.14
VI	10/12/00 11:30		7.28	10.0	620	3.43	0.00	2.4	122	12.68	11.2	43.3	328	2.8	523	0.18
VI	11/21/00 17:30		7.06	10.0		3.43	0.00	2.5	127	12.80	11.5	44.0	332	1.4	533	-0.02
VI	12/15/00 11:10	0.0007	7.82	10.1	608	3.31	0.22	2.5	117	12.65	11.3	44.3	326	4.6	517	0.70
VI	1/10/01 13:00	0.0005	7.08	10.0	630	3.32	0.22	2.5	121	12.58	11.2	45.5	331	3.7	527	-0.02
VI	2/27/01 12:20	0.0010	7.25	9.9	628	3.63	0.24	2.7	123	12.17	11.4	44.7	321	1.3	519	0.14
VI	3/27/01 11:00		7.15	10.0	618	3.64	0.31	2.8	121	10.96	11.6	43.3	321	1.8	514	0.04
VI	5/1/01 12:50	0.0006	7.61	10.2	622	3.14	0.18	2.5	122	8.77	10.2	40.0	318	0.1	505	0.50
VI	5/31/01 13:30		7.17	9.9	620	3.40	0.31	2.5	125	1.73	5.5	42.0	323	2.4	504	0.08
VI	6/28/01 14:00		7.43	10.0	619	3.49	0.28	2.6	125	11.54	12.4	44.2	327	1.3	527	0.34
VI	7/23/01 10:15	0.0008	7.41	10.0	625	3.35	0.20	2.5	125	11.64	12.7	44.5	326	1.5	526	0.32
VI	8/29/01 0:00		7.43	10.0		3.56	0.23	2.6	128	11.76	12.6	43.6	321	0.4	524	0.34
VI	9/27/01 0:00		7.39	10.0		3.34	0.23	2.5	120	11.06	11.6	43.3	325	3.0	516	0.28
VI	10/31/01 0:00		7.42	10.0	620	2.90	0.23	2.1	124	10.91	12.8	50.7	329	3.7	533	0.33
VI	11/27/01 0:00		7.66	10.0	613	3.45	0.23	2.4	120	9.97	11.8	46.1	321	2.5	515	0.54
VI	12/20/01 14:10		7.62	10.0	612	3.56	0.03	2.6	137	9.79	11.7	45.8	327	3.1	537	0.56
VI	1/31/02 16:30		7.30	10.0	644	3.28	0.20	2.4	124	10.95	12.3	42.9	329	2.1	525	0.21
VI	2/27/02 14:00		7.20	10.0	617	3.25	0.20	2.4	124	10.87	12.4	43.1	323	1.3	519	0.10
VI	4/10/02 11:30		7.21	10.0	612	3.52	0.19	2.6	133	9.49	11.9	43.1	321	2.9	525	0.13
VI	5/14/02 14:00		7.33	10.0	617	3.49	0.19	2.6	128	10.67	12.4	39.8	316	1.8	513	0.23

EN percolation water

Site	Date	Flow	pH	T(Wa)	Cond	Na	K	Mg	Ca	Cl	SO4	NO3	HCO3	E	TDS	Calcite_si
		[l/s]		[°C]	[µS/cm]	[mg/l]	[mg/l]	[mg/l]	[mg/l]	[mg/l]	[mg/l]	[mg/l]	[mg/l]	[%]	[mg/l]	
EN	6/24/99 18:00	0.020	7.21	9.8	590	2.90	0.30	1.4	125	6.00	12.1	16.8	356	0.5	521	0.15
EN	8/4/99 19:10	0.010	7.12	9.8	501	2.50	0.20	1.5	127	6.30	10.1	20.7	372	2.2	540	0.09
EN	9/9/99 16:20	0.004	7.20	9.9	546	2.50	0.30	1.5	128	6.40	9.7	20.9	359	0.2	528	0.16
EN	10/8/99 18:30	0.011	7.16	10.5	585	2.40	0.20	1.5	122	6.30	9.6	20.5	366	3.3	529	0.12
EN	11/25/99 13:15	0.020	7.17	9.7	611	1.61	0.39	1.5	120	6.00	11.0	19.8	354	3.0	514	0.09
EN	12/30/99 22:10	0.190	7.30	9.2	575	2.38	0.25	1.4	127	5.40	11.6	16.4	362	0.3	527	0.25
EN	1/26/00 18:40	0.038	7.80	9.5	520	2.19	0.48	1.6	113	5.79	12.7	17.4	357	5.5	511	0.69
EN	3/9/00 18:00	0.122	7.44	9.5	604	2.30	0.37	1.6	122	5.51	12.3	14.1	373	3.2	532	0.39
EN	4/18/00 12:15	0.008	7.18	9.7	604	2.43	0.23	0.9	133	6.22	13.9	20.5	354	1.5	531	0.14
EN	5/11/00 16:30	0.008	7.33	9.5	591	2.17	0.41	1.6	120	4.89	10.0	14.7	362	2.3	517	0.26
EN	6/14/00 17:10	0.005	7.29	10.2	589	2.49	0.32	2.1	119	6.50	13.7	20.9	356	3.4	522	0.22
EN	7/11/00 18:00	0.003	7.43	10.0	605	2.15	0.26	1.5	121	4.94	9.4	15.8	354	1.3	509	0.36
EN	10/11/00 10:00	0.003	7.14	10.0	591	2.65	0.00	1.4	132	4.96	9.5	16.4	362	1.7	529	0.11
EN	11/21/00 17:30	0.016	7.11	9.6	587	2.30	0.00	1.3	123	3.51	8.6	12.6	353	0.6	504	0.04
EN	12/15/00 10:50	0.000	7.65	9.9	589	2.39	0.24	1.4	122	3.95	9.4	13.3	372	2.6	525	0.60
EN	1/10/01 13:00	0.090	7.27	9.6	598	2.40	0.26	1.3	122	3.84	9.9	12.2	384	4.0	536	0.23
EN	2/27/01 11:30	0.020	7.26	9.9	602	2.70	0.28	1.5	125	4.63	10.6	15.0	360	0.0	520	0.21
EN	3/27/01 11:20	0.172	7.20	9.5	600	2.61	0.31	1.4	124	3.86	12.2	11.6	360	0.2	516	0.14
EN	5/1/01 12:45	0.061	7.40	9.8	595	2.34	0.23	1.4	124	3.43	11.1	10.4	366	0.7	519	0.35
EN	5/31/01 13:30	0.057	7.24	9.9	596	2.46	0.27	1.4	126	3.92	12.8	13.2	364	0.5	524	0.20
EN	6/28/01 13:45	0.012	7.51	9.7	590	2.66	0.46	1.5	126	3.98	11.3	13.5	362	0.1	521	0.46
EN	7/23/01 10:40	0.014	7.31	10.0	591	2.35	0.25	1.4	127	3.23	10.0	9.5	371	0.1	524	0.28
EN	8/29/01 0:00	0.005	7.30	10.0		2.44	0.25	1.5	129	3.97	10.4	14.9	354	2.2	516	0.26
EN	9/27/01 0:00	0.007	7.38	9.1	601	2.42	0.23	1.6	121	4.90	10.5	21.1	353	1.9	514	0.30
EN	10/31/01 0:00	0.007	7.42	10.2	592	2.27	0.33	1.4	124	3.66	10.4	17.3	345	0.9	505	0.35
EN	11/27/01 0:00	0.008	7.79	10.0	577	2.41	0.23	1.4	119	2.93	9.3	14.8	371	3.5	521	0.73
EN	12/20/01 14:10	0.010	7.68	10.0	565	2.46	0.06	1.5	137	2.92	9.1	15.0	361	4.6	529	0.66
EN	1/31/02 16:10	0.010	7.27	9.9	576	2.29	0.22	1.4	120	3.37	9.6	17.7	346	0.6	501	0.19
EN	2/27/02 14:00	0.042	7.20	9.8	557	2.14	0.20	1.2	117	2.45	9.3	12.6	344	0.5	489	0.11
EN	4/10/02 11:40	0.010	7.41	9.9	582	2.45	0.21	1.5	131	2.82	9.3	13.4	350	4.0	511	0.37
EN	5/14/02 14:00	0.052	7.21	9.9	590	2.50	0.24	1.4	129	3.47	11.7	11.9	345	3.7	506	0.15

ST percolation water

Site	Date	Flow	pH	T(Wa)	Cond	Na	K	Mg	Ca	Cl	SO4	NO3	HCO3	E	TDS	Calcite_si
		[l/s]		[°C]	[µS/cm]	[mg/l]	[mg/l]	[mg/l]	[mg/l]	[mg/l]	[mg/l]	[mg/l]	[mg/l]	[%]	[mg/l]	
ST	5/27/99 16:15	0.0033	7.20	9.6	623	2.40	0.40	1.5	140	11.50	16.8	53.0	361	2.6	587	0.14
ST	8/4/99 18:50	0.0200	7.11	10.1	581	2.80	0.40	1.3	144	10.80	16.0	55.7	375	2.9	606	0.13
ST	9/9/99 16:00	0.0020	7.19	9.7	632	2.70	0.30	1.3	145	10.50	16.1	56.0	368	1.9	600	0.19
ST	10/8/99 18:00	0.0033	7.12	10.7	680	2.60	0.30	1.2	138	10.20	16.0	55.2	360	3.3	584	0.11
ST	11/25/99 13:50	0.0120	7.29	9.7	693	1.64	0.35	1.3	129	9.90	16.4	54.7	356	6.2	570	0.24
ST	12/30/99 21:45	0.1000	7.31	9.4	665	2.21	0.37	1.3	139	9.90	16.2	53.3	357	2.3	580	0.28
ST	1/26/00 18:15	0.0130	7.42	10.3	645	2.45	0.45	1.5	130	9.59	17.1	55.8	355	5.7	572	0.38
ST	3/9/00 17:55	0.0222	7.35	9.8	690	2.38	0.55	1.5	134	9.41	16.3	54.8	357	4.0	577	0.31
ST	4/18/00 12:30	0.0075	7.16	9.9	681	2.69	0.31	1.1	149	10.99	20.2	66.7	346	0.4	597	0.15
ST	5/11/00 16:00	0.0047	7.34	10.3	681	2.39	0.56	1.5	135	8.87	15.7	55.9	359	4.0	578	0.32
ST	6/14/00 17:00	0.0015	7.27	10.2	682	2.74	0.37	1.9	135	8.66	16.2	53.0	350	2.3	568	0.24
ST	7/11/00 17:30	0.0001	7.31	10.0		2.47	0.41	1.3	132	8.91	16.0	54.2	349	3.8	564	0.26
ST	10/11/00 16:40	0.0001	6.98	10.0	691	3.00	0.10	1.2	141	9.11	16.8	56.8	343	0.5	571	-0.05
ST	11/21/00 17:00	0.0001								9.07	17.1	55.9				
ST	12/15/00 10:50	0.0006	7.58	10.8	678	2.76	0.37	1.3	134	8.84	16.5	52.6	357	3.7	574	0.56
ST	1/10/01 13:00	0.0047	7.16	10.0	678	2.66	0.34	1.3	135	8.43	16.4	49.3	357	2.8	571	0.13
ST	2/27/01 11:30	0.0072	7.36	10.0	670	2.90	0.38	1.4	137	8.09	16.9	46.9	351	1.0	565	0.33
ST	3/27/01 11:30	0.0383	7.19	9.9	667	2.72	0.41	1.3	136	6.77	17.9	45.2	351	1.2	561	0.16
ST	5/1/01 13:00	0.0080	7.32	9.9	654	2.38	0.35	1.3	133	5.48	15.8	37.5	355	0.9	551	0.28
ST	5/31/01 13:30	0.0073	7.15	9.9	660	2.56	0.39	1.3	139	6.39	17.7	41.0	364	0.8	573	0.14
ST	6/28/01 13:00	0.0039	7.41	10.0	657	2.78	0.50	1.3	139	7.33	18.1	39.0	366	0.9	574	0.40
ST	7/23/01 11:15	0.0023	7.15	10.3	660	2.56	0.33	1.3	138	7.32	18.6	38.1	364	1.1	570	0.14
ST	8/29/01 0:00	0.0012	7.32	10.0		2.60	0.32	1.3	142	7.39	19.2	36.1	356	1.3	565	0.31
ST	9/27/01 0:00	0.0003	7.15	10.0		2.72	0.29	1.2	133	7.41	17.0	33.9	360	1.8	555	0.12
ST	10/31/01 0:00	0.0016	7.21	10.0	661	2.38	0.39	1.1	136	6.82	19.1	38.4	361	1.6	565	0.19
ST	11/27/01 0:00	0.0018	7.44	10.0	653	2.82	0.33	1.2	136	6.15	17.3	35.2	367	1.4	566	0.42
ST	12/20/01 14:30		7.69	10.0	641	2.65	0.74	2.0	151	6.29	12.4	31.5	371	4.9	578	0.71
ST	1/31/02 16:00		7.30	10.0	628	2.45	0.31	1.2	129	6.53	18.0	33.4	346	1.4	538	0.24
ST	2/27/02 14:00		7.23	10.0	626	2.44	0.31	1.2	130	6.57	18.0	34.0	349	1.4	542	0.18
ST	4/10/02 11:40		7.36	10.0	628	2.21	0.27	1.1	130	5.83	17.1	32.1	340	0.1	530	0.30
ST	5/14/02 14:00		7.29	10.0	634	2.65	0.33	1.2	137	6.59	17.6	30.0	339	2.9	534	0.25

EG tributary

Site	Date	Flow	pH	T(Wa)	Cond	Na	K	Mg	Ca	Cl	SO4	NO3	HCO3	E	TDS	Calcite_si
		[l/s]		[°C]	[µS/cm]	[mg/l]	[mg/l]	[mg/l]	[mg/l]	[mg/l]	[mg/l]	[mg/l]	[mg/l]	[%]	[mg/l]	
EG	5/11/99 17:30	1.00	7.20	9.5	646	2.10	0.70	1.7	118	9.30	14.9	24.5	361	6.1	532	0.12
EG	6/24/99 17:30	0.50	7.33	9.7	638	2.60	0.70	1.6	135	8.20	13.5	27.5	386	2.4	575	0.33
EG	8/4/99 18:35	1.00	7.18	9.6	541	2.60	2.80	1.8	134	10.60	14.3	30.0	373	1.7	569	0.16
EG	9/9/99 15:40	0.50	7.30	9.5	655	2.30	0.80	1.8	136	8.80	12.8	29.9	381	1.9	573	0.29
EG	10/8/99 17:30	1.50	7.11	10.1	648	2.40	0.80	1.7	132	8.70	12.4	31.2	384	3.8	573	0.11
EG	11/25/99 14:10	2.50	7.34	9.7	672	1.70	1.01	1.8	130	9.30	12.4	36.9	367	3.6	561	0.30
EG	12/30/99 21:30		7.28	9.4	650	2.40	0.75	1.7	137	8.80	13.0	38.9	373	2.1	576	0.27
EG	1/26/00 17:45	1.50	7.44	10.5	599	2.06	0.87	1.9	139	8.31	12.9	32.9	366	0.4	563	0.44
EG	3/9/00 17:45	0.80	7.28	9.6	653	2.19	0.74	1.8	131	8.20	13.3	33.9	366	2.4	557	0.25
EG	4/18/00 12:45	0.60	7.17	9.6	645	2.15	0.74	1.0	143	8.44	15.6	30.1	361	2.2	563	0.16
EG	5/11/00 15:30	0.80	7.46	10.5	639	1.96	0.96	1.9	130	7.04	12.5	24.0	382	3.0	560	0.45
EG	6/14/00 16:30	0.27	7.31	9.8	637	2.24	0.95	2.1	129	6.96	11.9	23.8	368	1.5	545	0.28
EG	7/11/00 17:00	0.78	7.29	9.5	662	1.96	0.96	1.8	127	7.10	12.1	21.7	368	2.1	541	0.25
EG	10/11/00 16:50	1.00	7.09	9.8	649	2.43	0.78	1.8	134	7.94	12.5	26.4	376	1.1	562	0.08
EG	11/21/00 16:50	4.00	7.11	9.5	658	2.38	0.72	1.8	135	8.33	12.6	30.0	376	1.5	567	0.10
EG	12/15/00 10:50	1.50	7.49	9.9	660	2.70	0.91	1.9	133	8.23	12.3	35.7	375	2.7	569	0.47
EG	1/10/01 13:30	5.00	7.20	9.7	665	2.65	0.78	1.9	133	8.09	12.3	36.2	364	1.4	559	0.17
EG	2/27/01 11:30	1.80	7.30	9.9	660	2.81	0.93	2.0	134	8.11	12.3	35.3	364	0.7	559	0.28
EG	3/27/01 11:50	4.20	7.19	9.7	654	2.61	0.68	1.6	133	6.27	13.5	32.5	364	1.0	554	0.16
EG	5/1/01 13:15	1.00	7.31	9.7	642	2.16	0.62	1.6	130	5.12	12.1	24.2	372	1.6	548	0.28
EG	5/31/01 13:45	0.35	7.18	9.8	642	2.32	0.66	1.6	134	6.03	13.6	28.9	368	0.6	556	0.16
EG	6/28/01 13:30		7.26	9.6	638	2.32	0.76	1.7	133	6.75	13.9	26.1	371	1.0	555	0.24
EG	7/23/01 11:00	0.80	7.40	9.9	642	2.26	0.74	1.8	135	6.82	13.6	24.9	372	0.3	557	0.39
EG	8/29/01 0:00		7.30	7.5		2.27	0.82	1.8	140	6.94	13.6	26.3	356	3.2	547	0.25
EG	9/27/01 0:00	0.60	7.29	9.7	646	2.24	0.75	1.7	130	7.05	13.0	28.1	366	1.9	549	0.25
EG	10/31/01 0:00	0.30	7.29	10.0	648	2.20	0.81	1.7	134	7.06	14.0	31.9	362	0.6	554	0.27
EG	11/27/01 0:00		7.42	10.0	652	2.32	0.83	1.8	132	6.44	12.9	30.6	377	2.5	564	0.41
EG	12/20/01 14:40	0.83	7.80	10.0	623	2.66	0.15	1.2	150	6.03	17.4	33.6	359	4.5	569	0.81
EG	1/31/02 16:40	0.80	7.32	9.9	645	2.43	0.78	1.8	132	7.67	13.0	33.9	366	2.0	557	0.29
EG	2/27/02 14:00	10.00	7.14	9.8	636	2.44	0.83	1.8	132	7.29	13.1	34.1	359	1.2	550	0.10
EG	4/10/02 11:50	0.30	7.26	9.7	643	2.52	0.84	1.9	141	5.89	12.7	30.2	370	1.8	565	0.26
EG	5/14/02 14:00	0.30	7.34	9.9	645	2.53	0.78	1.8	138	6.39	13.2	29.4	359	2.0	551	0.32

GO percolation water

Site	Date	Flow	pH	T(Wa)	Cond	Na	K	Mg	Ca	Cl	SO4	NO3	HCO3	E	TDS	Calcite_si
		[l/s]		[°C]	[µS/cm]	[mg/l]	[mg/l]	[mg/l]	[mg/l]	[mg/l]	[mg/l]	[mg/l]	[mg/l]	[%]	[mg/l]	
GO	5/27/99 16:00	0.0017	7.27	10.0	646	2.30	4.30	2.3	145	6.60	13.5	32.0	427	2.8	633	0.30
GO	8/4/99 18:30	0.0030	7.23	10.2	608	2.34	4.04	2.0	146	6.50	12.8	38.9	427	3.3	640	0.31
GO	9/9/99 15:40	0.0020	7.29	10.3	738	2.70	4.30	2.1	148	6.30	13.1	41.2	409	1.0	627	0.35
GO	10/8/99 17:30		7.10	10.6	721	2.40	4.00	2.0	146	6.10	12.7	41.7	421	3.1	636	0.18
GO	11/25/99 14:20		7.42	10.3	720	1.60	4.58	1.9	143	5.60	12.3	38.7	420	3.8	627	0.48
GO	12/30/99 21:30		7.40	9.6	702	2.51	3.83	2.0	147	5.20	11.7	37.2	409	0.8	618	0.45
GO	1/26/00 17:50	0.0300	7.48	10.5	672	2.72	4.86	2.6	156	5.35	12.2	39.5	410	2.3	633	0.57
GO	3/9/00 17:45	0.0133	7.35	9.8	730	2.31	4.57	2.3	148	4.53	10.1	37.0	420	1.1	628	0.42
GO	4/18/00 12:45	0.0033	7.17	9.9	728	2.45	4.37	1.6	152	5.94	14.6	51.5	407	1.5	640	0.24
GO	5/11/00 15:30	0.0042	7.80	10.5	728	2.34	4.33	2.3	147	5.41	12.0	44.9	418	2.5	637	0.87
GO	6/14/00 16:30	0.0033	7.27	10.4	727	2.70	4.35	1.9	146	5.22	11.5	44.1	407	1.5	624	0.33
GO	7/11/00 17:00	0.0017	7.21	10.3	750	2.42	4.31	2.3	143	5.61	12.5	46.5	406	2.9	623	0.26
GO	10/11/00 17:00	0.0008	7.15	10.0	743	2.69	3.98	2.2	153	5.97	13.1	52.0	420	2.0	652	0.23
GO	11/21/00 16:50	0.0028	7.13	10.1	741	2.71	3.57	2.2	152	5.97	13.1	49.3	410	0.9	639	0.20
GO	12/15/00 10:50	0.0083	7.66	10.1	711	2.58	3.72	2.1	134	4.76	11.6	38.7	432	7.6	629	0.70
GO	1/10/01 13:30	0.0060	7.20	10.0	723	2.77	4.04	2.2	149	4.31	11.1	37.6	423	1.3	634	0.28
GO	2/27/01 11:30	0.0067	7.37	10.0	727	2.83	4.71	2.2	148	4.69	11.6	43.8	411	1.1	629	0.43
GO	3/27/01 11:50	0.0233	7.22	9.8	725	2.76	4.81	2.1	146	3.58	11.0	40.6	411	1.1	622	0.27
GO	5/1/01 13:15	0.0050	7.30	10.2	716	2.43	4.57	2.1	146	3.11	10.3	38.3	414	1.0	620	0.36
GO	5/31/01 13:45	0.0111	7.22	10.5	722	2.54	4.54	2.1	149	3.74	11.7	44.5	420	1.8	637	0.30
GO	6/28/01 13:30		7.40	10.0	717	2.77	4.74	2.1	149	4.42	12.7	43.7	417	1.5	636	0.47
GO	7/23/01 11:15	0.0017	7.29	10.2	732	2.62	4.45	2.1	150	4.83	13.1	45.6	409	0.6	632	0.36
GO	8/29/01 0:00		7.55	10.0		2.66	4.52	2.2	156	4.82	13.6	45.5	407	1.2	636	0.62
GO	9/27/01 0:00		7.19	10.0		2.65	3.87	2.1	143	4.75	12.0	46.3	409	3.0	624	0.24
GO	10/31/01 0:00	0.0008	7.22	10.0	706	1.89	3.29	1.5	148	4.00	13.0	49.8	409	2.5	630	0.28
GO	11/27/01 0:00		7.42	10.0	717	2.73	4.20	2.1	145	3.75	11.8	45.5	418	2.9	634	0.48
GO	12/20/01 14:40	0.0026	7.76	10.0	674	2.68	4.57	2.1	153	3.33	11.5	43.0	392	3.0	612	0.81
GO	1/31/02 16:40	0.0011	7.27	10.0	713	2.61	4.02	2.0	148	4.01	12.0	41.7	343	6.7	557	0.26
GO	2/27/02 14:00	0.0200	7.22	9.8	623	3.14	1.98	1.7	128	2.32	9.0	45.9	346	1.0	538	0.16
GO	4/10/02 11:50	0.0005	7.24	10.0	705	2.53	4.50	2.0	146	3.09	12.0	40.1	403	0.2	613	0.29
GO	5/14/02 14:00	0.0050	7.30	10.0	706	2.69	4.36	2.1	151	3.63	12.0	37.7	400	1.9	614	0.36

CA percolation water

Site	Date	Flow	pH	T(Wa)	Cond	Na	K	Mg	Ca	Cl	SO4	NO3	HCO3	E	TDS	Calcite_si
		[l/s]		[°C]	[µS/cm]	[mg/l]	[mg/l]	[mg/l]	[mg/l]	[mg/l]	[mg/l]	[mg/l]	[mg/l]	[%]	[mg/l]	
CA	5/27/99 15:30	1.00	7.10	9.6	695	2.50	1.00	2.3	143	14.10	12.9	43.8	376	1.5	596	0.05
CA	6/24/99 17:00	0.70	7.15	9.7	697	3.10	1.10	2.2	144	13.30	12.7	51.0	378	2.0	605	0.16
CA	8/4/99 18:10	1.00	7.06	9.8	581	2.70	1.10	2.1	142	13.00	12.5	49.6	371	1.8	594	0.06
CA	9/9/99 15:20	0.50	7.04	9.8	702	2.70	1.10	2.2	144	13.20	12.2	49.9	362	0.2	587	0.04
CA	10/8/99 17:00	0.45	7.12	10.2	693	2.50	1.00	2.1	138	12.90	12.1	48.4	377	3.7	594	0.13
CA	11/25/99 14:40	1.00	7.14	9.7	692	1.87	1.16	2.0	138	12.40	12.9	48.3	360	2.1	576	0.12
CA	12/30/99 21:10	2.00	7.22	9.8	678	2.66	0.94	2.1	141	12.00	13.8	45.4	364	0.8	581	0.21
CA	1/26/00 17:20	0.57	7.30	9.7	544	2.17	1.19	1.8	138	11.46	13.5	47.1	367	2.7	582	0.29
CA	3/9/00 17:30	0.90	7.22	9.6	692	2.36	1.16	2.1	136	11.28	14.0	46.2	371	3.2	584	0.20
CA	4/18/00 13:15	0.50	7.08	9.8	683	2.50	1.07	1.1	137	10.10	11.0	40.1	364	1.3	567	0.06
CA	5/11/00 15:00	0.53	7.10	9.7	681	2.44	1.31	2.4	135	11.10	11.8	45.0	376	3.5	585	0.09
CA	6/14/00 16:15	0.37	7.10	10.1	678	2.73	1.17	2.1	142	11.20	11.9	43.5	364	0.2	578	0.10
CA	7/11/00 16:45	0.41	7.10	9.8	705	2.40	1.19	2.5	134	11.58	11.2	43.2	362	2.2	568	0.07
CA	10/11/00 17:00		7.08	10.0	677	2.74	0.72	2.4	139	11.65	11.4	42.8	370	1.5	580	0.08
CA	11/21/00 16:30	0.30	7.12	9.7	683	2.55	0.66	2.3	138	11.56	11.7	42.0	367	1.5	576	0.11
CA	12/15/00 10:50	0.32	7.23	10.0	666	2.60	0.95	2.3	132	10.83	12.4	39.4	381	4.6	581	0.22
CA	1/10/01 13:45	0.32	7.12	9.8	672	2.59	0.91	2.2	132	10.54	12.9	39.6	371	3.4	572	0.10
CA	2/27/01 11:30	0.52	7.26	10.0	677	2.91	1.10	2.3	137	10.02	13.1	40.6	368	1.2	576	0.25
CA	3/27/01 12:20	0.74	7.15	9.7	683	2.77	1.09	2.0	136	7.77	14.8	38.6	368	1.4	572	0.13
CA	5/1/01 13:30	0.75	7.27	9.9	672	2.49	1.15	2.1	139	6.83	12.2	32.3	375	0.1	570	0.27
CA	5/31/01 14:00	0.87	7.11	10.0	676	2.68	1.18	2.1	139	8.26	14.1	38.6	384	1.9	591	0.12
CA	6/28/01 13:15		7.40	9.8	673	2.77	1.27	2.3	141	9.46	14.0	38.1	376	0.5	584	0.40
CA	7/23/01 11:15	0.38	7.11	10.0	678	2.64	1.18	2.3	140	9.68	13.6	41.6	371	0.9	581	0.11
CA	8/29/01 0:00		7.27	10.0		2.67	1.16	2.3	144	10.09	13.7	37.1	388	0.9	598	0.30
CA	9/27/01 0:00	0.45	7.19	9.7	683	2.56	1.04	2.2	135	9.45	12.5	38.1	375	2.3	576	0.18
CA	10/31/01 0:00	0.42	7.22	10.0	671	2.11	1.04	1.8	136	9.54	13.9	43.5	368	2.6	576	0.21
CA	11/27/01 0:00		7.29	10.0	663	2.49	1.06	2.2	134	8.32	12.9	39.3	375	2.8	575	0.28
CA	12/20/01 15:00	0.50	7.41	10.0	657	2.69	1.01	2.4	153	8.20	12.7	37.4	376	3.8	593	0.45
CA	1/31/02 17:00	0.50	7.23	9.9	664	2.66	1.03	2.1	135	8.87	13.7	37.1	366	1.2	567	0.21
CA	2/27/02 14:00	0.60	7.32	9.9	661	2.51	1.03	2.1	136	8.61	14.2	37.4	366	1.0	568	0.30
CA	4/10/02 12:00	0.54	7.10	10.0	667	2.77	1.16	2.3	149	7.42	13.5	35.3	364	4.4	575	0.12
CA	5/14/02 14:00	0.46	7.22	9.9	665	2.69	1.05	2.2	140	8.25	13.7	34.6	357	2.0	560	0.20

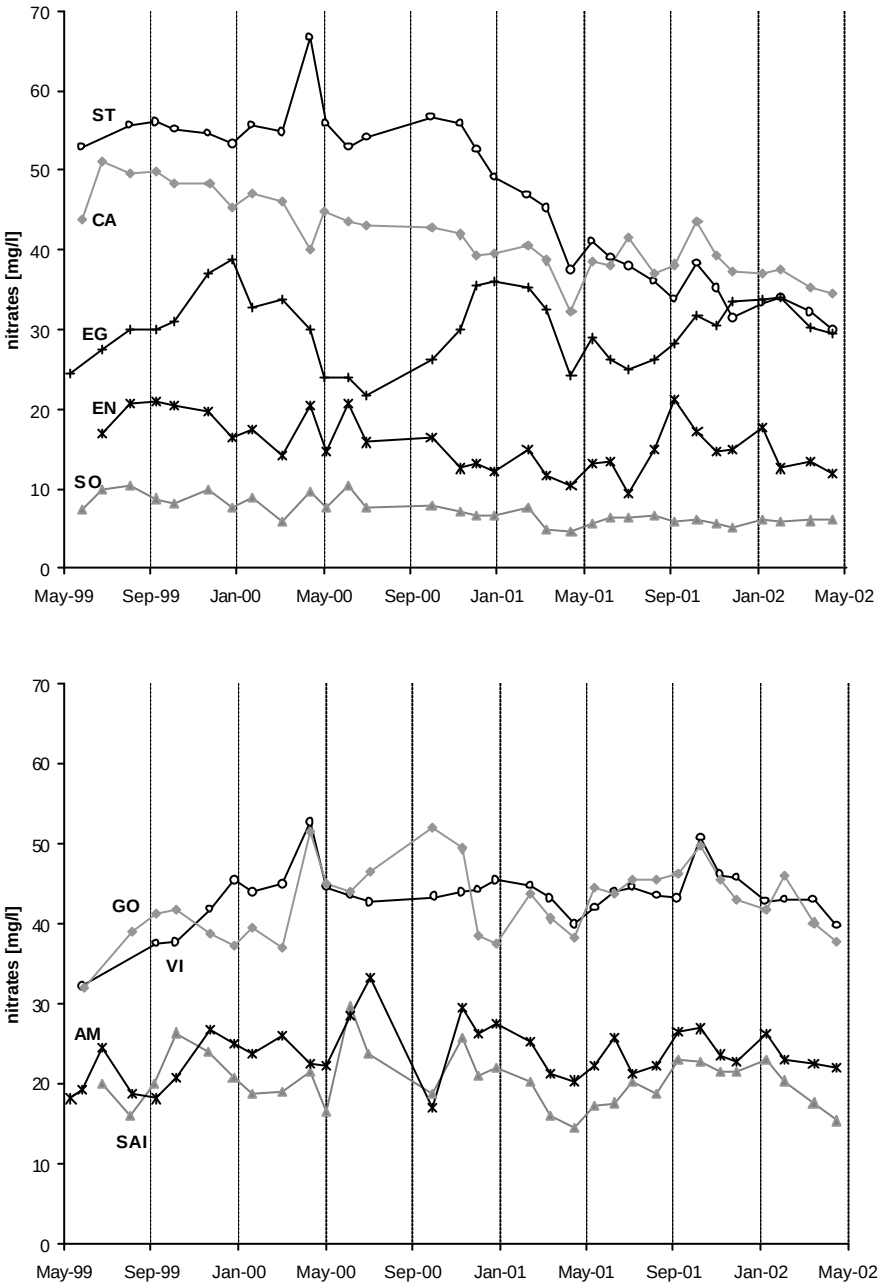

Appendix 3e : three years evolution of nitrates concentration in several tributaries at Milandre karst system. A clear decrease can be seen at ST and CA tributaries.

Appendix 5 : Oxygen and hydrogen stable isotope ratio in duplicate samples, Saivu spring.

	1st analysis	duplicate
19-Nov-99	-9.18	-9.20
	-62.70	-62.80
9-Dec-99	-9.02	-8.84
22-Mar-00	-9.21	-9.24
11-Jul-00	-8.61	-8.67
14-Jun-00	-9.00	-9.02

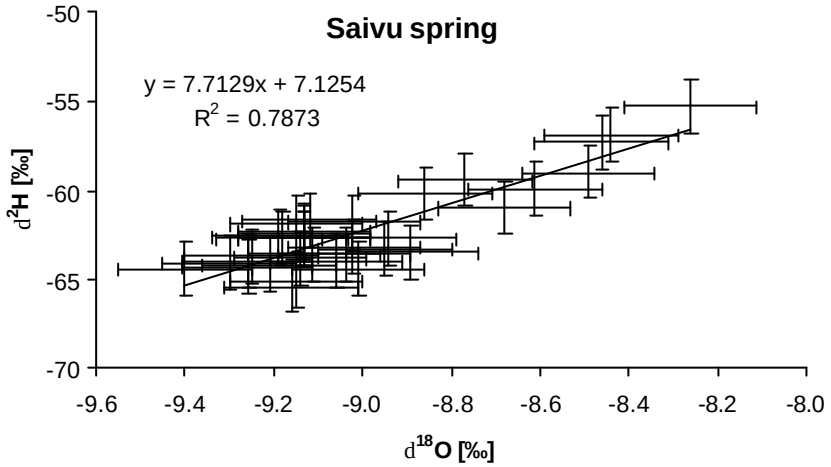

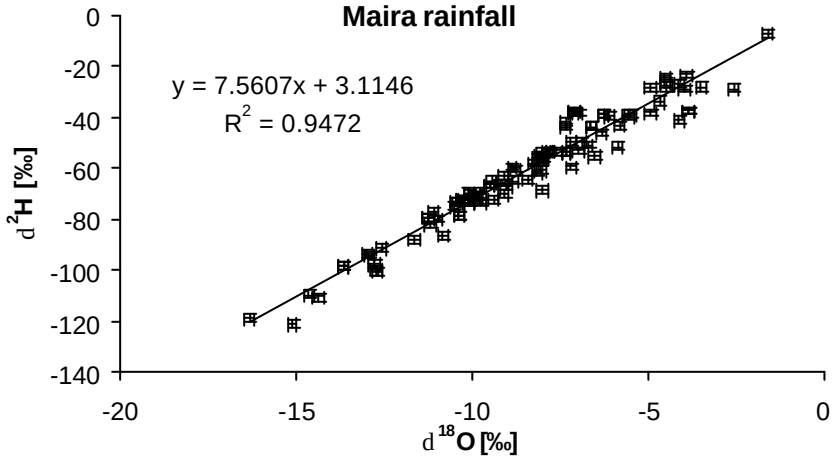

Relationship deuterium – oxygen isotopic ratio both at Saivu spring (above) and in rainfall (Maira village, below). Error bars are represented, and most of the points fall on the straight line representative of the meteoric water line for the region.

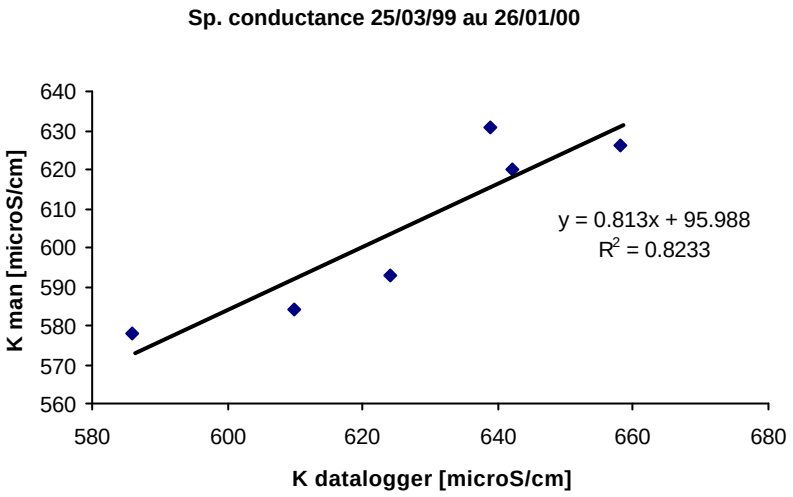

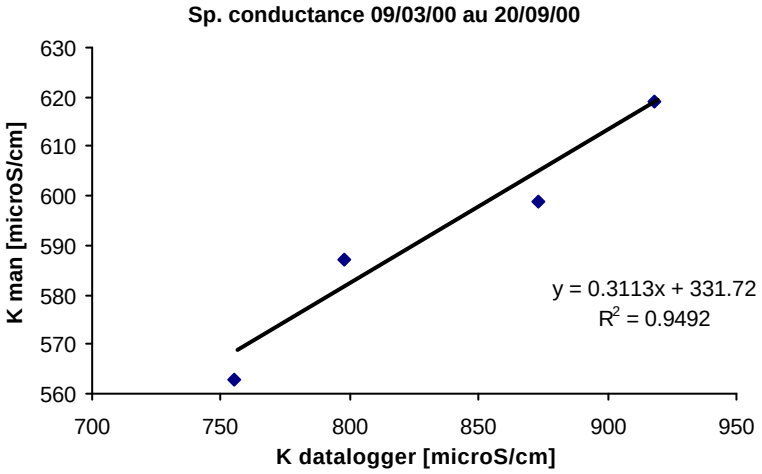

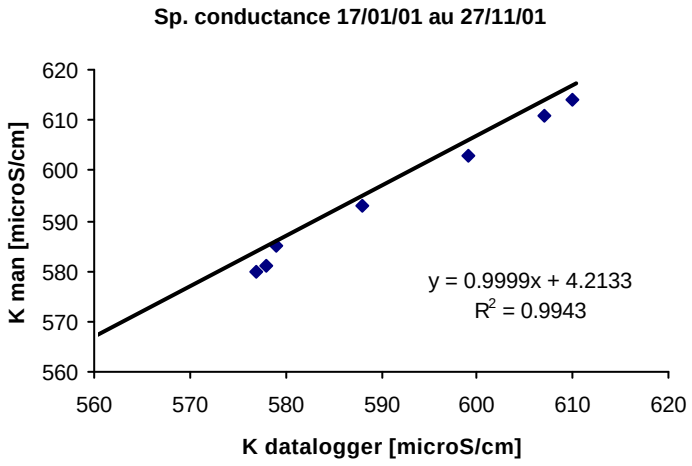

Appendix 6a: Bure tributary specific conductance calibration curves

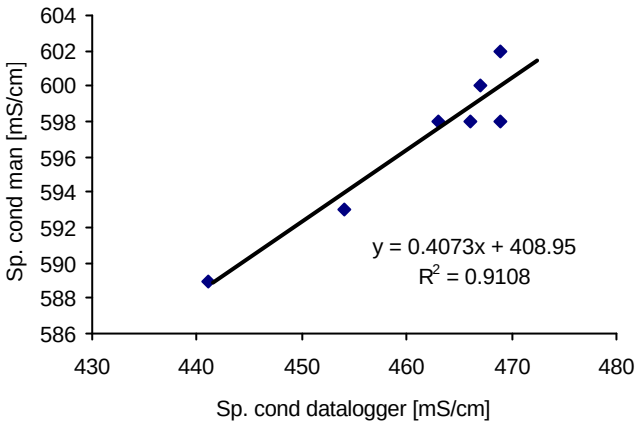

Appendix 6b : EN specific conductance calibration curve

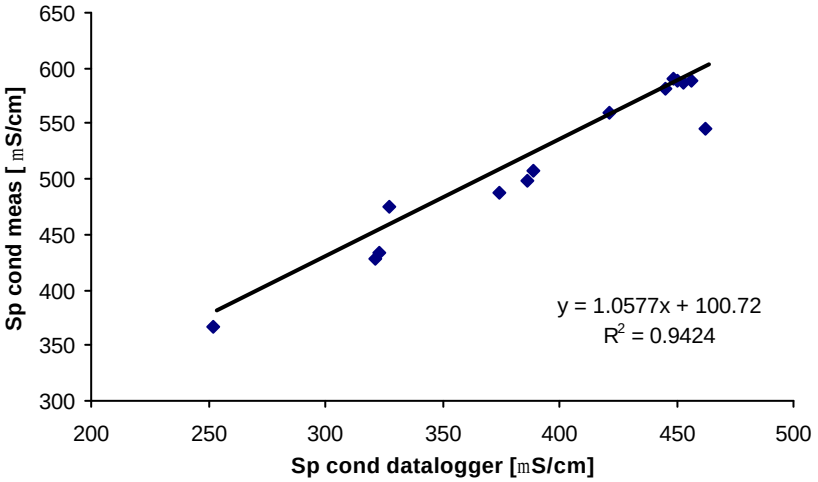

Appendix 6c : EC specific conductance calibration curve

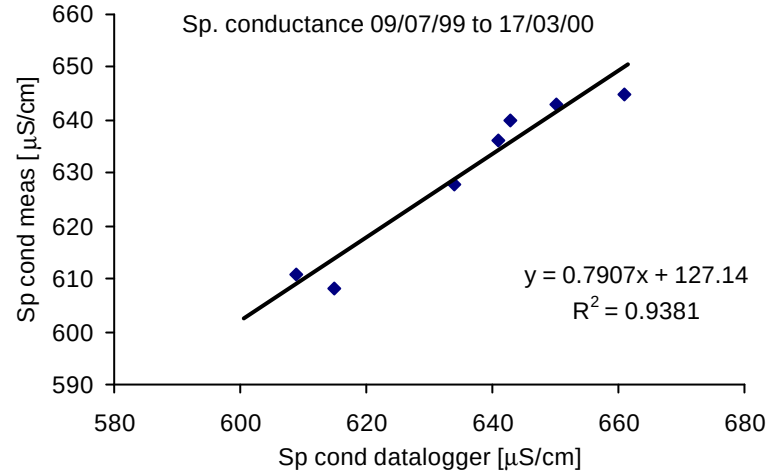

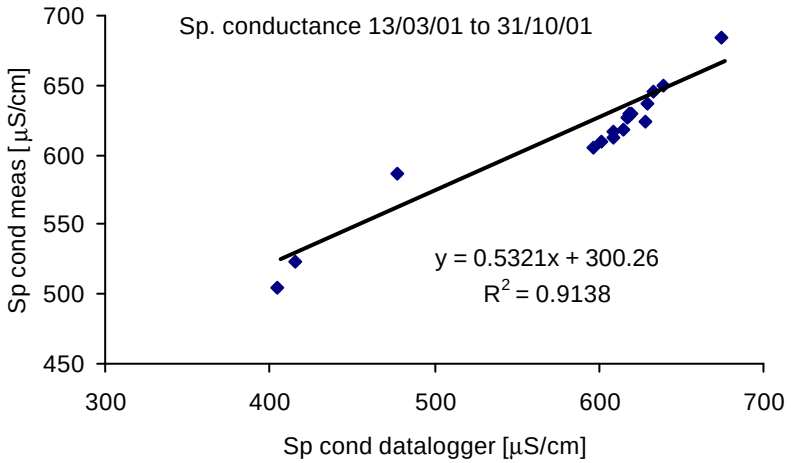

Appendix 6d : Milandrine upstream (AM) specific conductance calibration curves

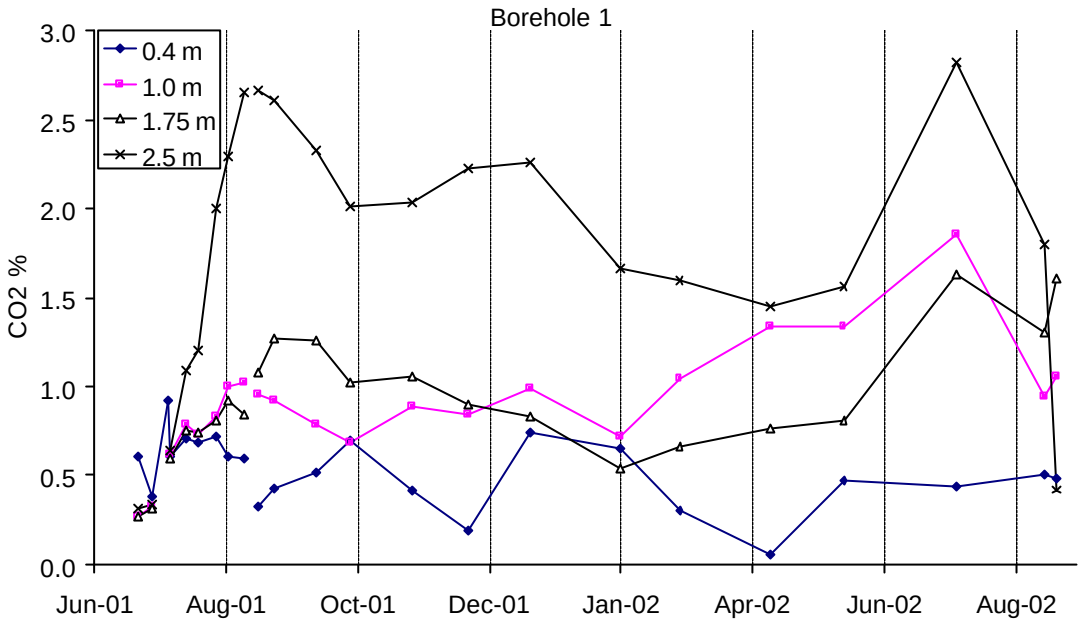

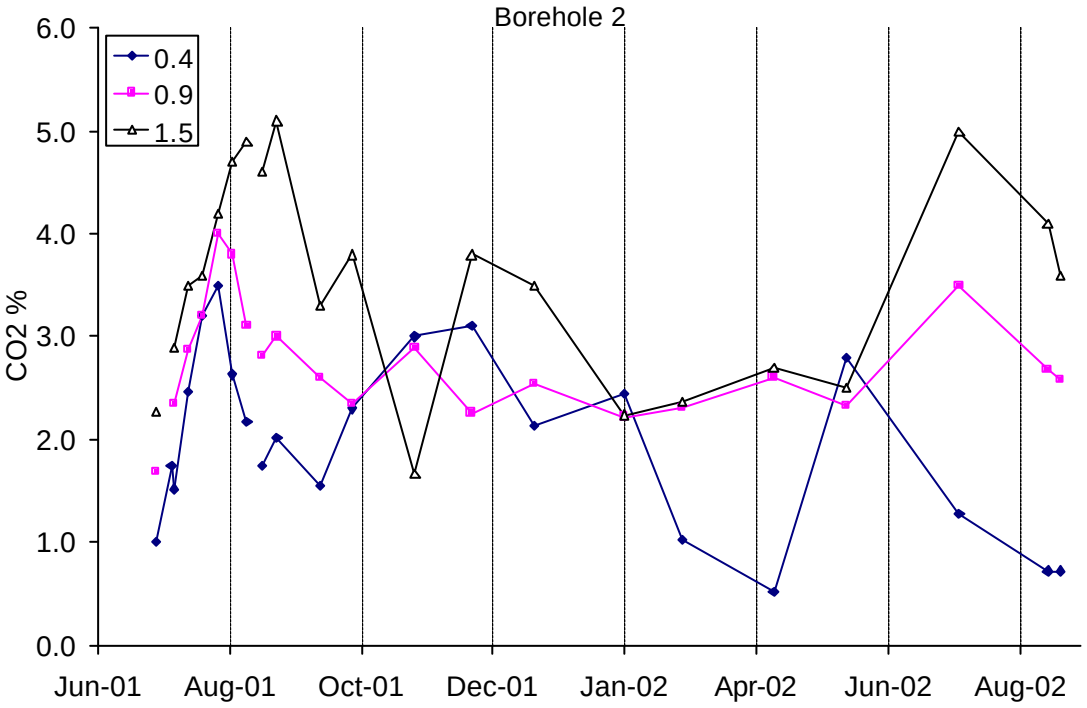

Appendix 7, page 1: soil air CO2 partial pressure, boreholes 1 and 2, Milandre test site

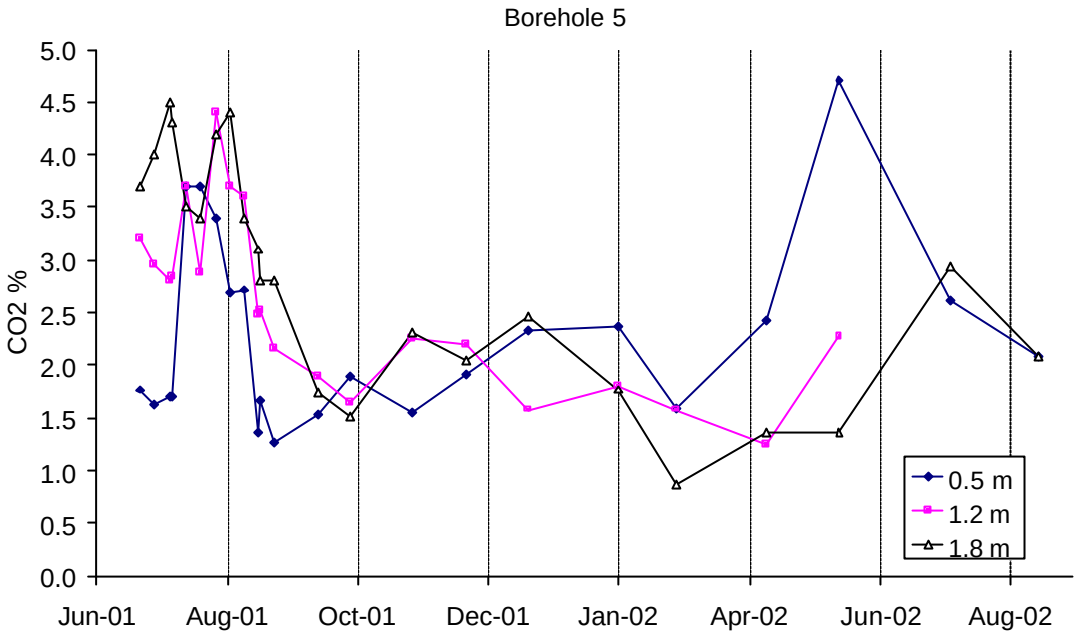

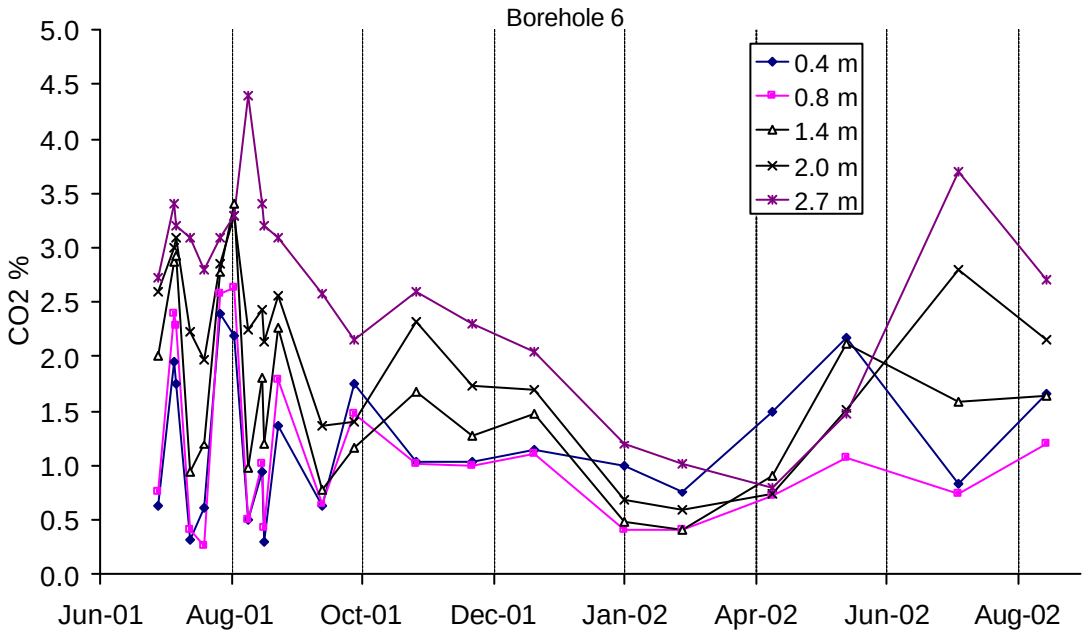

Appendix 7, page 2: soil air CO2 partial pressure, boreholes 5 and 6, Milandre test site

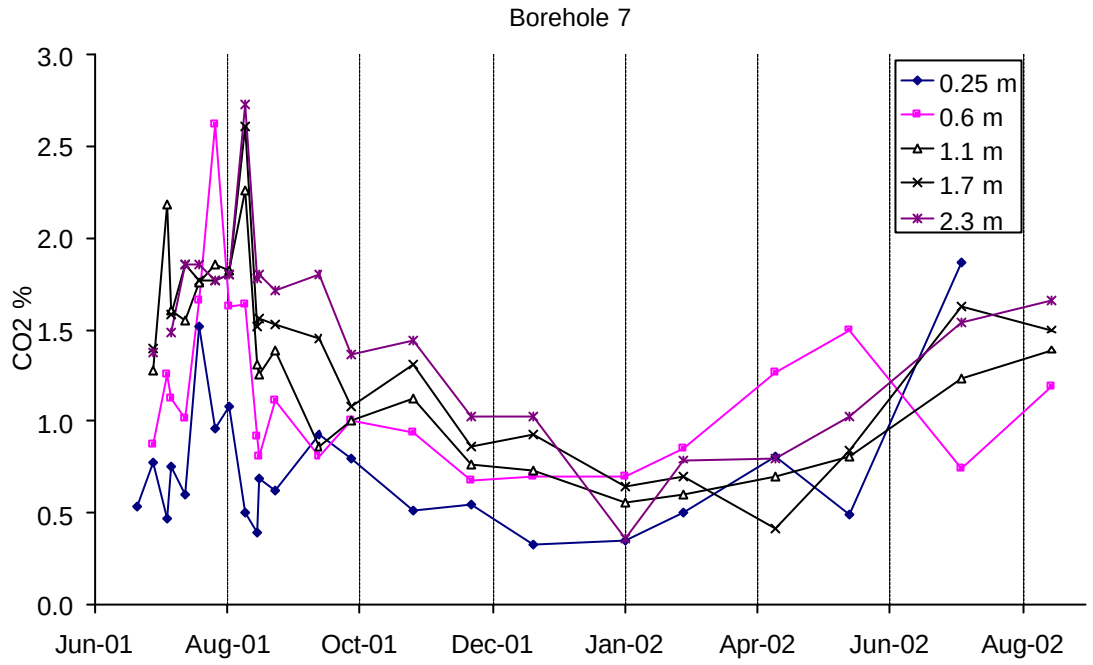

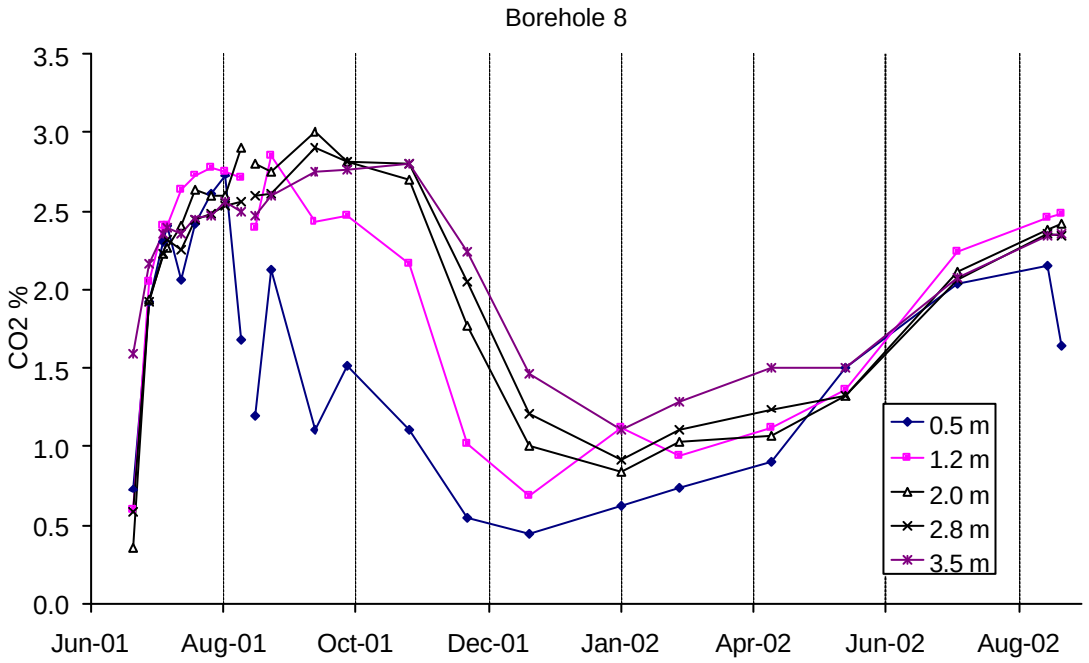

Appendix 7, page 3: soil air CO2 partial pressure, boreholes 7 and 8, Milandre test site

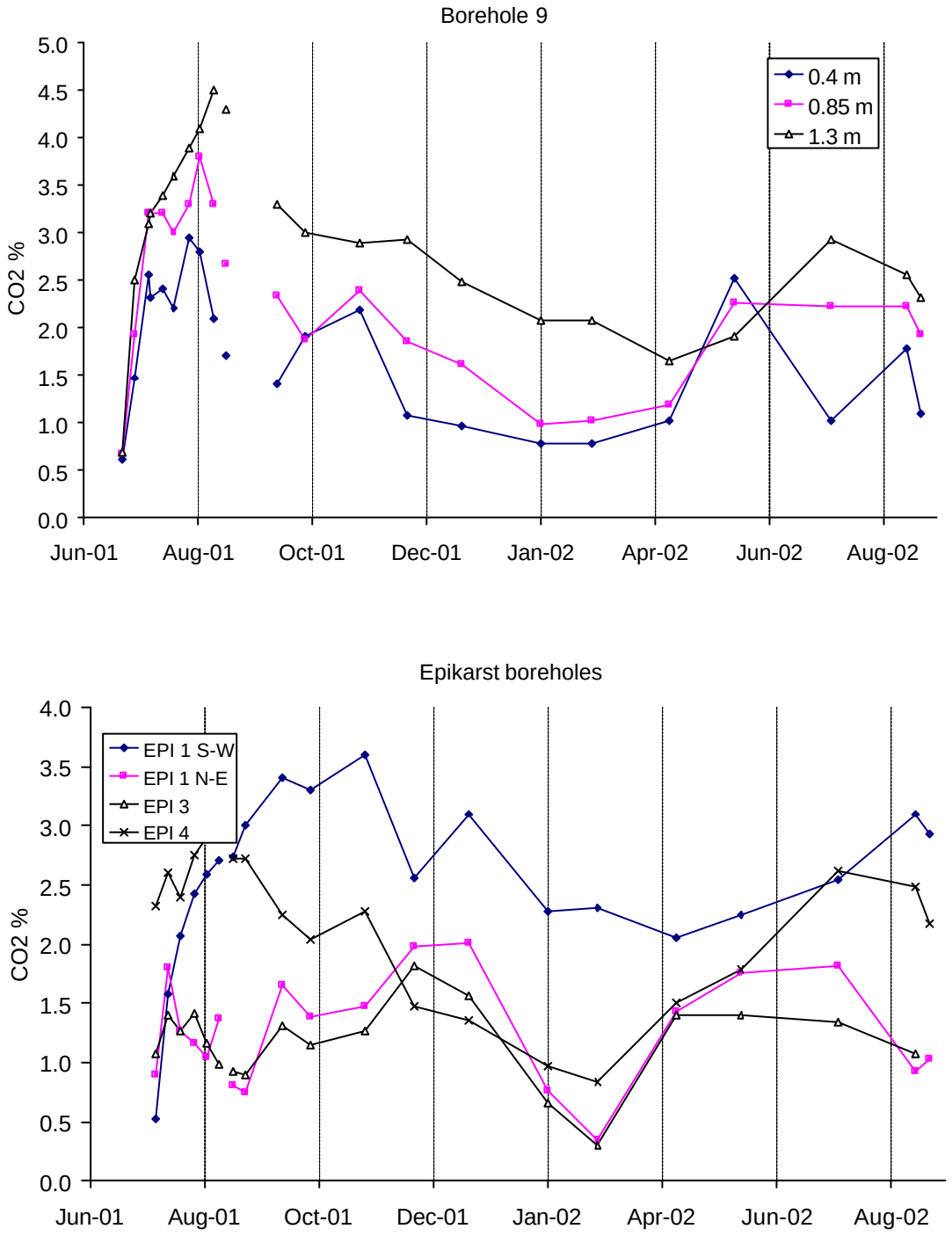

Appendix 7, page 4: Measurements of CO_2 partial pressure in soil air, borehole 9 (higher graph), and in epikarst boreholes (lower graph), Milandre test site.

site	28-Jun-01	23-Jul-01	9-Aug-01	18-Aug-01	12-Sep-01	27-Nov-01	31-Jan-02	27-Feb-02	10-Apr-02	14-May-02
Entrance Maira		1.83								
-5m in shaft		1.82								
-15m in shaft		1.95								
base shaft (-22m)	0.12	1.82								
start second ladder (-26m)		2.03								
base second ladder (-35m)		2.10	0.89							
EC (-38m)	0.77	2.15	1.56		0.43	0.13	0.69	1.30	2.10	1.63
5m before river	1.02									
SO			1.66							
AM (weir)	1.44/ 1.78*	2.18	2.15		0.87	0.84	1.97	2.13	2.02	2.02
EN	1.88	2.07	2.05							
start Gratte Roche gallery	1.91	2.36	2.24							
ST	2.13									
EG	2.17									
CA	2.22			2.70		2.38				
BU				2.46	2.22	1.33				
FA						1.18				
Salle SCJ				2.85						
ladder after salle SCJ				2.45						
AF						1.02				
AV				2.33		0.91				
start dry gallery						0.19				
end tourist gallery				2.01		0.15				

Appendix 7, page 5: Measurements of pCO_2 in Milandre cave. The measurements points are classified from the upstream entrance to the downstream part of the cave (ancient tourist gallery). The star indicates the measurement made at the river level.

Appendix 8 : Continuous measurements of nitrates at Milandrine upstream (AM)

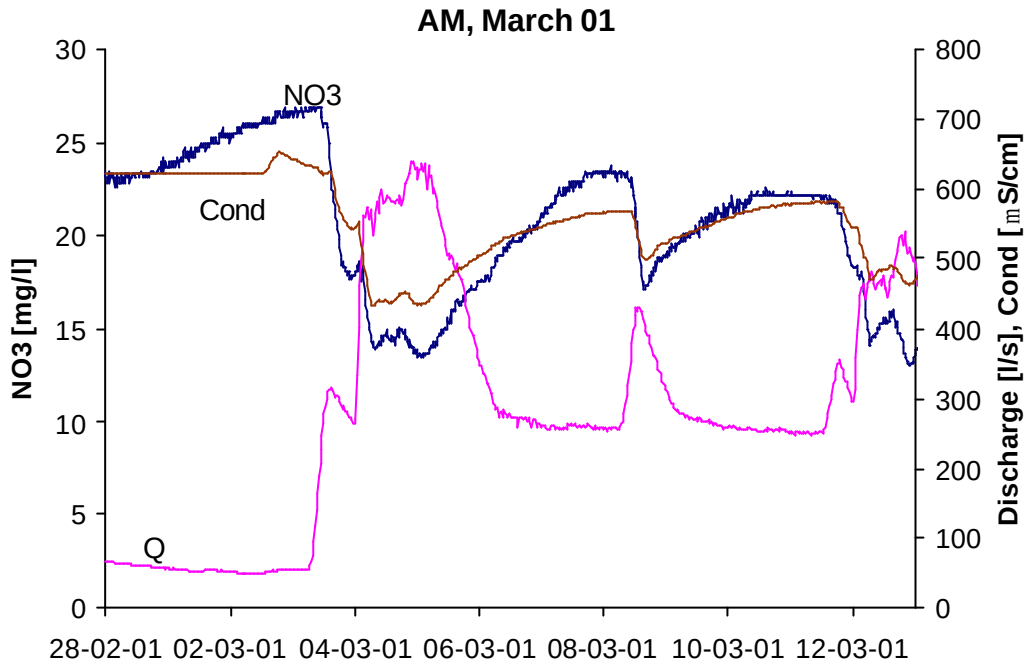

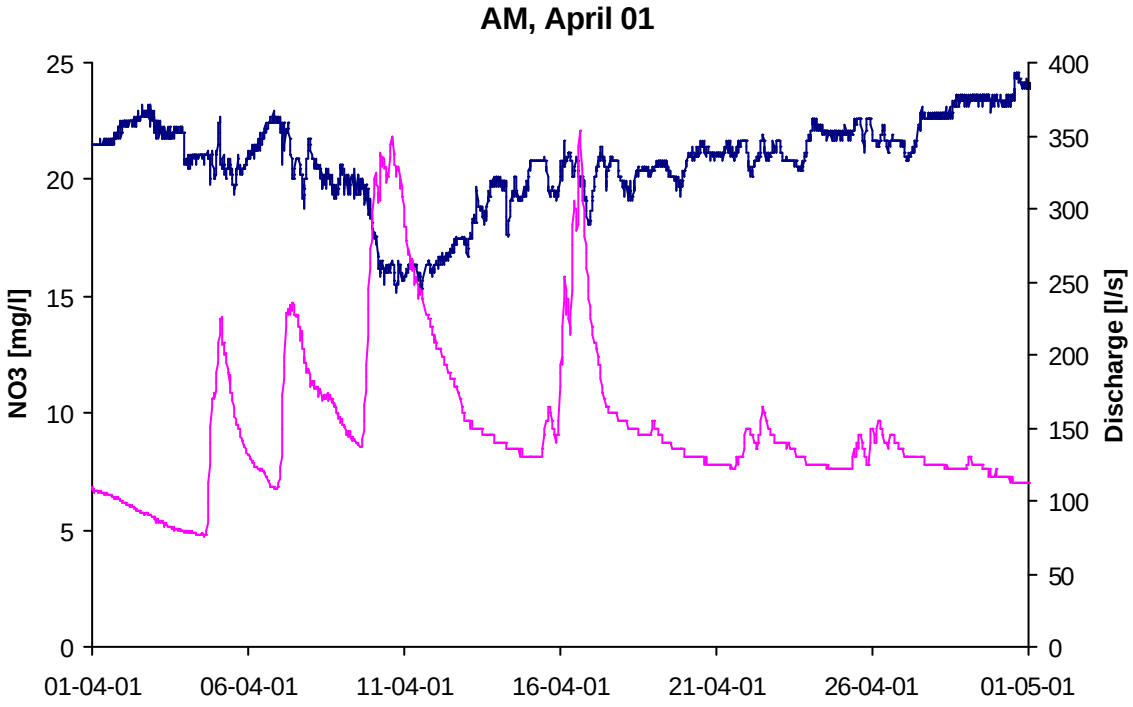

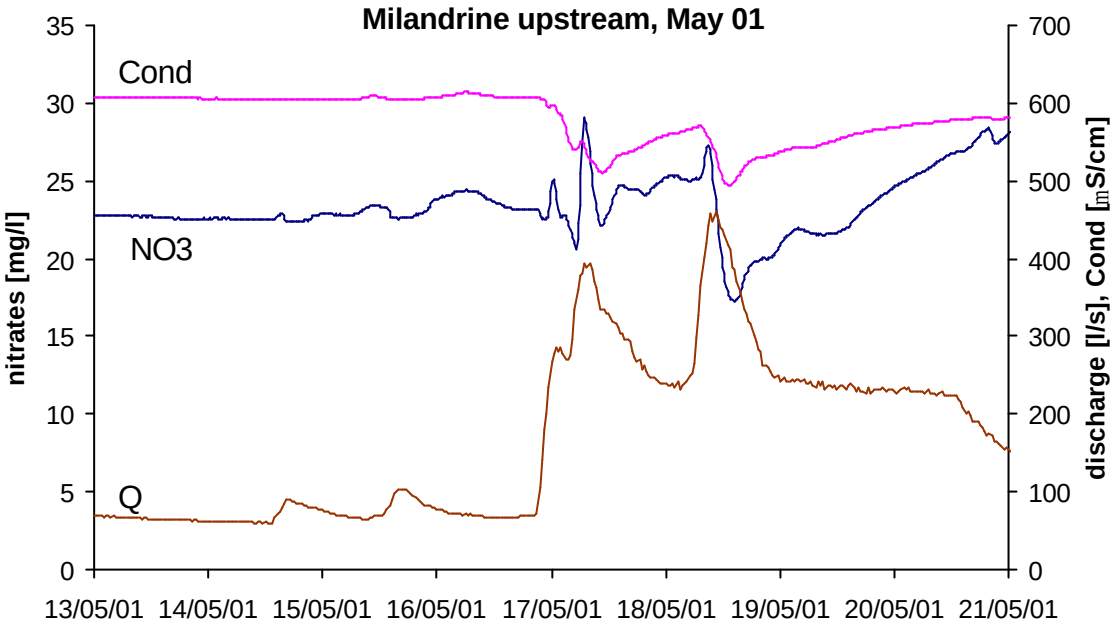
Milandrine upstream, May 01
Cond
NO3
Q
nitrates [mg/l]
discharge [l/s], Cond [µS/cm]
35
30
25
20
15
10
5
0
700
600
500
400
300
200
100
0
13/05/01
14/05/01
15/05/01
16/05/01
17/05/01
18/05/01
19/05/01
20/05/01
21/05/01

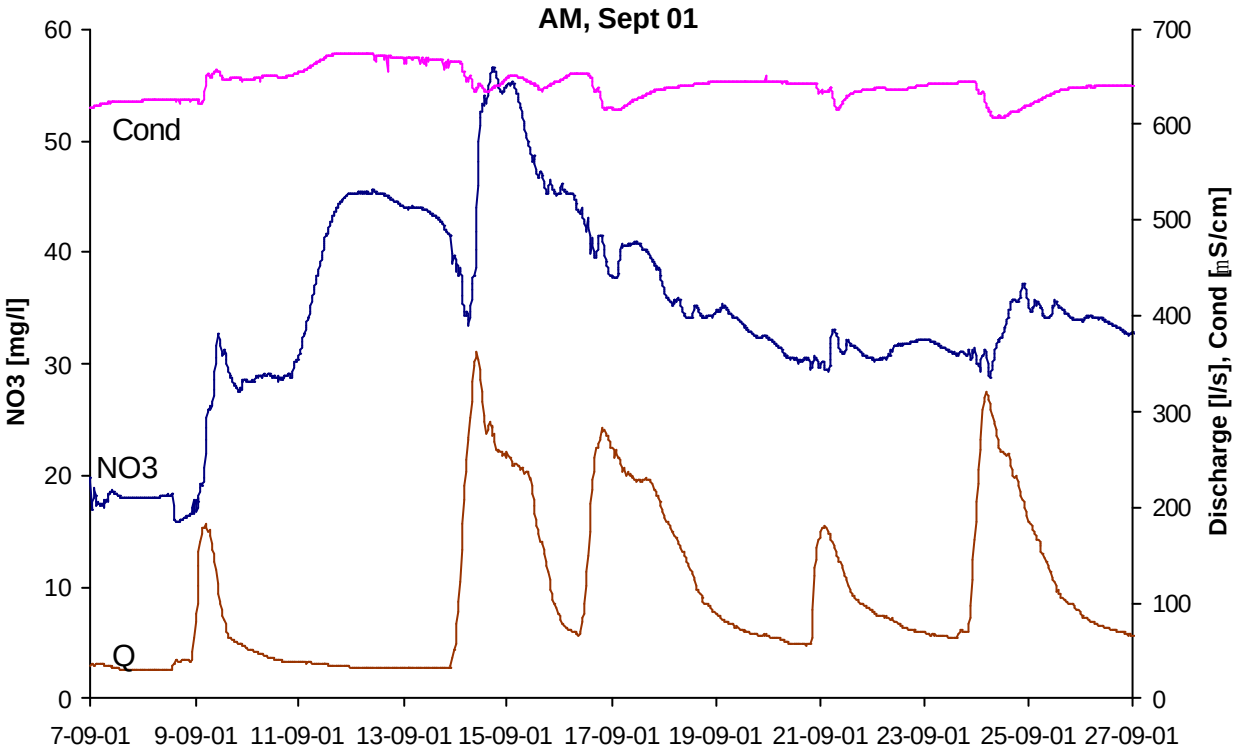
AM, Sept 01
Cond
NO3
Q
NO3 [mg/l]
Discharge [l/s], Cond [µS/cm]
60
50
40
30
20
10
0
700
600
500
400
300
200
100
0
7-09-01
9-09-01
11-09-01
13-09-01
15-09-01
17-09-01
19-09-01
21-09-01
23-09-01
25-09-01
27-09-01

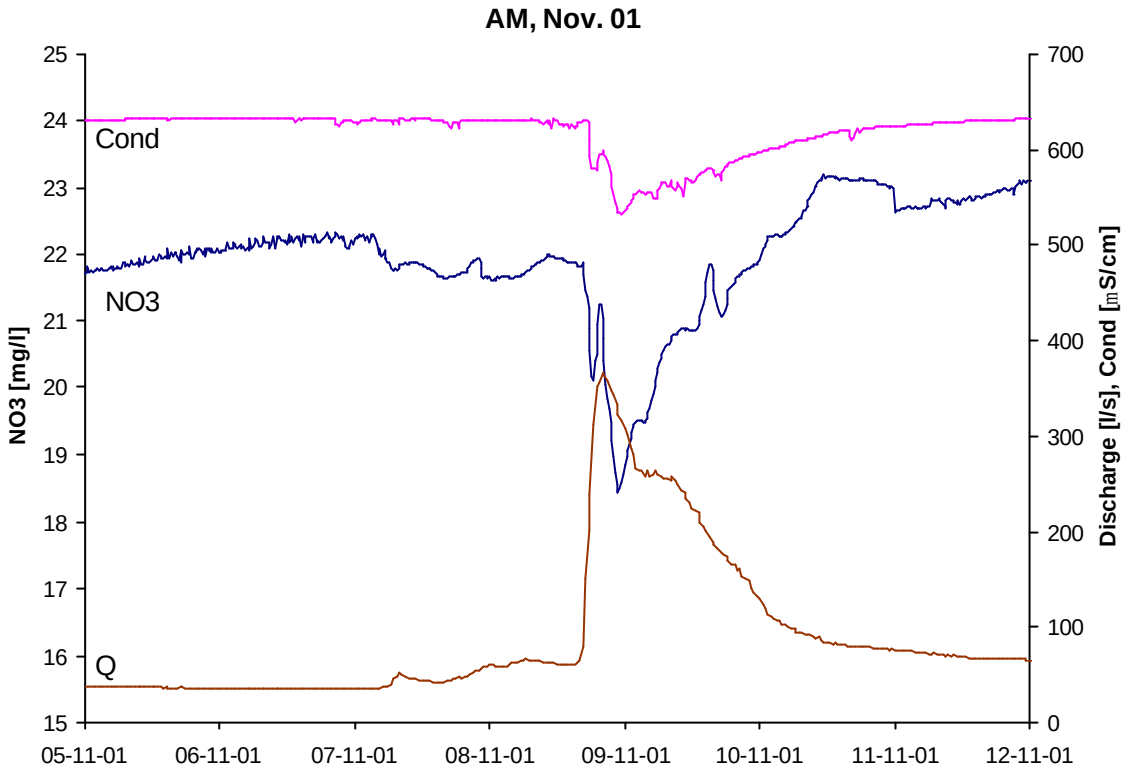
AM, Nov. 01
Cond
NO3
Q
NO3 [mg/l]
Discharge [l/s], Cond [mS/cm]
25
24
23
22
21
20
19
18
17
16
15
700
600
500
400
300
200
100
0
05-11-01
06-11-01
07-11-01
08-11-01
09-11-01
10-11-01
11-11-01
12-11-01

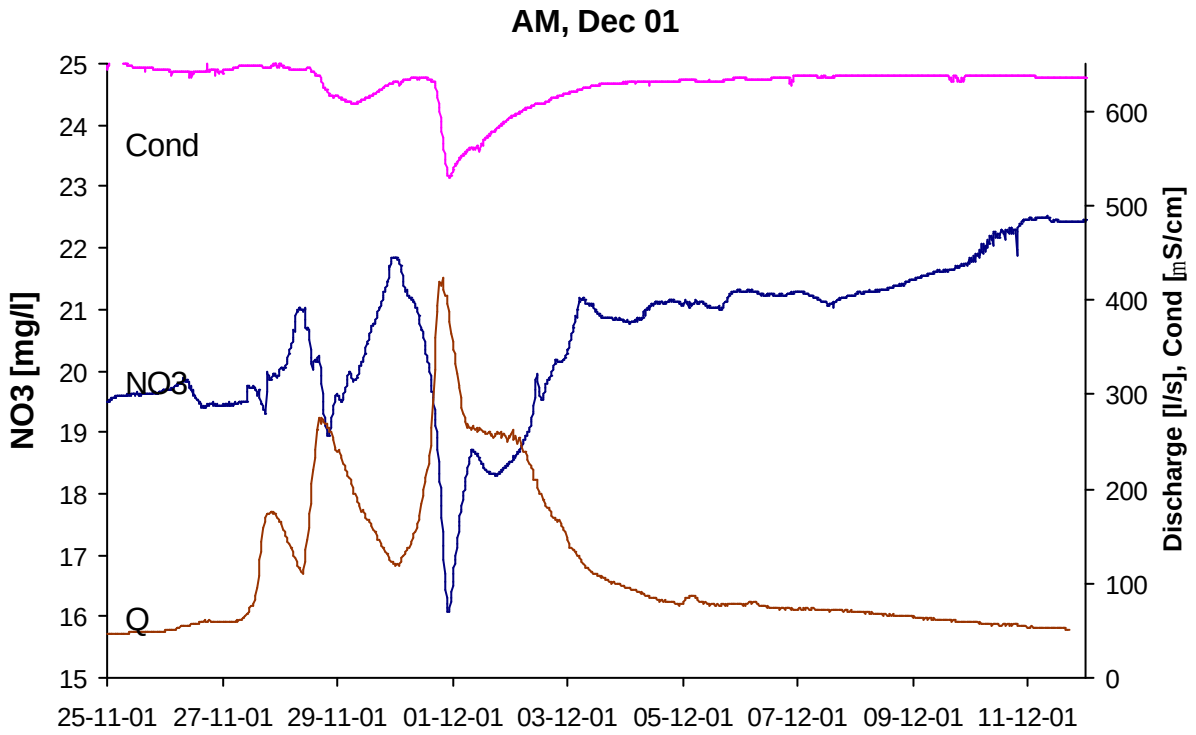
AM, Dec 01
Cond
NO3
Q
NO3 [mg/l]
Discharge [l/s], Cond [mS/cm]
25
24
23
22
21
20
19
18
17
16
15
600
500
400
300
200
100
0
25-11-01
27-11-01
29-11-01
01-12-01
03-12-01
05-12-01
07-12-01
09-12-01
11-12-01